GEOCHEMISTRY AND PETROGENESIS OF RHYOLITES HOSTING VMS MINERALIZATION IN THE EASTERN BETUL BELT, CENTRAL INDIA

Thesis Submitted to the

COCHIN UNIVERSITY OF SCIENCE AND TECHNOLOGY

in Partial Fulfillment of the Requirements

for the Degree of

DOCTOR OF PHILOSOPHY

IN GEOLOGY

(Faculty of Marine Sciences)

by

M.N. PRAVEEN

DEPARTMENT OF MARINE GEOLOGY AND GEOPHYSICS

SCHOOL OF MARINE SCIENCES

COCHIN UNIVERSITY OF SCIENCE AND TECHNOLOGY

COCHIN – 682 016

2016

Declaration

I M. N. Praveen, do hereby declare that the thesis entitled ***"Geochemistry and Petrogenesis of Rhyolites hosting VMS Mineralization in the Eastern Betul Belt, Central India"*** *is an authentic record of the research work carried out by me under the supervision and guidance of Prof. C.G. Nambiar, Department of Marine Geology and Geophysics, School of Marine Sciences, Cochin University of Science and Technology, Kochi - 682 016 in partial fulfillment of the requirements of the Ph.D. degree of Cochin University of Science and Technology and that no part thereof has been presented for the award of any other degree in any University.*

Kochi – 682 016 ***M.N.Praveen***

29th March, 2016

Certificate

I certify that the thesis entitled ***"Geochemistry and Petrogenesis of Rhyolites hosting VMS Mineralization in the Eastern Betul Belt, Central India"*** *is an authentic record of the research work carried out by Mr. M.N.Praveen under my supervision and guidance in partial fulfillment of the requirements for the degree of Doctor of Philosophy and no part thereof has been submitted for any other degree.*

Kochi – 682 016
29th March 2016

Dr. C.G. Nambiar
(Research Supervisor)
Professor
Department of Marine Geology and Geophysics
School of Marine Sciences
Cochin University of Science and Technology
Kochi-682 016

Acknowledgments

My sincere thanks to my research guide Dr. C.G. Nambiar for his able and inspiring guidance during all stages of my Ph.D. work. I also thank Dr. G.R. Ravindra Kumar, National Centre for Earth Science Studies (NCESS) for his valuable suggestions and also for facilitating XRF and REE analyses. I express my sincere gratitude to Dr. M.Satish Kumar, Niigata University, Japan for help with isotope analysis.

I express my deep gratitude to the Director General, Geological Survey of India for kindly permitting my Ph.D studies. I would also like to thank Shri. P.A. Ramesh Babu, Deputy Director General, GSI, SUAP and T, for his support during the period of submission of this thesis. I would like to thank several of my colleagues in GSI for various helps during the course of this work, especially, Dr. M.L.Dora, Shri. H.S. Shrivastava and Shri. M.N.Mishra who were associated with my field work in Betul Belt, and who have contributed by way of discussions.

My special thanks to Smt. Sonalika Joshi and Shri. Mahesh Korakoppa, who helped in carrying out petrographic and EPMA studies at GSI laboratories Faridabad and Bangalore. My sincere thanks to Dr. H.M.Ramachandra, for his insightful comments and discussions at the petrology lab in GSI, Bangalore.

I express my sincere gratitude to all faculty and office staff in the Department of Marine Geology and Geophysics, CUSAT for support and encouragement. My special thanks to Jishnu and Harisanth, research scholars of CUSAT and Sreejith, Nishanth and Eldhose (NCESS) for helping me in many ways during the course of my work.

Lastly, my thanks to my wife Divya, and my sons Aditya and Sidharth, who showed great patience during all these years and without whose support and understanding this work would not have been possible.

M.N.Praveen.

Dedicated to my Parents

Preface

The present work deals mainly with the geochemistry and petrogenesis of the rhyolites hosting the VMS deposits of eastern Betul Belt in Madhya Pradesh, central India. Other related aspects like mineral chemistry, metamorphism and sulphide mineralization have also been studied and discussed.

The first chapter introduces the topic and provides a review of VMS deposits and also the regional geology of the area.

The second chapter gives the field relations of the felsic volcanic rocks and sulphide mineralization.

The third chapter describes the petrographic aspects of the main rock types in the study area.

The chapters 4 and 5 deal with the geochemistry of unaltered rhyolites and altered rhyolites respectively and discuss the petrogenetic and hydrothermal processes involved in their evolution. A preliminary isotope study of the carbonate-bearing alteration is also included here.

The sixth chapter presents the mineral chemistry of the various metamorphic minerals and discusses their compositional variations in different alteration zones.

The seventh chapter describes the nature of sulphide mineralization, ore textures, sulphide mineralogy and their paragenesis.

The eighth chapter deals with the metamorphism in the area based on mineral paragenesis and EPMA-based geothermobarometry.

The summary and major conclusions are presented in the ninth chapter.

Contents

1. Introduction ---------- 1

1.1 Introduction ---------- 1

1.2 Volcanogenic Massive Sulphide Deposits (VMS) ---------- 3

1.2.1 Distribution ---------- 5

1.2.2 Types of Deposits ---------- 6

1.2.3 Association of VMS Deposits with Felsic Volcanism and Crustal Extension ---------- 6

1.2.4 Classification of Felsic Volcanics based on VMS Potential ---------- 7

1.3 Previous Work ---------- 9

1.4 Objectives and Scope of the Study ---------- 9

1.5 Methodology ---------- 10

1.6 Regional Geological Setting ---------- 11

1.6.1 The Central Indian Tectonic Zone (CITZ) ---------- 11

1.6.2 Geological setting of Betul Belt ---------- 14

1.6.3 Bimodal Volcanics ---------- 18

1.6.4 Base-metal Deposits ---------- 20

2. Geology of the Area ---------- 23

2.1 Geological Mapping ---------- 23

2.2 Lineament Studies in the Eastern Betul Belt ---------- 24

2.3 Lithology and Structure ---------- 29

2.4 Volcanic and Sedimentary Facies ---------- 36

2.5 Alteration Facies Mapping ---------- 41

2.5.1 Least Altered Rhyolites or unaltered Rhyolites ---------- 44

2.5.2 Quartz-muscovite-sericite-K feldspar ± biotite/phlogopite ± garnet schist and red silicified rhyolite ---------- 47

2.5.3 Quartz-biotite-phlogopite ± muscovite ± garnet ± plagioclase ± staurolite ± gahnite schist ---------- 49

2.5.4 Tremolite ± carbonate ± actinolite ± talc ± chlorite ± garnet rock ---------- 52

2.6 Summary and Conclusions ---------- 56

3. Petrography ---------- 59
3.1 Petrography of Least Altered Rhyolite ---------- 60
3.2 Petrography of Altered Rhyolites ---------- 64
3.2.1 Quartz-muscovite-K-feldspar ± garnet ± biotite/phlogopite schist ---------- 64
3.2.2 Quartz- biotite/phlogopite - garnet ± plagioclase ± staurolite ± gahnite schist ---------- 67
3.2.2.1 Quartz-phlogopite-garnet ± plagioclase schist ---------- 69
3.2.2.2 Zincian spinel (gahnite) bearing assemblage ---------- 71
3.2.2.3 Zincian staurolite bearing assemblage ---------- 74
3.2.3 Tremolite ± dolomite ± actinolite ± talc ± chlorite ± garnet rock ---------- 76
3.3 Mafic volcanic/ Metabasalt ---------- 82
3.4 Mafic Intrusives ---------- 84
3.5 Discussion ---------- 84
4. Geochemistry of Unaltered Rhyolites ---------- 87
4.1 Introduction ---------- 87
4.2 Aims of this Study ---------- 88
4.3 Methodology ---------- 88
4.4 Major and Trace Element Geochemistry of Rhyolite ---------- 90
4.4.1 High HFSE Contents ---------- 94
4.4.2 Magmatic Affinity ---------- 94
4.5 Zircon Saturation Temperatures ---------- 97
4.6 Rare Earth Elements (REE) Geochemistry of Least Altered Rhyolite ---------- 97
4.7 Rhyolite Classification and Petrogenesis ---------- 100
4.8 Tectonic Setting ---------- 105
4.9 Discussion ---------- 108
5. Geochemistry of Alteration Zones ---------- 113
5.1 Introduction ---------- 113
5.2 Sampling and Analysis ---------- 115
5.3 Results ---------- 116
5.3.1 Alteration Trends ---------- 120

5.3.2 Major and trace elements of alteration zones and relationship with AI ------- 126
5.3.3 Relative enrichments and depletions of elements compared to unaltered rhyolite ----------133
5.3.3.1 Relative percentage gains and losses----------138
5.3.4 Alkali-Alumina Molar Ratios of rhyolites----------141
5.3.5 Discussion on gains and losses (mobility) of major and trace elements------143
5.3.6 Immobile elements during Hydrothermal Alteration----------144
5.3.7 Rare Earth Elements of Alteration zones ----------146
5.4 Summary and Interpretation of REE in Altered Rocks ----------151
5.5 Geochemical Proximity Indicators to Mineralized Zone----------153
5.6 Discussion ----------154
5.7 Carbon and Oxygen Isotope studies of Carbonates ----------156
5.7.1 Introduction ----------156
5.7.2 Carbonate Bearing Rocks around Bhuyari----------157
5.7.3 Methodology ----------159
5.7.4 Results ----------160
5.7.5 Discussion----------164
6. Mineral Chemistry ----------169
6.1 Introduction----------169
6.2 Methodology ----------170
6.3 Results----------170
6.4 Summary and Conclusions----------209
7. Sulphide Mineralization ----------213
7.1 Introduction----------213
7.2 Objectives of this Study ----------216
7.3 Methodology ----------216
7.4 Surface Indications and Nature of Sulphide Mineralization----------217
7.5 Sulphide Texture and Mineralogy----------220
7.6 Mineral Chemistry of Sulphides ----------221
7.7 Discussion ----------225

8. Metamorphism and Geothermobarometry----------227

8.1 Introduction ----------227

8.2 Metamorphic Mineral Assemblages----------234

8.3 Use of Petrogenetic Grid for Estimating Pressure-Temperature ----------237

8.4 Geothermobarometry----------239

8.4.1 Garnet Biotite Thermometry ----------240

8.4.2 Ti in Biotite Thermometer ----------246

8.4.3 Phengite geochemistry and Barometry----------249

8.4.4 Garnet-Plagioclase-Muscovite-Biotite Barometry.----------255

8.4.5 Garnet-Muscovite-Plagioclase-Quartz Geobarometer ----------256

8.5 Conclusions----------260

9. Summary and Conclusions ----------261

References ---------- 271

Appendix ---------- 303

Chapter 1

INTRODUCTION

Contents

1.1 Introduction
1.2 Volcanogenic Massive Sulphide Deposits (VMS)
1.3 Previous Work
1.4 Objectives and Scope of the Study
1.5 Methodology
1.6 Regional Geological Setting

1.1 Introduction

The Betul Belt is an E-W trending, Proterozoic gneiss-supracrustal entity within the Central Indian Tectonic Zone (Fig.1.1) known for its base-metal deposits hosted by the felsic volcanic rocks. Recent studies on the base-metal deposits of the area have shown that they have several similarities with volcanogenic massive sulphide deposits (VMS) (Raut and Mahakud, 2004; Praveen et al, 2005; 2007 and Golani et al, 2006). However, detailed characterization of these deposits have not been attempted so far to convincingly demonstrate their VMS status and to understand their genesis.

The greenstone belts in Precambrian shield areas contain significant VMS deposits, the best example being those of the Canadian Shield. Although the Indian shield is known for the occurrence of several greenstone belts, they contain very few VMS deposits, which may be partly an artifact of non-recognition of these features or of inadequate exploration (Misra, 2000).

The base-metal deposits including the Ambaji and Deri deposits of Delhi Fold Belt in Rajasthan are known to be of VMS type which were formed around 1 Ga (Deb, 2000; Deb et al, 2001). However, it is possible that many other base-metal and base-metal-gold deposits in India may turn out to be of VMS origin following detailed studies. There also exists high potential for discovery of such deposits in the various volcanosedimentary sequences of India. Therefore, there is a need for reassessment of several of our base-metal deposits, especially those hosted by volcanosedimentary sequences. Recognition of some of these deposits as VMS-type will help vastly in exploration of such deposits within the same belt and other similar belts in India. Since the VMS deposit class is well studied, there exists a variety of exploration tools which can be applied for discovery of these deposits.

Application of lithogeochemistry and alteration studies are important methods used to explore for VMS deposits (Hashiguchi et al, 1983; Hodges and Manojlovic, 1993; Galley et al, 2000). The volcanosedimentary belts in India which host base-metal deposits and those that have potential for hosting such deposits occurs as deformed sequences in gneissic terrains. Recognition of the characteristic features of VMS deposits in gneissic terrains which have undergone medium to high-grade metamorphism and deformation is challenging and requires a combination of field-based, petrographic and geochemical studies (Bonnet and Corriveau, 2007).

Volcanic and alteration facies mapping along with petrological and geochemical characterization is crucial in understanding VMS deposits in deformed Precambrian terrains.

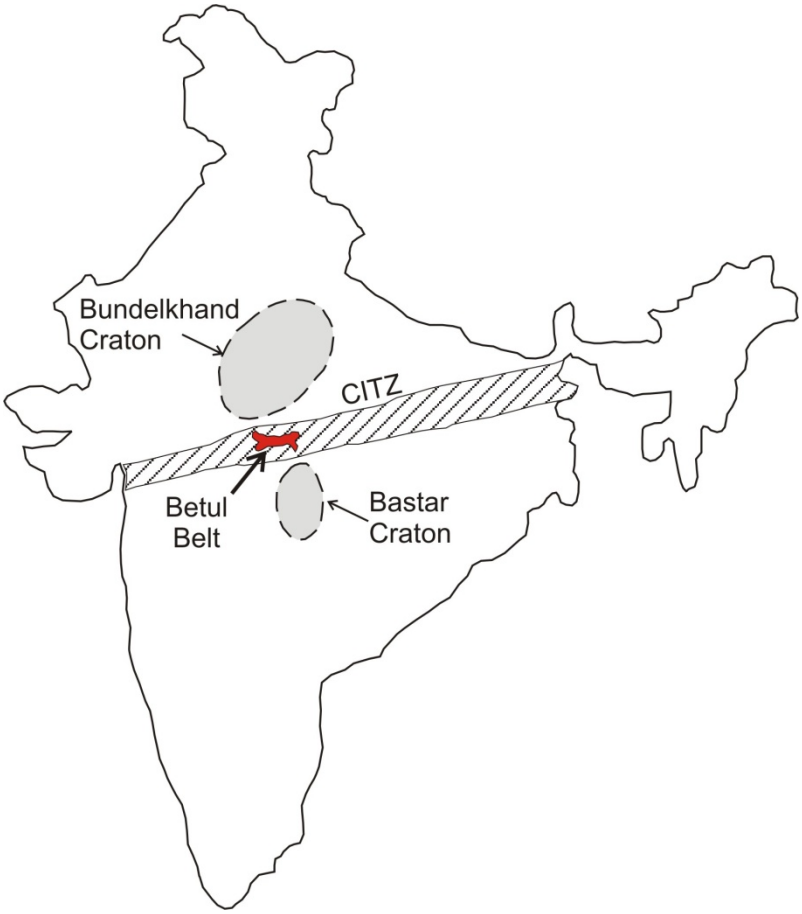

Fig. 1.1 Location map of Betul Belt within the ENW-WSW trending Central Indian Tectonic Zone (CITZ) modified after Radhakrishna (1989) and Jain et al (1991).

1.2 Volcanogenic Massive Sulphide Deposits (VMS)

Base-metal sulphide deposits with massive Zn-Pb-Cu ores associated with volcanic rocks have been described variously as 'volcanic-associated', 'volcanic-hosted' or 'volcanogenic'. The term volcanic-associated is considered more appropriate, because as per the definition of Franklin et al, (1981) these deposits include not only those enclosed entirely within volcanic-strata, but also those hosted by sedimentary rocks that formed in a dominantly

volcanic regime, such as the Besshi deposits of Japan which are locally hosted by pelite but occur in a mafic volcanic environment (e.g.Misra, 2000). The most important requirements of the volcanic-associated class are that penecontemporaneous volcanism must have accompanied the deposition of deposits and that volcanic rocks must comprise an essential part of the immediate stratigraphic sequence (Franklin et al, 1981)

Volcanic-associated massive sulphide deposits are an important source of zinc, copper, lead, silver and gold and a significant source of Co, Sn, Se, Mn, Cd, In, Bi, Ti, Ga an Ge (Hannington et al, 1999; Allen et al, 2002). These deposits form attractive exploration targets because of their clustered nature, compact and polymetallic ore bodies and well-defined alteration zones which act as guides.

VMS deposits have been extensively researched and copious literature is available for this class of deposits (e.g., Hutchinson, 1973, 1980; Solomon, 1976; Sangster and Scott, 1976; Large, 1977; Klau and Large, 1980; Franklin et al, 1981; Ohmoto and Skinner, 1983; Stanton, 1986; Lydon, 1984; Franklin, 1993; Franklin et al, 2005). VMS deposits have become the major focus of scientific studies since the discovery of active high-temperature (>300ºC) hydrothermal vents in the ocean-floor ridge shift systems in the eastern Pacific Ocean (Spiess et al, 1980).

The discovery in the 1960's of hot brine pools on the floor of the Red Sea indicated the possibility of direct precipitation of metalliferous sediments from hydrothermal brines on the seafloor (Shanks and Pat, 2012 and references therein). Later, the discovery of high-temperature black smoker-type venting on the modern sea-floor at the Mid Atlantic Ridge and the East Pacific Rise (Hekinian et al, 1980; Spiess et al, 1980; Rona et al, 1986) paved the way for more interest in this class of ore deposits.

VMS deposits form at or slightly below the seafloor where hot (>300°C) metal-bearing seawater solutions are discharged from submarine volcanoes and active faults (Allen et al, 2002). These solutions precipitate sulphide minerals due to the cooling by seawater. The hot solutions also cause hydrothermal alteration of the rocks below the seafloor. During hydrothermal alteration primary minerals of the rock are transformed into secondary (alteration) minerals. VMS deposits are generally underlain by large volumes of hydrothermally altered rocks (Allen et al, 2002).

There appear to be a common set of factors that contribute to the formation of VMS deposits in all major VMS-hosting terrains (Allen et al, 2002). These geological factors include: events such as major crustal extension, simultaneous presence of felsic and mafic volcanics and ore deposition in a relatively short time interval. Based on several studies involving volcanic facies analysis it is inferred that the VMS deposits formed at or slightly below the sea- floor in below wave base conditions (Misra, 2000 and references therin).

1.2.1 Distribution

VMS deposits are associated with volcanic and volcano sedimentary rocks of submarine origin and were formed in a wide variety of tectonic environments and range in age from Archean to Teritiary. The oldest recorded deposits are in pre-3700 m.y-old supracrustal rocks of Isua, Greenland (Appel, 1979), and in the pre-3400 m.y-old volcanic rocks of the Pilbara rocks of Western Australia (Sangster and Brook, 1977). The youngest deposits are the presently active black smokers in various ridge-rift systems on the ocean floor.

Some of the important regions with VMS deposits are Archean and early Proterozoic greenstone belts of the Canadian Shield, the lower Paleozoic

volcanic belts of the Caledonides in Scandinavia and the northern Appalachians of Newfoundland (Canada), the Upper Paleozoic Iberian pyrite belt extending from southern Portugal to northern Spain, and the Miocene Green Tuff belt of Japan (Misra, 2000). In Australia, the Cambro-Ordovician VMS deposits of Mount Read volcanics in Tasmania and Mount Windsor volcanics of Queensland are also significant (Large, 1992).

Within individual belts, VMS deposits commonly occur in clusters and are probably related to volcanic centers. Most of the deposits in each cluster occur within a restricted stratigraphic interval (the 'favourable horizon'), which occupies only a fraction of the volcanic sequence, and their localization appears to be controlled by topographical and structural features of the substrate (Misra, 2000).

1.2.2 Types of Deposits

Various classification schemes have been proposed for VMS deposits, which are based on one or more of the variables, like ore composition, host rock lithology and tectonic setting. The classification schemes based on the bulk composition of the ores are simpler, more reliable and not subject to uncertainties in the interpretation of tectonic settings (Misra, 2000). Based on bulk composition of the ores, a two-fold sub-division into (a) Cu-Zn deposits and (b) Zn-Pb-Cu deposits was proposed by Franklin (1993). This compositional grouping is similar to that proposed earlier by Hutchinson (1973) and Solomon (1976), except that no Cu type is recognized.

1.2.3 Association of VMS Deposits with Felsic Volcanism and Crustal Extension

An extensional regime is a common theme in the interpretations of tectonic setting in most VMS deposits worldwide. Cas and Wright (1987) have

shown that VMS deposits are closely related to proximal volcanic facies of submarine felsic volcanoes. Sillitoe (1982) for the first time advocated an extensional setting for rhyolite hosted VMS deposits. Association of VMS deposits with felsic volcanism was further studied by later workers (Ohomoto 1996; Lentz 1998; Allen et al. 2002). Lentz (1998) highlights the association between geotectonic environment (extension), felsic volcanism and VMS deposition which he studied from six different Phanerozoic VMS deposits. Ohomoto (1996) from the study of VMS deposits in Hokuroku district concludes that they were formed in an extensional setting. Although there is substantial evidence that mineralization was linked to extensional tectonism, the interrelationship between the crustal extension, felsic volcanism and VMS deposits are not very clear (Allen et al, 2002).

1.2.4 Classification of Felsic Volcanics based on VMS Potential

Volcanogenic massive sulphide (VMS) deposits occur primarily in subaqueous rift-related environments (e.g, oceanic, fore-arc, arc, back-arc, continental margin, or continental), are hosted primarily by bimodal, mafic-felsic volcanic successions, and are typically associated with felsic volcanic rocks with specific geochemical characteristics.

A preferential association of geochemically distinctive, subaqueous felsic volcanic rocks with VMS depostis was first highlighted in the Archean Superior province of the Canadian Shield by Thurston (1981) and Campbell et al. (1982). Subsequent studies have shown that all VMS depostis in the Superior province including Kidd Creek and the deposits in the Noranda and Sturgeon Lake camps, are associated with geochemically distinctive rhyodacites, rhyolites and high silica rhyolites (eg. Lesher et al., 1986; Barrie et al., 1993).

These rocks have been classified as calc-alkaline and tholeiitic felsic volcanic rocks by Campbell et al. (1982), felsic volcanic groups FII and FIII rhyolites by Lesher et al. (1986), groups I, II, and III rhyolites by Barrie et al. (1993) and transitional and tholeiitic rhyolites by Barrett and MacLean (1994). These classifications have been a useful area selection tool in the exploration for VMS deposits in Archean and Proterozoic volcanic successions.

Hart et al. (2004) have proposed a more acceptable classification retaining that of Lesher et al. (1986) with FI, FII, F III and FIV felsic volcanic rocks with specific geochemical attributes for each. FI felsic rocks are characterized by steep REE patterns with weakly negative to moderately positive Eu anomalies, high Zr/Y and low abundances of high field strength elements (HFSE; e.g., HREE, Y, Zr, Hf). FII felsic volcanic rocks are characterized by gently sloping REE patterns with vriable Eu anomalies, moderate Zr/Y, and intermediate abundances of HSFE. FIII felsic volcanic rocks are rhyolites and high silica rhyolites characterized by relatively flat REE patterns. FIV felsic volcanic rocks are rhyoltes and high silica rhyolites characterized by flat to slightly LREE depleted REE patterns and low REE and HFSE abundances.

The VMS potentials of these geochemically distinct felsic volcanic groups differ; FI alkalic dacites and rhyodacites, despite being abundant in the rock record, are typically barren; some FII calc-alkalic rhyodacites and rhyolites host VMS deposits, but most are barren; FIII tholeiitic and FIV depleted rhyolites and high silica rhyolites are much less abundant in the rock record but commonly host VMS deposits, regardless of age; and FIII rhyolites appear to host the largest deposits Hart et al.(2004).

1.3 Previous Work

The previous geological work in the area includes regional tectonic appraisal by Roy et al (2000), Roy and Prasad (2001), Chaturvedi (2001), Golani et al (2001) and Roy and Prasad (2003), geological mapping and exploration for base-metals in and around Betul Belt by Geological Survey of India (Mahakud, 1993; Shrivastava and Chellani, 1996; Mahakud et al, 2000, 2001; Golani and Dora, 2003; Raut and Mahakud, 2004; Dora and Praveen, 2007; Shrivastava et al, 2007; Praveen et al, 2010), works on geochemistry of mafic-ultramafic complex (Roy et al, 2004; Alam et al, 2009; Mishra et al, 2011; Chakraborty and Roy, 2012) and studies relating to various aspects of exploration for base-metal deposits (Praveen et al, 2005; 2007; Ghosh et al, 2006; Golani et al, 2006; Praveen and Ghosh, 2007; Ghosh and Praveen, 2007; Ghosh and Praveen, 2008; Praveen and Ghosh, 2009). The salient aspects of these works are incorporated in the review of regional geology (Section 1.6)

1.4 Objectives and Scope of the Study

The primary aim of this study is to understand the geological setting of the felsic volcanic hosted sulphide deposits in the eastern part of Betul Belt. For detailed study, the eastern part of Betul Belt around the Bhuyari Zn-Pb-Cu deposit has been selected. Studies have been conducted on the lithology, geochemistry and mineralogy of unaltered and altered rhyolites in and around Bhuyari Zn-Pb-Cu deposit to understand the petrogenesis, hydrothermal alteration, sulphide mineralization and metamorphism. The objective of the study is to thoroughly analyse the VMS status of the deposit and to understand its petrogenetic and ore-genetic aspects. Thus the study included:

1. Large scale geological mapping of the eastern Betul Belt;
2. Volcanic and alteration facies mapping and interpretation around Bhuyari prospect;
3. Petrographic studies of unaltered and altered rhyolite to understand the types of alteration;
4. Characterization of the primary lithogeochemistry of rhyolites hosting Zn-Pb-Cu mineralization at Bhuyari, including classification based on VMS potential and understanding the tectonic setting;
5. Study of the geochemistry and mineralogy of the altered rocks and to understand the chemical trends of alteration and understand the nature of protolith;
6. Stable isotope studies of carbonates from the Bhuyari Prospect to understand the nature and origin of hydrothermal fluids associated with alteration and mineralization;
7. Geothermobarometric studies using mineral chemistry and mineral assemblages to understand the metamorphic conditions in the area; and
8. Arriving at a genetic model for the evolution of these VMS deposits by synthesizing all of the above.

1.5 Methodology

The aims of this study were largely achieved by a combination of detailed field mapping and detailed analyses of major, trace and REE analyses of the least altered and intensely altered rhyolites associated with the mineralized zone.

Emphasis was placed on field mapping and identification of volcanic and alteration facies during this study. Large scale mapping on 1: 25,000 scale of the surrounding area has brought out the primary textures associated with submarine volcanics in the area and also the relationship between the bimodal volcanic rocks and younger felsic and mafic intrusives in the area. Detailed mapping on 1:2000 scale of the mineralized area helped in delineating the relationship between massive sulphides and the associated alteration zones.

Information on tectonic setting was deciphered from identification of primary volcanic textures and also by interpreting the geochemistry of least altered rhyolites. Hydrothermal alteration was characterized by detailed geochemistry of alteration zones as well as by mineralogical studies.

The laboratory work involved in this study included petrographic studies using polarizing microscope and ore microscope, XRF analyses of rocks for major and trace elements, ICP-MS analyses for REE, mineral chemical analyses by EPMA and isotope analyses using mass spectrometer. Details of the techniques and procedures involved are given in the respective chapters.

The geochemical and other data were interpreted using standard procedures like computations of specific parameters and ratios, normalizing the values with standard values, plotting in relevant diagrams and chemistry based computations.

1.6 Regional Geological Setting

1.6.1 The Central Indian Tectonic Zone (CITZ)

The Central Indian Tectonic Zone (CITZ) is a prominent structural feature of the Indian peninsular shield and is comprised of an ENE-WSW composite zone of Proterozoic fold belts, older migmatitic gneisses and shear

zones. The CITZ, as defined by Radhakrishna (1989) and Acharya and Roy (2000), covers an ENE-WSW trending linear tract lying between the Son-Narmada north Fault (SNNF) in the north and the Central Indian Suture (CIS) in the south (Fig. 1.2). CITZ contain three prominent supracrustal belts and a number of major shear zones/ faults of Precambrian age. The supracrustal belts include northern Mahakhosal (2.4-1.8 Ga), central Betul (1.8-0.85 Ga) and southern Sausar (1.1-0.95Ga) belts (Roy and Prasad, 2003). Linear zones of granulite rocks are present parallel to the shear zones along the CIS (Balaghat-Bhandara Granulite Belt) and north of the Sausar belt (Ramakona Granulite Belt) (Roy and Prasad, 2003) (Fig. 1.2).

The major shear zones of the CITZ are the Son-Narmada North Fault, Tan shear and the Central Indian Suture (Jain et al, 1991). Among the three, the Son-Narmada shear system and the CIS are well studied (Roy et al., 2000, Jain et al.; 1991: Yedekar et al., 1990). Some workers have inferred continuity of some of these lineaments into Madagascar and Eastern Africa (Crawford, 1978).

The Tan Shear (Jain et al, 1991) or the Gavilgarh-Tan Shear Zone (GTSZ) (Golani, et al, 2001) is located midway between the Son-Narmada South Fault in the north and the Central Indian Suture in the south (Fig. 1.2). The GTSZ is essentially a Precambrian feature, manifested in the form of sheared granites and gneisses, which separate the Betul and Sausar supracrustal belts (Fig. 1.2). In recent years, the studies in the CITZ have assumed significance due to the recurrence of seismic activities, which have been located along some of these lineaments. The evidence of faulting along the GTSZ includes brecciation, presence of hot springs and tilting of the otherwise horizontal Gondwana rocks and basaltic flows (Golani and Dora, 2003). The CITZ has been recognized to represent a zone of amalgamation along which the northern Bundelkhand and southern Bastar cratons were

amalgamated (Yedekkar et al, 1990; Jain et al, 1991; Roy et al, 2000). The CITZ is thought to have evolved through a prolonged and multiphase development during 2.5Ga to 1.0 Ga (Roy et al, 2000). Stein et al (2004) based on the Re-Os dating of molybdenite from Malanjhkhand Cu-Mo-Au deposit occurring in the southern margin of CITZ (not shown in map) suggested that the CITZ developed as a zone of convergence between the southern and northern Indian cratons during 2.5Ga and have subsequently experienced widespread Grenvillian and younger reactivations. Recent deep seismic profiling of the CIS shows a deeply penetrating crustal-scale imbricating structure below the CIS which is interpreted as representing the collisional suture along which the Bastar craton subducted northwards below the Bundelkhand Craton (Mandal et al, 2013).

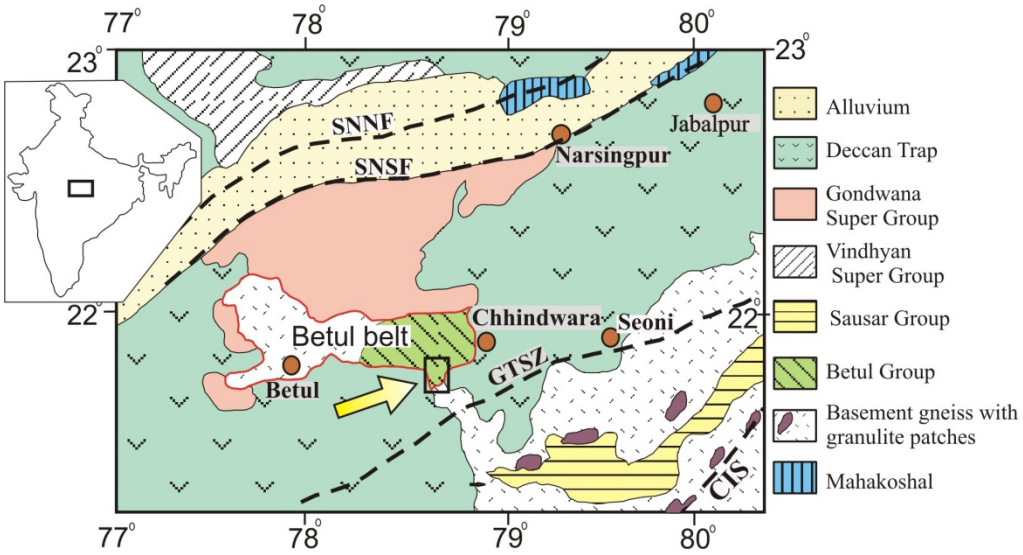

Fig.1.2 Regional Geological map showing the location of Betul Belt and adjoining areas (modified after, Roy et al., 2000; Roy and Prasad, 2001; Chakraborty and Roy, 2012 and GSI maps). Major shears: CIS- Central Indian Suture, GTSZ- Gavilgarh-Tan Shear Zone, SNNF- Son-Narmada North Fault, SNSF- Son-Narmada South Fault. The study area is shown in the box (arrow) south west of Chhindwara.

1.6.2 Geological setting of Betul Belt

The Betul Belt forms a narrow lithotectonic unit in the Central Indian Tectonic Zone (CITZ) between the Mahakoshal Belt in the north and the Sausar Group in the south. It forms a linear, E-W trending belt with Betul Group supracrustal rocks and basement gneisses with an approximate length of 135 km and an average width of 15 km (Mahakud et al, 2000; 2001). The basement gneisses comprises of granitic gneisses and migmatites with enclaves of older meta-sedimentaries. The basement gniesses and migmatites are exposed in the western part of the belt around Betul and the Betul Group volcanosedimentary sequence is exposed towards the eastern part (Fig.1.2). Field based evidences indicate that the basement gneisses are followed in chronological order by bimodal volcanics, meta-sedimentaries, utramafic-mafic complex and syntectonic and post tectonic granites.

There is a lack of precise age data for the gneisses; however they are interpreted to form the basement for the volcano-sedimentary sequence (Chaturvedi, 2001; Mahakud et al., 2001). These gneisses contain enclaves of of quartzites, quartz-mica schsits, graphitic schist, marble, tremolite-actinolite schist and calc-silicates which represent older metasedimentary/ supracrustal rocks. The Betul Belt comprises three distinct rock suites: 1) supracrustal rocks, 2) an ultramafic-mafic suite, and 3) a syn- to post-kinematic granitic suite (Roy and Prasad, 2001). The Betul Group supracrustal rocks are composed of quartzite, meta-pelite, bimodal volcanic rocks, meta-exhalites, calc-silicate rocks and banded iron formation (Roy and Prasad, 2001). The generalized stratigraphic succession (after Mahakud et al., 2000) is given in Table 1.1.

The central and eastern part of Betul Belt contains the volcanosedimentary complex which comprises of bimodal volcanics and associated metasedimentary rocks. The bimodal volcanics are composed of metabasalt and metarhyolite. Available whole rock data indicate the dominantly bimodal nature of the volcanics and their tholeiitic affinity (Raut and Mahakud, 2004; Praveen et al., 2007). Zn-Pb-Cu and Zn-Cu ore bodies are associated with metamorphosed hydrothermal alteration zones which contain various assemblages of metamorphic minerals which include chlorite, biotite, garnet, staurolite, sillimanite, gahnite, anthophyllite, actinolite and tremolite (Praveen et al., 2005).

Table.1.1 Stratigraphic succession of the Betul Belt (after Mahakud et al., 2000)

Cretaceous	Deccan Trap	Basalt flows
Permo-Carboniferous	Gondwana Supergroup	Lower and upper Gondwana rocks
	-----unconformity-----	
	Basic intrusives	Gabbro and Pyroxenites
Late Proterozoic	Acid intrusives	granites, aplites, pegmatites and quartz veins.
Middle Proterozoic	Younger metasediments	Phyllites, quartz-mica schist
	------sheared contact---------	
	Volcano-sedimentary sequence	Acid volcanics- metarhyolite, tuffs with intercalations of metasediments. Basic volcanics- pillowed and non pillowed basalt
Early Proterozoic	Granitoid complex	Granite gneiss, porphyroblastic gneiss and pegmatoid granite
	Older metasediments	Graphite schist marble, calc-silicate, tremolite-actinolite schist
	-- --- ---Base not seen---------	

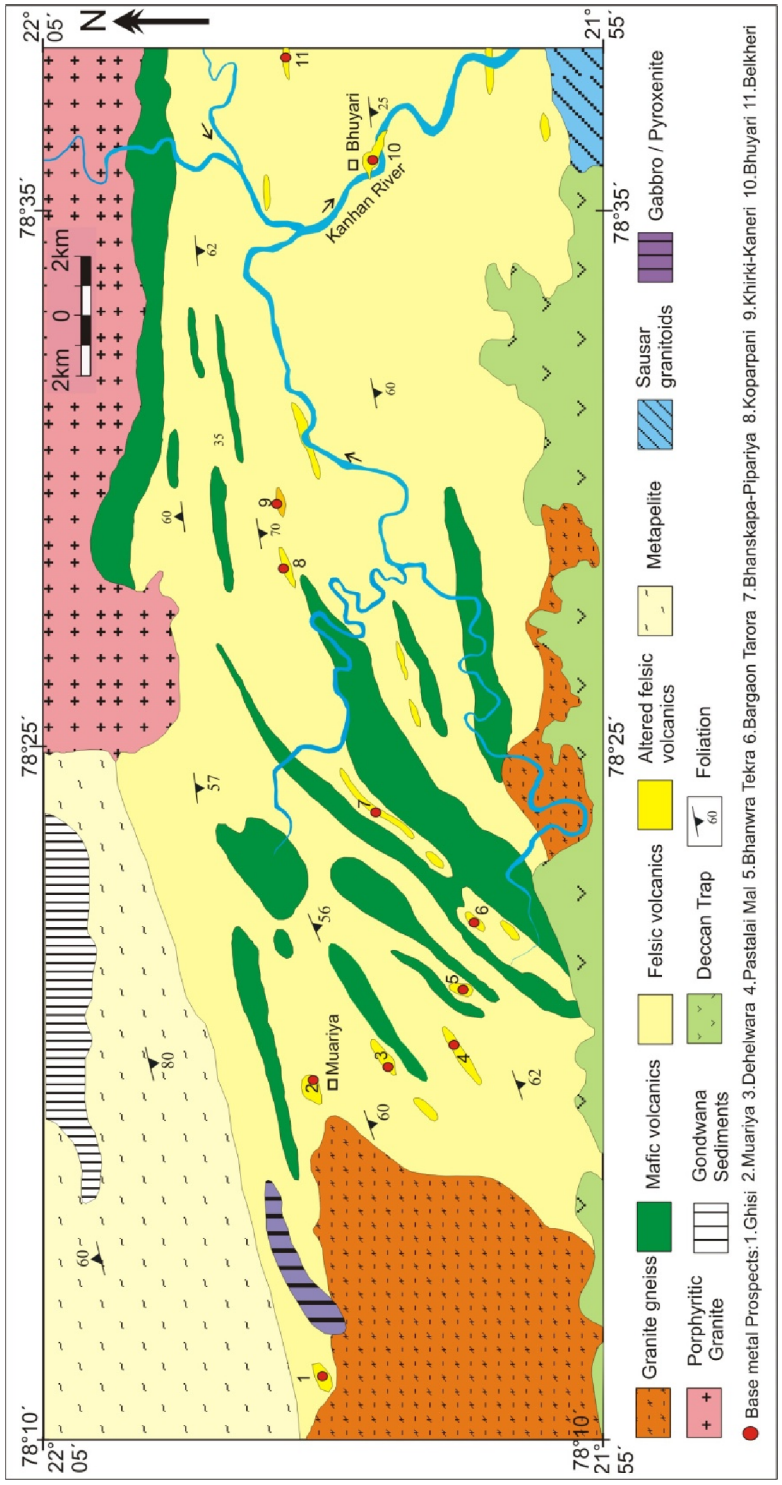

Fig. 1.3. Generalized geological map of central and eastern parts of Betul Belt showing the location of the various base-metal prospects (modified after Mahakud et al., 2001 and Praveen et al., 2007)

The volcanic sequence is overlain conformably by younger metasediments towards the north-west which comprises of phyllites, ferruginous quartzites and banded hematite quartzites and minor carbonate rocks. The entire volcano-sedimentary sequence is intruded by younger granites and basic intrusives (Mahakud et al., 2001).

The central Betul Belt consists of a suite of mafic-ultramafic rocks which are intrusive into the volcano-sedimentary sequence. They show similarities with layered mafic-ultramafic sequences (Roy et al, 2004). These mafic-ultramafic suites consist of pyroxenite, gabbro and diorite and are interpreted as products of mantle wedge melting in a subduction zone (Chakraborty and Roy, 2012). The basic intrusives comprising of gabbro and pyroxenite occur as dykes in the eastern and northern part of Betul Belt (Fig. 1.3).

Syntectonic to post-tectonic granite occur within the Betul Belt as ENE-WSW trending plutons emplaced along the ductile shear zones. The deformed syntectonic granite towards the western part of Betul Belt has given a Rb-Sr date of 1550 ± 50 Ma (Mahakud et al., 2001). These granites represent the older granitoids of Betul Belt. A younger phase of granitic activity represented by pink coloured feldspar-porphyritic granites well exposed around the north-eastern part of Betul Belt intrudes the bimodal volcanic sequence (Fig.1.3). The post-tectonic granite near Navegaon has given a Rb-Sr date of 850 Ma (Mahakud et al., 2001). The Betul Belt is covered by Deccan Traps in the south and east and Gondwana sedimentary rocks in the north and west (Fig. 1.2).

The belt is traversed by several ENE-WSW trending ductile shear zones having sub-vertical to steep dips, which were developed during deformation and were subjected to low to medium grade metamorphism (Roy and Prasad, 2001). According to them the area has experienced two phases of

metamorphism, with an earlier amphibolite facies and a later retrograde phase. Structural history of the volcanic region is not clearly understood due to the lack of marker horizons. A well-developed regional foliation is present striking ENE-WSW to E-W with moderate to steep southerly dips. The foliation plane is found to be generally parallel to the contact between the felsic and mafic volcanics and also to the bedding planes in the volcaniclastics.

Mahakud et al (2001) reported that the rocks were metamorphosed to staurolite-almandine subfacies of almandine-amphibolite facies, and subsequently subjected to retrograde metamorphism. Based on the study of metamorphic minerals in the alteration zones of sulphide mineralization, Ghosh and Praveen (2007) proposed that most of the minerals formed in a single metamorphic regime of continually decreasing growth kinetics generally linked to progressive cooling.

1.6.3 Bimodal Volcanics

Bimodal volcanics forms an important component of the Proterozoic volcanosedimentary sequence of Betul Belt. The volcanics are bimodal in nature and are entirely composed of metabasalt and metarhyolite. No intermediate volcanics have been convincingly documented, although there are some reports of minor proportion of andesite occurring along with basalt, (eg. Mahakud et al., 2001; Alam et al., 2009). The bimodal volcanics are present in the central and eastern part of the belt (Fig.1.3 and Fig. 2.2a). Volumetrically rhyolite is dominant over basalt and their relative proportions are approximately 60: 40. However, towards the eastern part of Betul Belt contain predominantly rhyolite with only minor mafic volcanic (Fig.1.3 and Fig. 2.2a)

The stratigraphy of the bimodal volcanics is complex with felsic and mafic volcanics showing interfingering relationships. Mafic volcanics are

present as elongate lensoid enclaves within more widespread felsic volcanics (Fig. 1.3). Within the bimodal volcanic sequence, the proportion of mafic volcanic rocks is higher in the western part when compared to the eastern part of the Betul Belt (Fig. 1.3). They comprise of pillowed and non-pillowed metabasalts (Fig. 2.3b). The mafic volcanic rocks are known to posses tholeiitic affinities (Mahakud et al, 2001., Raut and Mahakud, 2004). Recent work on the geochemistry of mafic volcanic flows in Betul Belt further confirms their tholeiitic geochemical affinities (Alam et al, 2009). Based on the trace element characteristics, it is inferred that the basalts are derived from partial melting of the enriched mantle. The REE abundances are low, with slight enrichment in LREE (20-60 times chondrite) and low enrichment in HREE (10 times chondrite). The general REE pattern indicates less fractionated nature of the volcanics with nearly flat MREE and HREE. Based on geochemistry a rift-tectonic environment is inferred (Alam et al, 2009).

Felsic volcanics comprise of massive rhyolite and volcaniclastics, Rhyolite is generally quartz-porphyritic, with 2mm phenocrysts showing resorbed grain margins in a recrystallized quartzo-feldspathic groundmass. Primary volcanic textures like flow banding, autobreccias and hyaloclastites have been documented in relatively unaltered rhyolites from the eastern Betul Belt (Praveen and Ghosh, 2007). Volcaniclastics also include fine-grained laminated tuff and lapilli tuff in the central parts of Betul Belt (Mahakud et al, 2001). Available data on the geochemistry of felsic volcanics show that they are tholeiitic in their affinities (Mahakud et al., 2001; Raut and Mahakud, 2004). The felsic volcanic rocks are hydrothermally altered near the mineralized zones and show extreme enrichments and depletions in various major elements (Praveen et al., 2005).

1.6.4 Base-metal Deposits

The sulphide deposits are hosted by the felsic volcanic rocks of the bimodal volcanic sequence in the central and eastern part of Betul Belt (Fig. 1.3). The mineralized zones within the felsic volcanic rocks are locally enclosed by typical assemblages including anthopyllite and tremolite-bearing rocks and biotite-garnet-staurolite-gahnite bearing rocks. These rock types were interpreted by previous workers as altered ultramafics (anthophyllite and tremolite-bearing rocks) and metasedimentary-tuff intercalations (biotite-garnet-staurolite-gahnite bearing rocks) (Mahakud et al, 2001; Raut and Mahakud; 2004). Later workers have suggested that these rocks represent metamorphosed hydrothermal alteration zones in felsic volcanic rocks (Praveen et al, 2005; Ghosh et al, 2006; Golani et al, 2006; Praveen et al, 2007). The Geological Survey of India has explored the base-metal deposits since the 1990's and several small deposits like Banskhapa - Pipariya, Bhanwra - Tekra, Bargaon - Tarora, Ghisi, Muariya, Koparpani, Dehalwara and Bhuyari have been identified (e.g., Mahakud et al. 2001; Raut and Mahakud, 2004; Golani and Dora 2003; Praveen et al. 2007) (Fig. 1.3). Most deposits are small (< 3 million tons) and low grade with 2 to 10 % (Zn + Pb + Cu). The Bhuyari base-metal deposit which is the focus of this study is a sub-economic zinc deposit with 1.56 million tonnes of ore containing 2 % zinc, 0.44% lead, and 0.12% copper and 5ppm silver (Praveen et al., 2010). Although the deposits are small in size, there exists the possibility of discovering larger deposits at depth, which may require a better understanding of the entire bimodal volcanic sequence and delineation of prospective horizons by a combination of detailed volcanic facies and alteration facies mapping and geochemical and mineralogical characterization of these rocks. Geophysical tools like ground and air-borne geophysics will also help in

locating sub-surface and concealed deposits. The felsic volcanic host rocks in Betul Belt are covered by Deccan Traps in the eastern and southern part. In the eastern part of Betul Belt, the altered rhyolites constitute first-order controls/guides for exploration and are observed to continue beneath the Deccan Traps. Since the thickness of the Deccan Trap cover in these parts are not very significant, it would be worthwhile to explore the inferred extension of the prospective altered felsic volcanics by a combination of geophyscis and deep drilling by scout bore holes.

******

Chapter 2

GEOLOGY OF THE AREA

Contents

2.1 Geological Mapping
2.2 Lineament Studies in the eastern Betul Belt
2.3 Lithology and Structure
2.4 Volcanic and Sedimentary Facies
2.5 Alteration Facies Mapping
2.5 Summary and Conclusions

2.1 Geological Mapping

As part of this Ph.D work mapping on different scales were carried out to better understand the geology, volcanic facies and alteration facies in the area. Accordingly, the previous maps of GSI has been modified and updated. The mapped area forms part of Survey of India Toposheets 55 J/12 and 55 K/9.

The objectives of the mapping were (1) to update the regional geological map around Bhuyari Prospect to delineate the various lithounits in the eastern Betul Belt and (2) to prepare a detailed map (1:2000 scale) of an area of about 2 sq.km around the Bhuyari prospect to delineate the metamorphosed alteration zones.

These objectives have been achieved by carrying out reconnaissance field work across strike from north to south and demarcating and refining the lithological contacts of various lithounits by modifying the earlier maps. The new map was prepared by integrating data from the available large scale maps in the area (Golani and Dora, 2003; and Dora and Praveen, 2007).

The alteration facies map was prepared by carrying out close-spaced traverses around Bhuyari Prospect. During the mapping work representative samples from least altered and different alteration zones were collected simultaneously for pertographic and geochemical analysis. Before the geological mapping of the area, an appraisal of the regional structure of the area was carried out by interpretation and lineament analyses of the aerial photographs of the eastern Betul Belt.

2.2 Lineament Studies in the Eastern Betul Belt

The detailed understanding of the regional structure is an important prerequisite to the understanding of the Bhuyari base metal prospect. This provides a regional perspective vis a vis the adjacent lithotectonic domains in the area and helps in arriving at better interpretation of the geological evolution of the deposit and terrain in general.

For this purpose, the aerial photographs (1: 62, 000 scale) of the area available with GSI were studied in detail to analyze the structural aspects in the area (Fig. 2.1a). The selected area comprises approximately 300 sq.km along the N-S Kanhan River corridor, which is the only continuously exposed link of Precambrian rocks between the Betul Belt and the Sausar Belt.

The prominent lineaments were demarcated with the help of the aerial photographs in an attempt to correlate the known geological boundaries and features with the lineament analyses brought out as part of this work (Fig. 2.1b). Based on lineament analysis, the terrain in the eastern part of Betul Belt can be sub-divided into three broad domains (Fig.2.1a and b)

1. The Betul Belt Domain
2. The Lawagoghri Shear Domain
3. Sausar Belt Domain

Two sets of lineaments predominate in the area,

1. EW lineaments
2. NW-SE lineaments

The EW lineament corresponds to the penetrative deformational fabric developed in the rocks which are represented by a well-developed schistosity in the phyllosilicate bearing rocks in Betul Belt. Whereas, the NW-SE lineaments are later generation features.

The **Betul Belt domain** is represented mostly by the E-W striking lineaments, which corresponds to the general strike of the rocks in the area. A prominent set of NW-SE striking lineament is also present in the area. This NW-SE lineament appears to be later and cuts the earlier E-W to ENE-WSW structural fabric. These later set of lineaments may represent faults and fractures, however substantial displacement have not been identified along these features. These set of NW-SE lineaments appear to have controlled the Kanhan River course which at places flow parallel to it.

A closed fold with EW trending axial plane is deciphered by structural analyses of aerial photo. This fold occurs to the NNE of Lawagoghri village. Around the Bhuyari Prospect, the EW set of lineaments are dominant, which is

consistent with a E-W to ENE-WSW foliation developed in the rocks as is evident in the detailed map (Fig. 2.2b).

The **Lawagoghri Shear Zone domain** is about 2 km wide and extends in the E-W direction. This domain has close-spaced and predominantly E-W striking lineaments. This at places swerves to ENE-WSW direction. These lineaments are the manifestation of intense shearing in the area with the development of mylonite. This shear zone demarcates the boundary between the Betul volcanics to the north and the Sausar granitoids to the south. This corroborates with the well developed EW striking mylonitic foliation as is seen in the geological map (Fig. 2.2a).

The **Sausar Belt domain** is characterized by EW trending lineaments and also NW-SE trending lineaments. The E-W trending lineaments are close spaced near the Lawagoghri shear domain, but further away towards south this fabric is not very prominent. The NW-SE set of lineaments are also present in the Sausar belt domain as is preresent in the Betul Belt domain.

Overall, the aerial photo interpretations are consistent with the known geological domains as mapped by previous workers. The E-W trending lineaments in the Lawagoghri shear domain (Fig. 2.1b) correspond well with the mylonite zone in the geological map (Fig.2.2a).

The lineament analysis provides a sound structural framework for the geological and tectonic interpretations in the later part of the thesis. The aerial photograph study substantiates the presence of a major shear zone in the area which has juxtaposed two different Precambrian terrains.

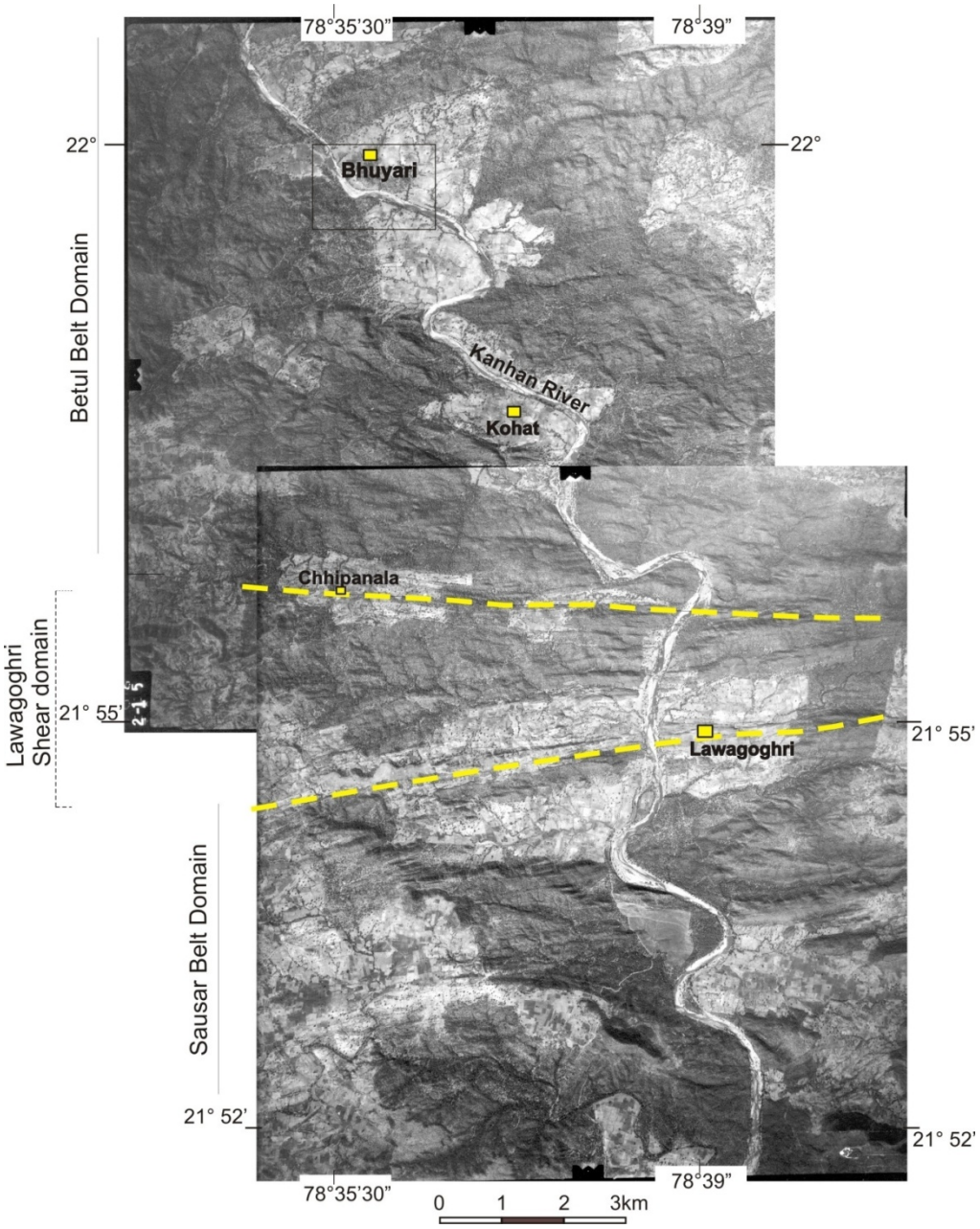

Fig.2.1a Aerial photo of parts of eastern Betul Belt along the Kanhan River corridor showing the physiographic and structural features. Note the Kanhan River flows south, perpendicular to the strike of the lithounits and structural fabric in the area. The dashed lines represent the boundaries of the major shear.

.

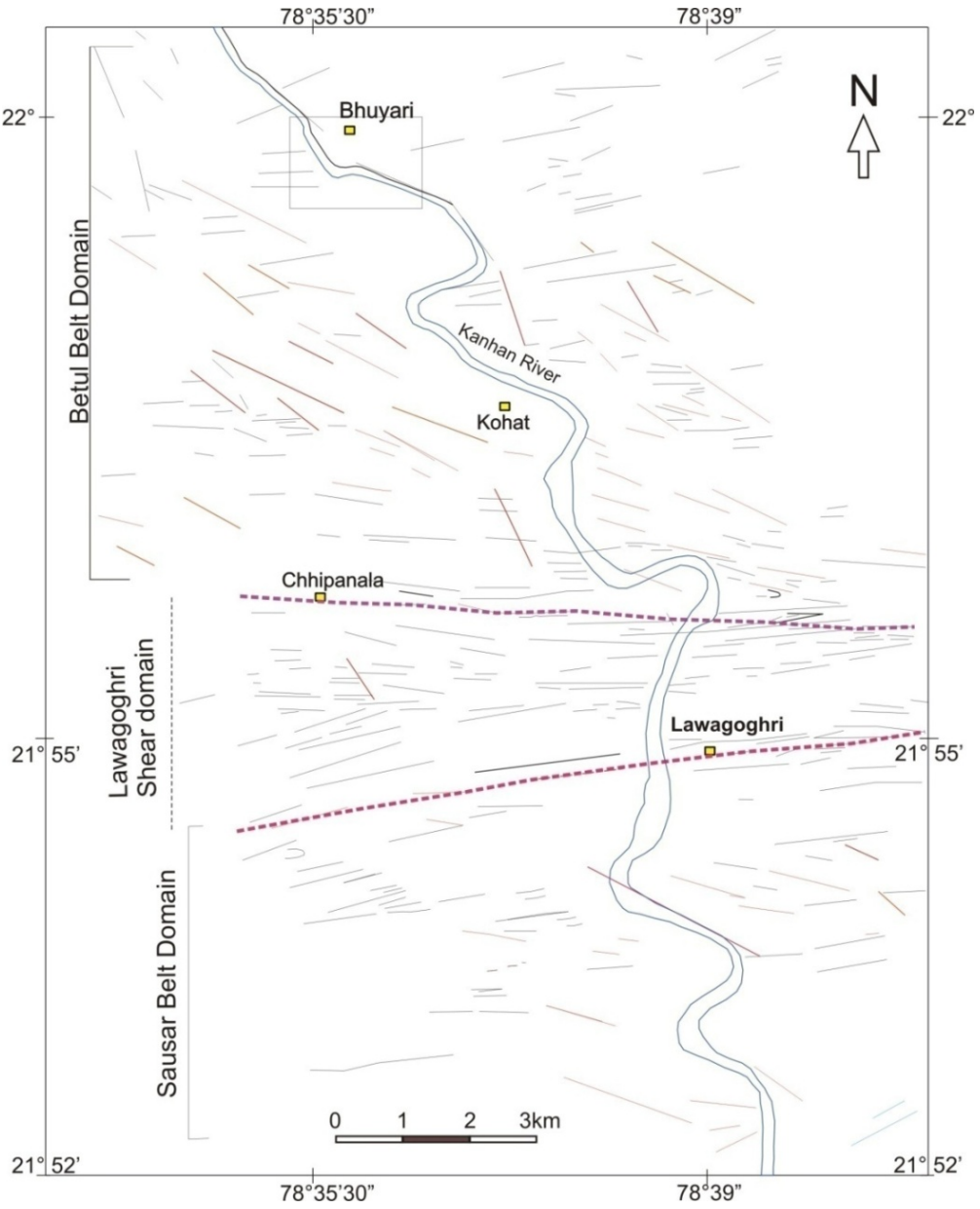

Fig.2.1b Lineament map of eastern part of Betul Belt around Bhuyari Prospect. The contact with Sausar Belt is manifested by a E-W striking shear zone (Lawagoghri Shear). The Lawagoghri shear zone is bounded between the Chhipanala village in the north and the Lawagoghri village in the south.

2.3 Lithology and Structure

The geological map prepared as part of this work is based on additional across-strike traverses in an area covering 150 sq. km from north of Mordongri to near Chippanala in the south (Fig. 2.2a). The modified geological map integrates the data from earlier maps (Golani and Dora, 2003; Dora and Praveen, 2007; Praveen et al, 2010) with new data. The area has a wide sequence of felsic volcanic rock (more than 15 km) dominated by rhyolite containing lensoid and conformable bands of altered rhyolites which represent zones of hydrothermal alteration and mineralization (Fig. 2.2a). Mafic counterpart of the bimodal volcanics occurs towards the north of the felsic volcanic sequence. The thick sequence of felsic rocks also contains small patches and bands of amphibolites (representing metabasalts) and metasedimentary rock. The rhyolite is also punctuated by mafic and ultramafic intrusives which are represented by hornblendite and hornblende gabbro (Fig. 2.3a). Porphyritic granites are present to the north of the area and are intrusive into the bimodal volcanic and ultramafic rocks.

Mafic volcanics occur as a 500m to 2 Km wide band which occurs in contact with the felsic volcanic towards the north (Fig. 2.2a). The EW contact of the mafic volcanic and felsic volcanic indicate that the stratigraphic contacts of the rocks are along the EW direction. This inference is also validated by the presence EW striking primary bedding in the metasedimentary enclaves (Fig. 2.3f). The disposition of the pillows in the mafic volcanic suggests that the stratigraphic top of the volcanic sequence in the area is towards the north (Fig. 2.3b). It is therefore inferred that the bimodal volcanic sequence in this part of Betul Belt has younging direction towards north. This field based

interpretation can only be validated by detailed geochronological studies across the E-W trending stratigraphy of the bimodal-volcanic sequence which is beyond the scope of this work. The bimodal volcanic in the area mapped is felsic-dominant with felsic to mafic ratio of approximately 6:1. Minor, conformable bands of amphibolite occurring within the felsic volcanics may also represent the mafic component of the bimodal volcanics.

Strictly speaking, the felsic rocks of the area are metamorphosed rhyolites including those which have been variably affected by hydrothermal alteration and drastic modification in chemistry. It is preferred to use the term 'rhyolite' instead of 'meta-rhyolite' for these rocks because most of the processes aimed at understanding in this work are syn-volcanic in nature. The term 'altered rhyolite' is used to denote 'metamorphosed felsic volcanic rocks which had undergone hydrothermal alteration prior to their metamorphism. The terms 'unaltered rhyolites' or 'least altered rhyolites' are used for meta-rhyolites which have undergone insignificant to mild degrees of hydrothermal alteration.

The felsic volcanic rocks mapped in the area comprise rhyolites and felsic volcaniclastic rocks and form a wide sequence from Chippanala in the south to north of Jilharidev temple. The unaltered felsic volcanics in the area comprise mainly of grey rhyolite and hornblende-bearing rhyolite (Fig. 2.3c). The rhyolite is massive, and exhibits a porphyritic texture with 2mm phenocyrsts of quartz and occasionally plagioclase. Primary textures like flow-banding are preserved at places. At places, the rhyolite outcrops become reddish in colour due to the oxidation of disseminated pyrite (Fig.2.3a). The rhyolites at places in many areas contain disseminated, metamorphic

hornblende (Fig. 2.3c) and such rhyolites are delineated as hornblende-bearing rhyolites (Fig. 2.2a). The hornblende-bearing rhyolite may represent a variant of grey rhyolite which has undergone mild effects of alteration. This is evidenced based on their slightly higher contents of pyrite, magnetite, epidote and chlorite when compared to grey rhyolites. However, the hornblende rhyolites can be considered as least altered rhyolite because the primary volcanic textures are generally preserved and they do not show any marked difference in their major element composition when compared to unaltered rhyolites. Such hornblende bearing grey rhyolites are present around the peripheral areas of Bhuyari Prospect towards the north and in the Kanhan River area south of Bhuyari (Fig. 2.2a).

Metasedimentary rocks comprising dark meta-argillite/ mudstone with intercalations of light coloured meta-siltstone occurs as conformable lensoid bands within the rhyolite and they contain well-preserved sedimentary textures like planar laminations, convoluted laminae/bedding, flame textures and syn-sedimentary deformation textures (Fig. 2.3d). The volcanosedimentary sequence is intruded by mafic-ultramafic intrusive comprising of hornblende gabbro and hornblendite (Fig. 2.3a). The major intrusive body of mafic-ultramafic rock comprises the 6 x 2 km ENE-WSE trending body occurring to the south of Mordongri village. This rock preserves cumulus textures and primary igneous layering at places (Praveen et al, 2010). Primary hornblende and plagioclase are the major minerals in this rock, which also contain variable epidote, chlorite, iron-oxides and pyrite.

Towards the north, the volcanic sequence is intruded by younger porphyritic granite related to the Neoproterozoic Navegaon granites (Fig. 2.3 e

& f). The granites north of Mordongri village are coarse grained, light pink in colour and porphyritic with large (1-4 cm) sized phenocrysts of alkali feldspar. The ground mass consists of quartz-feldspar and biotite. The coarse-grained porphyritic granite at places shows the presence of enclaves of older rocks like the mafic volcanics and mafic and ultramafic rocks (Fig. 2.3f). These granites are interpreted to be the last phase of igneous activity in the area and may have been intruded after the main deformation event in the area.

Structurally, the area is highly deformed. Secondary structures in the area are present in the form of a pervasive regional foliation which generally strike in the ENE-WSW to EW direction in the mapped area. This regional foliation is better manifested in the altered phyllosilicate-rich rocks when compared to the unaltered rocks with low content of phyllosiclicates. The ENW-WSW regional trend is sub-parallel to the E-W trending mylonite zone represented by the Lawagoghri Shear Zone. The regional foliation has moderate to shallow southerly dips near Bhuyari Prospect which becomes progressively steeper towards the shear zone around Chippanala and has steep northerly dips near Lawagoghri (Fig. 2.2a). This reversal of foliation may suggest the existence of a folded sequence. However, this cannot be confirmed due to absence of marker horizons like BIF or chert horizons in the area. Alternatively, the northerly dips near the shear zone may be due to rotation of regional foliation along the steeply dipping shear-fabric. A second type of foliation related to shearing (mylonitic foliation) is developed in certain zones which overprint the earlier regional foliation. The mylonitic foliation is manifested as close-spaced planar cleavages with steep to moderately steep northerly dips and is developed in the gneisses north of Lawagoghri (Fig. 2.2a).

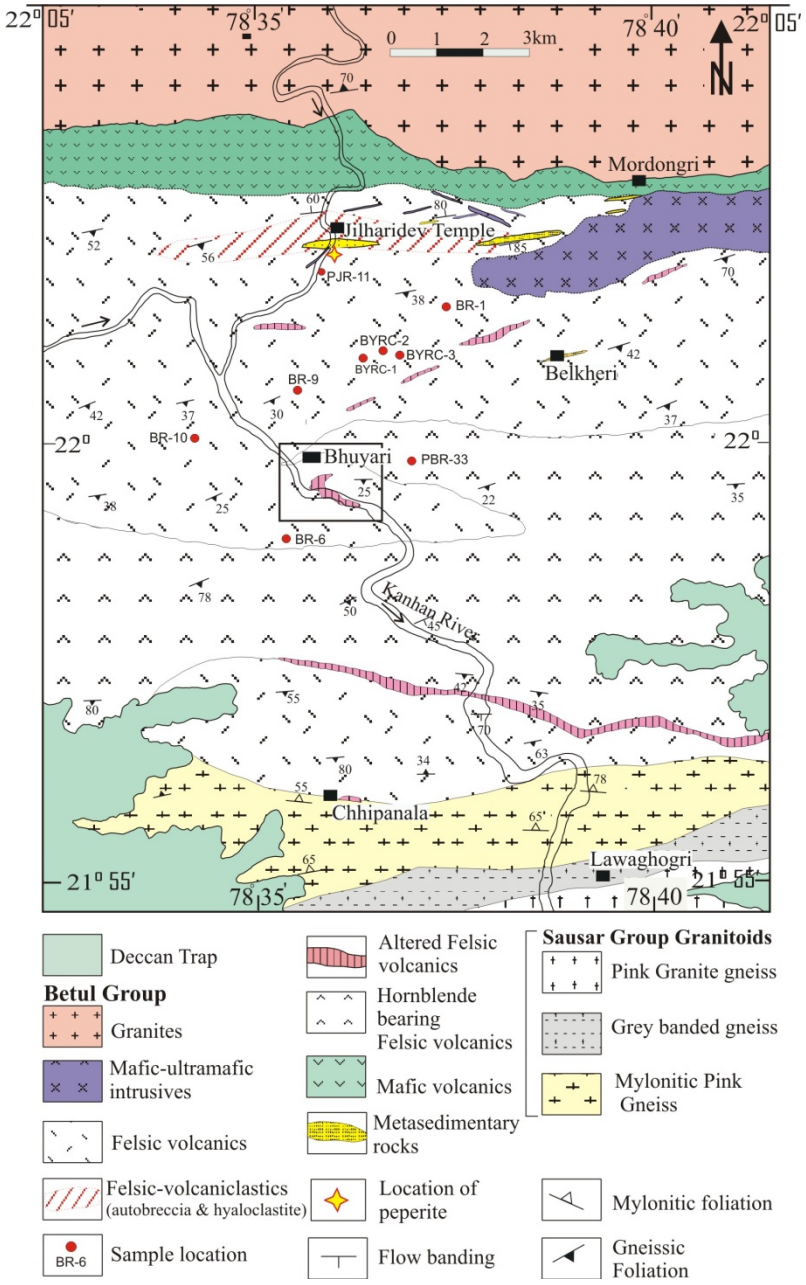

Fig.2.2.a Geological map of the eastern Betul Belt, modified after Golani and Dora (2003), Dora and Praveen (2007) and Praveen et al (2010). The box denotes the Bhuyari prospect area which has been covered by detailed mapping shown and in Fig. 2.2b which also shows the locations of most of the samples studied. The sample locations falling outside the detailed map area are shown in this map.

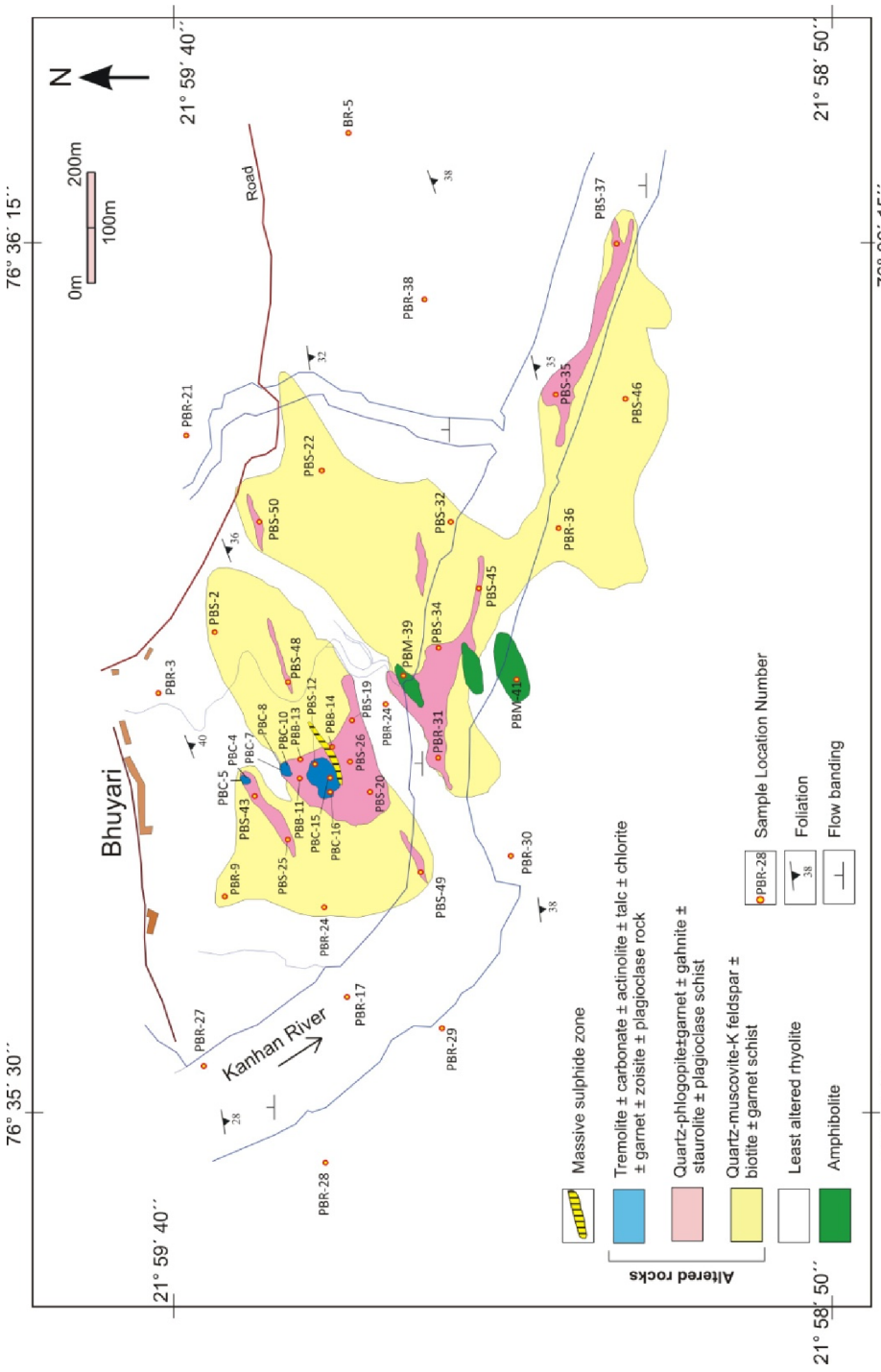

Fig. 2.2.b Detailed geological and alteration facies map of Bhuyari (1: 2000 scale) (modified after Praveen et al, 2010) showing the different metamorphosed alteration zones, the associated massive sulphide zone and sample locations. Note the discordant and zoned nature of the alteration within least altered rhyolite.

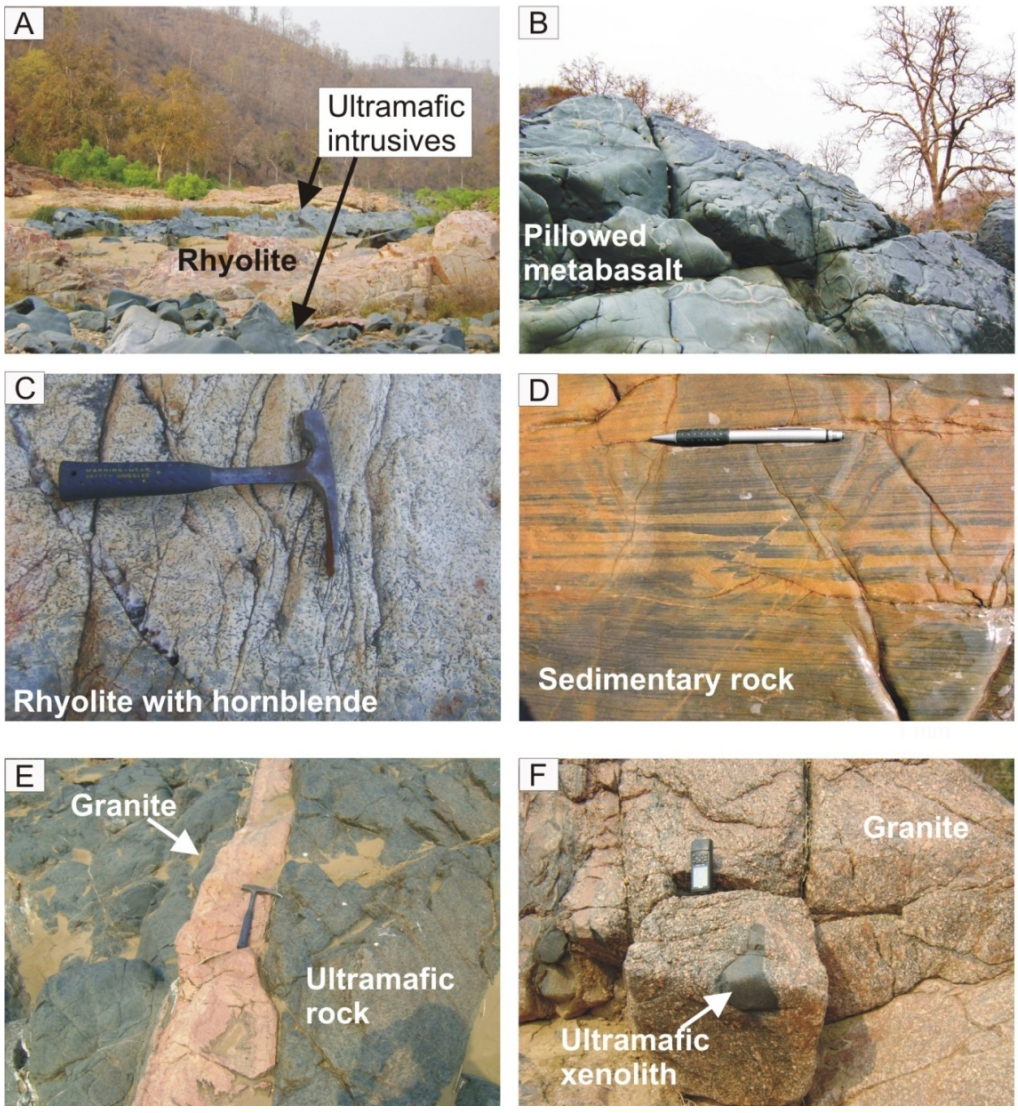

Fig.2.3 Field photographs of various lithounits in the eastern part of Betul Belt around Bhuyari Prospect a) rhyolite (red coloured) intruded by sub-parallel bands of ultramafic rocks north of Bhuyari area, b) pillowed mafic volcanic (metabasalts), c) hornblende bearing rhyolite, d) thinly laminated sedimentary rock (argillite-siltstone intercalations, e) ultramafic rock intruded by granite, f) pink poprhyritic granite with xenoliths of ultramafics.

2.4 Volcanic and Sedimentary Facies

Volcanic and sedimentary facies provide important clues in understanding the tectonic setting during volcanism and sedimentation. The eastern part of Betul Belt around Bhuyari is dominated by volcanic rocks (predominantly felsic) with rare intervals of fine-grained clastic rocks (Fig.2.2a). This implies that volcanism was the dominant process with only minor hiatuses in which sedimentation could take place.

The term 'facies" refers to a distinct deposit that demonstrates consistent observable attributes, like composition and volcanic structure (Fisher, 1961). For example, a felsic flow can be represented by two facies: 1) a massive facies and 2) a flow-banded facies. The term "volcaniclastic" refers to clastic deposits that contain predominantly volcanic components.

Nowadays, most studies depend solely on geochemistry for deciphering tectonic setting of volcanic rocks with very little corroborating field evidences. But field data, especially volcanic textures and facies can provide direct evidences for tectonic setting. Such an analysis (Praveen and Ghosh, 2009) has already proved efficient in identifying several types of felsic volcanic facies (the paper is provided as Appendix at the end of the thesis). Certain additional volcanic and sedimentary facies have been identified as part of this study and the same are described below.

The felsic volcanic facies documented in the previous study from Betul Belt (Praveen and Ghosh, 2009) are 1) massive, 2) flow-banded, 3) autobreccia and 4) hyaloclastite. Autobreccia and hyaloclastite constitute the volcaniclatic rocks (fragmented volcanic rocks) in the area. These felsic volcaniclatics are formed by autoclastic processes (non-explosive) like chill fragmentation (hyaloclastites) and flow-fragmentation (autobreccia). Based on

the presence of flow-banded and autobreccia facies, it was inferred that the felsic volcanics in the area were part of non-explosive, effusive eruptions in submarine volcanic centres. Based on associated volcanic textures, this study interprets a depth of more than 500m for the emplacement of the volcanics.

During the present work, an important volcanic facies - peperite and thin bands of fine-grained sedimentary rocks have been identified. These volcanic and sedimentary facies have been identified solely based on field characteristics and on the basis of preserved primary textures. The identification of peperite provide evidence for magma-sediment interactions and the identification of thin bands of sedimentary rocks comprising meta-argillite and siltstone gives evidence for a deep water setting. In this work, a combination of mapping and study of volcanic and sedimentary facies is used to understand the environment of deposition of felsic volcanic sequence and understand the implications for the formation of VMS deposits in the area.

Peperite

The peperite outcrops are present near the contact of rhyolite with sedimentary rocks approximately 200m south of the Jilharidev temple (near sample PJR-11) (Fig. 2.2a). This study is the first report of peperite from the Betul Belt. Peperite is a rock resulting from the mixing of magma and wet unconsolidated sediment (Schmincke 1967; Busby-Spera and White 1987; McPhie et al. 1993). As defined by White et al (2000), *peperite is a genetic term applied to a rock formed essentially in situ by disintegration of magma intruding and mingling with unconsolidated or poorly consolidated, typically wet sediment.*

The importance of peperite lies in the fact that their presence demonstrates approximate contemporaneity of magmatism and sedimentation and is therefore important in palaeoenvironmental reconstructions and relative chronology (Busbery-Spera and White, 1987; Brooks, 1995 and White et al.2000).

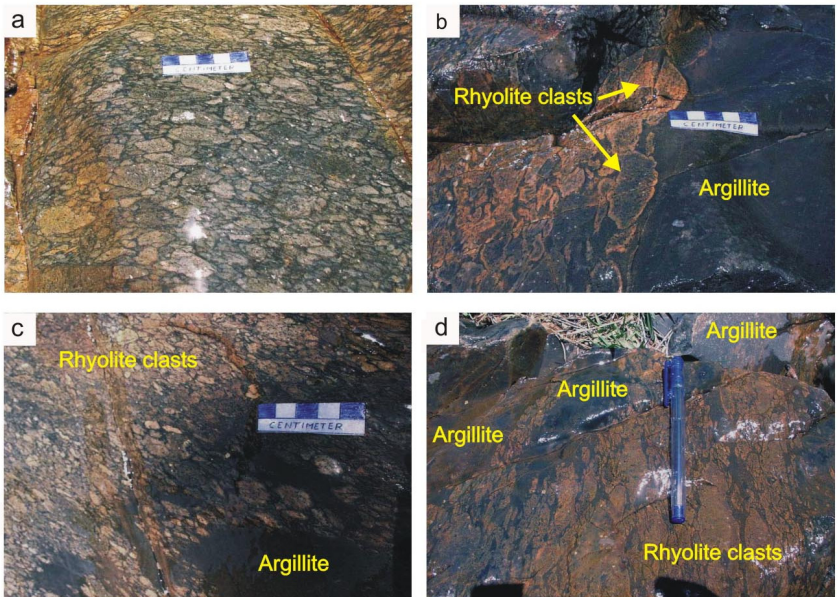

Fig. 2.4 Field photographs of peperite, a) angular to rounded clasts of rhyolite with a matrix of dark argillite, b) rhyolite-argillite interface with rounded clasts of rhyolite c) smaller rhyolite clasts within argillite, d) larger clasts of rhyolite in dark argillite.

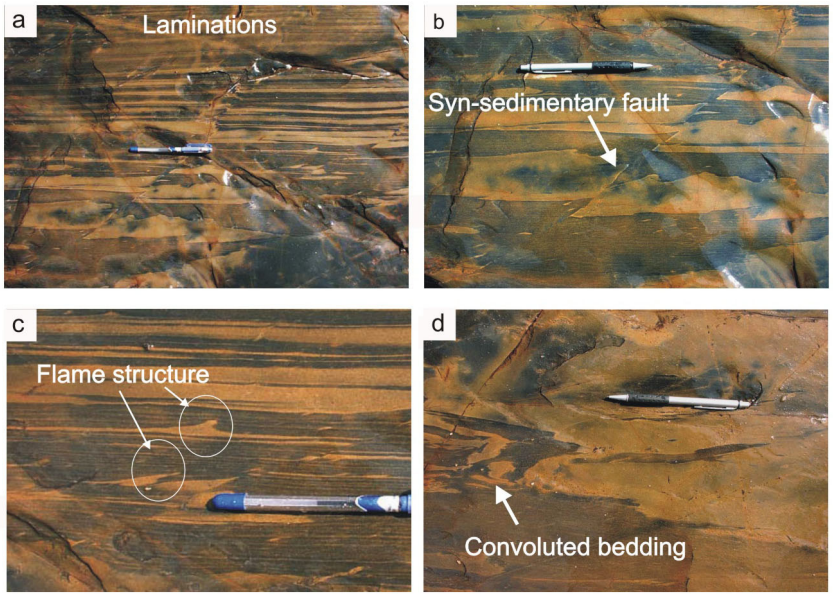

Fig. 2.5 Field photographs of sedimentary textures, **(a)** thin planar-laminated mudstone/argillite (black) and siltstone (pale) **(b)** syn-sedimentary faulting, **c)** flame structures, **d)** soft-sediment deformation textures shown by convoluted laminations.

The peperite reported in the present study consists of rhyolitic clasts (up to 5cm) with angular to rounded margins occurring in a matrix of dark, fine-grained meta argillite/mudstone (Fig.2.4a). The peperite is present at the contact of a massive rhyolite with fine-grained, black, meta-argillite which occurs as thin, impersistent enclaves within the rhyolites (Fig.2.4b). The margins of the massive-coherent rhyolite grades into insitu-hyaloclastite with jig-saw fit textures which again grades into peperite near the contact of the meta-argillite. Near the contact with the argillite, the rhyolite clasts are more rounded and contain higher proportion of dark mudstone matrix (Fig.2.4c and d). The relatively rounded nature of the clasts near the contact with the meta-argillite shows that they are similar to globular peperite which develop when magma interacts with fine-grained sediments like silt or mud (Busby Spera and White, 1987).

The identification of peperite is based on the following observations

1. The peperite occurs at the contact of rhyolite with fine grained sedimentary rock
2. There is a progression from massive quartz-porphyritic rhyolite to brecciated rhyolite with jig-saw fit textures to globular breccias with matrix occupied by dark metasediment and then into dark coloured metasediments.
3. The clasts are rhyolitic in composition whereas, the dark matrix is composed of fine-grained material and is contiguous with laminated meta-argillite, which contain well-preserved primary sedimentary textures (fig. 2.5).
4. The rock represents a composite rhyolite-sediment entity, with varying proportions of rhyolite clasts and sedimentary rock.

Associated deep-water sedimentary facies

Sedimentary rocks were identified for the first time in the study area. These are found as enclaves within the felsic volcanic sequence 2 Km to the south of Mordongri village (Fig.2.5). The sedimentary rocks are represented by thin bands and lenses of fine-grained clastic sedimentary rocks within the predominantly volcanic sequence. These are composed of thinly bedded siltstone intercalations within dark argillaceous rock are found approximately 3 km to the SE of Mordongri village (Fig.2.2a). These lithounits occur as impersistant bands with a maximum width of 20m. They rocks show thin, planar intercalations of black, meta-argillite and light-colored meta-siltstone (Fig. 2.5a). The dark meta-argillite could represent ambient deep water sedimentation in anoxic conditions, and the light-siltstone may represent periodical influxes of fine-grained volcaniclastic material derived from submarine felsic volcanoes.

Soft-sediment deformation structures (SSDS) are present in the form of well-preserved, cm-scale, syn-sedimentary faults (Fig.2.5b) which indicates contemporaneous volcanic or tectonic activity in the basin. These mudstone-siltstone beds could have deposited as turbidity currents in the sea-floor. Such turbidity currents can occur in the deep parts of the basin due to periodic volcanic eruptions. Flame structures developed during compaction by overlying strata are present at places, and are developed in the light-colored siltstone layers (Fig.2.5 c) These rocks at places show disturbed bedding lamina in the form of convoluted bedding (Fig.2.5 d), which is again indicative of sudden catastrophic event possibly tremors related to volcanism in the basin. These convolute bedding is localized in nature and are clearly not developed due to tectonic deformation (Fig.2.5 d), which is consistent the observation in the felsic volcanics that primary textures are occasionally preserved despite regional deformation in the area.

By definition-SSDS in clastic sediments are deformations that occur in still unlithified sediments or in sedimentary rocks that had not yet undergone lithification before the deformation structures started to be formed (van Loon, 2009). Well studied examples of Precambrian soft sediment deformation structures are those described from the Paleoproterozoic Chaibasa Formation from eastern India (Majumdar et al, 2006), which is ascribed to seismic activity in a tectonically active basin. SSDS are particularly common in tectonically active areas such as forearc basins (Campbell et al., 2006) and back-arc basins (Bryan et al., 2001). Although relatively few SSDS are present in deep marine environment, these are mostly related to seismics (Long, 2004).

The thin sedimentary units within the volcanics around Bhuyari preserve primary structures and SSDS, shown by thin laminations, flame structures, syn-sedimentary faults and convolute laminations indicative of deep sea turbidite deposits. The thin planar laminations of siltstone within dark argillite/mudstone indicates ambient deep water sedimentation punctuated by periodic influxes of more coarse-grained volcaniclastic debris, which may be related to active volcanism in distal parts of the basin. Such a sedimentary sequence give evidence for moderate to deep water setting for the emplacement of the felsic volcanics in the eastern part of Betul Belt. Associated peperite gives unequivocal evidence for rhyolite emplacement and concomitant deposition of sediments. Such a relatively deep-water environment is therefore envisaged to be prevalent in a back-arc basin.

2.5 Alteration Facies Mapping

Alteration mapping based on visual estimates of rock types, mineral modal assemblages, and mineral assemblages are effective in qualitatively measuring the variations in major elements associated with pre-metamorphic

hydrothermal alteration and establishing the chemical zoning with a reasonable degree of confidence (e.g. Bonnet and Corriveau, 2007).

The metamorphosed alteration facies have been demarcated by detailed mapping on 1: 2000 scale, carried out by GSI (Praveen et al, 2010). During the present work, the previous map was further refined by additional detailed mapping and the boundaries of the alteration zones and their contacts were further modified and refined. Each alteration facies consists of a characteristic set of mineral assemblages that can be recognized and mapped in the field. The modified alteration facies map prepared as part of this shows that metamorphosed alteration zones forms a NW-SE trending entity (Fig. 2.2b). This alteration zone shows a slight discordant nature with the ENE-WSW regional foliation which might reflect the original discordant and pipe like nature of the alteration zone with respect to the rhyolite sequence. Such discordant alteration zones are a common feature of most VMS deposits (Franklin et al, 1981), and in Bhuyari, despite the effects of deformation the primary discordant nature of the alteration zone is partly preserved. The alteration zone contains the massive sulphide lenses at its NW periphery (Fig. 2.2b).

Depending upon the intensity of the alteration and mineral assemblage, various alteration zones or alteration facies have been mapped in the block. Rocks with a characteristic set of mineral assemblage which can be easily identified in the field were grouped into one particular alteration facies. The rhyolite that preserved the primary volcanic textures like flow-banding and phenocryst-groundmass relationships and exhibits minimum mineralogical changes were mapped as unaltered rhyolites. These unaltered rhyolites are represented in the area by grey rhyolite and hornblende bearing rhyolites. It

must be noted that due to the highly gradational nature between one alteration facies to the other, the boundaries depicted in the alteration facies map are approximated. Intensely altered rhyolites grade into moderately altered and further into less altered rhyolites.

Three distinct metamorphosed alteration zones have been identified and mapped within the least altered rhyolite in the area (Fig. 2.2b). The mapping results show that the alteration system is zoned with intensely altered quartz-biotite-phlogopite ± garnet ± plagioclase ± staurolite ± gahnite schist forming the core zone which is enveloped by the moderately to intensely altered quartz-muscovite ± K-feldspar ± garnet schist. This zoning corresponds to the inner core zone with Mg-Fe-K alteration enveloped by an outer zone showing K-Fe alteration. Such a zoned alteration system is consistent with a primary hydrothermal chlorite-sericite core zone enveloped by a sericite-rich outer zone. The tremolite-carbonate rocks are present as pockets near the mineralized zone and could represent carbonate-altered rhyolites or meta-exhalites.

The unaltered or least altered rhyolite in the area comprise of the following types

1. Grey rhyolite and Hornblende rhyolite

The altered rhyolite comprise of the following types

1. Quartz-muscovite-K feldspar ± garnet schist and red silicified rhyolite
2. Quartz-phlogopite ± garnet ± staurolite ± gahnite schist ± plagioclase schist
3. Tremolite ± carbonate ± talc ± chlorite ± garnet rocks

2.5.1 Least Altered Rhyolites or unaltered Rhyolites

The least altered or unaltered rhyolites in the area comprise of massive grey rhyolite which preserves relatively well preserved primary volcanic textures at places. The hornblende-bearing rhyolites are a variant of the grey rhyolites that contain variable amounts of disseminated hornblende.

Grey rhyolite

Grey rhyolite is relatively unaltered rhyolite and is a widespread rock type in the area that envelops the more altered rocks. This rock type is a grey coloured massive rhyolite which at places preserves primary volcanic textures like quartz-phenocrysts and flow banding and is exposed in the Kanhan River Section south of Bhuyari (Fig. 2.6a & b). A characteristic feature of grey rhyolite is the presence of discrete, euhedral, 1-2 mm, and grey to dark grey quartz porphyroblasts which can be identified during field mapping in relatively unaltered rhyolites (Fig.2.6d). The phenocryst percentage generally ranges from 5 to 8 % of the rock. The groundmass is generally composed of recrystallized quartz, plagioclase, orthoclase, biotite, sericite, garnet and magnetite. Pyrite and pyrrhotite are sometimes present. Rarely, the feldspar phenocrysts in the form of white laths of plagioclase can also be identified in the unaltered rhyolite (Fig. 2.6e). Small, discrete magnetite grains (<1mm) frequently have a biotite-free halo, which indicates that they possibly formed from biotite during metamorphism. Though the grey rhyolite has undergone slight alteration, it preserves the primary volcanic textures like phenocryst-ground mass relationship and flow banding. Flow banding is represented by 1mm to 1cm thin, faint alternate dark and light coloured laminations represented by biotite rich and siliceous layers (Fig. 2.6c). These flow bandings are sometimes contorted indicating that they formed during viscous flow of the lava.

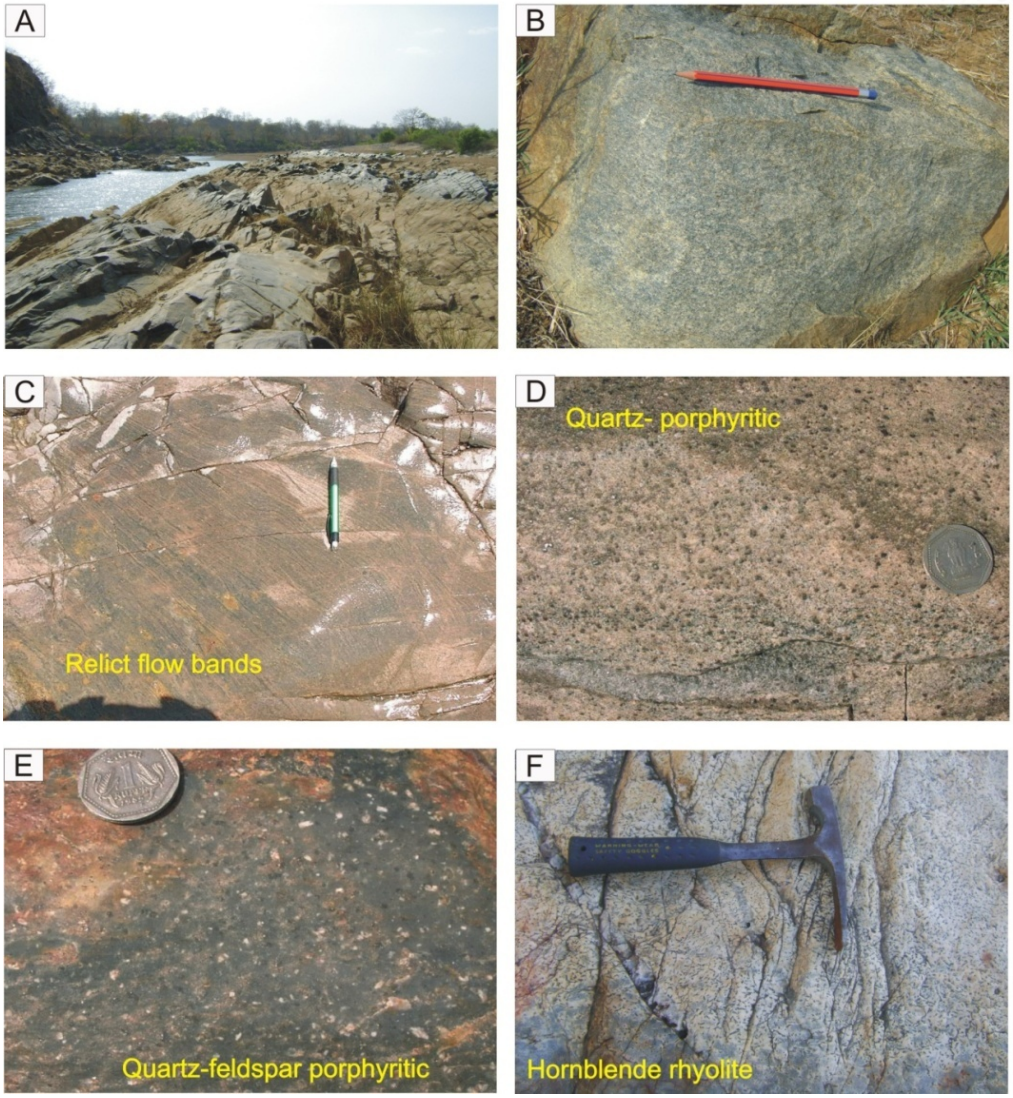

Fig.2.6 Field photographs of least altered rhyolite showing a and b) grey massive rhyolite, c) relict flow banding in grey massive rhyolite, d) quartz-phenocrysts in (dark rounded spots), d) feldspar (white laths) and quartz (dark rounded spots) phenocrysts, f) disseminated hornblende in rhyolite.

A 50 to 100m wide, NE-SW trending unaltered grey rhyolite band occurs within the alteration zone in the Kanhan River Section (Fig. 2.2b). Such a tongue-like band also separates the northern-most tremolite-carbonate rock from the middle tremolite-carbonate outcrop. Although the contacts are not well exposed, it is inferred that they may represent post-mineralization sills and feeder channels for the overlying grey rhyolite towards the north.

Hornblende rhyolite

In the mapped area, this facies occurs as patches and lensoid bodies with the grey rhyolites, outcrops of which can be seen in the Kanhan river valley and further south of it. The rock is characterized by the presence of green 0.5 to 3cm long laths of hornblende porphyroblasts in a recrystallized quartzofeldspathic matrix (Fig.2.6f). The hornblende crystals are mostly randomely oriented. Apart from hornblende porphyroblasts, the rhyolites show rounded 1-2 mm quartz phenocrysts in a recrystallised groundmass of quartz, feldspar, sericite, biotite and chlorite. Magnetite, garnet and epidote occur as accessory minerals. The hornblende is frequently poikiloblastic with quartz, garnet and magnetite inclusions and is commonly altered to chlorite. Petrographic evidence indicate that the hornblende is not a primary igneous phase and is probably formed late in metamorphism. The hornblende porphyroblasts generally have a biotite free halo around them indicating that they might have formed from biotite during prograde metamorphism. Presence of hornblende may indicate alteration caused due to seawater-rhyolite interaction.

The least altered rhyolites comprising quartz and feldspar porphyritic rhyolite and flow-banded rhyolites are suggestive of proximal volcanic facies which are close to submarine volcanic centers. Presence of hydrothermal alteration and mineralization within this facies is consistent with this interpretation.

2.5.2 Quartz-muscovite-sericite-K feldspar ± biotite/phlogopite ± garnet schist and red silicified rhyolite

This rock type is easily identified based on the reddish colour of the outcrops due to the oxidation of disseminated pyrite present in this rock. This assemblage is characterized by the assemblage muscovite and K-feldspar and represents potassic alteration. This potassic altered assemblage forms a broad envelop over the more intensely altered phlogopite-bearing schists. Based on the muscovite content of this assemblage, it can grade from pink coloured massive rhyolite with high silica content and low muscovite content (silicified rhyolite) and quartz-muscovite-sericite schist in which the muscovite contents are higher and quartz-contents are lower.

Silicified rhyolite outcrops have a characteristic pink-red colour on the surface, which is due to the oxidation of abundant disseminated pyrite (Fig: 2.7a and b). Silicified, rhyolite act as guides for base-metal mineralization in Betul Belt, since this rock easily stands out as resistant bodies and can easily be identified during field mapping.

Primary textures are generally obliterated due to effects of alteration and relict flow-banding is rarely preserved (Fig. 2.7b). Freshly broken surfaces show presence of disseminated pyrite and at times other base-metals (Fig. 2.7e). Freshly broken surfaces have a characteristic white colour which is due to the high silica content as well as due to the absence of biotite (Fig.2.7e). Silicification is pervasive and is evidenced in the form of minute mm-sized network of quartz veins and also by overall silicification of the rock and at times contains more than 80 wt. % SiO_2. The rock shows 2-3mm rounded to sub-rounded quartz phenocrysts in a recrystallised matrix of quartz, feldspar and sericite. This rock is characterized by the enrichment of pyrite, which occurs as disseminations of <1mm, euhedral grains and also as networks of cross cutting stringer veins which at times contain sphalerite and galena. This rock contains

varying proportions of muscovite and sericite and due to increase in mica content, it grades at many places into quartz –muscovite-sericite schist.

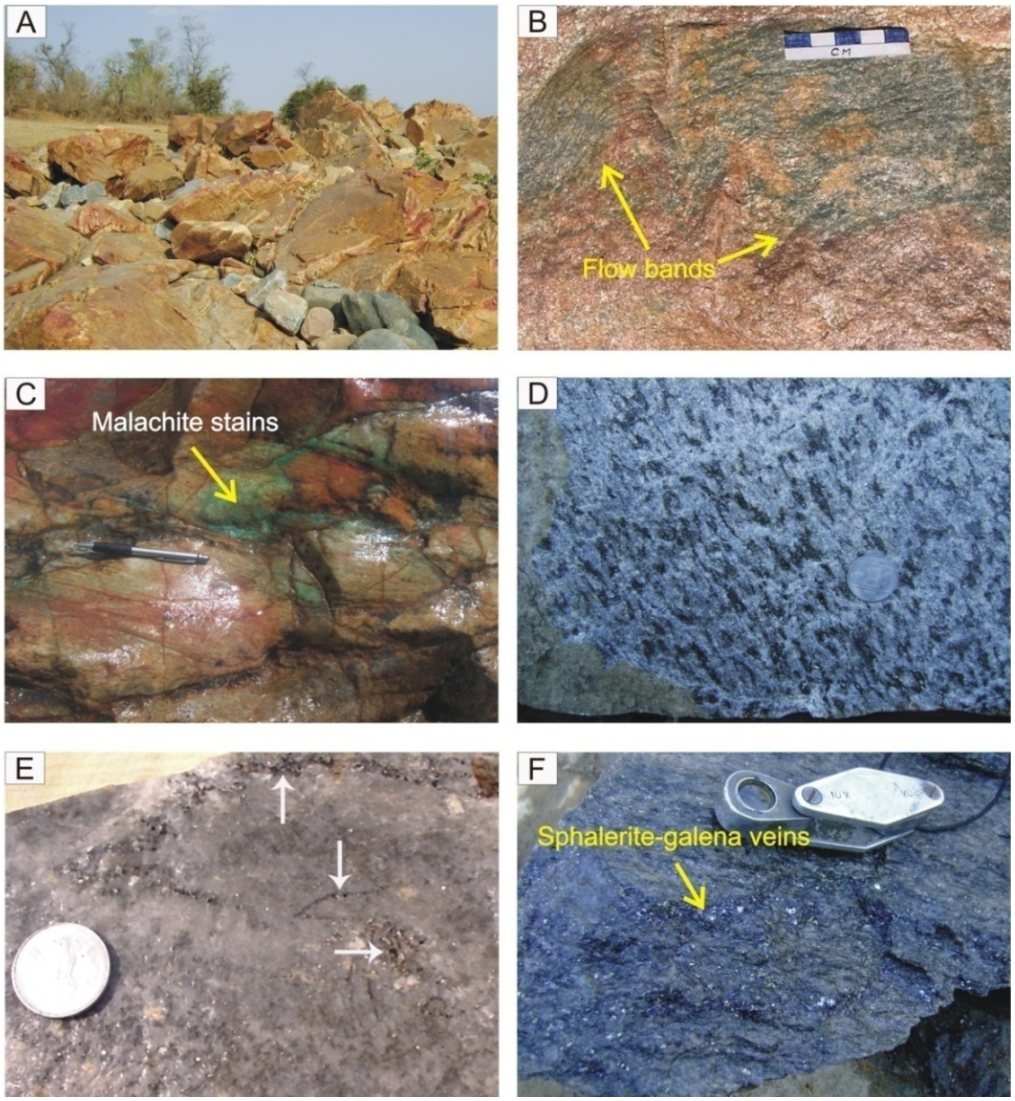

Fig.2.7. Field photographs of quartz-muscovite - K-feldspar altered rhyolite showing **a)** red silicified rhyolite outcrops due to presence of pyrite **b)** relict flow bands in red silicified rhyolite **c)** malachite staining on weathered outcrops **d)** quartz-muscovite-biotite schist showing spotted nature of biotite, **e)** silicified zones with veins of sphalerite and pyrite, **f)** sphalerite-pyrite veins along foliation in quartz-muscovite-sericite - K-feldspar- biotite- garnet schist.

Quartz–muscovite-K feldspar ± biotite ± garnet schist is characterized by the enrichment of phyllosilicates like muscovite and sericite and is thereby variably schistose in nature. This alteration type is intimately associated with silicified rhyolite and has gradational contact with it. With increasing proportion of muscovite/sericite content the rock changes from massive silicified rhyolite to quartz - muscovite-sericite schist. This rock is also silicified to varying degrees and essentially comprises of quartz and muscovite/sericite. Garnet is present at places as minute 2-3m sized, light pink porphyroblasts. The rock generally has only very little biotite, but at places biotite is present and occurs as 5mm to 1cm spots giving the rock a spotted look (Fig. 2.7d). As the proportion of biotite increases, this rock type grades into biotite-muscovite bearing schist. This alteration assemblage hosts mineralization at places which is in the form of veins and bands of pyrite, sphalerite, galena and chalcopyrite (Fig.2.7f). Weathered outcrops show the presence of malachite stains indicating the presence of mineralization (Fig. 2.7c).

Based on the presence of higher proportion of potassic mineral assemblages in this rock like muscovite, sericite and K-feldspar, these rock types are inferred to represent potassic alteration zones. These zones be identified in the field and mapped as part of alteration facies mapping. The potassic nature of the alteration has been further confirmed by petrographic and geochemical studies (See Chapter-3 and Chapter-5).

2.5.3 Quartz-phlogopite ± muscovite ± garnet ± plagioclase ± staurolite ± gahnite schist

This rock type represents a highly altered form of massive rhyolite and is characterized by the enrichment of Mg-Al bearing minerals like Mg-rich biotite and phlogophite along with porphyroblasts of garnet, staurolite, gahnite

and plagioclase and generally occur in the field as dark-colored outcrops which form bands/zones within relatively light coloured quartz-muscovite-schist. Despite intense alteration, these rocks locally preserve relict flow-banding manifested as thin, alternate light and dark coloured layers (Fig. 2.8c & d). The random and contorted nature of the layering, similarity with flow-banding in unaltered rhyolites and lack of correlation with regional foliation show that these represent relict flow banding texture.

This phlogopite bearing alteration facies has close spatial relationship with mineralization and define the core zone of the alteration system. Outcrops of this rock type contain disseminations and veins of sphalerite, pyrite, galena and minor chalcopyrite at many places in the Kanhan river section. Within this facies there is wide variation in the proportion of the constituent minerals.

The rock is variably schistose in nature depending upon the phlogopite content and can range from relatively massive porphyroblastic rock with lower phyllosilicate content (Fig.2.8a) to highly schistose phlogopite rich rock. Most of the biotite in the rock type is high-Mg biotite or phlogopite as identified from EPMA studies (See Chapter 6). Monomineralic phlogopite schist and phlogopite - garnet schist occurs towards the north of the main tremolite - carbonate outcrop south of Bhuyari village. In the Kanhan river valley, the phlogopite-garnet-gahnite bearing assemblage occurs as parallel bands along the foliation. Phlogopite defines the schistosity in the phyllosillicate-rich variants.

Plagioclase at places occurs as white coloured, randomly oriented, 1-3 cm sized porphyroblasts in a groundmass of biotite, and at places (Fig.2.8d). Staurolite generally coexists with biotite and garnet in the quartz-biotite-garnet-staurolite schist. This rock type is restricted in 150 X 200m area

adjacent and south of the massive sulphide zone (Fig. 2.2b). Staurolite forms euhedral porphyroblasts ranging in size from 1 cm to 5 cm and garnets are light pink in colour, euhedral and range in size from 2mm to 5mm (Fig. 2.8b). Staurolite porphyroblasts frequently show inclusions of garnets. The staurolite crystals are randomly oriented which suggests that they have not undergone any deformation after their formation.

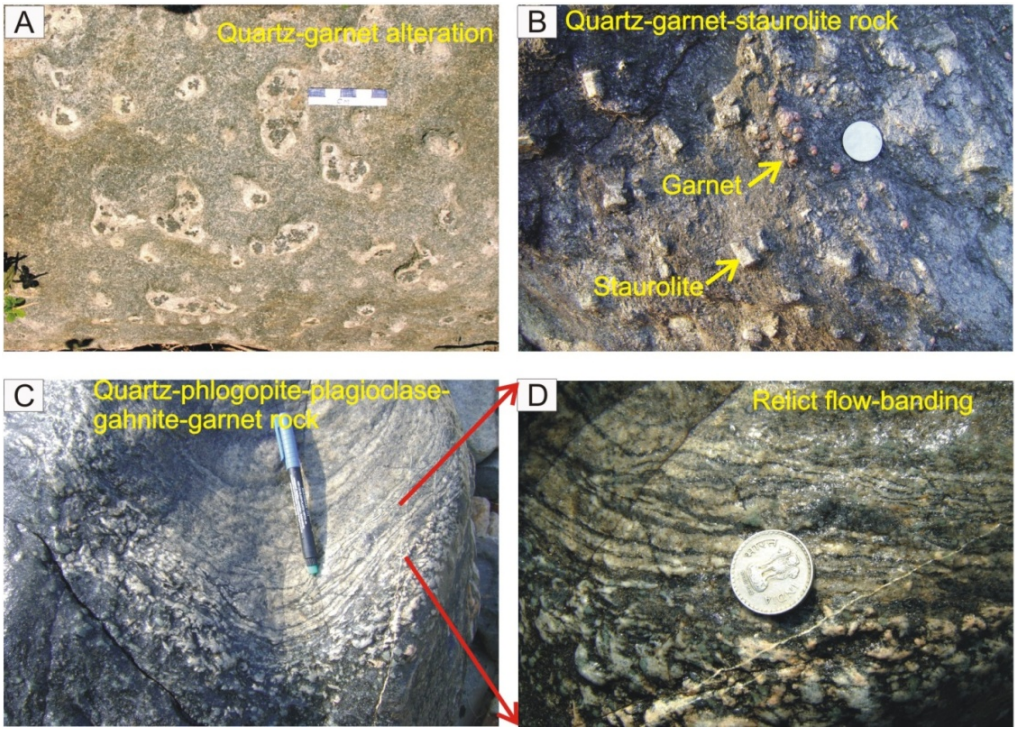

Fig.2.8 Field photographs of quartz-biotite-phlogopite ± plagioclase ± garnet ± gahnite a) spotted quartz-garnet alteration in massive rhyolite (b) dark biotite-garnet-staurolite rock (c) relict flow banding in phlogopite- bearing schist. Plagioclase is seen as white grain-sized minerals below the flow-bands (d) close-up view of relict flow bands and white plagioclase laths.

Gahnite occurs in an assemblage consisting of quartz - biotite - muscovite - plagioclase-gahnite schist (Fig. 2.8c and d). This rock type is also closely associated with mineralization. Outcrops of gahnite-bearing assemblage are found in a 100 X 25m area in the Kanhan river valley. This rock shows encrustations of malachite and smithsonite besides mm to cm thin veins and dissemination of base-metal sulphides. It is observed that gahnite is developed in sphalerite-rich zones or adjacent to sphalerite-rich zones. The sizes of gahnite crystals vary from < 1mm to nearly 1 cm and coexist with plagioclase which occurs as subhedral to euhedral, white porphyroblasts (Fig: 2.8d). Distal to the highly altered zone, the rock grades into a rock which contain centimeter-sized patches of spessartine-garnet and quartz.

2.5.4 Tremolite ± carbonate ± actinolite ± talc ± chlorite ± garnet rock

These rocks occur as three separate and discrete lensoid bodies on a hillock south of Bhuyari village and are disposed in a linear north-south fashion (Fig. 2.2b), and for descriptive purposes, they are named CS hill-1, CS hill-2 and CS hill-3 starting from the south to north. The southernmost outcrop (CS hill 1) is the largest and closest to mineralized zone whereas the northernmost outcrop (CS hill 2) is the smallest. The southernmost outcrop (CS hill-1) is the biggest and has a dimension of approximately 100m x 70m and forms a small rocky hillock. Because of the presence of carbonate minerals, the rock is extensively leached and has a craggy, pockmarked appearance. The tremolite-carbonate outcrops occur within the highly altered phlogopite-bearing assemblages and are in close spatially association with the massive sulphide lenses (Fig. 2.2b). Major element data of this rock type show high enrichment of MgO (up to 25wt. %) and CaO (up to 13.5wt. %) (Table 5.4).

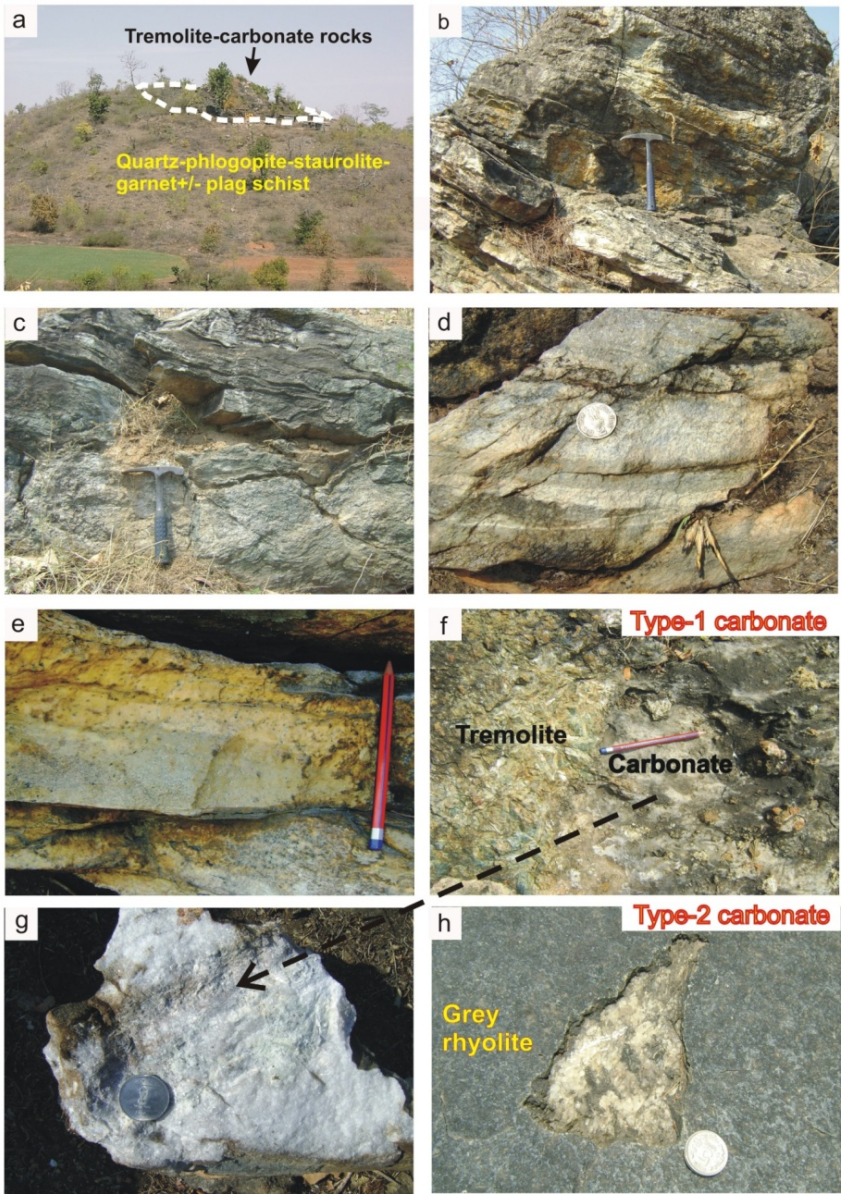

Fig. 2.9 a) Panoramic view of hillock south of Bhuyari village showing outcrops of tremolite-carbonate rocks on top of hillock, surrounded by phlogopite-staurolite-garnet bearing schist. b) primary layering (c) folded laminations,(d) colour banding due to compositional variation displayed by alternate greenish chlorite-tremolite and white/cream coloured carbonate-chert layers. f) carbonate segregations of carbonate associated with coarse-grained tremolite (Type-1 carbonate), (g) freshly broken piece of carbonate from tremolite-carbonate rocks, (h) Type-2 carbonate occur as patches in unaltered grey rhyolite

This rock shows wide variation in the constituent mineral assemblage with varying proportions of tremolite, carbonate, actinolite, sericite, talc, chlorite and garnet. The southernmost outcrops consists mainly of massive, monomineralic tremolite rock, in which tremolite laths are randomly oriented and range in length from 5mm to as large as 10 cm (Fig.2.9f). Occasionally these rocks also show the presence of light pink garnets 0.5 to 1 cm in size and locally attains high proportions in the layered outcrop (CS Hill-3). More commonly, they consist of tremolite porphyroblasts in groundmass of carbonate, sericite, chlorite and talc. At places this rock becomes dominantly composed of carbonate minerals in which tremolite occurs as isolated porphyroblasts. Carbonate is dolomitic in composition and the rocks at places contain segregations and patches of free dolomitic-carbonate (Fig. 2.9f). Towards the western margin of the southern outcrop the rock grade into greenish, monomineralic actinolite rock. Actinolite-carbonate rocks also occur as small pockets in the northernmost tremolite-carbonate outcrop. Presence of minerals like tremolite, dolomite and talc, indicate high Mg-enrichment caused due to hydrothermal alteration prior to metamorphism. In addition presence of actinolite at places indicates local Fe-enrichment.

The tremolite-carbonate rocks at many places show apparent primary bedding and depositional layering. The main outcrop (CS-Hill 1) shows 1 to 5 cm wide apparently bedded nature represented by fine to medium grained tremolite with minor carbonate at places (Fig.2.9b). The northern-most outcrop (CS-Hill 3) shows millimeter to centimeter scale laminations which are deformed and folded (Fig. 2.9c). These laminations comprise of alternate layers of fine-grained, cream-coloured cherty-carbonate and light-green coloured chlorite-tremolite layers (Fig.2.9d and e). At places, the layers display sagging and convolute laminae resembling soft-sediment deformation

structures (Fig. 2.9c). These apparent layering may point to a primary depositional feature, which may have been modified by later deformation.

The light-coloured areas at places contain high contents of sub-millimeter sized light-pink garnets which locally attains high proportions of the rock (> 20 %). EPMA analyses of these garnets have shown that they are spessartine-rich (See Chapter 6, Table 6.9). It is important to note that spessartine garnet-rich lithounits are characteristic of metaexhalites associated with VMS deposits (Spry et al, 2000). The presence of possible primary layering, close spatial association with mineralization and local enrichment of spessartine garnets suggest that these rocks could represent metaexhalites-metamorphosed exhalites from a hydrothermal vent on the sea-floor.

Chlorite-tremolite-carbonate alteration assemblages are not generally characteristic of VMS-related alteration systems Lydon (1984). However, carbonate-bearing assemblages are present in a number of VMS deposits like the Cambrian-Ordovician, Thalanga Zn-Pb-Cu-Ag deposit in North Queensland, Australia, some Cambrian deposits in the Mount Read Volcanics like Hellyer, Que River, Rosebery and South Herculus (Large, 1992; Herrmann and Hill, 2001), in the Proterozoic Skellefte and Bergslagen areas in Sweden (Allen et al. 1996, 1997), and the Miocence deposits of Hokuroko district, Japan (Shikazono, 1998). In most areas, the carbonates have a hydrothermal origin, except in the Bergslagen district, Sweden, which are interpreted to be skarns derived from metasomatised pre-existing limestones. In these deposits the carbonate bearing assemblages formed at or close to the palaeo seafloor, towards the upper regions of the hydrothermal vent, where carbonate precipitation is caused by heating of seawater and / or neutralization of acid-hydrothermal fluids mixing at moderate temperatures.

2.6 Summary and Conclusions

Lineament studies of the N-S Kanhan River corridor using aerial photographs show that the area can be classified into three distinct structural domains- Betul Belt domain, Lawagoghri Shear zone domain and Sausar belt domain. The structural and lineament studies show that the Betul domain is separated from the Sausar domain by a E-W trending zone with close-spaced lineaments (Lawagoghri shear zone).

Presence of pillowed basalt provides good evidence for submarine emplacement of the volcanic sequence. Based on disposition of pillows in the metalavas, the inferred stratigraphic top of the volcanic sequence is towards the north. The new mapping carried out around Bhuyari reveals that the eastern Betul Belt is dominated by felsic volcanic rocks with the mafic volcanic component restricted largely towards the north of the felsic volcanic sequence. Study of volcanic textures and facies is attempted to understand the environment of rhyolite emplacement. However, recognition of volcanic facies in Precambrian terrains is fraught with difficulties as the volcanic strata are invariably subjected to effects of multiple deformation and alterations. Correct recognition of primary volcanic textures gives direct evidence for the environment of deposition and thereby offers valuable evidences for tectonic setting.

The study of volcanic facies in the eastern part of Betul Belt gives overwhelming evidence for emplacement in sub-aqueous conditions. The predominance of felsic volcanic flows with well-developed planar flow lamination and lack of pyroclastics are similar to rift-related volcanism rather than arc-related volcanism (eg. Lentz, 1996).

Presence of deep water sedimentary facies like dark mudstone and argillite interlayered with volcaniclastic siltstone indicate moderate to deep

water emplacement for the rhyolite. Hydrothermal fluids venting near the proximal massive rhyolite likely gave rise to focused discharge resulting in a zone alteration pipe and massive to disseminated sulphide mineralization. Presence of peperite textures in the felsic volcanic provides unequivocal evidence for emplacement of rhyolite in a deep water conditions which contained wet, unconsolidated sediments. Secondly, deep water conditions favours deposition of massive sulphides. The Bhuyari prospect area is dominated by massive quartz-porphyritic and flow banded rhyolite representing proximal volcanic facies.

Alteration facies mapping has helped delineate the zoned alteration system at Bhuyari which is disposed partly parallel to the regional foliation and partly oblique or discordant to the regional foliation. The current disposition of the alteration zone may be the result of the originally discordant nature of the alteration zone which has been later rotated and transposed parallel to the strike of the E-W regional foliation during deformation which possibly accompanied convergent margin tectonics in the area.

The unaltered rhyolite near Bhuyari is represented by grey rhyolite which preserves primary volcanic textures like flow-banding and 1-2mm quartz-phenocrysts and can be recognized during field mapping. The hornblende bearing rhyolite forms an outer zone around the grey rhyolite and contains upto 1 cm sized hornblende phorphyroblasts. These rocks may have formed due to metamorphism of rhyolites which have undergone mild degrees of alkali metasomatism during seawater-rock interactions.

The core zone of the alteration system is characterized by phlogopite-garnet-staurolite-gahnite-plagioclase bearing assemblage which may correspond to pre-metamorphic hydrothermal Mg-chlorite + sericite alteration

zones representing Mg-Al rich alteration. The muscovite-K feldspar-garnet zone occurs as an envelope over the core zone and possibly represents pre-metamorphic sericite-K-feldspar rich zones representing potassic alteration. The tremolite-carbonate rocks occurring as pockets near the top of the alteration system has spatial proximity with mineralization. The presence of possible relict banding and apparently bedded nature at places suggest their derivation as exhalites on the sea-floor.

Alteration facies mapping around Bhuyari prospect has helped in identifying certain controls for mineralization viz. (1) proximal volcanic facies comprising massive and flow-banded rhyolites, (2) presence of lithounits containing magnesium and aluminosilicate-bearing minerals within felsic volcanics (3) presence of tremolite-carbonate lithounits within felsic volcanics (possible metaexhalites). The presence of one or more of the above criteria can be useful as exploration guides for VMS deposits in other parts of Betul Belt or similar terrains elsewhere containing submarine felsic volcanic rocks.

******

Chapter 3

PETROGRAPHY

Contents

3.1 Petrography of Least Altered Rhyolites
3.2 Petrography of Altered Rhyolites
3.3 Mafic Volcanic/ Metabasalt
3.4 Mafic Intrusives
3.5 Discussion

Detailed petrographic studies were carried out on the unaltered rhyolites, various types and sub-types of altered rhyolites and other rock types in the area. Petrography of unaltered rhyolite was carried out to characterize the primary volcanic textures which include quartz and feldspar phenocrysts and the nature of groundmass. The effects of metamorphic modifications of primary volcanic texture are also documented. Through detailed petrography of altered rhyolites, it is aimed to study and document the textural relationships between various metamorphic minerals and understand the mineral paragenesis during metamorphism. Identification of primary textures in highly altered rhyolites will help to substantiate the field-based assumptions for a rhyolite-protolith for most of the highly altered rocks in the area. The petrographic study of the various alteration types will help in linking these assemblages to possible precursor hydrothermal mineral assemblages. The characterization of mineral assemblages in each alteration zone is important so that it can be used in tandem with the major and trace element geochemistry of these alteration zones to trace the nature and type of premetamorphic hydrothermal alteration as discussed later in the thesis (Chapter 5).

Since precise spatial location of specific alteration assemblages are critical in such studies where mineral assemblages and mineralogy vary with respect to distance to the centre of the hydrothermal system and the ore zones,

the sample numbers of the rock samples studied are shown against each photomicrograph which can then be referred with the geological and alteration facies maps in Fig. 2.2a & 2.2b.

Apart from the detailed studies carried out on the unaltered and altered rhyolites, representative thin sections of mafic volcanics and the mafic-ultramafic intrusive rocks were also studied to corroborate the field identification of these rocks.

3.1 Petrography of Least Altered Rhyolite

Petrography of unaltered or least-altered rhyolite shows that it is composed mainly of quartz, plagioclase, K feldspar, biotite, sericite and minor to accessory amounts of garnet, hornblende, epidote, magnetite, pyrite, rutile and zircon. Generally the rhyolite exhibits porphyritic texture which is evident even in hand specimen. Thin section studies show rounded to oval shaped quartz-phenocrysts (Fig. 3.1a), however, well preserved plagioclase phenocrysts are rare (Fig. 3.1 c). The quartz and feldspar phenocrysts occur in a relatively fine-grained, recrystallized groundmass (Fig. 3.1a, b and c). Accessory zircon, garnet, magnetite, epidote and pyrite are also common. Among the accessory minerals zircon is a magmatic phase, while the rest show evidence for metamorphic growth. Zircons are euhedral, elongated and typically less than 50 micron in size (Fig. 3.1d). The opaque minerals rutile and magnetite occur as discrete, small (< 1mm) disseminations in the rock and are commonly present in the rhyolite. The modal composition of the typical unaltered grey rhyolite is approximately: quartz 50%, microcline 20%, plagioclase 10-12 %, biotite 15%, opaques (magnetite + rutile) <3 %.

Rhyolites which have undergone slight effects of alteration show the presence of garnet, magnetite, epidote and hornblende as discrete crystals. The garnets occur as discrete, light pink euhedral crystals and are associated with biotite (Fig. 3.1e & f). Generally garnets show inclusions of quartz and biotite. Metamorphic biotite is green in colour and flaky (Fig. 3.1e & f).

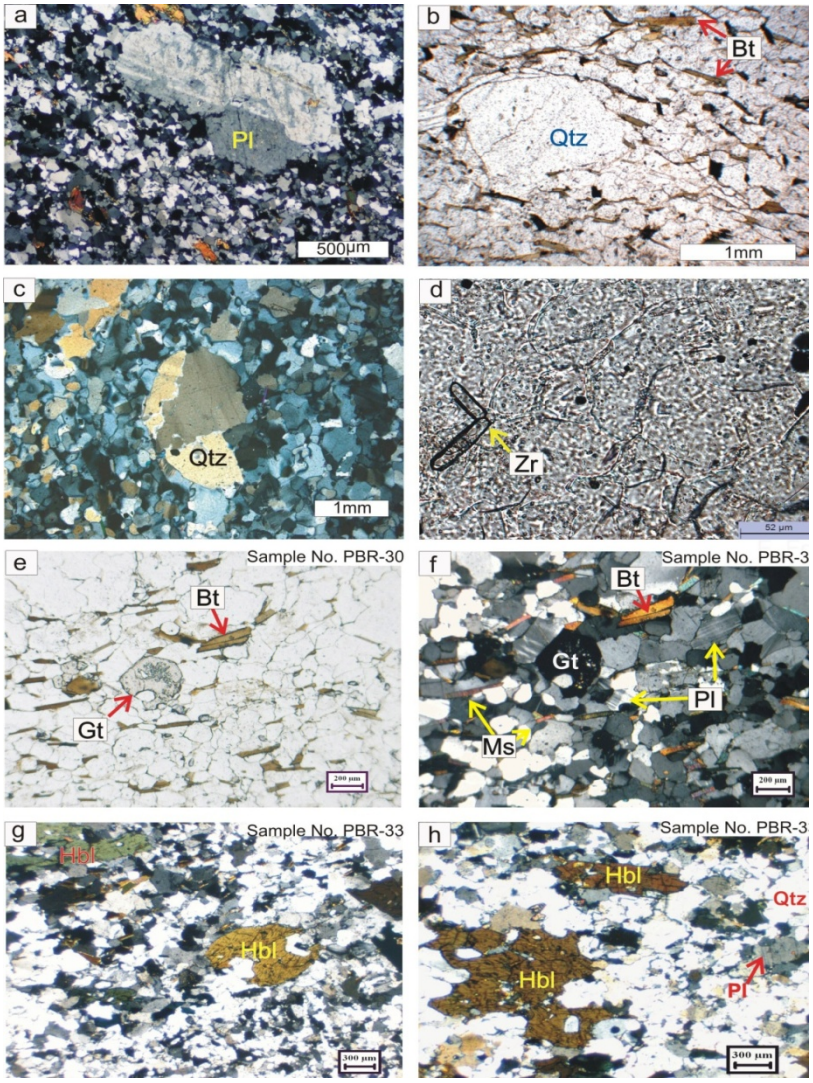

Fig.3.1 Photomicrographs of least altered rhyolite showing (a) euhedral plagioclase phenocryst (Pl) in a quartzo-feldspathic groundmass (b) rounded quartz phenocryst (Qtz) in a fine-grained quartz-feldspar groundmass with biotite defining foliation, (c) embayed and recrystallised quartz phenocryst (Qtz) in a recrystallized quartz-rich groundmass, (d) euhedral and elongated zircons (Zr) in a fine-grained groundmass (e) garnet porphyroblasts (Gt) as discrete grains in a recrystallised groundmass of quartz + feldspar + biotite, with biotite (Bt) defining the foliation (f) plagioclase, garnet and biotite in crossed nicols. (g) and (h) Hornblende (Hbl) occurring as poikiloblastic grains with quartz and biotite inclusions in the hornblende-bearing felsic volcanics in a quartz (Qtz) and plagioclase (Pl) groundmass

Hornblende occurs as 0.5mm to 2 cm sized, inclusion-rich, poikiloblastic grains in Hornblende rhyolite (Fig.3.1g & h). Hormblende occurs in a recrystallized quartz-feldspar rich groundmass (Fig.3.1g). Inclusions of quartz, feldspar and biotite and replacement textures suggest a metamorphic origin (Fig. 3.1h). The approximate modal composition of the typical hornblende-bearing rhyolite is: quartz 50%, plagioclase 20%, K feldspar 10%, hornblende 5-10 %, biotite 5%, opaques (magnetite + rutile) < 5 %.

Table 3.1 Summary of mineral assemblages studied in thin sections from the least altered rhyolite from Bhuyari Prospect.

Sample No.	**Assemblage** (major minerals)*	**Accessory minerals**
PBR-3	qtz, k-feld, pl, bi, ms, mt	py, po, zr
PBR-9	qtz, pl, k-feld, ep, gt, mt	py, po
PBR-30	qtz, pl, k-feld, bi, ms, gr,mt	ep, py
PBR-32	qtz, k-feld, pl,,ms, se	py
PBR-21	qtz, pl, k-feld, bi, mt, gr	zr
PBR-27	qtz, k-feld, pl, bi,ms	zr
PBR-28	qtz, pl, k-feld, bi,	zr
PBR-29	qtz, pl, bi,	zr
PBR-17	qtz, bi, ms, pl, gt, ch	zr
PBR-38	qtz, pl, k-feld, bi, mt, se	zr
PBR-24	qtz, pl, k-feld, bi, ms	zr, py, sp
PBR-36	qtz, pl, k-feld, bi, mt, se	ep, py,
PBR-33	qtz, pl, k-feld, hbl,ep, mt,	py, zr, rt
PBS-17	qtz, pl, bi, ms	zr
PBR-36	qtz, pl, k-feld, ms, gt,	zr, sp
BR-7	qtz, pl, k-feld, ms, gt,	zr
BR-8	qtz, k-feld, ms, bt, rt	zr, py ap

***Abbreviations** (for tables 3.1 to 3.3): act-actinolite, ap-apatite, an-anorthite, bi-biotite, ch- chlorite, do-dolomite, ep-epidote, gah-gahnite, gn-galena, ilm- ilmenite, k-feld - K-feldspar, qtz-quartz, hbl-hornblende, ms-muscovite, mt-magnetite, gt-garnet, phl-phlogopite, se-sericite, sp-sphene, st- staurolite, tc- talc, tr-tremolite, zo-zoisite, zr-zircon, rt-rutile, po- pyrrhotite, py-pyrite and sph-sphalerite.

Table 3.2 Mineral assemblages from altered rhyolite: quartz-biotite-phlogopite ± garnet ± ± gahnite ± staurolite schist (Mg-K-Fe alteration zone) and quartz-muscovite-K-feldspar ± garnet± biotite schist (K-alteration zone)

Sample No.	Alteration Type	Assemblage (major minerals)	Accessory minerals
PBS-19	Mg-K-Fe	qtz, bi, phl, st, gt, se, ch	mt, py
PBS-20	Mg-K-Fe	qtz, bi, phl, ms, st, gr, se	ch, ilm, mt
PBS-26	Mg-K-Fe	qtz, st, phl, gt, ch, se	py, sp
PBS-31	Mg-K-Fe	qtz, phl, ms, pl, gah, gr, ch	py, sp,
PBS-48	Mg-K-Fe	qtz, phl, gt, pl, ilm, sp	py, sp, ch
PBS-34	Mg-K-Fe	qtz, bi, pl, K-feld, ms	py
PBS-1	K-Fe	qtz, ms, bi, K-feld,pl, gr	py, ccp, sp, gn, zr
PBS-2	K-Fe	qtz, ms, bi, K-feld,gr	py, ccp, sp, gn,pl, zr
PBS-51	K-Fe	qtz, bi, ms, k-feld, gr	Py
PBR-22	K-Fe	qtz, ms, k-feld, gr	Py, bi

Table 3.3 Mineral assemblages from the tremolite-carbonate assemblage (Ca-Mg alteration).

Sample No.	Alteration Type	Assemblage (major minerals)	Accessory minerals
PBC-4	Mg-Ca	tr, tc, qtz, zo, ap, an, gt	ch
PBC-5	Mg-Ca	an, tc, tr, act, gt, qtz, zo, ap,sph	sp,ch
PBC-7	Mg-Ca	do, tr, chl, ms	sph
PBC-8	Mg-Ca	do, tr, chl, ms	sph
PBC-10	Mg-Ca	do, tr, tc	sp, ch
PBC-10	Mg-Ca	do, tre, tc	ch
PBC-16	Mg-Ca	tr,qtz,talc, chl	sp, gn
PBC-15	Mg-Ca	tr, do, phl	ap
PBC-18	Mg-Ca	tr, act, tc,ch	-
BY-5	Mg-Ca	tr, zo, ch, tc, ap	sp
BY-4	Mg-Ca	tr, ch, tc	zo

3.2 Petrography of Altered Rhyolites

The characteristic mineral assemblages in the different alteration zones are given in Tables 3.1, 3.2 and 3.3. Petrographically, most of these rocks are medium grade metamorphic rocks. However, their precursor nature (i.e, rhyolites that have undergone varying degrees and types of hydrothermal alteration) is evident from field relations and presence of relict textures as described below.

3.2.1 Quartz-muscovite-K-feldspar ± garnet ± biotite/phlogopite schist

This alteration assemblage is intimately associated with the biotie-phlogopite alteration zones. Generally, the muscovite- K-feldspar rich alteration assemblage, envelop the more intensely altered phlogopite-bearing (Mg-rich) alteration zone thus displaying a crude zoning which is apparent both in outcrop/hand-specimen scale as well as in map-scale (Fig.2.2b). This rock is characterized by high K_2O (2.5 to 9 wt. %) and slightly high FeO contents (upto 4 wt. %) (See chapter 5 for detailed chemistry). Approximate modal composition for this assemblage is quartz 50-60%, microcline 20%, muscovite 15%, plagioclase 5%, biotite 2-5%, sulphides 2-5%, garnet < 5 %. However, this rock can grade into quartz-muscovite schist which is dominantly composed of quartz (20-40%) and muscovite (40-60%) with minor K feldspar (5%) and garnet (< 5%).

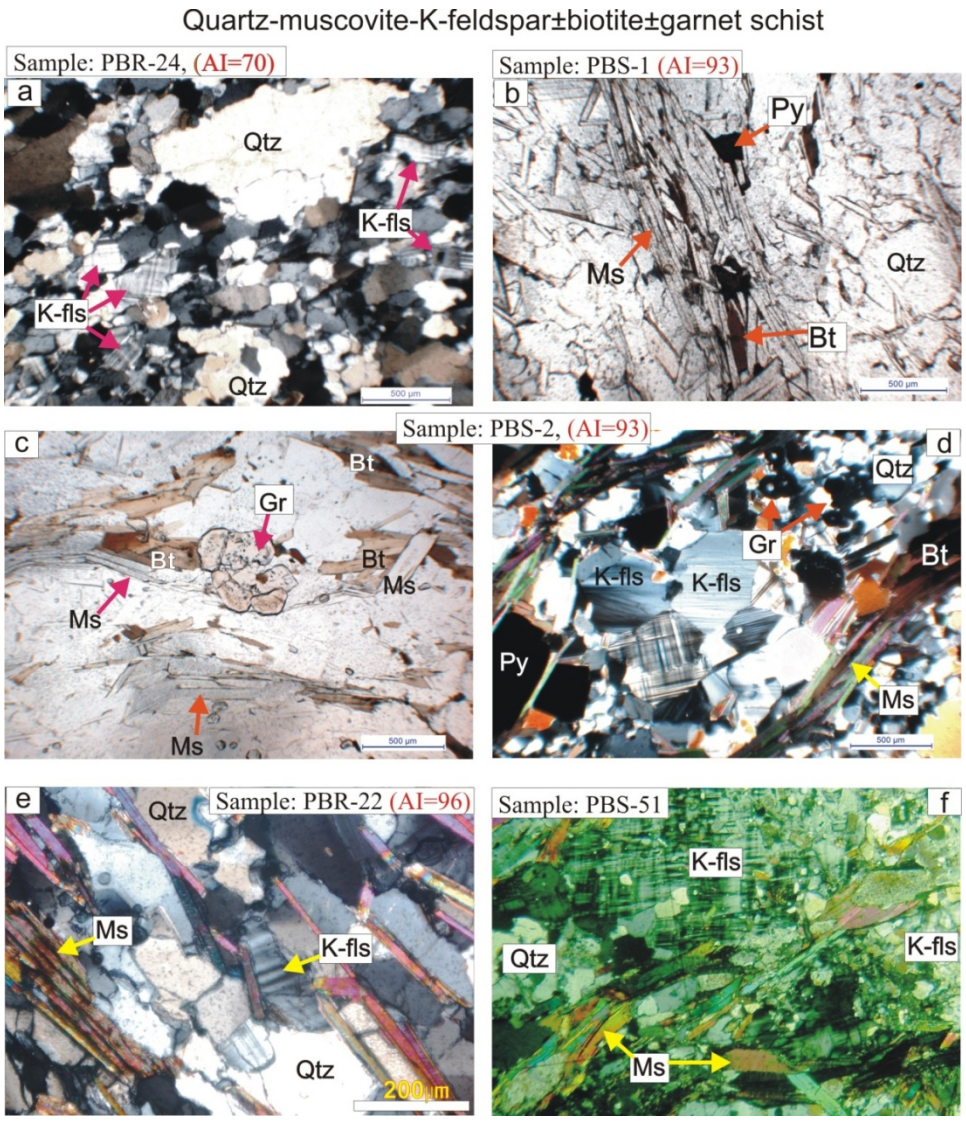

Fig. 3.2 Texture of quartz-muscovite-K-feldspar alteration a) preserved primary texture in the form of relict quartz phenocryst (Qtz) in a ground mass comprising of quartz + K-feldspar/microcline (K-fls), b) muscovite (Ms) and minor biotite (Bt) defining the foliation in the mineralized zone with sphalerite (Sph) along foliation, **c**) garnet (Gt) overprinting the foliation defined by muscovite (Ms) and biotite (Bt) foliation, **d)** microcline/K-feldspar (K-fels) forming aggregates in quartz-muscovite groundmass with muscovite defining foliation, **e)** muscovite defining foliation in quartz-muscovite-K-feldspar schist**, f)** quartz-muscovite-K-feldspar schist in X nicols showing large poikilitic K-feldspar with numerous quartz-muscovite inclusions, muscovite (Ms) defines foliation.

The typical rock type representing this alteration assemblage is a white to reddish white rock which is commonly schistose due to the high content of muscovite and/or sericite. At places the rock appears massive with a sericite-sheen. The protolith of these rocks is inferred to be rhyolite which has undergone intense potassic alteration possibly in the form of hydrothermal sericite. Primary volcanic textures like quartz phenocrysts are preserved despite high alteration indices (70) (Fig. 3.2a). The rock is characterized by high proportion of K-feldspar and muscovite (Fig. 3.2a). Generally, sericite/muscovite is the major phyllosicate with minor biotite and rare chlorite. Quartz- K-feldspar and muscovite are aligned parallel to the foliation with muscovite defining the foliation (Fig 3.2e). The main feldspar in this type of alteration is K-feldspar which is mostly microcline (Fig. 3.2a). Typical, cross-hatched microcline occurs as porphyroblasts and form aggregates at places which show poikiloblastic texture with numerous inclusions of quartz and muscovite (Fig. 3.2f).

Garnet is commonly found in the rock as <1mm, euhedral crystals. They contain inclusions of biotite and quartz and they cut across the foliation and therefore are possibly formed late in the deformation event (Fig 3.2c & d). This rock has sulphide mineralization at places, pyrite and sphalerite are generally present along the foliation planes (Fig.3.2b). Pyrite also occurs as euhedral porphyroblasts, which were formed during metamorphic recrystallization (Fig.3.2d) and they contain inclusions of sericite and quartz. The pyrite is generally associated with sphalerite and minor galena. At places the sulphides are replaced by silicate minerals especially muscovite. Zircon is a common accessory mineral and discrete, euhedral crystals are present in the groundmass.

Garnet is commonly found in the rock as <1mm, euhedral crystals. They contain inclusions of biotite and quartz and they cut across the foliation and therefore are possibly formed late in the deformation event (Fig 3.2c & d). This rock has sulphide mineralization at places, pyrite and sphalerite are generally present along the foliation planes (Fig.3.2b). Pyrite also occurs as euhedral porphyroblasts, which were formed during metamorphic recrystallization (Fig.3.2d) and they contain inclusions of sericite and quartz. The pyrite is generally associated with sphalerite and minor galena. At places the sulphides are replaced by silicate minerals especially muscovite. Zircon is a common accessory mineral and discrete, euhedral crystals are present in the groundmass.

3.2.2 Quartz- phlogopite - garnet ± plagioclase ± staurolite ± gahnite schist

This alteration assemblage is closely associated with mineralization and represents the Mg-rich core zone of the alteration system. This assemblage is a highly altered form of rhyolite found in the footwall alteration zones and within the mineralized zones and thin sections frequently contain disseminations of sulphides (Fig. 3.3c). This Mg-rich core zone is enclosed by the quartz-muscovite K feldspar alteration. Chemically, this zone is characterized by high MgO (4-18 wt.%), FeO (2-8 wt.%) and K_2O (2-7 wt.%) (See Chapter 5). This alteration facies display wide range in the proportion of the constituent minerals, at places it is in the form of monomineralic phlogopite schist and at places this rock can grade into an assemblage comprising about 50% plagioclase (mostly oligoclase).

Typically, the alteration is dominated by quartz + phlogopite bearing assemblage with varying proportions of plagioclase, garnet, staurolite, gahnite,

and muscovite. The mica present in the rock is essentially phlogopite or high-Mg-biotite as revealed by EPMA (See chapter 6, Tables 6.5 and 6.6). The phlogopite forms a major constituent in the rock and defines the foliation (Fig. 3.3a, 3.3b and 3.3c). Generally, the alteration is distinguished in the field by its grey to dark grey colour, phlogopite rich composition and presence of a variety of porphyroblasts. This rock has a granoblastic texture where garnet, plagioclase, staurolite and gahnite occur as porphyroblasts. The phlogopite is possibly derived from metamorphism of Mg-chlorite rich hydrothermal alteration zones in the rhyolite. Textural aspects of gahnite (zincian spinel) and staurolite in these rocks are discussed in more detail in this chapter as they provide better clues for metamorphic conditions. The growth of garnet, staurolite, plagioclase and gahnite during metamorphism and their existence as porphyroblast provides reasonable constraints for peak metamorphic conditions achieved in the area.

At Bhuyari, the phlogopite-bearing core alteration zone shows variation with respect to their mineralogical composition. The overall quartz-biotite-garnet-plagioclase alteration contains zones with either zincian staurolite or zincian spinel. The phlogopite-bearing assemblages are therefore broadly classified into three different sub-types for the sake of description. The corresponding commonly occurring rock type is given in italics.

1) Quartz - phlogopite - garnet ± plagioclase assemblage *(Quartz-phlogopite-garnet ± plagioclase schist)*
2) Zincian spinel (gahnite) bearing assemblage *(quartz-phlogopite-plagioclase-gahnite-garnet-chlorite schist)*
3) Zincian staurolite-bearing assemblage (*quartz-biotite-phlogopite-staurolite-garnet-chlorite-muscovite schist)*

3.2.2.1 Quartz-phlogopite-garnet ± plagioclase schist

This assemblage is the most abundant in the entire phlogopite-bearing alteration zone in Bhuyari. The rock is characterized by quartz, phlogopite, garnet and plagioclase with phlogopite defining the foliation. Typically the modal composition is quartz (40-50%), phlogopite (20-60%), garnet (5-20%) and plagioclase (5-20%). Phlogopite in this assemblage is phlogopitic and is the main Mg-bearing mineral and can attain up to 60 % or more of the rock (Fig. 3.3a). Despite intense alteration, the protolith of these rocks are inferred to be rhyolite based on the presence of relict volcanic textures like relict quartz phenocrysts and flow bands (Fig. 3.3a &b). The quartz phenocrysts are generally less than 2mm in size and are resistant to alteration, while the groundmass is replaced by phlogopite (Fig. 3.3a). Despite intense alteration which is manifested texturally as well as chemically (Alteration Index= 88) the quartz-phlogopite-garnet altered rhyolite (Sample No.PBR-48) shows relict quartz phenocrysts (Fig. 3.3a). The quartz phenocrysts are elongated along the direction of foliation due to the effects of deformation.

Garnets are ubiquitous in this alteration zone and reaches high proportions in the mineralized zone, with profuse development of < 1mm light pink garnets with high spessartine component (Fig. 3.3c and d). The garnets contain numerous inclusions of quartz and biotite, and give textural evidence for having formed by a reaction involving biotite. The garnets at places shows evidence of deformation in the form of fractures filled with quartz veinlets (Fig. 3.3d. This rock is closely associated with mineralization and frequently contains sphalerite, galena and chalcopyrite (Fig.3.3c).

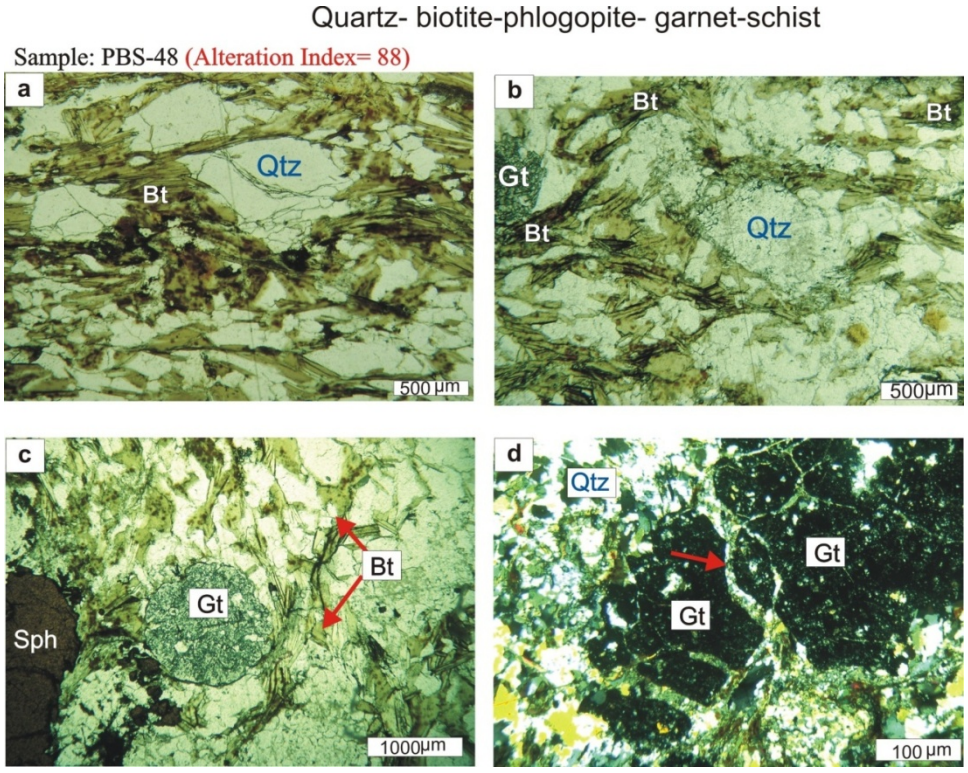

Fig.3.3 Photomicrograph of phlogopite-garnet bearing assemblage from mineralized zone at Bhuyari. **(a)** and **(b)** The phlogopite (Bt) defines foliation, relict quartz-phenocryst (Qtz) are still preserved in spite of intense alteration and metamorphism **(c)** Garnet (Gt) porphyroblasts show numerous inclusions of quartz, large patch of sphalerite (Sph) is seen **(d)** Garnets (Gt) in crossed nicols, show quartz veins along fractures.

This assemblage occurring immediately south of the massive sulphide zones at Bhuyari provides an opportunity to texturally interpret the PT paths experienced by the rocks during metamorphism. The pophyroblastic garnet likely grew during prograde metamorphism involving chlorite and muscovite. Chlorite and muscovite and/or biotite were likely consumed during garnet growth. The garnets frequently contain inclusions of biotite and chlorite (3.3d). The chlorite present in the matrix gives textural evidence for formation during retrogressive metamorphism. This chlorite is frequently seen as alteration of phlogopite and garnet.

3.2.2.2 *Zincian spinel (gahnite) bearing assemblage*

Gahnite or zincian spinel is well developed in the magnesium-rich alteration zone characterized by the biotite (phlogopite) bearing assemblage close to the mineralized zone. This rock is characterized by presence of gahnite porphyroblasts reaching up to 1 cm in size. Gahnite in this study contains up to 37 wt. % ZnO and is generally formed by desulphidation reactions involving sphalerite (ZnS) during metamorphism (Spry and Scott, 1986a). The representative mineral chemistry of gahnite is given in Table 6.12 (Chapter 6).

The approximate modal compositions of gahnite-bearing assemblage are quartz (30-40%) (phlogopite) (20-30%) plagioclase (15-20%), gahnite (20%) and garnet (5-10%). Petrographic studies show that some gahnites are euhedral with inclusions of sphalerite, and others which form pseudomorphs after biotite. These two types of gahnite show evidence for forming in different processes. Gahnite with sphalerite in their core suggests formation by desulphidation process where the sphalerite reacts with an aluminosilicate like garnet during prograde metamorphism to form gahnite. Gahnite at places form rounded grains with sizes ranging from 0.5mm to 1 cm (Fig 3.4a, b & c). These gahnites attain euhedral shapes and are possibly formed by desulphidation process involving the reaction of sphalerite with an aluminosilicate. The presence of sphalerite disseminations as inclusions within gahnite supports the view that desulphidation could have been the ideal mechanism of gahnite formation.

Calculations of f_{O2}-f_{S2} relations in the system Zn-Fe-Al-Si-S-O by Wall and England, (1979) suggest that sphalerite and almandine react to form gahnite, quartz and Fe sulfide at low f_{O2} and f_{S2} values by the following reaction:

$$Fe_3Al_2Si_3O_{12} + ZnS + 2.5\ S_2 = ZnAl_2O_4 + 3\ FeS_2 + 3\ SiO_2 + O_2$$

Almandine garnet + Sphalerite = Gahnite + pyrite + quartz

Gahnites also show textural evidence for formation by breakdown of biotite during retrogression (Fig 3.4d). Petrographic studies indicate varying stages of replacement of biotite by gahnite accompanied by chloritization of biotite (Fig. 3.4d). Thus the textural study of gahnite suggests that the area underwent a prograde amphibolite facies metamorphism characterized by development of gahnite by a reaction involving sphalerite and garnet, which was followed by a retrogressive event in which the gahnite was formed by the breakdown of zinc-rich biotites during chloritisation.

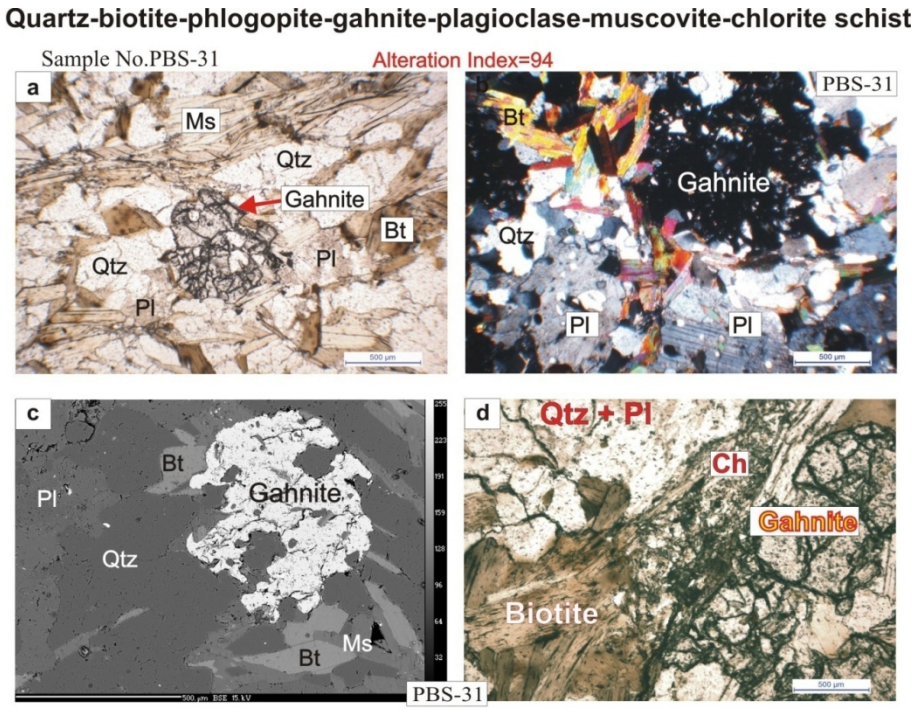

Fig.3.4 Texture of gahnite-bearing assemblages in the proximal alteration zone of Bhuyari showing **(a)** quartz-gahnite-biotite-muscovite assemblage with gahnite porphyroblasts overgrowing the foliation defined by biotite (Bt) and muscovite (Ms), **(b)** gahnite coexisting with plagioclase (Pl) quartz (qtz) and biotite (Bt), Plagioclase and gahnite porphyroblasts show similar quartz inclusions, **(c)** BSE image showing large (0.5mm) gahnite with inclusions of biotite and quartz, Biotite (Bt) and muscovite (Mt) are also seen **(d)** Incipient gahnite formation by breakdown of biotite. Note that the edges of the biotite are converting to an assemblage comprising of chlorite (Ch) and porphyroblastic gahnite.

Porphyroblastic plagioclase with An_{10-22} is reported in the alteration assemblages in the late Proterozoic Bleikvasslli Zn-Pb (Cu) deposit, Nordland, Norway (Cook, 1993). The rocks at Bleikvassli has undergone garnet-amphibolite facies regional metamorphism resulting in the development of garnet, staurolite, kyanite, microcline, muscovite, biotite, chlorite in the alteration zones close to the ore bodies. The mineral assemblages at Bleikvassli are more or less similar to that of Bhuyari, except the fact that kyanite is not present in the assemblage. The absence of aluminosilicate indicates that the primary hydrothermal alteration was not advanced argillic (Al-rich alteration). However, the presence of staurolite indicates that the alteration was at places argillic (Fe + Al alteration) within a wider zone of chloritic alteration- characterized by the phlogopite bearing rocks.

Bassed on a previous study on gahnites from the area Praveen and Ghosh (2007) interpreted that the gahnites formed by desulphidation process as well as by retrograde breakdown of biotite. The additional detailed work carried out as part of this work confirms the two modes of gahnite formation. Plagioclase is present in the gahnite-bearing assemblage as 0.5 to 2mm sized porphyroblasts. The plagioclase shows evidence for formation in a prograde metamorphic event and coexists with biotite, garnet and gahnite. They form euhedral porphyroblasts with poikiloblastic texture with inclusions of biotite, quartz and muscovite (Fig. 3.4b). EPMA studies have shown that the plagioclase is oligoclase. The presence of oligoclase with $An_{24\ to\ 35}$ is an unusual feature of the alteration zones at Bhuyari which is unique among other VMS deposits of Betul Belt, where plagioclase is generally absent in the highly altered zones. The development of plagioclase requires the bulk composition to have calcium, which may be related to the carbonate altered assemblage occurring in close proximity.

The plagioclase-bearing metamorphosed alteration assemblage although quite rare is similar to the alteration zone proximal to VMS deposits of Snow Lake, in the Paleoproterozoic Trans-Hudson Orogen, Manitoba, Canada (Menard and Gordon, 1997). Menard and Gorton (1997) based on detailed metamorphic P-T path studies of the mineral assemblages, interpreted that an additional Ca- bearing phase (either epidote or calcite) would be required for simultaneous development of garnet and plagicoclase. This interpretation may hold true for the garnet and plagioclase bearing assemblages in the Bhuyari footwall as well. Dolomite is present in the tremolite carbonate rocks which occur in spatial association with the plagioclase-garnet-phlogopite bearing rocks, however, carbonates could not be identified in the other magnesium rich or potassic alteration zones. Although calcite/dolomite is not preserved in these rocks, it is possible that the precursors of these rocks had undergone some degree of carbonate alteration and the calcite may have been completely consumed during metamorphism.

3.2.2.3 Zincian staurolite bearing assemblage

This study is the first report of zincian staurolite from the Bhuyari area. Like gahnite, staurolite occurs only proximal to the mineralized zones. This shows that the formations of these minerals are dependent on bulk compositions and not on variations in grades of metamorphism.

Stuarolite coexists with biotite, garnet, chlorite and muscovite. Approximate modal compositions in this assemblage are quartz (50%), biotite (20%) staurolite (20%), garnet (5-10%), chlorite (< 5%), sericite (<5 to 20 %).

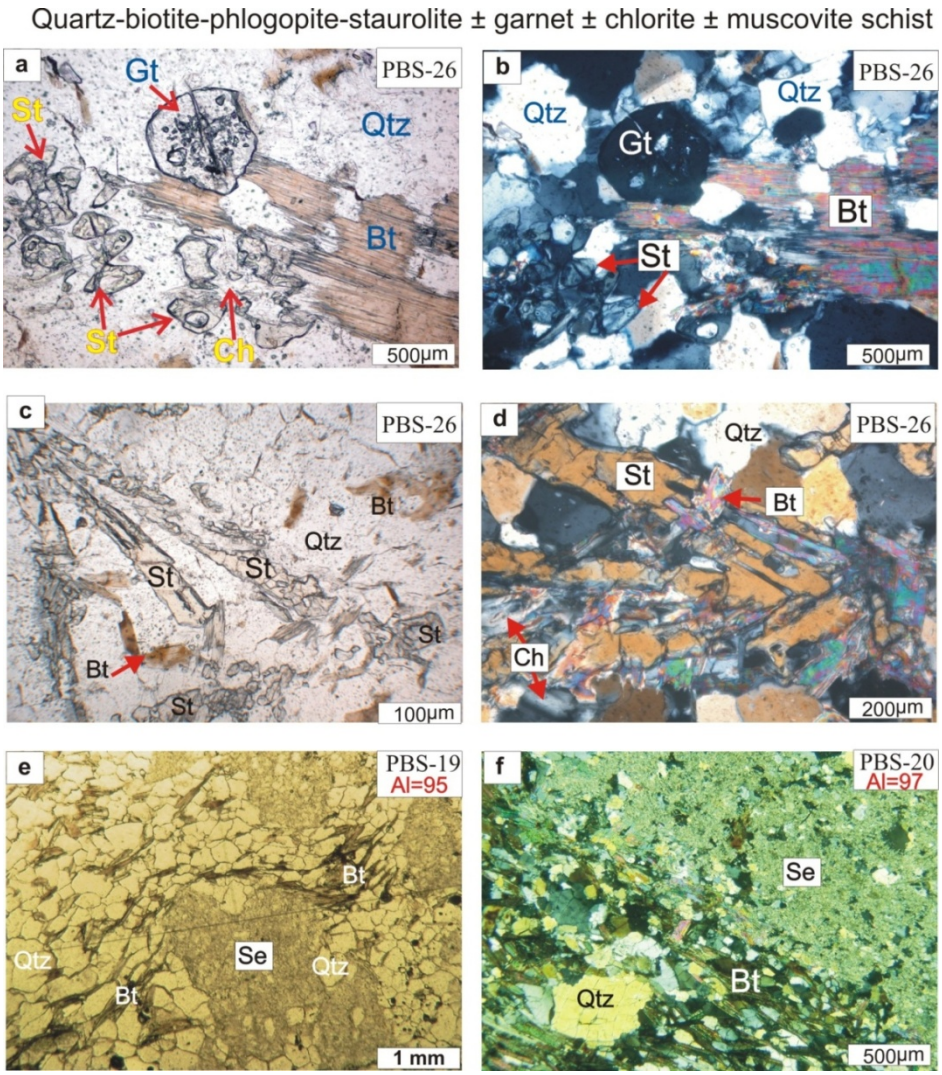

Fig.3.5 Photomicrographs of staurolite-biotite bearing rocks, **(a)** in plane polarized light (PPL) shows incipient development of staurolite (St) by breakdown of biotite (Bt), biotite near the contacts with staurolite appear frayed and is converting to chlorite (Ch), garnet porphyroblast (Gt) with inclusions is also seen, (b) in crossed nicols, garnet (Gt) show inclusions of chlorite and quartz (Qtz), incipient staurolite (St) is also seen (c) staurolite (St)form elongate pseudomorphs after biotite in a quartz-rich groundmass ,biotite altering to chlorite (Ch) is also observed (d) staurolite (St) formation involving retrograde breakdown of biotite (Bt) into chlorite (Ch), **(e)** porphyroblastic staurolite now completely replaced by sericite (Se), biotite (Bt) swerves around the staurolite porphyroblast, **(f)** close up view of sericite (Se) replacing the staurolite.

Two types of staurolite are seen in Bhuyari- either as large, euhedral porphyroblasts (up to 3cm) or as smaller (< 2 mm), incipient anhedral grains. Petrographic study of the smaller staurolite-bearing assemblages shows that staurolite coexists with garnet and biotite in a quartz-rich ground mass (3.5a and b). The coexisting biotite shows evidence for breaking down to form staurolite (Fig. 3.5a and b). The staurolite in this assemblage is frequently elongated and possibly forms pseudomorphs after biotite, which is evidenced by the presence of biotite in the matrix and also as inclusions in the staurolite (Fig. 3.5c and d). This assemblage also contains chlorite and garnet. Garnets in this assemblage are small (< 1mm), euhedral and are in contact with biotite (Fig. 3.5a and b). Texturally, garnet and staurolite appear fresh and unaltered and could have possibly formed in the same episode. The biotite in contact with staurolite appears frayed and shows alteration to chlorite (Fig 3.5a and b)

Petrography of the larger euhedral staurolite show that it is completely altered to sericite preserving only its euhedral outlines (Fig. 3.5 e and f). The larger staurolites occur in a more biotite-rich groundmass than the smaller staurolites. The high zinc contents in the staurolite (up to 9 wt. %) indicates that zinc was available in the system during its growth (Table 6.13). Zn can substitute for Fe in the staurolite structure. The randomly oriented garnet and staurolite porphyroblasts indicate that they formed after the peak deformation event in a strain-free environment.

3.2.3 Tremolite ± dolomite ± actinolite ± talc ± chlorite ± garnet rock

This assemblage is the carbonate bearing alteration assemblage at Bhuyari and is present as three separate outcrops which occur in close proximity of the massive sulphide zone (Fig.2.2b). The most common mineral in this alteration is tremolite and many other minerals occur in varying

proportions at different places within this rock. The rocks range at places from monomineralic tremolite rock (Fig. 3.6a) to one that is a carbonate dominant rock with minor tremolite (Fig. 3.6c). This rock exhibits wide variation in the proportion of its constituent minerals.

The rock at places is almost wholly composed of massive, coarse-grained tremolite. The tremolites is known to have Mg-numbers (> 0.9) as observed by EPMA studies. This rock grades into a more carbonate-rich rock with more than 80% carbonate minerals. The carbonate is identified as dolomite by EPMA analyses. The representative mineral chemistry of tremolite and carbonate are given in chapter 6 (Tables 6.14 and 6.15). Chemically, this rock is characterized by high MgO (7-23 wt. %) and CaO (13-14.5 wt. %) and is representative of both calcium and magnesium-rich alteration.

Petrographic studies show that tremolite + carbonate assemblage are mainly composed of tremolite and carbonate minerals with varying proportions of talc, chlorite, actinolite, anorthite, apatite, garnet, biotite and muscovite. Petrographic study of monomineralic tremolite rock show randomely oriented laths of tremolite with minor talc occurring in the interstitial spaces (Fig. 3.6a). At places this rock becomes carbonate-rich and is made up predominantly of equigranular carbonate (dolomite) with 5-10% tremolite. The tremolite occurs as large poikilitic grains which occur in a groundmass of carbonate minerals (Fig 3.6b). The tremolite porphyroblasts contain abundant inclusions of carbonate minerals (Fig.3.6.b). The tremolite laths show alteration to chlorite and portions of the rock become chlorite-rich (Fig. 3.6d). Thin veins of carbonate are present in this rock which cross-cuts the tremolite porphyroblasts. The tremolite laths are randomly oriented indicating growth in a strain-free environment possibly postdating peak deformation (Fig.3.6a).

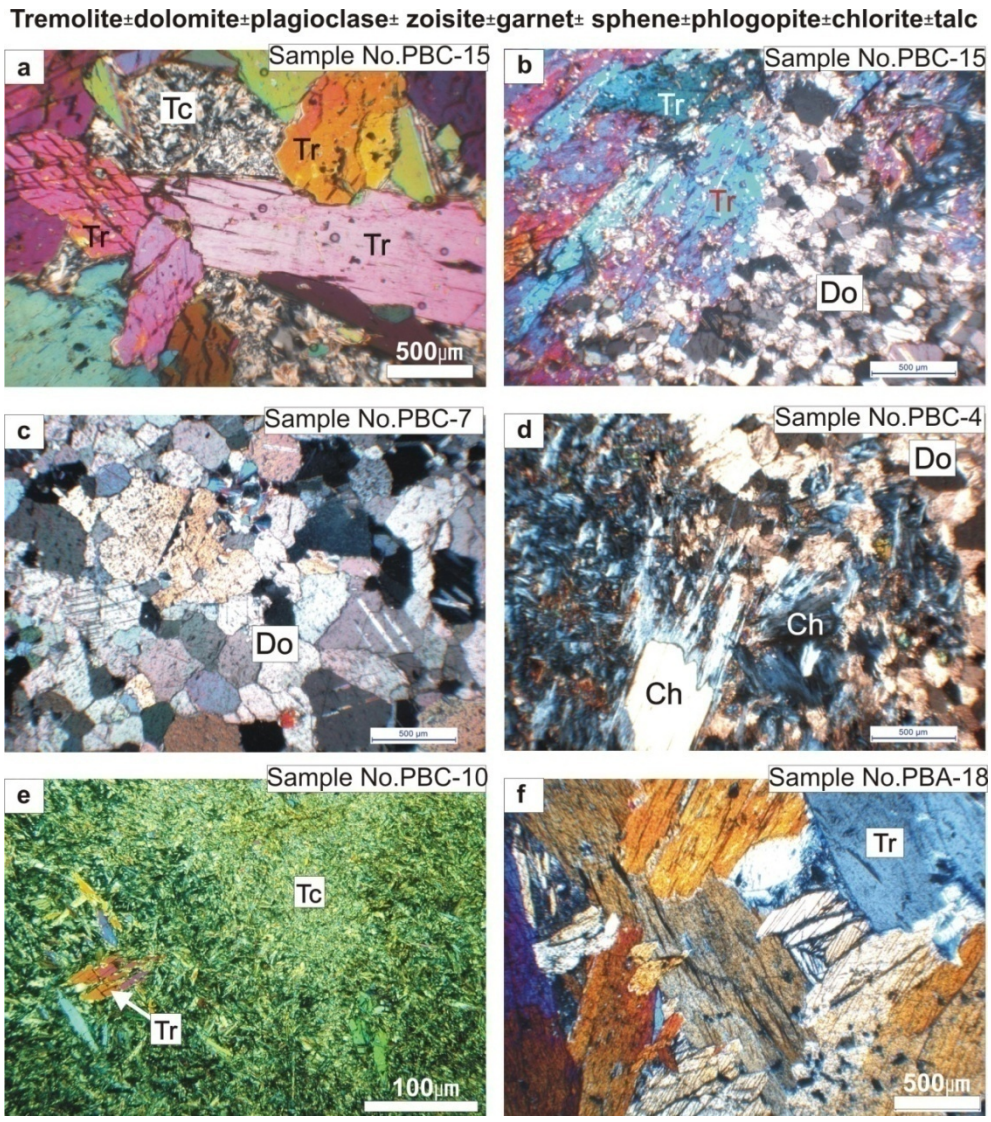

Fig.3.6 Photomicrographs of tremolite- carbonate bearing rocks, **(a)** porphyroblasts of tremolite (Tr), a) large porphyroblasts of tremolite (Tr) in a monomineralic assemblage consisting of mainly tremolite and minor talc, **(b)** large poikilitic tremolite lath in a groundmass of dolomite, **(c)** carbonate-dominant assemblage consisting of recrystallised dolomite (Do) with minor tremolite, **(d)** flaky chlorite (peninite) altering to chlorite forming aggregates in a dolomite-rich groundmass, chrlorite appear to be the alteration product of Mg-rich amphibole, **(e)** talc-tremolite rock with larger laths of tremolite (Tr) in a fine-grained talc-rich (Tc) groundmass, **(f)** monomineralic actinolite rock showing coarse, randomely oriented actinolite laths

At places the rock is entirely composed of fine-grained talc, with occasional bunches of tremolite porphyroblats (Fig.3.6e). The rock contains disseminations of sulphide (sphalerite and galena) minerals at places. Flaky, euhedral chlorite showing high relief form clusters in the rock, this chlorite is further altered to possibly iron-rich chlorite showing anomalous blue interference colours (Fig. 3.6d). At places the rock grades into monomineralic tremolite rock, which show alteration to talc along grain margins and cleavage traces (Fig.3.6f).

The petrographic study of the foliated/layered tremolite carbonate outcrops (CS-Hill 3), show that it is composed of fine-grained tremolite aligned along the foliation and also grey coloured plagioclase (anorthite) (Fig. 3.7a). The plagioclases are highly altered and show grey interference colours and lamellar twinning in crossed nicols (Fig. 3.7b). This rock also contains garnet which form aggregates along certain zones along the foliation and also as discrete euhedral crystals (Fig. 3.7b &c).

At places the rock contains high proportion of sphene and zoisite along with phlogopite (Fig. 3.7c &d). Sphene occurs as brown, euhedral grains and is sometimes rimmed by zoisite (Fig. 3.7c).

The colour-banding or apparent layering observed in this rock is at places made up of alternate bands of fine-grained garnet rich zones (light-cream) and tremolite-rich zones (green). The garnet rich zones contain around 30 to 40 % garnet and are therefore similar to some coticules which are a variety of garnet-rich metaexhalites (e.g.Spry et al, 2000; Slack et al, 2009). However, the spessartine-garnet rich coticules described by Spry et al (2000) are made of garnet and quartz as the major components, in this case the rock comprises of garnet and tremolite as major constituents.

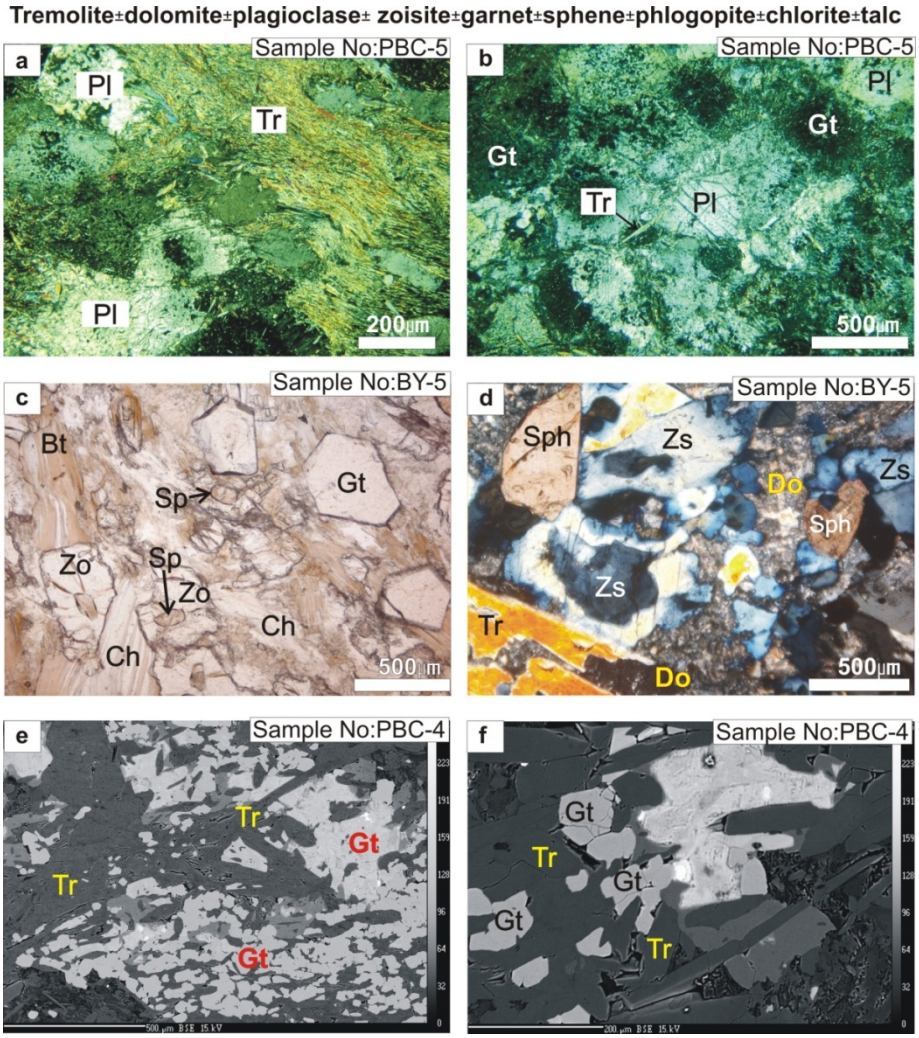

Fig. 3.7 Photomicrographs of tremolite-bearing rocks with (**a)** tremolite (Tr) and plagioclase (Pl) showing crude alternate banding which correspond to greenish and creamy-white layering seen in the outcrop, (**b)** plagioclase (Pl)-rich zones in crossed nicols, (**c)** zoisite (Zo) and garnet (Gt) form euhedral crystals in a groundmass of plagioclase and chlorite (Ch) in plane polarized light (PPL) (**d)** Euhedral sphene (Sph) showing reddish brown body colour and zoisite (Zs) showing anomalous blue interference colours and tremolite (Tr) showing bright second order yellow interference colour in a fine grained carbonate groundmass, (**e)** Back scattered electron images of garnet (Gt)-bearing zones in banded tremolite-chlorite-garnet rock from CS Hill-3, garnets show intergrowth texture with tremolite (Tr) **(f)** garnets (Gt) show euhedral to skeletal shapes and are intergrown with tremolite laths (Tr), the bright spot in the centre of the image is an unidentified REE-carbonate mineral.

Petrographic studies of sample PBC-4, show that the garnet-bearing layers are composed of minute (<1mm) euhedral to subhedral garnets which have an interlocking texture with the tremolite. The texture gives evidence for simultaneous formation of tremolite and garnet (Fig. 3.7e). Garnets also contain minute inclusions of fine-grained tremolite and dolomite. At places these rocks show the presence of an unidentified REE carbonate mineral (Fig. 3.7f). The presence of REE bearing phase in this rock is consistent with very high Total REE values (up to 1650ppm) obtained in this rock (See Chapter 5, Table 5.7). The REE-bearing phase occurs as bright patches associated with an unidentified calc-silicate mineral present in this rock.

Chemically, the rock is characterized by high CaO and MgO (Table 5.4) and is possibly formed by amphibolite grade metamorphism of carbonate-altered protoliths and also possibly a mixture of metaexhalites and altered volcanics. Detailed petrographic, mineralogical, and geochemical studies have been conducted on the tremolite-carbonate rocks as part of this Ph.D. work to understand the genesis of these rocks. This rock type is inferred to have developed as a result of intense carbonate alteration of the rhyolites near the hydrothermal vent.

Similar carbonate alteration is well-documented in other areas with VMS-type mineralization. In these deposits the carbonate bearing assemblages formed at or close to the palaeo seafloor, towards the upper regions of the hydrothermal vent, where carbonate precipitation is caused by heating of seawater and / or neutralization of acid-hydrothermal fluids mixing at moderate temperatures. The primary hydrothermal minerals could possibly have been dolomite, chlorite and talc which replaced the rhyolites close to the vent. Subsequent amphibolite grade metamorphism of this assemblage produced the present mineralogy comprising tremolite ± carbonate ± actinolite ± chlorite ± talc ± biotite ± garnet. The tremolite could have formed by a reaction involving dolomite, quartz and chlorite:

dolomite + quartz + talc + chlorite = tremolite + dolomite + actinolite

The absence of diopside in this assemblage show that these rocks have not attained granulite facies, as calcic pyroxene starts appearing in such an assemblage at the upper amphibolite - granulite facies transition (Spear, 1993). Detailed study of tremolite-carbonate-chlorite bearing assemblage at VMS deposit of Thalanga, Australia (Herrmann and Hill, 2001) has indicated that the precursors for tremolite-dolomite bearing rock could be chlorite + quartz + dolomite ± calcite or Mg-smectite + quartz + dolomite ± calcite bearing hydrothermal assemblages in altered rhyolites. The textural relations indicate that the tremolite formed in a prograde amphibolite facies event. The large porphyroblasts of tremolite contain inclusions of dolomite, chlorite and talc. The tremolite-carbonate-bearing assemblage is closely similar to that of the Thalanga assemblage except for the fact that the Thalanga assemblage has more chlorite when compared to the Bhuyari assemblage. This could be due to the higher metamorphic grade of Bhuyari (amphibolite) when compared to Thalanga (upper-greenschist). However, the precursors of the tremolite-carbonate assemblage in Bhuyari could have similarly developed involving a prograde reaction involving Mg-rich chlorite or smectite, dolomite and quartz. The prograde reaction could have proceeded along the following lines: Quartz + chlorite + dolomite + H2O = tremolite + calcite + CO_2.

This reaction proceeds at about 450ºC at 2 kb pressure and low to moderate activities of CO_2 (Slaughter et al., 1975). At Bhuyari, higher temperatures could have converted the remaining calcite to dolomite, resulting in a predominantly tremolite + dolomite bearing assemblage.

3.3 Mafic volcanic/ Metabasalt

The metabasalt in the area is represented by amphibolites, which is present as hornblende-quartz-plagioclase-magnetite-rock. This rock is present as small bands within the felsic volcanic sequence at Bhuyari (Fig. 2.3). The rock contains approximately 60% hornblende, 15-20 % plagioclase, 10-15% quartz, and 5-10% magnetite. Chlorite and epidote are common in altered varieties. Hornblende is green, pleochroic in yellow-green colours, randomly

oriented with interstitial space occupied by fine-grained and recrystallized aggregates of altered plagioclase and quartz (Fig. 3.8 a to d). Hornblende laths show a crude alignment parallel to the foliation (Fig.3.8a). Magnetite and ilmenite occurs as small grains scattered in the matrix (Fig. 3.8a).

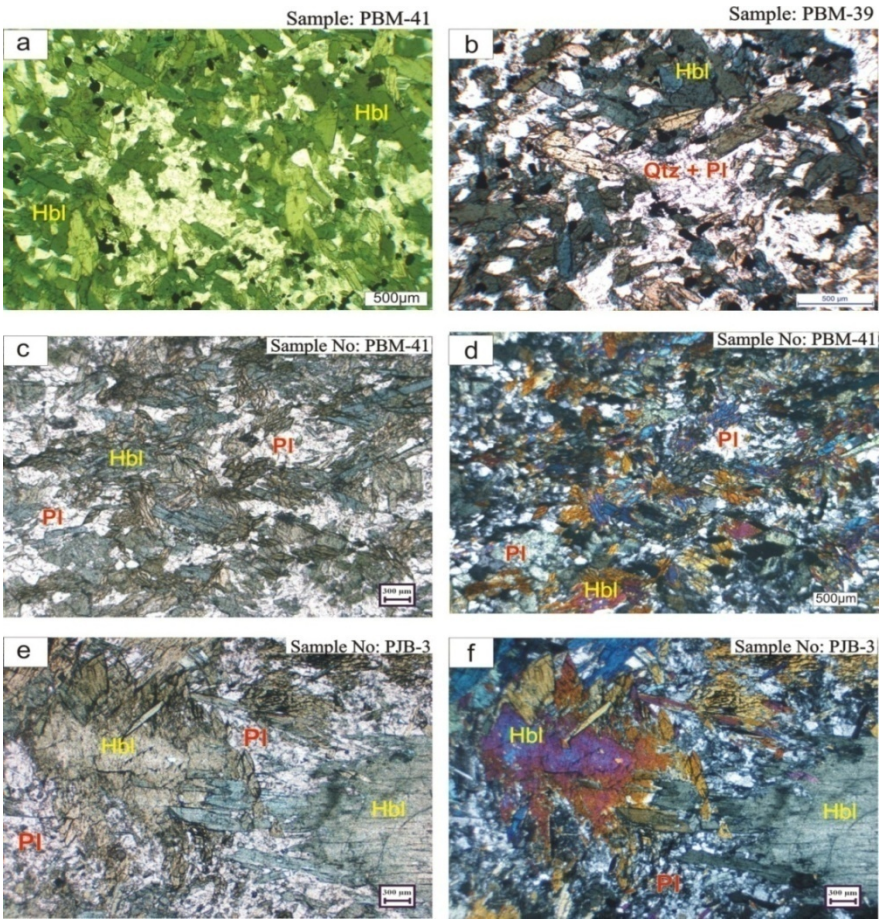

Fig.3.8. Photomicrographs of mafic rocks (amphibolites) (a) showing green hornblende (Hbl) and plagioclase and quartz constitutes the light-coloured areas (in plane polarized light), dark grains are magnetite and ilmenite, (b) Hornblende (Hbl) show blue-green interference colour in crossed nicols, light areas are plagioclase and quartz. (c) hornblende showing yellow to bluish green pleochroism and the light-grey areas are quartz + plagioclase. **e**) Photomicrograph of hornblende gabbro showing coarse-grained green hornblende (Hbl) with interstitial fine-grained plagioclase (Pl) (in PPL), (f) hornblende gabbro in crossed nicols with hornblende (Hbl) showing higher order brown-red purple interference colours, grey fine-grained material in the interstitial spaces are plagioclase (Pl).

3.4 Mafic Intrusives

The sample of hornblende gabbro is collected from the large E-W trending mafic intrusive south of Mordongri village (Fig. 2.1). The rock is predominantly composed of coarse-hornblende and interstitial medium to fine grained plagioclase and minor quartz. It contains hornblende (60-70%) and plagioclase (30-40%) and up to 5 % biotite and 2-5 % quartz. Texture is sub-ophitic to at places cumulus with plagioclase occupying interstitial spaces of large cumulus hornblende (Fig.3.8e & f). Large laths of hornblende are randomly oriented with interstitial euhedral plagioclase and are poikilitic with numerous inclusions of plagioclase and biotite (Fig.3.8e and f). The hornblende and plagioclase show igneous textures which reveals that the hornblende is primary. At places there is presence of aggregates of epidote grains which may have formed due to alteration from hornblende. At places the rocks show small clusters of biotite which are altered to chlorite.

3.5 Discussion

Petrographic studies show that unaltered rhyolites preserve primary volcanic textures like phenocryst-groundmass relationships and resorbed nature of the quartz-phenocrysts. Presence of substantial proportion of accessory zircons shows that the magma was zircon-rich and possibly formed at high temperatures. Texture of metamorphosed alteration zones show that most minerals were formed during late stages of deformation. This is evidenced by the relatively random orientation of the garnet, staurolite, gahnite and plagioclase porphyroblasts. Earlier episode of mineral formation is evidenced by the foliated nature of phlogopite, muscovite and biotite, which indicates that these minerals formed during the deformation event. The mineral assemblages are indicative of amphibolite facies metamorphism.

Textural relations suggest that most porphyroblasts developed during an amphibolite facies prograde event possibly late in the deformation event. This was followed by a lower grade retrogressive event evidenced in the chloritisation of biotite and amphiboles and also the development of gahnite by breakdown of biotite. Gahnite possibly formed in two stages- a prograde amphibolite facies in which gahnite formed by desulphidation reaction involving garnet which was followed by a retrograde event in which gahnite formed by breakdown of zinc-bearing biotite.

The assemblage containing staurolite + garnet + biotite represent the peak metamorphic assemblage in the area. Tremolite carbonate rocks with spessartine garnets may be products of metamorphosed hydrothermal exhalites (e.g. Spry et al, 2000; Slack et al, 2009). The high proportion of garnets at places in the banded tremolite-bearing rock suggests that these are similar to coticules- a variety of metaexhalites (Spry et al, 2000). The presence of relict banding or layering, close association with sulphide lenses, presence of Mn-rich garnet bearing zones (coticule) suggest that these rocks may have formed from precipitation of hydrothermal material from a sea-floor vent.

******

Chapter 4

GEOCHEMISTRY OF UNALTERED RHYOLITES

Contents

4.1 Introduction
4.2 Aims of this Study
4.3 Methodology
4.4 Major and Trace Element Geochemistry of Rhyolites
4.5 Zircon Saturation Temperatures
4.6 Rare Earth Elements (REE) geochemistry of Least Altered Rhyolites
4.7 Rhyolite Classification and Petrogenesis
4.8 Tectonic Setting
4.9 Discussion

4.1 Introduction

The study and characterization of volcanic geochemistry is a powerful tool in the exploration for volcanogenic massive sulphide (VMS) deposits. Such studies can help characterize potential host rocks from those that are likely to be barren of VMS deposits and thereby help save exploration expenditure. Primary lithogeochemical signatures of volcanic rocks (petrochemical signatures) provide critical information on the petrogenetic history and tectonic setting of volcanic rocks which in turn provide information on the thermal and geodynamic regime in which the belt has formed. When the geochemistry of volcanic rocks is combined with the stratigraphic context, it is possible to delineate potentially fertile and less fertile volcanic basins on a regional scale (Piercey, 2009). VMS deposits are typically associated with sub-aqueous felsic volcanic rocks with specific geochemical characteristics (Hart et al., 2004, Gaboury and Pearson, 2008).

The relationship between high-temperature rhyolites and VMS deposits are well documented (e.g., Hart et al., 2004). These high temperature rhyolites are also enriched in HSFE and REE and have been recognized from Archean to present

(Lentz, 1998; Piercey et al., 2001; Dusel-Bacon et al., 2004). There also appears to be a link between tectonic history of rhyolites and genesis of massive sulphides (Pearce et al., 2008).

4.2 Aims of this Study

The aims of this study are to characterize the major, trace and REE geochemical features of the rhyolite hosting sulphide mineralization in the eastern Betul Belt, to deduce the petrogenetic evolution of the rhyolite bassed on geochemical signatures and understand process that form VMS-bearing rhyolite and to constrain the tectonic setting of rhyolite emplacement with help of geochemistry.

Least rhyolite around the Bhuyari Prospect was analysed for major and trace elements and classified based on parameters by Lesher et al (1986) and Hart (2004). This chapter documents high-temperature rhyolite with elevated HFSE and REE, and low Zr/Y and La/Yb ratios (similar to F-111 type) which evolved in an extensional geodynamic setting with high heat-flow, possibly in a continental back-arc basin. It is proposed that a combination of field identification of specific volcanic textures and geochemistry can help in quickly evaluating VMS-potential of rhyolites in bimodal sequences. A petro-tectonic model for the evolution of the Betul Belt is postulated from this study.

4.3 Methodology

The samples of least altered rhyolite were collected during field work carried out as part of this study. Given the fact that most volcanic rock around the Bhuyari Prospect has undergone various degrees of hydrothermal alteration, extreme care was taken to collect samples from least altered rhyolites in the area. Sampling was carried out around the Bhuyari Prospect

and sample locations are shown in Fig.2.2a & b. The following criteria were used while sampling:

1. Samples collected from rhyolites preserving primary volcanic textures like quartz-phenocryst relationship and flow banding.
2. Samples having low to negligible contents of metamorphic minerals like biotite, muscovite, garnet which may indicate that it has undergone primary hydrothermal alteration.
3. After the analytical results were received from the lab, a set of 15 samples were selected based on their position when plotted in the alteration box plot. The 15 selected samples plot within the unaltered rhyolite box or close to it (Fig.4.1a)

The Bhuyari area and surrounding localities have good and relatively unweathered outcrops particularly in the Kanhan River section and the streams flowing into it. Large massive outcrops are also present in a series of low E-W trending ridges in the area. Around 2 Kg of freshly broken samples were collected from each location. The weathering rinds were carefully chipped away with the help of a hammer in the field so as to remove effects of oxidation. The fresh broken pieces are then crushed to -200 mesh sizes in a tungsten carbide pulverizer at the National Centre for Earth Science Studies (NCESS), Ministry of Earth Sciences, Thiruvananthapuram. A total of 40 samples were analyzed for whole-rock major and trace elements at NCESS by Bruker model S4 Pioneer sequential wavelength-dispersive x-ray spectrometer under pressed pellet and presented in Table 4.1 and 4.2. Analytical procedures are described in Sreejith and Ravindrakumar (2013). Analytical results for 15 unaltered rhyolites are provided in Tables 4.1 and 4.1. The remaining 25

samples are from various types of altered rocks and are given in Tables 5.1, 5.2, 5.3 and 5.4 (See Chapter 5).

REE and certain trace elements were analyzed at the National Geophysical Research Institute (NGRI) at Hyderabad by ICP-MS (Perkin Elmer, Sciex Elan DR (II). The procedure for REE and trace element analyses are described in Balaram et al (1996). REE analytical data of least altered rhyolites are presented in Table - 4.3. The REE data of altered rhyolites are given in Tables 5.6 and Table 5.7 (See Chapter 5).

4.4 Major and Trace Element Geochemistry of Rhyolite

The major and trace element analytical data are presented in Tables-4.1 and 4.2. The major element data of the 15 samples were plotted in the Alteration Box Plot of Large et al (2001a) to assess the degree of alteration (Fig. 4.1a). When plotted in the Alteration Box Plot, the majority of samples fall within the least altered rhyolite field, while the remaining samples plot close to the outer boundary showing minor effects of alkali metasomatism. However, they do not fall into the highly altered field. Since immobile elements are used for discrimination diagrams and classification these slightly altered rhyolites are also used as their immobile element ratios are little affected despite combined effects of hydrothermal alteration and metamorphism.

The alteration box plot of Large et al. (2001a) is a graphical representation that depicts two alteration indices: the Ishikawa alteration index (AI) = 100 (K_20 + MgO) / (K_2O + MgO + Na_2O + CaO) and the chlorite-carbonate-pyrite index (CCPI) = 100(MgO+FeO) / (MgO + FeO + Na_2O + K_2O) to characterize the nature and type of hydrothermal alteration related to VMS deposits. Least altered volcanics plot towards the centre of the diagram and hydrothermally altered volcanics plot at varying positions dependent on the principal hydrothermal minerals present. The box plot shows that the 15 rhyolite samples are relatively

unaltered and not significantly affected by hydrothermal alteration (Fig.4.1a). The samples plot within and close to the unaltered field and show slight trend towards the sericite and K-feldspar nodes due to effects of hydrothermal alteration, but they do not enter the strongly altered fields.

Table 4.1. Analytical results for major and trace elements of least altered rhyolite (oxides in wt.% and trace elements in ppm)

Sr.No.	1	2	3	4	5	6	7	8
Sample No	BR-1	BR-5	BR-6	BR-9	BR-10	PBR-21	PBR-30	PBR-38
Alteration Type	least altered	least altered	least altered	least altered	least altered	least altered	least altered	least altered
SiO2	72.00	74.37	73.78	75.42	74.60	76.93	73.86	75.97
TiO2	0.46	0.37	0.17	0.31	0.32	0.34	0.36	0.40
Al2O3	11.74	12.67	13.84	11.29	12.26	11.17	11.29	11.70
MnO	0.09	0.11	0.03	0.18	0.10	0.09	0.20	0.12
Fe2O3	5.05	4.07	2.41	3.89	3.65	4.10	3.94	4.65
CaO	1.29	1.36	0.54	1.29	1.81	1.37	1.28	1.32
MgO	0.74	0.43	0.53	0.48	0.23	0.55	0.50	0.67
Na2O	3.38	3.73	4.39	3.11	3.36	3.61	2.49	3.48
K2O	3.25	3.28	3.17	3.13	3.10	2.87	4.56	3.01
P2O5	0.09	0.05	0.02	0.03	0.05	0.04	0.06	0.06
Total	98.1	100.4	98.9	99.1	99.5	101.1	98.5	101.4
Co	9	7	5	7	7	0	0	5
Cu	0	6	2	4	0	5	24	11
Zn	121	155	32	762	154	101	92	240
Ga	21	22	20	20	20	20	19	20
Rb	99	99	99	97	95	50	75	55
Sr	78	61	39	54	75	45	66	73
Y	208	154	90	153	176	124	172	118
Zr	904	881	480	788	881	646	861	760
Nb	39	31	29	33	33	23	29	21
Ba	1200	1300	1300	1300	1100	1300	1600	1400
Pb	26	16	16	21	56	24	62	127
Zr/Y	4	6	5	5	5	5	5	6
Zr sat. Temp.	962	961	908	952	958	920	955	944
Alt Index	46	42	43	45	39	41	57	43
CCPI	44	37	26	39	35	40	36	43

Table 4.2 Analytical results for major and trace elements of least altered rhyolite

Sr.No.	9	10	11	12	13	14	15
Sample No	PBR-3	PJR-11	PBR-17	PBR-27	PBR-28	PBR-29	PBR-33
Alteration Type	least altered	least altered	least altered	least altered	least altered	least altered	least altered
SiO2	74.32	74.37	75.48	79.68	79.38	77.25	73.10
TiO2	0.32	0.20	0.41	0.14	0.18	0.17	0.36
Al2O3	11.82	14.11	11.12	10.59	11.48	12.10	10.38
MnO	0.12	0.06	0.25	0.03	0.07	0.04	0.21
Fe2O3	3.82	2.96	5.04	1.26	2.88	2.07	5.37
CaO	0.90	2.11	0.60	0.37	0.87	0.52	2.59
MgO	0.48	0.67	1.12	0.17	0.39	0.40	0.47
Na2O	1.68	0.94	2.07	2.41	5.37	6.19	3.84
K2O	6.49	4.87	3.36	5.60	1.21	0.64	2.09
P2O5	0.04	0.01	0.03	0.01	0.00	0.00	0.04
Total	100.00	100.30	99.47	100.26	101.84	99.38	98.45
Co	0	0	4	0	0	0	0
Cu	4	6	7	8	9	9	0
Zn	111	112	505	120	116	34	82
Ga	21	21	24	17	25	23	23
Rb	146	223	72	68	19	22	41
Sr	47	132	40	21	39	29	82
Y	186	90	143	96	173	131	168
Zr	889	617	822	380	552	544	912
Nb	28	26	27	24	34	33	26
Ba	1600	1400	1700	1800	1000	1500	1100
Pb	63	34	42	17	19	134	14
Zr/Y	5	7	6	4	3	4	5
Zr sat. Temp.	963	950	930	872	906	908	922
Alt Index	73	64	63	67	20	13	28
CCPI	32	36	51	14	31	25	47

A detailed account of altered rhyolites in the area is presented and discussed in comparison to their unaltered counterparts in the next chapter (Chapter -5).

The major element data shows that they contain high silica contents (SiO_2=72 to 79.68%) which are similar to high silica rhyolites (e.g. Hildreth,

1981, Barrie et al, 1993). Some rhyolites with higher SiO_2 contents (up to 85%) show evidence for silicification and are included in altered rhyolite (Table 5.3) in Chapter-5.

The rhyolites also show low Al_2O_3 (<14 %, average: 12 %) and low MgO (<1%) contents. They also are characterized by high FeO^T (1.1 to 4.5wt. %) and FeO^T / (FeO^T + MgO) ranging from 0.8 to 0.91.

The rhyolites are all aluminous, (metaluminous to peraluminous) and most samples have A/CNK (molar $Al_2O_3/Na_2O + K_2O + CaO$ ratio) close to unity (Fig.4.1b). Most of the samples plot in the boundary between the metaaluminous to peraluminous fields. The spread shown by some samples towards the peraluminous field is evidently due to effects of alkali mobility during alteration. Elsewhere in the world, the rhyolites of bimodal provinces, i.e. those with A-type affinities, are mainly metaluminous to mildly peralkaline (Eby, 1990; Frost et al, 2001). The Bhuyari rhyolites however, do not show a peralkaline character in this plot.

Major and trace element data when plotted in standard discrimination diagrams (Winchester and Floyd, 1977; Le Bas et al, 1986) plot well within the rhyolite field (Fig.4.2a & b). The data show that they can be classified as high-K rhyolites.

The trace elements were normalized against the primitive mantle with normalizing values from Sun and Mcdonough (1989) (Fig. 4.3a). Primitive mantle-normalized plots are characterized by high concentration of HFSE relative to primitive mantle. The plot also shows moderate negative Nb anomaly and strong negative Sr and Ti anomalies (Fig.4.3a). The spider plot shows an overall gentle slope from left to right.

4.4.1 High HFSE Contents

Trace elements show high concentrations in the rhyolite samples. The Bhuyari rhyolites contain some of the highest HFSE and REE contents for felsic rocks hosting deposits when compared to any other in the world (see Pearce et al, 2008; Lentz, 1998). The Zr (380 to 912ppm) and Y (89-163ppm) and Nb (21-39ppm) contents are particularly high. The high Zr and Nb contents are comparable to rhyolites from several well known VMS terrains like those from the Proterozoic Bathurst in Canada (Fig.4.5). Petrographical studies have shown high content of zircons in the rhyolites (Fig.3.1d). The elongated zircons observed in some samples are characteristic of rapid crystallization as is common in lavas and high level porphyriic intrusions (Corfu et al, 2003). The total REE contents of the rhyolites are also high and reaches about 100 times chondritic values. The high concentration of HFSE and REE are typical and is recognized in VMS terrains from Archean to recent (Lesher et al., 1986; Lentz, 1998). Bimodal successions with High Field Strength Elements (HFSE)-enriched high- silica rhyolites are associated with significant proportion of VMS deposits in Abitibi Subprovince, Canada (Barrie et al, 1993) although they form only a minor component of the greenstone succession.

4.4.2 Magmatic Affinity

When the major element data are plotted in the AFM diagram of Irvine and Baragar (1971), the rhyolites closely follow the boundary of the tholeiitic and calc-alkaline series (Fig.4.1c). Use of major element data of rocks affected by even minor hydrothermal alteration for constraining magmatic affinity can

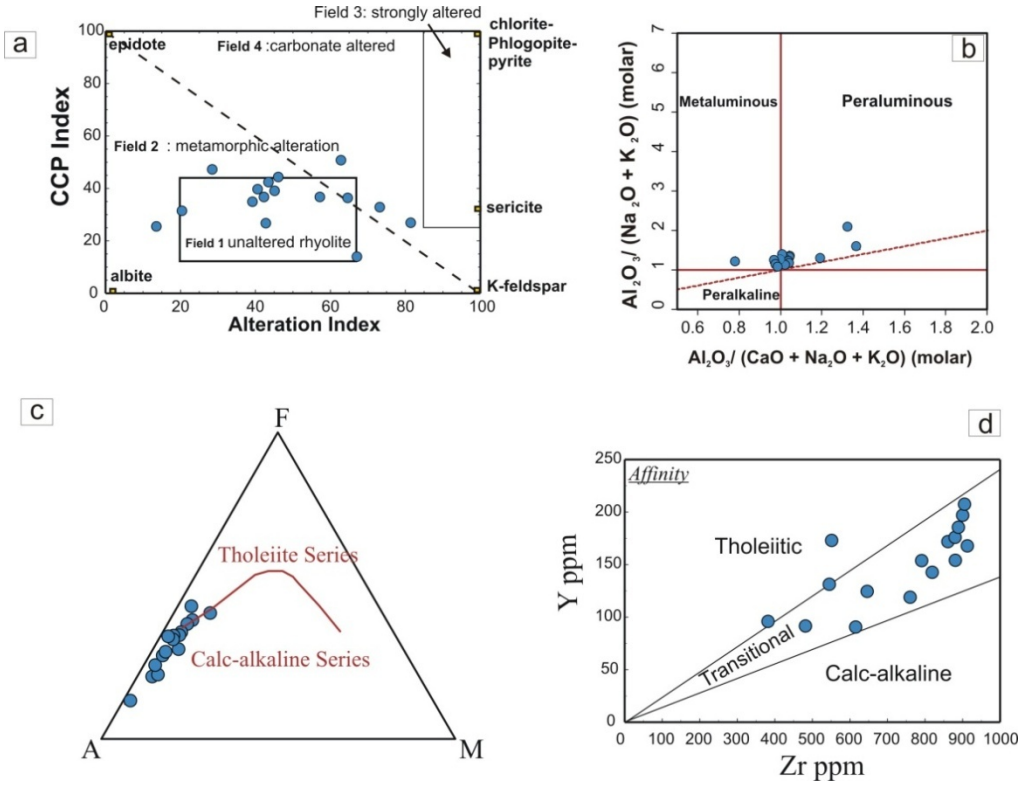

Fig.4.1 Unaltered rhyolite samples plotted in **(a)** the alteration box plot (Large et al.2001b). Note that some samples fall outside the least altered-field, but do not enter into the strongly altered field. The samples falling within the Field-1 and those plotting around the periphery of the field-1 are therefore considered relatively unaltered. **(b)** molar Al_2O_3/ (Na_2O + K_2O) versus Al_2O_3/ (CaO + Na_2O + K_2O) plot of Shand (1943), the most unaltered samples plot near unity **(c)** the AFM diagram of Irvine and Baragar (1971) shows a transitional to calc-alkaline trend **(d)** Immobile element plot using Zr vs.Y show a tholeiitic to transitional trend for the rhyolites.

be potentially erroneous due to mobility of alkalies. Therefore, trace elements which are relatively immobile are used to constrain magmatic affinity. Ratios of incompatible and immobile HFSE (e.g., Zr/Y, Y/Nb, La/Yb) and normalized REE profiles provide simple ways to monitor the magmatic affinity of volcanic rocks in mineral exploration (Barrett and MacLean, 1994b). For hydrothermally altered rocks, magmatic affinity can be assessed more precisely by using these

incompatible and immobile trace element ratios. These ratios are generally not affected by typical VMS-type alteration and provide simple ways to monitor the magmatic affinity of volcanic rocks in mineral exploration (Barrett et al, 2008).

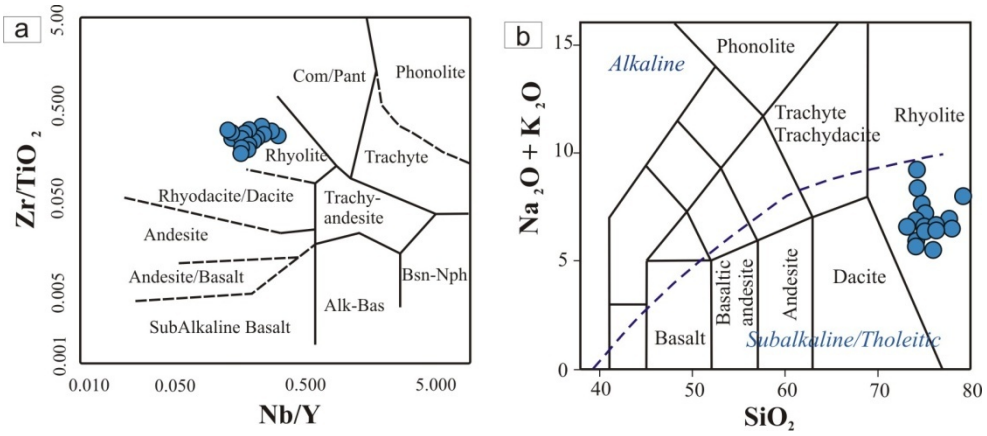

Fig.4.2 Unaltered rhyolites plotted in volcanic rock nomenclature diagrams after (a) Winchester and Floyd (1977) and (b) Le Bas et al (1986).

In a magma that fractionates to yield a spectrum of mafic to felsic compositions, there is generally little change in these ratios (unlike, for example, the ratio of TiO_2 to Zr). Fractionation trends remain nearly linear and directed away from the origin. Subsequent alteration will shift sample points toward or away from the origin, along an essentially parallel trend. For this reason, altered as well as unaltered samples can be used in magmatic affinity plots involving Zr, Y, Nb, and the REE (Barrett et al, 2001).As a general guideline, rocks with Zr/Y ratios <4 are tholeiitic, rocks with ratios above 7 are calc-alkaline and ratios between 4 and 7 are considered transitional (Barrett and MacLean, 1999, Barrett et al, 2008). Based on the Zr/Y ratio (3 to 7), the Bhuyari rhyolites show tholeiitic to transitional affinities (Fig. 4.1d).

4.5 Zircon Saturation Temperatures

The abundant euhedral and elongated zircons are indicative of magmatic crystallization at high temperatures. There is no petrographic evidence for xenocrystic / xenogenic zircons which may have been captured during interaction with the gneissic basement. This petrographic observation is supported by the spiderogram of the Bhuyari rhyolite which shows that most samples have no marked positive zircon anomalies (Fig. 4.3a). Only a few samples show weak positive zircon anomalies, and many samples show negative zircon anomalies, this shows that zircons were not accumulated or inherited. The zircon temperature estimated would turn out to be unrealistic if zircons were accumulated in this rock.

Zircon saturation thermometry, which is calculated for Zr concentration in a bulk rock analysis (Watson and Harrison, 1983), provides an estimate of melt temperatures. Following the zircon saturation method, the calculated magma temperatures for Bhuyari rhyolites ranges from 872°C to 991°C (average 940°C), Table-4.1 and 4.2. The zircon saturation temperatures were calculated using the GCD software which is free software available online.

Barrie (1995) studied the zircon thermometry of high-temperature rhyolites in the Abitibi subprovince in Canada and found that those associated with the VMS deposits recorded the highest zircon saturation temperatures (840ºC-940ºC), which are closely similar to the temperatures obtained for the Bhuyari rhyolite.

4.6 Rare Earth Elements (REE) Geochemistry of Least Altered Rhyolite

A total of 17 samples were analyzed for REE, out of which 6 samples are from unaltered rhyolite and will be used for characterization of rhyolites.

The REE analytical results of the 6 unaltered samples and their chondrite normalized ratios are given in Table 4.3. The REE analytical results of altered rhyolites are discussed separately in Chapter-5 and are provided in Table 5.6 and Table 5.7.

The unaltered / least altered rhyolite has high total REE contents ranging from 352 to 402ppm (Table 4.3). The chondrite normalized plot for the least altered rhyolites show enrichment in LREE with respect to HREE and the patterns display a narrow range (Fig.4.3b). The REE patterns of the rhyolites show similar patterns except for vertical shifts. Such vertical variations are caused mainly by mass changes in mobile elements, which produce either dilution or residual concentration of the REE (Barrett et al., 2005). The rhyolites are strongly enriched in LREE (>100 times chondrite). The profiles are characterized by LREE fractionation with $(La/Sm)_N$=2-2.3 and flat HREE profiles ($(Gd/Lu)_N$=0.9-1.2), which are typical of crustally-derived melts. They are also characterized by a pronounced negative Eu anomaly (Eu/Eu* < 0.6). The slopes of rare-earth element patterns (as approximated by the La/Yb ratio) also provide information on magmatic affinity. La/Yb ratios, normalized to chondrite, are generally about 0.5 to 2 for tholeiitic rocks, 2 to 5 for transitional rocks, and 5 to10 or more for calc-alkaline and alkaline rocks (Barrett et al., 2008).

Based on REE slopes and $(La/Yb)_{N,}$ the Bhuyari rhyolites show transitional affinities ($[La/Yb]_{N=}$ 2.5-4.4 (avg. 3.4). $(La/Yb)_N$ ratios of 4 to 6 and moderately high Σ_{REE} contents are common in rift-related settings where the underlying crust is continental (Hildreth, 1979).

Flat to slightly inclined chondrite normalized REE patterns with high total REE contents are typical of tholeiitic felsic volcanic rocks (Barrett et al.,

2001). Between the various altered groups and unaltered rhyolite, the patterns are essentially parallel, but are separated by vertical shifts which are primarily due to the addition and removal of mobile mass. Various studies have shown that the REE essentially behaves as immobile elements during hydrothermal alteration (e.g. Barrett et al., 2001).

Table 4.3 Rare Earth Element (REE) analyses of least altered rhyolite. Chondrite normalization values are after Nakamura (1974).

	1	2	3	4	5	6
	PBR-3	**PBR-21**	**PBR-27**	**PBR-28**	**PBR-29**	**PBR-30**
La	67.237	68.1	66.508	72.918	68.97	68.906
Ce	139.806	140.92	135.856	149.531	144.41	144.701
Pr	16.345	16.549	15.528	17.154	15.957	16.792
Nd	70.218	70.793	63.733	71.113	66.277	71.25
Sm	17.845	18.002	15.305	17.001	15.66	18.1
Eu	3.276	3.259	2.135	2.438	1.99	3.294
Gd	16.215	16.309	13.049	14.565	13.735	16.46
Tb	3.403	3.439	2.603	2.902	2.609	3.483
Dy	19.964	19.82	14.129	15.329	14.126	20.446
Ho	3.945	3.885	2.619	2.742	2.597	4.063
Er	13.491	13.298	8.755	8.876	8.759	14.126
Tm	2.271	2.238	1.442	1.441	1.465	2.37
Yb	14.398	14.061	9.29	9.353	9.697	15.267
Lu	2.203	2.157	1.432	1.465	1.517	2.367
ΣREE	390.617	392.83	352.384	386.828	367.769	401.625
La/Yb(N)	2.62	2.72	4.02	4.38	3.99	2.53
Eu/Eu*	0.58	0.57	0.45	0.46	0.41	0.57
(Gd/Lu)N	0.90	0.93	1.12	1.22	1.11	0.85
(La/Sm)N	1.95	1.96	2.25	2.22	2.28	1.97

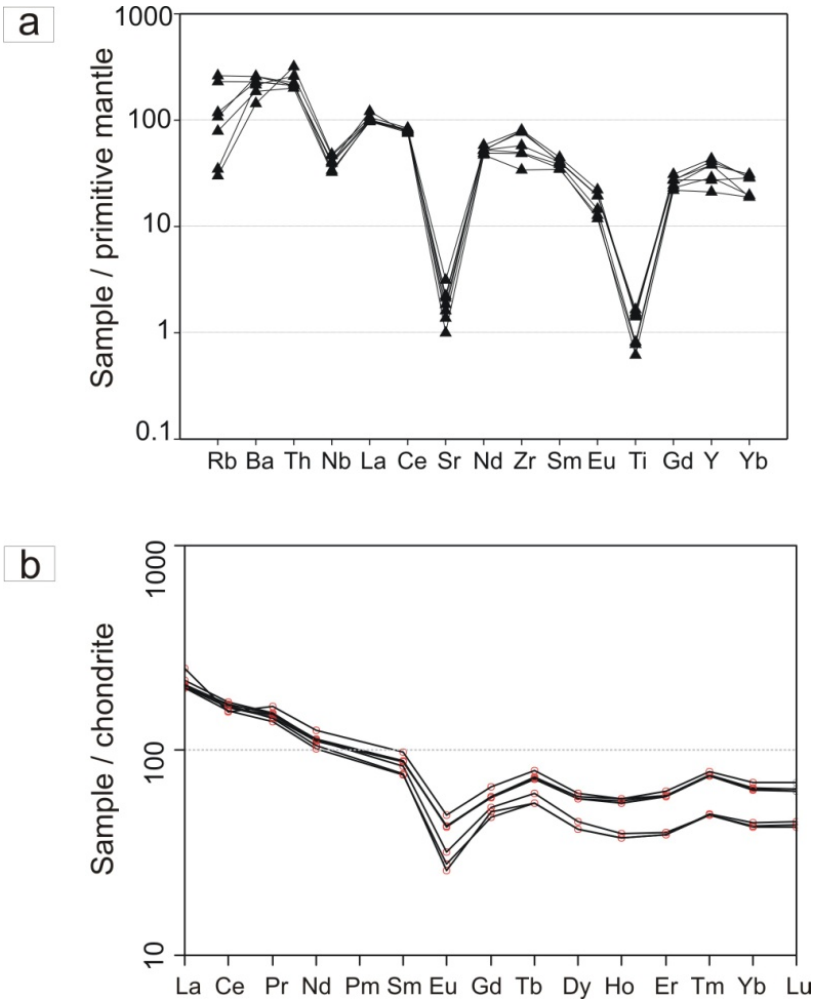

Fig. 4.3. (a) Primitive mantle-normalized trace element plots for the Bhuyari rhyolites, with primitive mantle values from Sun and McDonough (1989). **(b)** Chondrite-normalized, rare-earth element plot of rhyolites from Bhuyari, with chondrite values from Nakamura (1974).

4.7 Rhyolite Classification and Petrogenesis

Based on the potential for hosting VMS deposits, Precambrian felsic volcanics are classified geochemically into four type's viz. FI, FII, FIIIa and FIIIb, as identified by Lesher et al, (1986). Hart et al (2004) added another F

IV class, which is present mostly in Phanerozoic volcanic successions. These classification schemes have relied on immobile elements like Zr, Y, La and Yb and primitive mantle-normalized plots (Gaboury and Pearson, 2008).

FI and FII are alkalic and calcalkalic rhyolites and rhyodacites, with low to moderate HFSE contents, high Zr/Y ratios and steep REE patterns, and are abundant in the rock record but have low VMS potential, whereas the tholeiitic FIII type, with higher HFSE contents, low Zr/Y ratios and flatter REE patterns, although less abundant in the rock record, host the maximum number of VMS deposits.

The FI suite is characterized by high La/Yb_n ratios and lower HFSE contents. The FII group has signatures intermediate between the two groups. The majority of Archean VMS deposits are hosted by FIII and FII felsic rocks, which are interpreted to have formed from Archean rift sequences with high temperature melts (> 900°C) derived from melting of hydrated basaltic crust at shallow levels (Lesher et al, 1986; Hart et al, 2004). The melt generations at shallow depths facilitated these melts to rise to the surficial levels without losing much of their heat and therefore, are capable of generating long-lived hydrothermal convection systems (e.g. Barrie et al, 1999).

The Zr/Y vs. Y plot of Lesher et al. (1986) as modified by Lentz (1998) show that the Bhuyari rhyolite occupies the FIIIb rhyolite field (Fig. 4.4a). Similarly, in the $(La/Yb)_{CN}$ vs. Yb_{CN} diagram of Hart et al (2004), the samples plot within the FIIIb rhyolite (Fig.4.4b). Their tholeiitic to transitional affinity, elevated HFSE, Zr (380 to 912), Y (89-163) and low Zr/Y ratios of < 6 (3 to 6) together with their pronounced negative Eu anomalies (0.6 to 0.4) makes them

similar to FIIIb rhyolites of Hart et al (2004) which are considered highly prospective for VMS deposits.

In the Proterozoic and Phanerozoic terrains, lithogeochemistry is dependent on whether or not the felsic rocks were associated with juvenile or evolved environments. Most felsic host rocks of VMS from evolved terrains have elevated HFSE and REE contents and show FII to FIII signatures.

Some rocks in these evolved settings, particularly in continental rifts and continental back arc rifts show extremely elevated HFSE contents that are peralkaline in composition (Zr > 500ppm) (Dussel Bacon et al., 2004). It is assumed that like their Archean equivalents the felsic rocks in evolved settings represent high-temperature (>900°C) melting of crust within rift environments' (e.g. continental arc and back arc rifts) (Lentz,1998). The Zr and Nb contents of the Bhuyari deposit are similar to several Proterozoic VMS deposits like Finyalson, Avoca and Bathurst in Canada (Fig 4.5 a and b).

The relationship between felsic-volcanic geochemistry and VMS-formation is attributed to depth of partial melting and also source mineralogy in extensional tectonic settings (e.g. Hart et al., 2004; Gaboury and Pearson, 2008). The F1 magma is interpreted to have equilibrated with garnet-bearing residua at a depth of > 30 km, the FII magma with amphibole-plagioclase residua at 30 to 10 km, and the F111 magma with plagioclase-dominant, garnet-amphibole-free residua at < 15 km depth. The presence of plagioclase in the residuum is corroborated by the strong negative Eu anomaly shown by the Bhuyari rhyolite. Pronounced Eu anomalies can result from either partial melting with a plagioclase residuum, subsequent feldspar fractionation or a

combination of both processes (Lentz, 1998). Petrogenetic models proposed for the FIIIb rhyolites include formation by partial melting of granulite lower crust with fractionation producing higher silica contents; extreme fractional crystallization of tholeiitic mafic liquid resulting in liquid immiscibility with possible wall-rock contamination (Thurston and Fryer, 1983); higher temperature partial melting of crustal material with magma compositions controlled by differences in composition of crust (Lentz, 1998).

For rocks generated by melting of more evolved crust as is envisaged for the Proterozoic Bhuyari rhyolite, the trace element and REE budget could be a function of efficiency of melting of HFSE- and REE-enriched accessory phases rather than the depth of melt-generation (Pearce et al., 2008).

The relatively flat REE profiles, low Zr/Y and La/Yb_N ratios of the rhyolites at Bhuyari indicate lack of extensive hornblende fractionation, which are similar to tholeiitic to transitional-calc-alkaline sequences in extensional settings (Lentz, 1998). The close similarities of these ratios with those of the continental crust are indicative of a crustal source for the Bhuyari rhyolites.

The high SiO_2, HSFE and REE contents of the Bhuyari rhyolites broadly fits the definition of high-silica rhyolites of Barrie et al (1993) (>73% SiO_2, high HSFE and REE contents, flat REE profiles, negative Eu anomalies).

Field evidences for the high eruption temperatures and low volatile content of the FIII rhyolites of Bhuyari are present in the form of planar flow-banding, low-crystal contents and general absence of pyroclastics. Such high-temperature subaqeous felsic lavas tend to form flows rather than pyroclastics.

Low Zr/Y and (La/Yb)n ratios have been related to large degrees of melting and high zircon saturation temperatures indicative of high magma temperatures (Watson and Harrison, 1983; Barrie, 1995) or alternatively, melting at low pressures (Hart et al., 2004). Field and geochemical indicators are not supportive of fractional crystallization origin from basaltic magmas for the Bhuyari rhyolites. In Betul Belt, the large volume of felsic volcanics when compared to the mafic volcanic preclude the derivation of felsic melts by fractional crystallization of the mafic rocks. This is also consistent with the general absence of intermediate volcanic rocks in the stratigraphy.

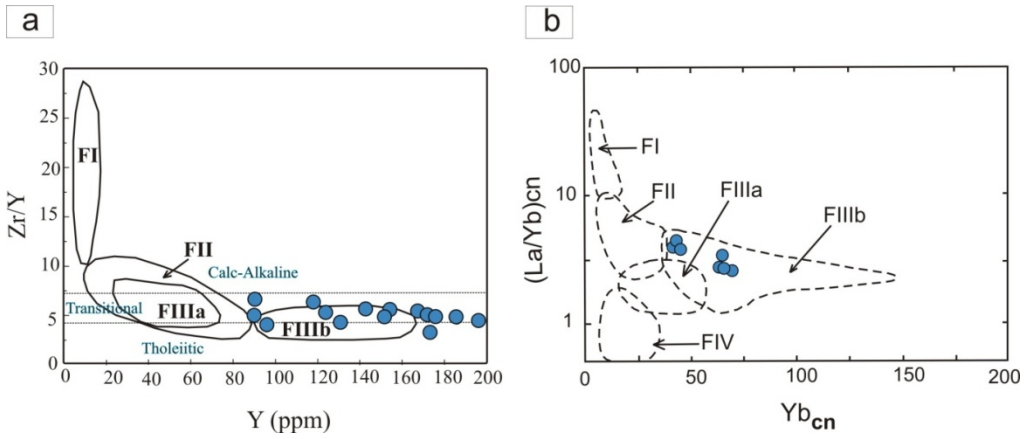

Fig.4.4. Rhyolite discrimination diagrams based on VMS-hosting potential **(a)** Zr/Y vs. Y diagram of Lesher et al (1986) as modified by Lentz (1998), with magmatic affinities based on Zr/Y ratios from the concepts of Barrett and MacLean (1999). **(b)** Chondrite-normalised plots of rhyolites from Bhuyari area in the $(La/Yb)_N$ versus Yb_N geochemical classification diagram of (Hart et al.2004). Normalizing factors from Nakamura (1974). In both the diagrams, the rhyolite samples plot well within the FIIIb field

4.8 Tectonic Setting

The rhyolites of Bhuyari have chemical characteristics consistent with a rifted continental margin setting. These include tholeiitic to transitional Zr/Y ratios of 3 to 7, $(La/Yb)_N$= 2 to 4 and high Zr contents of 380 to 912ppm. The higher Nb contents (21 to 39 ppm) are indicative of an interior continental rift setting rather than a setting close to a subduction zone.

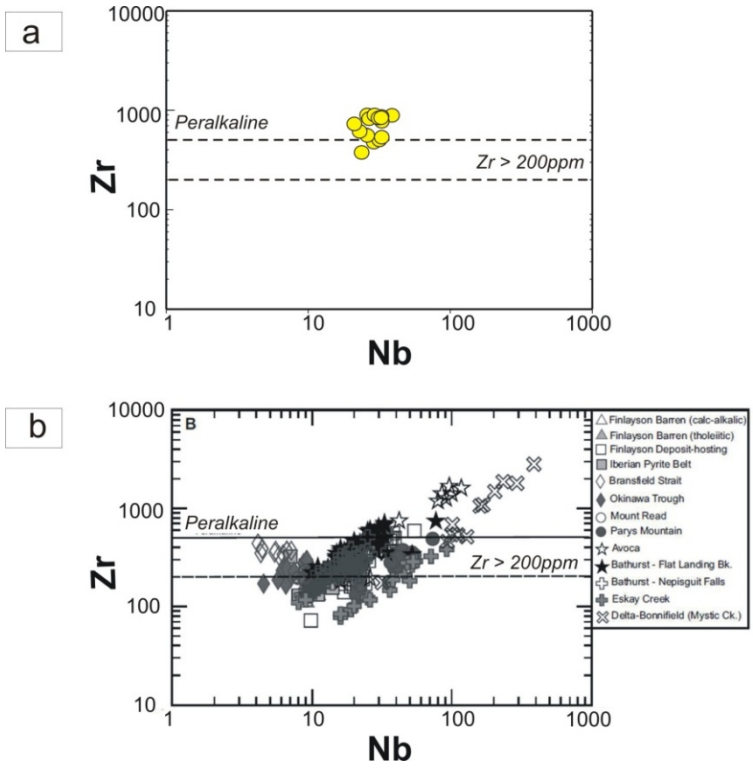

Fig.4.5. (a) Bhuyari rhyolites plotted in the Zr-Nb diagram showing similarities with rhyolites from other Proterozoic VMS deposits. **(b)** Zr-Nb diagram illustrating the HFSE variations in rhyolitic rocks associated with VMS environments (after Dussel Bacon et al, 2004). Note that the Bhuyari rhyolites are similar to the rhyolites hosting the Bathurst, Avoca and Finyalson VMS deposits.

To understand the tectonic setting of these rhyolites, they are plotted on several standard discrimination diagrams like the Rb vs. Y + Nb and Nb vs. Y

of Pearce et al, (1984) (Fig. 4.6a and 4.6b). The diagram which plot Rb against the sum of two incompatible elements (Fig. 4.6a), are designed to characterize the tectonic setting in which A-type granites are emplaced (Pearce et al., 1984). When plotted in these tectonic discrimination diagrams, the rhyolites have a consistent A-type, within-plate affinity (Fig.4.6a & b).

Trace element signatures and high Ga/Al ratios are similar to metaluminous A-type felsic rocks. When plotted in the Zr vs. Ga/Al and Nb vs. Ga/Al tectonic discrimination diagrams of Whalen et al (1987), all samples plots in the A-type granite field (Fig. 4.6c & d). These diagrams are useful to discriminate A-type granites from the I and S type granites. For further classification, the Rb/Nb versus Y/Nb diagram and the Y-Nb-Ga triangular diagram of Eby (1992) can be used (Fig. 4.6e and Fig. 4.6f). These diagrams subdivide A-Type granites into two classes; A-1, Mantle derived granites emplaced in an anorogenic setting and; A-2 granites, derived from the melting of continental or underplated mafic crust and emplaced in various tectonic environments. When plotted in these diagrams, the rhyolites fall in the A2 (crustally derived anorogenic granitoid) field (Fig. 4.6e & f).

Tholeiitic to transitional-calcalkaline magmatic affinity and within plate A-type characteristics are suggestive of a non-arc origin. The negative Ti (Ti/Ti^*= 0.03-0.08) and Nb([Nb/Th]n=0.1-0.2) anomalies are suggestive of an arc affinity. However, many workers have shown that such arc signatures like the negative Nb and Ti anomalies can arise due to remelting of arc-crust (Whalen et al., 1998; Morris et al., 2000) and/or fractionation of HSFE and Ti-enriched phases (Green and Pearson, 1987; Ryerson and Watson, 1987; Lentz, 1999). The negative Nb anomaly can also be inherited from the crust as the upper continental crust has a negative Nb anomaly on primitive mantle-normalized plots (Taylor and McLennan, 1985). Their metaluminous to peraluminous character, similarity to average continental crust and their within plate signatures are suggestive of low pressure partial melting of continental crust.

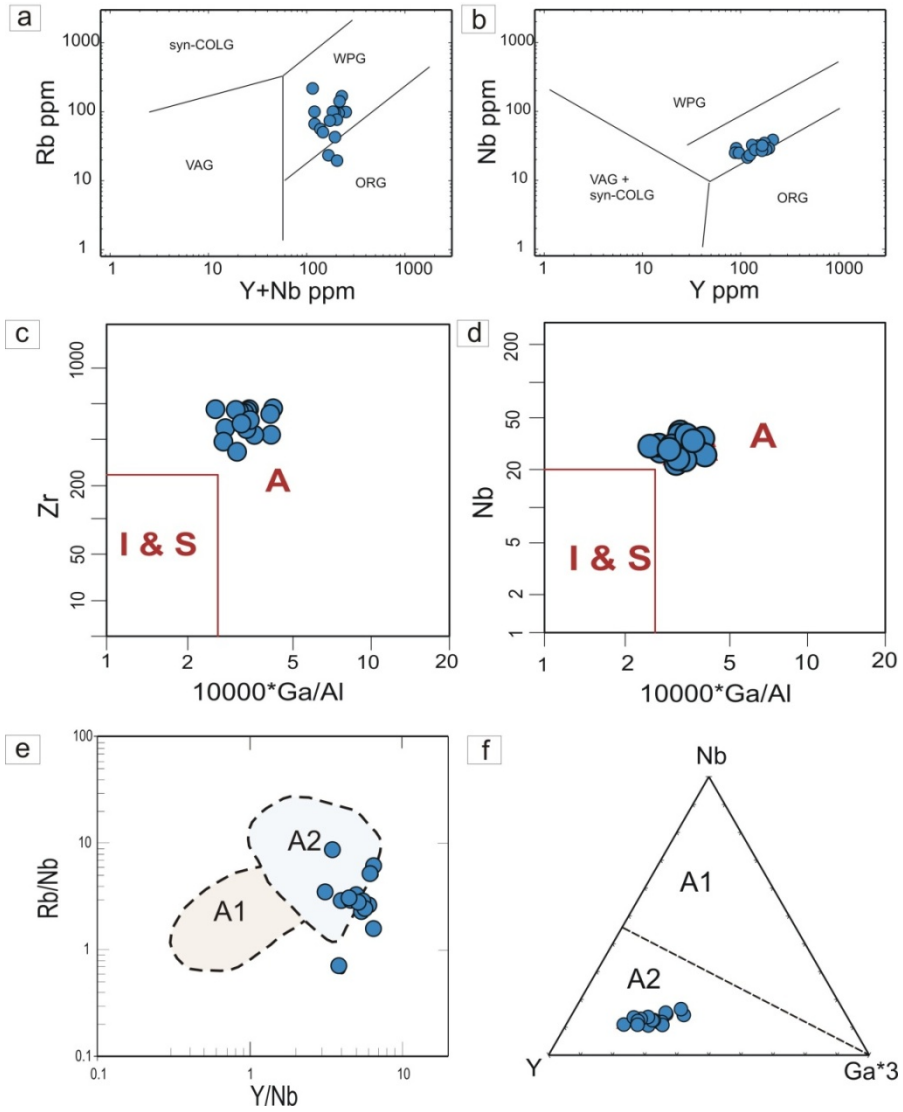

Fig.4.6. Tectonic discrimination diagrams of Pearce et al (1984) for granitoid rocks **(a)** Rb vs. Y+Nb plot **(b)** Nb vs. Y plot.
(c) and **(d)** Trace element discrimination diagrams for tectonic setup of granites **(c)** Zr vs. Ga/Al & (d) Nb vs. Ga/Al, all samples plots in the A-type granite field (Whalen et al., 1987).
(e) Rb/Nb versus Y/Nb diagram, A1, mantle derived and A2, crustal-derived granitoid rocks (Eby, 1992), **(f)** Y- Nb-Ga, trace element discrimination diagrams for tectonic setup of granites, A1=mantle-derived anorogenic granitoid rocks and A2=crustally derived anorogenic granitoid rocks (Eby, 1992).

Overall, the geochemical evidence shows that the rhyolites were emplaced in a within-plate anorogenic setting and were formed by partial melting of continental crust.

The vast domains of gneissic and migmatitic rocks representing the basement near the central and western part of Betul Belt are the likely source for these rhyolites. It is known that experimental melting of calc-alkaline granitoids at low pressures produce chemical characteristics similar to metaluminous A-type granites (Patino-Douce, 1997).

4.9 Discussion

The unaltered rhyolite show only minimum effects of alteration when plotted in the alteration box plot of Large et al (2001a). The rhyolite has high silica (> 72 wt. %) and FeO^T (1.1- 4.5 wt. %) contents and low Al_2O_3 (< 14 wt. %) and MgO (< 1%) contents. They show metaaluminous to peraluminous characters. Major and trace element discrimination plots show that they fall well within the rhyolite fields. The rhyolites also show transitional to tholeiitic magmatic affinities. Tholeiitic nature of the bimodal volcanics were assigned by earlier workers also (Raut and Mahakud, 2004; Praveen et al, 2007).

Rhyolite emplacement temperatures determined by zircon thermometry show that these are generated from high temperature melts (872-991°C).

Primitive mantle normalized trace element plots show high HFSE along with moderately negative Nb and strong negative Sr and Ti anomalies. Rhyolite classification plots based on VMS prospectivity show that they belong to FIIIb type which is considered highly prospective for VMS deposits (Lesher et al, 1986; Hart et al, 2004). The high SiO_2, HFSE and REE broadly fit the definition of high-silica rhyolite (Barrie et al, 1993).

Geochemistry of felsic volcanics have provided insights into tectonic settings and metallogenic evolution of host rocks for VMS deposits (eg., Lesher et al.1986; Barrie et al., 1993; Lentz, 1998,1999; Barrett and MacLean, 1999). The REE patterns of the Bhuyari rhyolite with deep, negative Eu anomalies and relatively flat and elevated LREE and HREE (Fig.8.B), display the 'seagull' pattern characteristic of hot-dry rhyolites occurring above areas of mantle upwelling (hotspots and continental rifts) (Glazner et al., 2008). In comparison, subduction zones are characterized by cold-wet-oxidised rhyolites with more U-shaped patterns that lack a pronounced europium anomaly because plagioclase crystallization is delayed in water-rich environments (Christiansen, 2005 and Christiansen and McCurry, 2008). Evidences for generation as a hot and dry rhyolite are seen in the observed high HFSE and REE contents and high zircon saturation temperatures. Abundant experimental and empirical work has shown that for felsic rocks the higher the temperature of melt generation, the greater the HSFE and REE content of the felsic melts (Watson and Harrison, 1983; Clemens et al., 1986; Skjerlie and Johnston, 1992; Bea, 1996; Watson, 1996; King et al, 2001).

The anomalously hot and dry rhyolites were generated by high heat flows by rapid ascend through the rifting process undergoing minimal fractional crystallization and forming high-level magma chambers. The pronounced strong negative Eu anomaly could be the result of plagioclase fractionation in the high-level magma chambers. The existence of such high-level crustal magma chambers in Precambrian basement rocks beneath the rhyolites along the Ethiopian rift was indicated by recently acquired geophysical findings (e.g. Keranen and Klemperer, 2008).

VMS deposits have formed throughout earth history right from the Archean to present day in extensional geodynamic regimes, and particularly in

rift environments (e.g. Piercey, 2009). These rift environments include mid-ocean ridges, back arc basins, intra-oceanic arc rifts, and continental arc rifts (e.g. Dussel Bacon et al, 2004; Barrett et al, 2001). Extensional settings are common to all tectonic environments where there is abundant volcanism (Cas and Wright, 1987).

It is possible that the Bhuyari rhyolites were emplaced in an extensional domain related to a continental arc setting, which could be a continental back-arc rift. This perhaps explains some of the 'arc-like' signatures like the negative Nb and Ti anomalies, which are likely inherited from the arc-magmatic source rocks.

Trace element characteristics show that the rhyolites have witin-plate, A-type affinities and more specifically belong to the A-2 type, which are the crustally-derived anorogenic sub-type. Recent studies on geochemistry of mafic volcanics and mafic intrusive of Betul Belt have suggested a continental margin arc setting (e.g. Ramachandra and Pal, 1992; Roy and Prasad, 2003; Roy et al., 2004; Chakraborty and Roy, 2012) or a rift-related tectonic setting for their emplacement (Alam et al., 2009; Mishra et al., 2011).

Bimodal volcanism is a common feature of rift-related tectonic environment worldwide (Wilson, 1989), in continental or oceanic arcs (Lentz, 1996) and are commonly associated with VMS mineralization (Lentz, 1998; Barrett and MacLean, 1999). An extensional setting provides heat to the near-surface environment for driving the hydrothermal convection, forms faults that would promote seawater circulation, and develop basins that may accumulate exhalative mineralization (e.g., Lentz, 1996).

The dominance of felsic metavolcanic rocks in this area argues against this unit being formed in a primitive, intra-oceanic island arc. Primitive intra-

oceanic arcs are characterized by tholeiitic, dominantly basaltic volcanism with only a small proportion of felsic volcanic rocks (e.g., Baker, 1968; Gill, 1981).

In Betul Belt, field relations of the bimodal volcanic rocks in spatial association with the gneiss-granitoid rocks are an indication for a continental basement/proximity for the bimodal volcanics (Fig.1.2). In the eastern Betul Belt, map-pattern and field evidence indicates that bimodal volcanism followed a prolonged period of felsic volcanism (Fig.1.3 and Fig. 2.2a). Felsic volcanism preceding mafic volcanism is a typical feature of back-arc rifts (Wilson, 1989). In such cases, the early crustal melts are felsic and generally peraluminous with A-type signatures and their generation can act as mid-crustal barriers to the ascent of co-magmatic mantle-derived mafic magmas (Pankhurst et al., 1998). A back-arc basin can be envisaged to have developed in a zone of convergence between the Bundelkhand craton in the north and the Bastar craton in the south during the early Proterozoic.

The volcanism in Betul Belt can be envisaged to have proceeded initially as rhyolites generated by melting of mid-crustal arc basement, which resulted in the generation of high-silica rhyolites with high HFSE and REE contents. This was followed by progressive widening of the rift and generation of tholeiitic basalts. After the basaltic volcanism the basin became shallower and received clastic sedimentary rocks represented by the shale and phyllite of the younger metasedimentary rocks.

******

Chapter 5

GEOCHEMISTRY OF ALTERATION ZONES

Contents

5.1 Introduction
5.2 Sampling and Analysis
5.3 Results
5.4 Summary and Interpretation of REE in Altered Rocks
5.5 Geochemical Proximity Indicators to Mineralized Zone
5.6 Discussion
5.7 Carbon and Oxygen Isotope Studies of Carbonates

5.1 Introduction

Recognition of mineralogical and chemical attributes of the alteration zones is very important in understanding the genesis of VMS deposits. As the alteration zones commonly are much larger than the deposits themselves, they may be recognized in the field and thus be a highly significant exploration guide (Franklin et al. 1981). The intense hydrothermal alteration of the footwall of some VMS deposits may be associated with significant changes in the mass of mobile chemical components (eg. Barrett and MacLean, 1991, 1994b; Barrett et al., 1993).

There has long been a question mark on the status of biotite-garnet-staurolite-gahnite and the anthophyllite and tremolite-bearing rock types associated with base-metal deposits in Betul belt. Earlier workers have suggested that the anthophyllite-cummingtonite-grunerite schists could represent altered ultramafic rocks. Similarly, the biotite-garnet-staurolite-gahnite schists hosting sulphide mineralization in Betul Belt have been classified as metasedimentary rocks as well as metasedimentary-tuff intercalations (e.g. Mahakud et al, 2000, 2001 and Raut and Mahakud, 2004).

Later workers have suggested that that these assemblages could represent intensely altered felsic volcanic rock (Praveen et al, 2005; Ghosh et al, 2006; Golani et al, 2006, Praveen et al, 2007). However, detailed geochemical studies have not been carried out so far to convincingly demonstrate that the protolith of these rock types have a felsic volcanic origin.

The objectives of the work presented in this Chapter are to geochemically characterize the various metamorphosed alteration zones around Bhuyari already identified by alteration facies mapping (Fig. 2.2b). Here an attempt is made to compare the major, trace and REE contents in metamorphosed alteration zones to those of the unaltered rhyolites, to assess the enrichment and depletion patterns of major, trace and REE in different alteration zones with respect to least altered rhyolite, to understand the alteration trends in the altered rocks and to identify geochemical proximity indicators to mineralization. Also, carbon and oxygen isotopic studies of the tremolite-carbonate rocks are carried out to understand the origin of hydrothermal fluids responsible for alteration. Through detailed geochemistry, it is also aimed to understand the nature of the protolith of these highly altered rocks.

The above-mentioned objectives are met by detailed study of major, trace and REE geochemistry of the representative alteration zones. These results are then assessed and interpreted by comparing among various alteration zones and also to the unaltered rocks described in the previous chapter.

Volcanogenic massive sulphide (VMS) deposits have petrologically distinctive alteration zones that underlie (footwall alteration) and sometimes overlie (hanging wall alteration) mineralized zones. These are produced by the reaction of the ore-forming fluids with the wall rocks. Hydrothermal alteration of footwall rocks is a diagnostic feature of VMS deposits (Franklin et al. 1981, Lydon 1984). Footwall alteration in VMS systems can be broadly classified as of two major types ie. a) discordant footwall alteration pipes, comprising of funnel shaped or carrot shaped zones associated with copper-bearing stringer

mineralization which exists immediately below the massive sulphides and b) stratabound or semiconformable footwall alteration which occur immediately adjacent to the ore horizon. Various types of hydrothermal alteration have been recognized in submarine volcanic terranes in Australia, North America, Japan and Europe and its mineralogy and geochemistry have been well-constrained. Large et al (2001c) have given a detailed classification of the various kinds of hydrothermal alteration zones associated with VMS deposits.

Alteration pipes are generally mineralogically zoned with a chlorite rich core surrounded by a sericite rich shell in many Cu-Zn deposits like that of Noranda in Canada. Zonation from sericite-rich alteration assemblages to more chlorite-or quartz-rich alteration has been recognized as an empirical vector towards the center of the hydrothermal system associated with VMS deposits (e.g., Sangster, 1972; Lydon, 1984). Chlorite-rich alteration is more common close to copper-rich ores, such as the Archean Noranda-type Cu-Zn deposits (eg., Franklin et al, 1981; Franklin,1995). The highly chloritised zones are generally converted to anthophyllite in metamorphosed deposits as in the Millenbach mine in Noranda, Canada (Franklin et al.1981).

Three distinct alteration zones have been identified and mapped within the least altered rhyolite (Fig. 2.2b). The metamorphosed alteration system is zoned with a high-Mg core represented by biotite-phlogopite-garnet bearing rocks which are enveloped by potassic-rich envelop characterized by muscovite-K feldspar bearing rocks. Tremolite-carbonate rocks occur as pockets in three discrete outcrops close to the massive sulphide lenses (Fig. 2.2b).

5.2 Sampling and Analysis

Sampling from alteration zones were carried out following the method outlined by Piercey (2009). According to the methodology of Piercey (2009), sampling to understand alteration is fundamentally different from petrochemistry. In the later we are interested in the primary lithogeochemical

attributes of the rocks, whereas alteration lithogeochemistry involves understanding the distribution of mobile elements. The first step is to identify and sample a suite of representative least altered samples. The samples could be the same samples as used for petrochemistry and provide a background against which all other altered samples are compared. Altered rocks were sampled as a function of alteration and alteration intensity. A reasonable degree of spatial coverage is also to be maintained while collecting samples.

A total of 35 samples of representative altered rhyolites were collected from representative alteration types/zones and analyzed for assessing the behavior of major and trace elements during hydrothermal alteration. The analytical procedures and equipment involved are the same as described in previous chapter (section 4.3).

The representative samples from different alteration zones were collected as follows:

1. Quartz-muscovite-K feldspar ± garnet schist (K-altered) : 7 samples
2. Quartz- phlogopite ± chlorite ± plagioclase ± garnet ± staurolite ± gahnite rock (Mg- altered) : 13 samples
3. Tremolite ± actinolite ± carbonate ± talc ± garnet ± quartz rock (Ca-Mg altered): 5 samples

5.3 Results

The analytical results data show that there exist large variations in the major elements of the altered rocks (muscovite-K-feldspar bearing schists, biotite-phlogopite-garnet bearing schist and the tremolite-carbonate rocks) (Table 5.1 to 5.4). The highest variations are shown by SiO_2 contents which vary from 44 to 83 wt. %, CaO from 0.02 to 7.84 wt. %, MgO from 0.37 to 18.02 wt. % and K_2O from 2 to 8 wt. %. The major and trace element data are plotted in various diagrams to show that the muscovite-K-feldspar bearing

schists and biotite-phlogopite-garnet bearing schists represent hydrothermally altered rhyolite. The tremolite-carbonate rocks may have alternate origins.

Table: 5.1 Major and trace element analyses of biotite-phlogopite-garnet bearing rocks (Mg-altered) around Bhuyari prospect

Sr.No.	1	2	3	4	5	6	7
Sample No	PBB-14	PBS-19	PBS-20	PBS-25	PBS-31	PBS-34	PBS-35
Alteration Type	Mg	Mg	Mg	Mg	Mg	Mg	Mg
SiO2	43.94	76.30	61.97	54.35	74.42	71.66	71.78
TiO2	0.24	0.15	0.21	0.21	0.16	0.19	0.34
Al2O3	16.12	12.00	16.32	18.64	7.98	11.13	10.93
MnO	1.57	0.15	0.37	0.92	0.19	0.30	0.25
Fe2O3	3.04	3.13	5.90	5.14	4.07	2.57	3.41
CaO	7.84	0.04	0.04	0.15	0.04	0.52	0.22
MgO	18.02	3.04	6.76	11.07	6.05	5.69	4.21
Na2O	0.53	0.25	0.33	0.53	0.52	1.79	0.64
K2O	4.18	2.06	4.62	4.06	3.21	4.96	7.20
P2O5	0.00	0.01	0.01	0.03	0.01	0.00	0.03
Total	95.48	97.13	96.53	95.10	96.65	98.81	99.01
Co	1	6	10	3	8	4	5
Cu	0	18	105	22	5	10	0
Zn	2971	3455	2884	7358	22551	582	178
Ga	45	21	35	34	23	15	13
Rb	127	97	128	84	106	162	155
Sr	68	2	4	0	2	19	29
Y	0	36	109	139	132	136	127
Zr	429	430	658	373	515	484	796
Nb	0	21	26	28	19	33	21
Ba	771	423	1269	886	406	873	1442
Pb	157	421	558	101	597	402	628
Alt Index	73	95	97	96	94	82	93
CCPI	82	72	71	77	72	54	48

Table: 5.2 Major and trace element analyses of biotite-phlogopite-garnet bearing rocks (Mg- altered) around Bhuyari prospect

Sr.No.	8	9	10	11	12	13
Sample No	PBS-37	PBS-43	PBS-45	PBS-48	PBS-49	PBS-50
Alteration Type	Mg	Mg	Mg	Mg	Mg	Mg
SiO2	73.90	50.90	69.40	64.31	67.19	69.30
TiO2	0.26	0.32	0.16	0.23	0.18	0.19
Al2O3	8.92	14.32	7.69	10.95	11.20	12.77
MnO	0.30	0.83	0.98	1.97	0.40	0.38
Fe2O3	4.16	5.07	8.08	4.65	2.92	2.99
CaO	0.27	0.58	0.15	0.88	0.80	0.04
MgO	4.67	17.23	7.34	10.09	9.30	6.63
Na2O	0.73	1.44	0.17	1.08	1.25	0.25
K2O	5.35	6.99	4.85	4.10	4.89	5.63
P2O5	0.03	0.01	0.01	0.00	0.01	0.00
Total	98.59	97.69	98.83	98.26	98.14	98.18
Co	7	1	15	0	5	5
Cu	17	16	3	18	9	10
Zn	816	6612	1470	5125	220	705
Ga	14	35	20	11	23	17
Rb	159	318	129	174	144	161
Sr	20	62	3	67	27	2
Y	93	176	141	138	217	118
Zr	672	383	303	268	453	469
Nb	21	47	13	36	38	29
Ba	1008	512	435	329	672	975
Pb	289	141	51	1490	54	825
Alt Index	91	92	97	88	87	98
CCPI	58	72	74	73	66	61

Table: 5.3 Major and trace element analyses of quartz-muscovite-K-feldspar altered rhyolite (potassic-altered) around Bhuyari prospect

Sr.No.	1	2	3	4	5	6	7
Sample No	PBR-24	PBR-32	PBS-22	PBS-46	PBR-36	PBS-2	PBR-9
Alteration Type	K	K	K	K	K	K	K
SiO2	83.27	78.08	85.21	74.87	80.73	71.84	72.55
TiO2	0.11	0.16	0.13	0.13	0.27	0.38	0.31
Al2O3	7.78	10.64	8.25	12.14	10.50	11.18	11.73
MnO	0.06	0.01	0.25	0.09	0.05	0.55	0.09
Fe2O3	1.56	0.98	1.32	2.11	1.73	4.22	3.29
CaO	0.42	0.01	0.04	0.11	0.02	0.15	0.44
MgO	0.45	0.15	0.82	0.74	0.15	2.30	0.37
Na2O	1.59	0.42	0.11	0.92	0.69	0.52	1.39
K2O	4.19	8.76	2.51	8.07	7.59	6.92	7.58
P2O5	0.01	0.02	0.02	0.01	0.05	0.06	0.04
Total	99.42	99.21	98.66	99.19	101.78	98.12	97.79
Co	0	0	3	3	0	0	0
Cu	9	15	21	9	244	61	3
Zn	277	22	86	65	21	629	602
Ga	16	15	17	21	11	17	16
Rb	67	151	97	109	96	117	166
Sr	19	25	2	25	25	19	34
Y	129	40	0	151	52	124	197
Zr	340	447	110	427	718	882	902
Nb	20	19	5	31	19	22	29
Ba	170	110	379	1787	110	130	1800
Pb	33	54	170	35	367	422	128
Alt Index	69.75	95.46	95.69	89.53	91.65	93.18	81.30
CCPI	24.27	10.17	43.40	22.71	17.11	45.03	27.13

Table: 5.4 Major and trace element analyses of tremolite-carbonate rocks around Bhuyari prospect.

Sr.No.	1	2	3	4	5
Sample No	PBA-18	PBC-5	PBC-16	PBC-4	PBC-10
Alteration Type	Ca-Mg	Ca-Mg	Ca-Mg	Ca-Mg	Ca-Mg
SiO2	53.61	51.13	58.83	56.19	55.24
TiO2	0.09	0.17	0.04	0.21	0.01
Al2O3	6.90	18.76	0.00	4.04	0.00
MnO	1.05	1.12	0.79	1.99	0.65
Fe2O3	3.49	1.76	1.23	3.45	1.14
CaO	12.76	13.99	13.43	14.55	11.49
MgO	16.32	7.76	23.13	15.85	25.68
Na2O	0.82	1.53	0.12	0.62	0.17
K2O	1.20	0.94	0.00	0.18	0.00
P2O5	0.02	0.09	0.01	0.02	0.02
Total	96.27	97.25	97.58	97.10	94.40
Co	5	2	1	4	1
Cu	133	255	27	87	833
Zn	4900	2135	360	3721	817
Ga	0	22	0	9	0
Rb	105	98	99	102	98
Sr	22	167	2	45	2
Y	0	189	0	155	0
Zr	736	78	21	142	24
Nb	0	23	0	25	0
Ba	363	142	0	0	9
Pb	8687	1275	206	449	10851
Alt Index	56.34	35.92	63.06	51.38	68.77
CCPI	90.60	79.10	99.51	95.95	99.37

5.3.1 Alteration Trends

Hydrothermal alteration trends during VMS alteration has been classified by Large et al (2001a) and is described in Fig. 5.1a. The altered samples were

plotted along with the unaltered samples in the alteration box plot to understand the alteration trends from unaltered to altered samples (Fig. 5.1b). The least altered rhyolite data is given in Tables 4.1 and 4.2 (Chapter 4), these data are plotted in various diagrams along with the altered samples for comparison.

The least altered rhyolites from Bhuyari plot within the Field-1 bounded by Alteration Index (AI) 20 to 65 and Chlorite Carbonate Pyrite Index (CCPI) 10 to 45 (Fig. 5.1b). The intensely altered rhyolites mostly have alteration indices above 80.

The samples of biotite - phlogopite ± garnet rocks plot well within the strongly altered footwall field which generally is characterized by chlorite. They plot along a well defined trend from the sericite node towards the chlorite node. They plot between AI 80 to 100, and have CCPI between 40 to 80 and plot in Field-3 representing the strongly altered footwall chlorite-sericite. These samples plot towards the ore centre and therefore represent proximal footwall altered assemblages (Fig. 5.1b).

The samples of muscovite-K-feldspar altered rhyolites show a distinct trend from the unaltered field towards the K-feldspar node in the lower right corner of the box plot. The potassic altered rhyolite represented by muscovite-K feldspar rocks is bounded by AI 80 to 95 and CCPI from 10 to 50. Petrography of these samples reveals presence of K-feldspar and muscovite. Two potassic altered samples also plot near the sericite node and towards the chlorite field. These are quartz-muscovite-biotite schist which represents intensely altered rhyolite. The tremolite carbonate samples plot above the unaltered rhyolite box and towards the upper part of the box plot (Fig. 5.1b). The tremolite-carbonate samples plot near the Field 4 which represent the carbonate altered field.

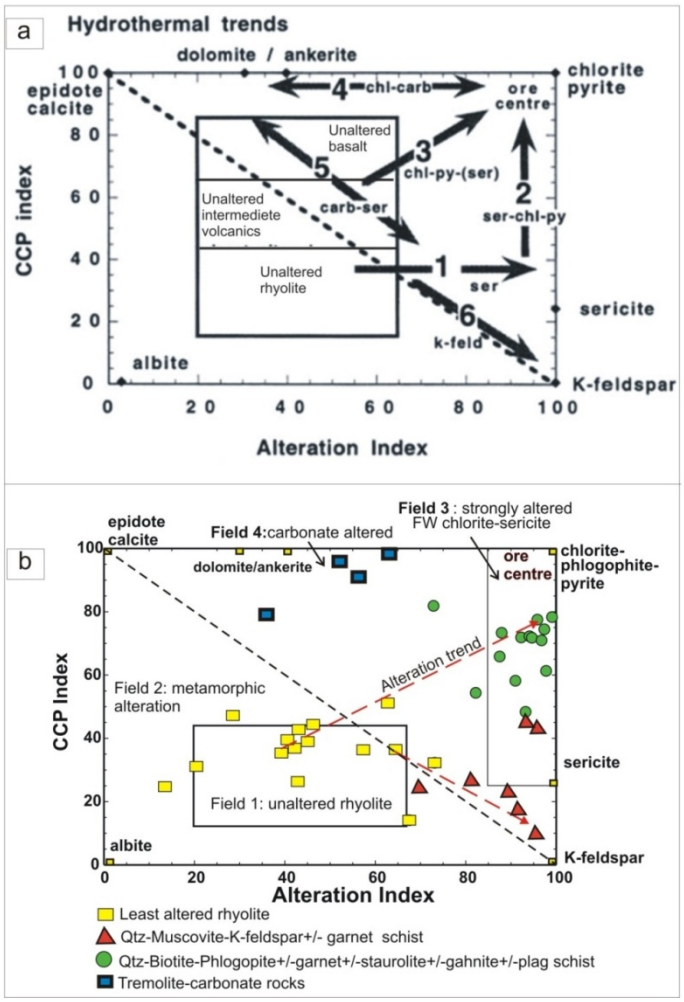

Fig. 5.1. **(a)** Hydrothermal alteration trends commonly observed in VMS deposits (Large et al, 2001a). *Trend 1:* Weak sericite alteration at the margins of a hydrothermal system in felsic volcanic host rocks, *Trend 2:* Intense sericite-chlorite ± pyrite alteration typical of the proximal footwall alteration, *Trend 3:* Chlorite ± sericite ± pyrite alteration typical of chlorite-dominated footwall alteration, *Trend 4:* Chlorite-carbonate alteration typically developed immediately adjacent to massive sulfide lenses in a footwall position, *Trend 5:* Sericite-carbonate alteration—immediate hanging wall to massive sulfide or along the favorable stratigraphic host unit, *Trend 6:* K feldspar-sericite - an uncommon trend developed locally within felsic footwall volcanics.

(b) The samples when plotted in the Alteration Box Plot (Large et al. 2001a) shows three clear trends: (1) Chlorite ± sericite ± pyrite alteration trend (2) K-feldspar-sericite trend and 3. Sericite-chlorite ± pyrite alteration.

Three distinct hydrothermal alteration trends are evident, which relates to the trends described by Large et al (2001a) in Figure (5.1a).

1. Trend 1, Chlorite ± sericite ± pyrite trend typical of chlorite dominated footwall alteration (Trend 3 in Fig.5.5a)
2. Trend 2, Intense sericite-chlorite ± pyrite alteration typical of proximal footwall alteration systems in VMS deposits (Trend 2 in Fig.5.5a).
3. Trend 3, K-feldspar-sericite trend-an uncommon trend developed locally within felsic footwall volcanic (Trend 6 in Fig.5.5a)

The trends 1 (chlorite ± sericite ± pyrite) and trend-2 (sericite-chlorite ± pyrite) are common in VMS systems and represent intense footwall hydrothermal alterations. However, the trend-3 (K-feldspar-sericite alteration) appears to be a uncommon alteration trend (Large et al, 2001a). This K-feldspar-sericite trend represents intense potassic alteration and is present in the Thalanga Zn-Pb-Cu deposit in Australia (Paulick et al, 2001).

There is also a weak chlorite-carbonate trend displayed by the tremolite-carbonate rocks. Although there are no field evidences for considering the tremolite-carbonate rocks as altered volcanics, such rocks have been known to have formed by carbonate alteration in some VMS deposits (e.g. Herrmann and Hill, 2001). The tremolite-carbonate rocks fall near the carbonate altered field in the alteration box plot (Fig.5.1b).

The hydrothermal alteration paragenesis at Bhuyari shows that initial alteration by sericite and quartz was later superimposed by pervasive fracture-controlled magnesium–rich chlorite alteration which was perhaps followed by low-temperature carbonate-smectite alteration. The high-Mg alteration was associated with the formation of massive sulphides as these occur in the core zones of the hydrothermal system.

The whole rock data were also plotted in the Al_2O_3/Na_2O versus Na_2O diagram of Ruks et al (2006) to appreciate the Na-loss which accompanies footwall alteration zones from unaltered and weak hydrothermally altered zones (Fig. 5.2a).The plot shows that 12 of the 15 least altered rhyolite falls in the field of fresh to weakly altered rhyolite. Two samples plot in the Na-altered and 2 in the Na-loss fields. All samples of biotie - phlogopite ± plag ± garnet schists (13 numbers), muscovite - K feldspar ± garnet schists (7 numbers) and tremolite - carbonate rocks (5 numbers) plot in the Na-loss field.

This plot shows that all the altered samples have undergone significant Na-loss. This plot very clearly distinguishes the footwall hydrothermal alteration associated with the sulphide mineralization in Bhuyari. The whole rock data is plotted in the $MgO-Al_2O_3$-Alkali diagram (MacDonald et al, 1996) to understand how the geochemical data corroborates with the mineralogy of these rocks. The distribution of the data in the $MgO-Al_2O_3$-Alkali space shows that the least altered rhyolite forms a coherent bunch in-between the albite and muscovite nodes, showing varying degrees of sericite alteration (Fig.5.2b).

The potassic-altered samples also plot along with the least altered samples and near the muscovite node. The magnesium altered samples show a clear trend towards the biotite and phlogopite nodes which is consistent with the phlogopite-rich mineralogy in these rocks. The tremolite-carbonate rocks plot near the actinolite and tremolite nodes which very well match with the mineralogy of these rocks in which the major amphibole is tremolite followed by actinolite.

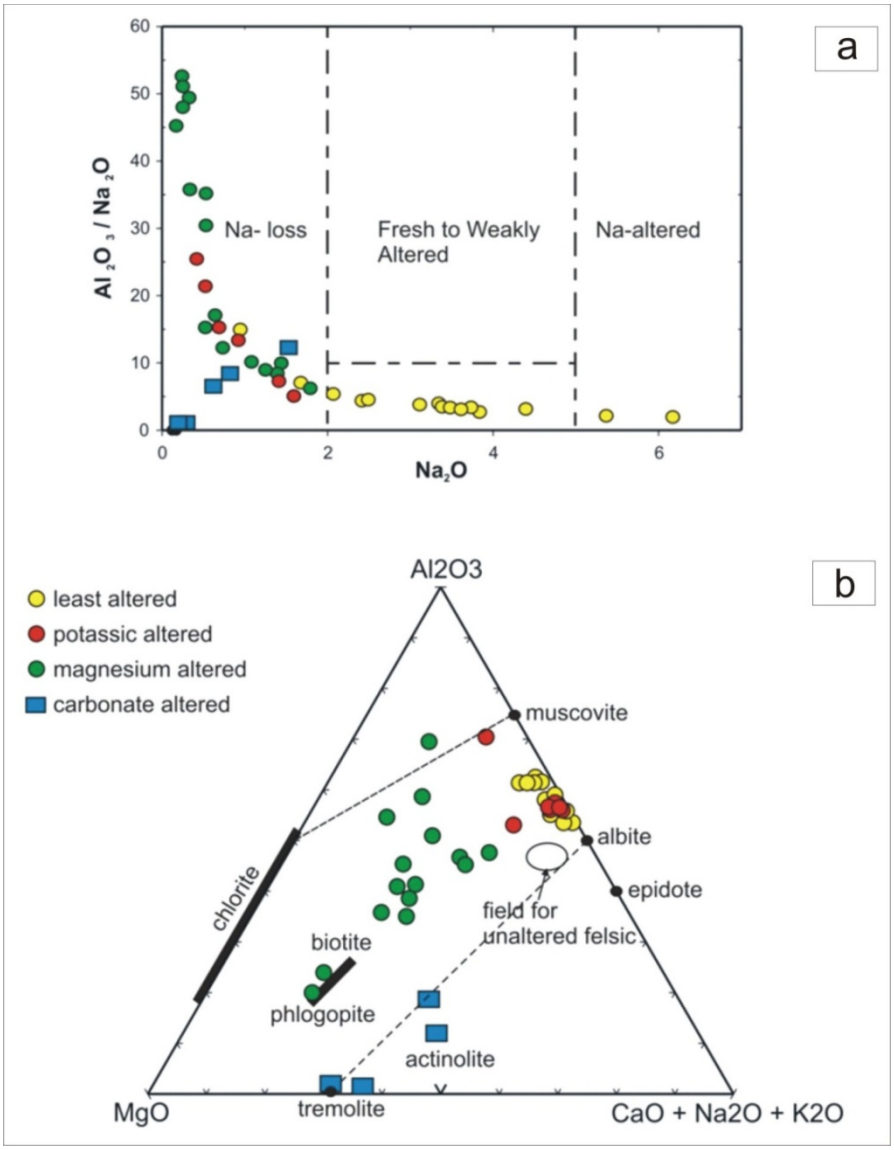

Fig. 5.2 a) Al_2O_3/Na_2O vs Na_2O plot for outlining fresh rock versus those with Na-gains (spillitised) and losses. Diagram from Ruks et al (2006). This diagram is useful for delineating semiconformable alteration (spillitization, Na gains) versus pipe-like alteration (Na-depletions).
b) Ternary plots of major element and normative mineral contents outlining volcanogenic massive sulphide –associated alteration- MgO-Al_2O_3-(CaO + Na_2O + K_2O) diagram with various mineral nodes (Diagram after MacDonald et al., 1996). The plot shows definite trends towards phlogopite, tremolite and muscovite. The field for unaltered felsic rocks is also shown.

5.3.2 Major and trace elements of alteration zones and relationship with AI

Major and trace elements show wide variations in the different alteration zones. To understand the behavior of various major and trace elements during hydrothermal alteration, the various types of altered rhyolites were studied with reference to their alteration index. Binary plots with the concentration of the various elements on the Y axis and the Alteration Index (AI) on the X axis is a convenient way to graphically represent and study the variations of the major and trace elements during hydrothermal alteration.

The major and trace element data are discussed in the previous chapter (Chapter-4). The least altered rhyolite data are also plotted in the binary plots using Alteration Index along with the altered rhyolite data for comparison (Fig.5.4 to 5.7). The least altered rhyolites show clear and systematic increase in the K_2O and corresponding depletion of Na_2O with increasing AI. Oxides like SiO_2 and Al_2O_3 show variable enrichments and depletion. However, MgO, Al_2O_3 and TiO_2 are relatively constant with increasing AI (Fig. 5.4)

Quartz-muscovite-K-feldspar ± garnet ± biotite schist.

The analytical data of this rock type is given in Table 5.3. These rocks have higher SiO_2 contents when compared to least altered rhyolites and range from 73 to 85 wt. % (average 78 wt. %). This may be to the effects of silicification which are noticed in these rhyolites in thin sections. This group has the highest enrichment in K_2O, which ranges from 2.5 to 8.7 wt. % (average, 6.5 wt.%), which indicates that these rocks have undergone potassic alteration. This is confirmed by petrographic studies which show higher sericite, biotite and K-feldspar contents in these samples. When compared to the least altered rhyolite, this group also posses higher MgO contents (up to

2.3 wt. %), MnO contents (up to 0.54 wt. %) and show depletions in Na_2O (< 1.6 wt. %) and CaO contents (<0.5 wt. %).

When plotted in the binary plots against AI, K_2O and Na_2O contents show systematic enrichments and depletions with increase in AI (Fig. 5.4). CaO maintains very low contents with increase in AI. Fe_2O_3 show significant increase with increase in AI which may be the result of presence of more pyrite in the altered rocks. Among trace elements, Ga, Zr, Nb and Rb do not show any significant effects due to increase in AI apart from minor perturbations in some samples. Sr and Y show significant depletion in a few samples with increase in AI. However, Zn, Pb and Cu show wide variations as is expected in altered samples.

Quartz-biotite-phlogopite ± plagioclase ± muscovite ± garnet schist

This group represents the most intensely altered rhyolites from Bhuyari area. The major and trace element analytical results of biotite-phlogopite-garnet bearing rocks are given in Table 5.1 and 5.2. Their SiO_2 contents show wide variation from 40 to 76 wt. % with an average value of 62 wt. %. It shows a general increase with increasing AI (Fig.5.3). There is wide variation in the Al_2O_3 contents which vary from 7.69 to 18.64 wt.% with an average value of 12.2 wt.%. The Al_2O_3 contents show extreme enrichment as well as depletion with high AI, which indicates that Al_2O_3 is highly mobile during intense hydrothermal alteration. These rocks are enriched in magnesium and their MgO contents vary widely from 3 to 18.04 (average 8.47 wt. %). As is seen from the MgO wt.% vs. AI diagram most of the samples with MgO contents (>5 wt.%) have very high alteration indices (AI 80 to 100) and the highest MgO contents corresponds to the samples with highest AI (Fig. 5.3). K_2O is highly variably enriched and ranges from 2 to 9.67 wt.% with an average value of 5.42 wt.%. Na_2O contents are quite low and depleted when

compared to least altered rhyolite. The Na_2O contents range from 0.17 to 1.79 wt. % (average 0.67 wt.%). MnO contents for this group is also relatively high when compared to least altered rhyolite and range from 0.15 to 1.97 wt.% (average 0.64 wt. %). Many of these samples also contain spessartine garnet which explains their higher MnO contents and the sample with the highest MnO contents (2 wt. %) is from the sample (PSS-48) containing higher proportion of spessartine garnet. This also shows that garnets are the chief manganese bearing mineral at Bhuyari. CaO contents are very low and range from 0.04 to 0.88, except one sample PBB-14, which has a high value of 7.84%, possibly due to presence of tremolite. Calcium bearing minerals are generally absent from this alteration type.

Among trace elements, Ga and Rb show increase with respect to higher AI, and they also show higher contents than the least altered and K-altered rock types. Strontium show extreme depletion in many samples with high AI. Zn, Cu and Pb show significant enrichment in most samples and show higher values with increasing AI, which is due to the presence of ore minerals in this rock (Fig.5.6 & 5.7). Ba and Zr show depletion in some samples with higher AI. The trace elements like Y, Nb and Zr remain relatively immobile in spite of intense alteration (Fig. 5.6 & 5.7).

In summary, the biotite-phlogopite bearing rocks show extreme enrichment of MgO contents (up to 18 wt. %), increase in MnO (up to 2 wt. %), higher K_2O contents and show depletion in their CaO contents (< 1 wt %) and Na_2O contents (< 2 wt %). Trace elements like Y, Nb and Zr remain relatively immobile during intense alteration. Strontium shows depletion with increasing AI.

Tremolite-Carbonate rocks

Since the tremolite-carbonate rocks may have formed partly by carbonate alteration of rhyolite and partly as precipitates on the seafloor from

hydrothermal vents (exhalites), it may be treated as an altered rock type for the sake of comparison.

The major and trace element analytical results 5 tremolite-carbonate rocks are given in Table 5.4. The tremolite carbonate rocks are mainly composed of SiO_2, MgO, CaO and Al_2O_3. Some carbonate-rich samples lack Al_2O_3. The very low contents of Al_2O_3 and TiO_2 suggest that these rocks may not represent altered rhyolite.

The SiO_2 contents range from 51.1 to 58.8 wt.% (average 55 wt.%). The MgO contents are high and range from 7.7 to 25.68 wt.%, (average 17.7 wt.%). All tremolite-carbonate rocks contain CaO more than 10 wt. % and range from 11.5 to 14.55 wt.% (average 13.25 wt.%) (Fig. 5.4). MnO show enrichment in some samples which is consistent with the higher contents of spessartine garnets. In the binary diagrams plotting major elements against AI, the only systematic trend is displayed by MgO which shows a positive correlation with AI.

Among trace elements, Rb remains constant with increase in AI. Sr shows a negative correlation with AI. Some samples of Y and Nb show immobility with increase in AI.

In summary, when compared to least altered rhyolite precursor, the tremolite-carbonate rocks show wide variations in major elements. They are highly enriched in MgO, CaO and MnO and depleted in Na_2O and CaO. Total depletion of Al_2O_3 is seen in a few carbonate-rich rocks. TiO_2 is also depleted. The increase in MgO and MnO and decrease in Na_2O are similar to those of other intensely altered rhyolites, however, very low Al_2O_3 and TiO_2 contents show that these rocks may not be related to rhyolite and may have alternate origins: for example as chemical precipitates on the seafloor.

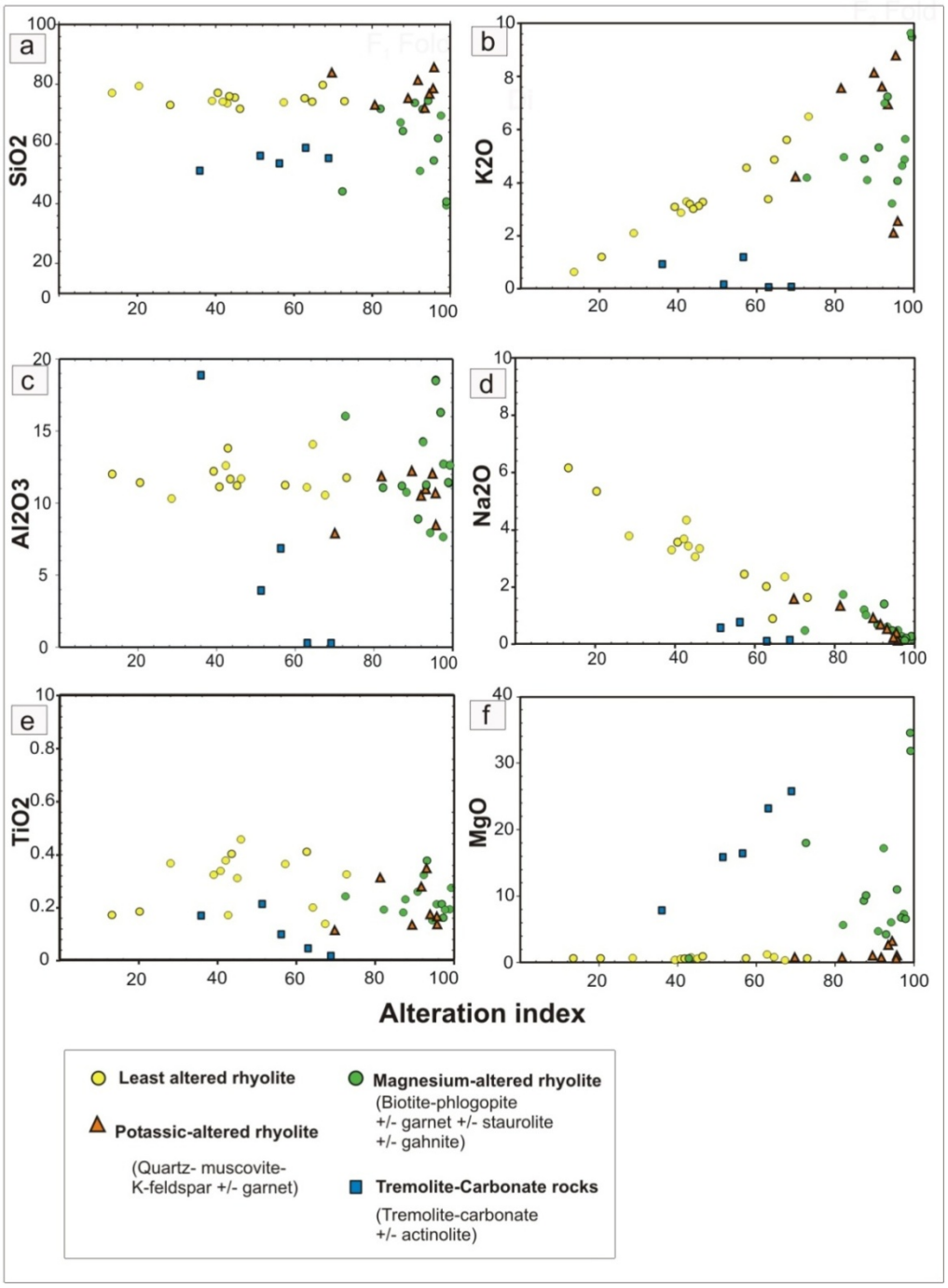

Fig.5.3 Plots showing major elements versus Alteration Index for the altered and least altered rhyolite and tremolite-carbonate rocks.

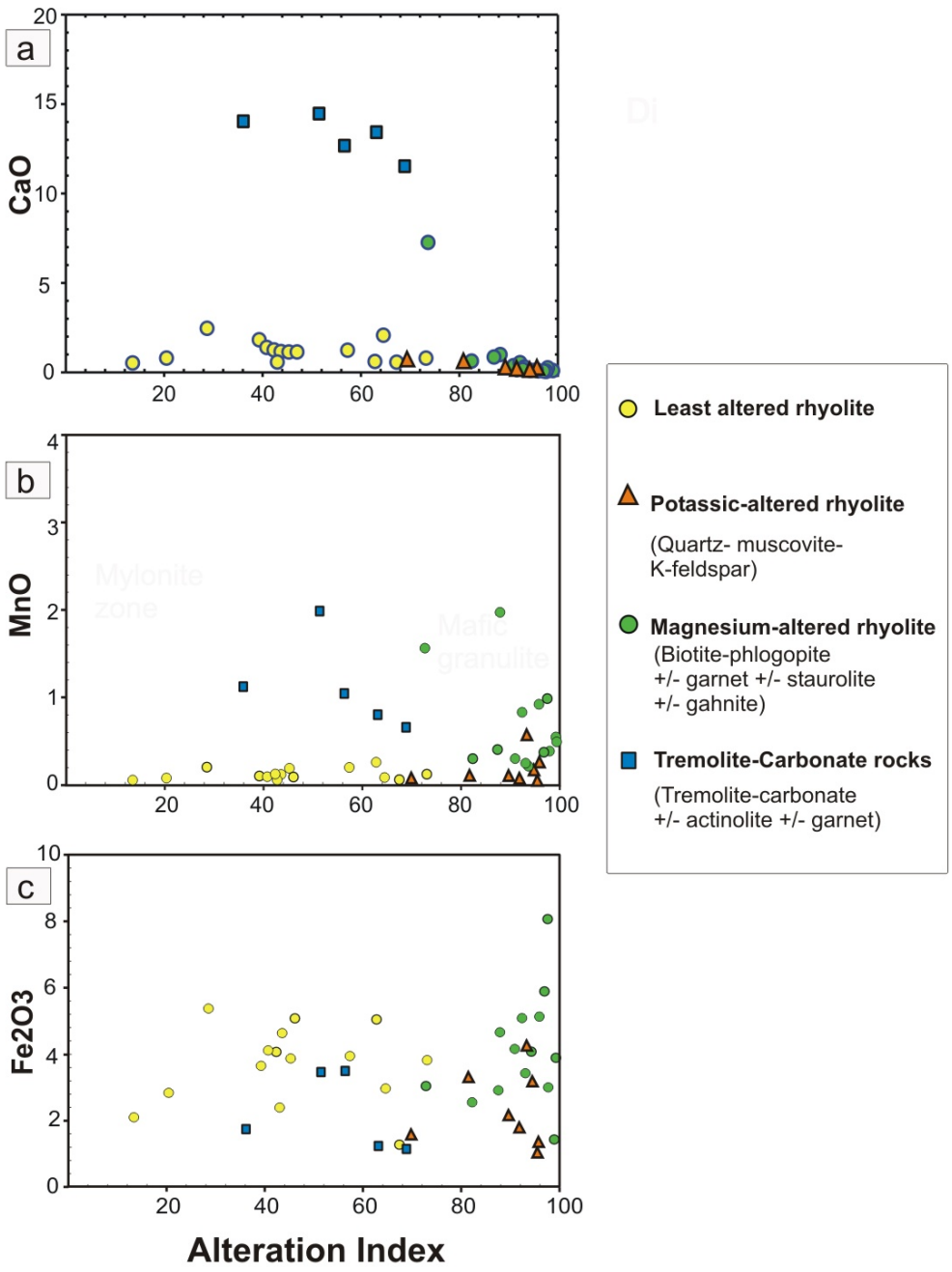

Fig 5.4 Plots showing major elements versus Alteration Index for the altered and least altered rhyolite and tremolite-carbonate rocks.

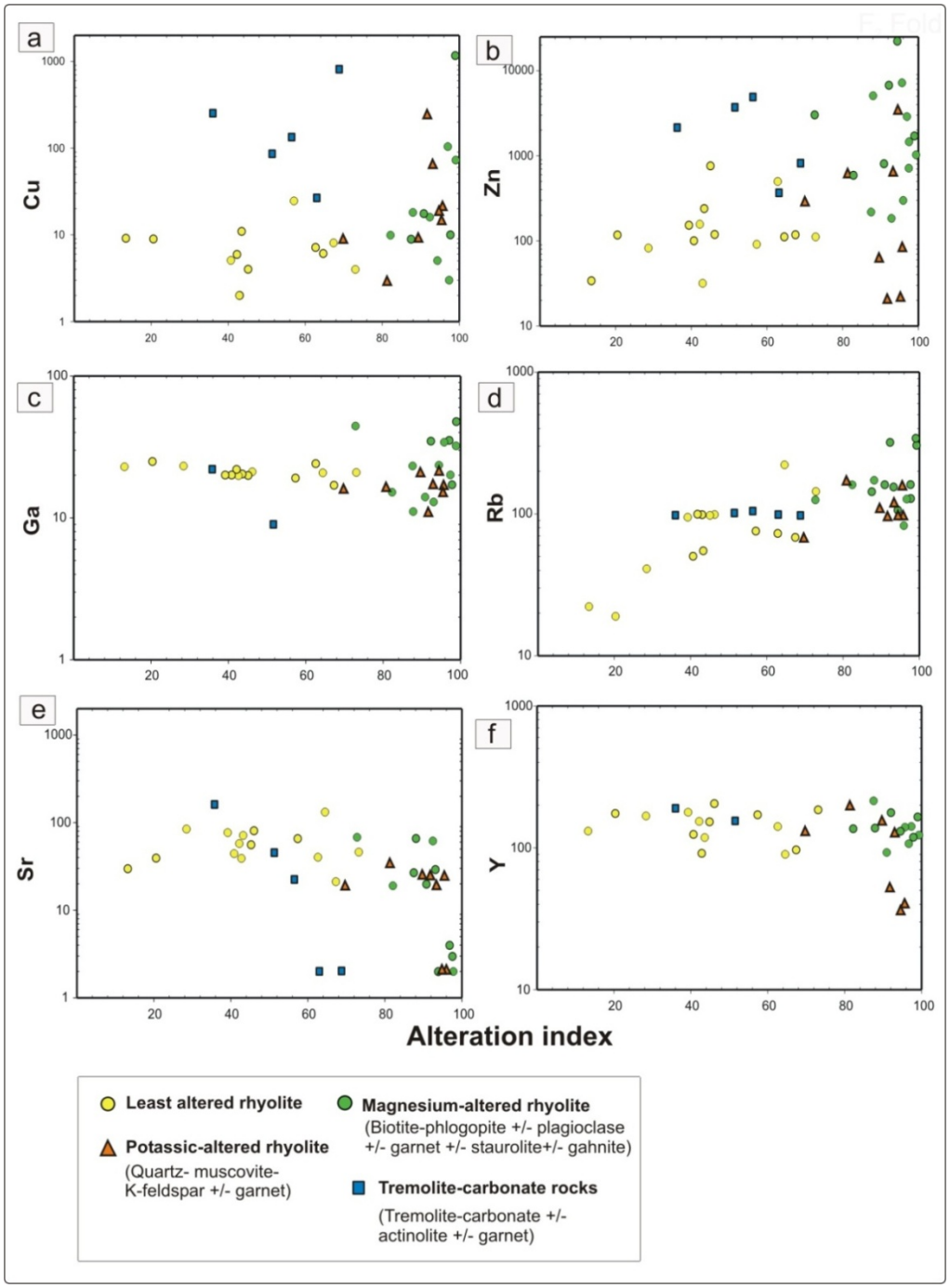

Fig. 5.5 Plots showing Trace elements versus Alteration Index for the altered and least altered rhyolite and tremolite-carbonate rocks.

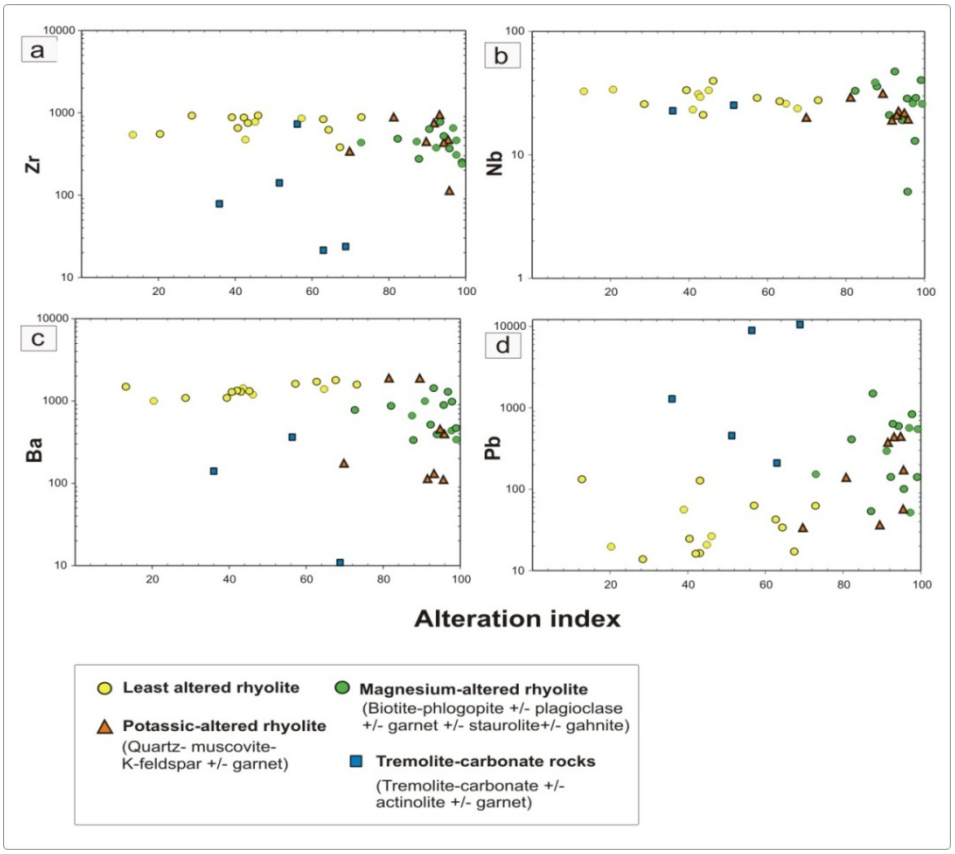

Fig.5.6 Plots showing Trace elements versus Alteration Index for the altered and least altered rhyolite and tremolite-carbonate rocks.

5.3.3 Relative enrichments and depletions of elements compared to unaltered rhyolite

Various methodologies have been used to identify precursor rocks in highly altered areas (e.g. MacLean and Barrett, 1993; Barrett and MacLean, 1994b; Barrett et al, 2001). A common method of dealing with hydrothermal alteration involves calculating gains and losses of mobile elements in altered samples relative to precursor samples. In some cases, the precursor is simply a least-altered sample thought to represent or approximate the pre-alteration composition of the altered samples. In still other cases, precursors are

calculated from fractionation curves which, in turn, are compiled from a series of least-altered samples.

In the present study, since there are unequivocal field and petrographic evidence for alteration of rhyolite, it is considered safe to assume that all the altered rock types in the area except perhaps the tremolite-carbonate rocks represent various forms of altered rhyolites. Therefore, the ideal way of generating the precursor composition will be to get the composition of the most unaltered rhyolite in the area.

In the present study, a total of 15 analyses of least altered rhyolite were available, out of which 8 samples were selected as the most ideal samples representing unaltered rhyolites and averaged to represent the precursor composition (Table 5.5). The 8 samples representing unaltered rhyolites were selected based on the following criteria:

a) They were collected from fresh outcrops showing primary volcanic textures like relict flow banding and quartz-phenocryst-groundmass relationships which can be identified in the field and by petrographic studies.

b) The major and trace element geochemistry show typical rhyolite composition.

c) These samples plot within the unaltered rhyolite field in the Alteration Box Plot of Large et al (2001a) (Fig 5.1b)

This precursor rhyolite therefore will have ideal major element and trace element composition. All other forms of altered rhyolite can then be compared against this precursor composition and relative mass gains and losses can be estimated. For understanding the relative changes in the major and trace elements in the altered rhyolites with respect to the unaltered

rhyolites, the major and trace element concentrations of different groups of altered rhyolites are compared with the unaltered rhyolite precursor. The other groups are normalized against the precursor rhyolite composition and can be visualized graphically (Fig.5.7).

Table 5.5. Relative percentage changes for major oxides (wt.%) and trace elements (ppm) for the three representative alteration types when compared to unaltered precursor rhyolite. (average compositions are recalculated to 100)

	n=8	n=13		n=7		n=4	
Alteration Type	**Unaltered rhyolite**	**Bt-phlo-Plg-Gt**	**Bt-phlo-Plg-Gt**	**Qtz-Mus-K-feld**	**Qtz-Mus-K-feld**	**Tre-Carb**	**Tre-Carb**
	Precursor composition		**% change**		**% change**		**% change**
SiO2	74.90	66.97	-11	78.73	5	56.61	-24
TiO2	0.34	0.22	-35	0.21	-38	0.13	-61
Al2O3	12.04	12.53	4	10.40	-14	7.65	-36
MnO	0.12	0.68	489	0.16	37	1.27	1007
Fe2O3	3.99	4.35	9	2.19	-45	2.56	-36
CaO	1.29	0.91	-29	0.17	-87	14.10	995
MgO	0.52	8.68	1580	0.72	39	16.25	3045
Na2O	3.46	0.75	-78	0.81	-76	0.80	-77
K2O	3.31	4.90	48	6.57	99	0.60	-82
P2O5	0.05	0.01	-76	0.03	-40	0.04	-24
Trace elements (ppm)							
Co	5.00	5.31	6	0.86	-83	3.00	-40
Cu	6.50	17.92	176	51.71	696	126	1831
Zn	207	4225	1941	243	17	2779	1243
Ga	20.25	23.54	16	16.14	-20	7.75	-62
Rb	84	150	79	115	37	101	21
Sr	61	23	-62	21	-65	59	-4
Y	149	120	-20	99	-34	86	-42
Zr	775	479	-38	547	-29	244	-68
Hf	12.72	23.99	89	14.46	14	3.88	-70
Nb	29.75	25.54	-14	20.71	-30	12	-60
Ta	1.99	1.42	-29	1.71	-14	11	452
Ba	1313	769	-41	641	-51	126	-90
Pb	44	440	910	173	297	2654	6002
Cs	0.27	1.24	361	0.36	36	0.20	-24

The major and trace element of different alteration groups are normalized against the precursor rhyolite and plotted as spiderogram to graphically view the relative enrichment and depletion during hydrothermal alteration (Fig.5.7a and b). This method is a simple way to quickly understand the behavior of major and trace elements in the three altered groups- 1. Biotite-phlogopite schists 2. Muscovite-K-feldspar schists and 3. Tremolite-carbonate rocks.

When the major and trace element data of different altered types are normalized against that of the unaltered precursor; they show wide variations in their major elements and trace elements (Fig. 5.7a and b). The spiderogram shows that the biotite-phlogopite samples show higher MnO and MgO and lower Na_2O, K_2O and CaO with respect to unaltered precursor (Fig. 5.7). The muscovite-K feldspar altered samples, show depletion of major elements when compared to the unaltered precursor. The tremolite-carbonate samples show high enrichment in MgO, CaO and MnO and depletion in all other major elements when compared to the unaltered precursor. The quartz-muscovite-schists show the strongest depletion of CaO among all groups (Fig. 5.7a). This plot also shows that the tremolite-carbonate rocks have the highest enrichment in MgO. It also shows that in all the groups SiO_2 and Al_2O_3 are the most inert and do not show major fluctuations. Among trace elements, Co, Zn, Pb, Cu and Ba behave in a highly mobile manner (Fig. 5.7b). The other trace elements like Ga, Rb, Sr, Y, Zr, Hf, Nb and Ta are relatively immobile with respect to least altered rhyolite precursor. This is shown by the relatively their relatively flat profile from Ga to Ta.

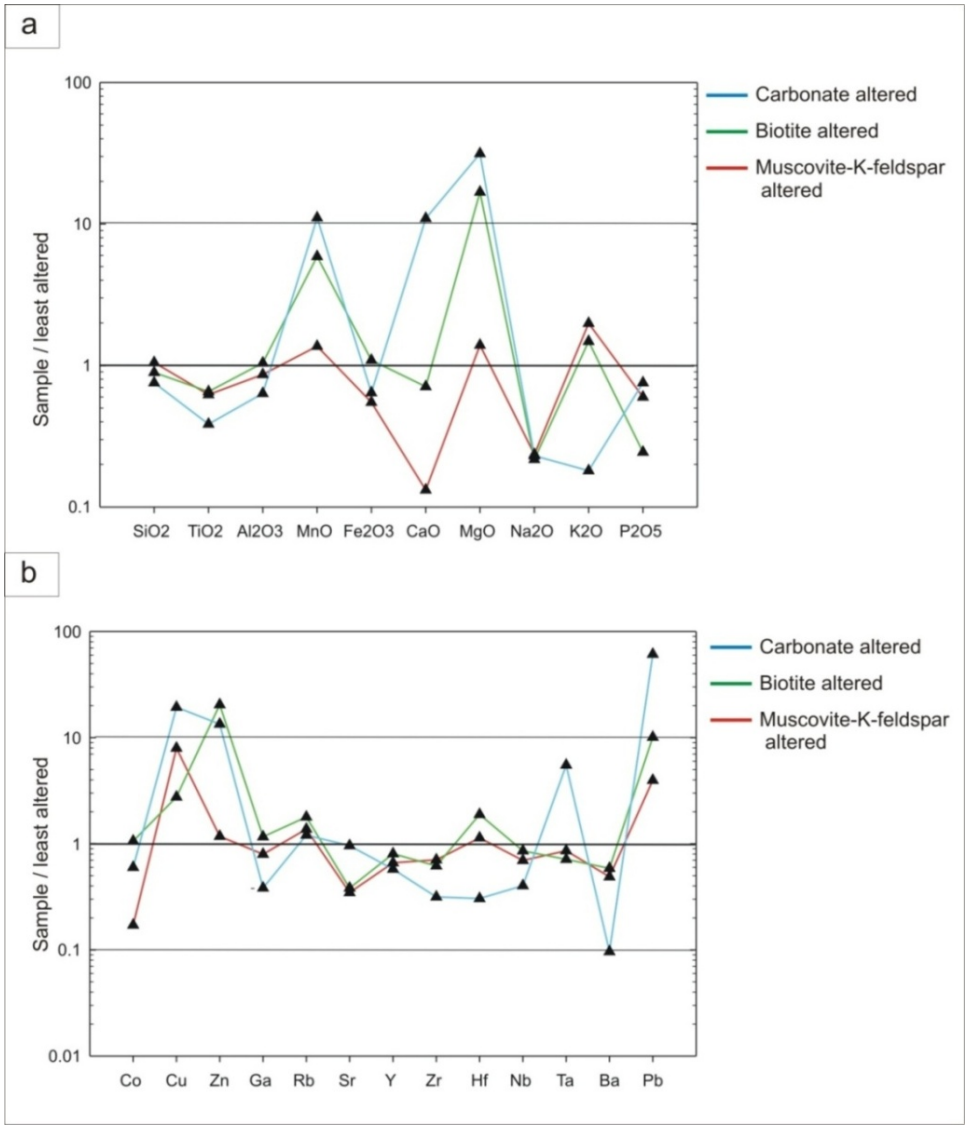

Fig. 5.7 The average values of representative alteration types including the tremolite-carbonate rocks are normalized against the least altered precursor rhyolite.

(**a)** Major elements of representative alteration types normalized against the least altered precursor rhyolite composition show high to very high MnO, MgO and K_2O enrichments, while there is severe depletion of CaO and Na_2O and marked depletion in TiO_2 contents. (**b)** Trace elements of representative alteration types normalized against least altered rhyolite show that they are relatively immobile except for Co, Cu, Zn Pb and Ba.

5.3.3.1 Relative percentage gains and losses

The average compositions of the various groups of altered rhyolites were estimated and compared with the composition of the precursor rhyolite (Table 5.5). The table shows the average compositions of the three major alteration types and the unaltered rhyolite.

The representative composition for the quartz- muscovite-k feldspar schist (potassic altered rhyolite) was derived by averaging 7 quartz- muscovite-k feldspar schist samples (Table 5.5). The average of 13 biotite-phlogopite bearing assemblage was calculate to represent the average composition of the Mg-rich alteration type. Four samples of tremolite carbonate rocks were averaged to represent this alteration type. The percentage gains and losses (compared to unaltered rhyolite) of major oxides and trace element for the three alteration types are then calculated and given in the same table (Table 5.5). Based on the relative percentage gains and losses in the altered rhyolites, bar charts were plotted for all three alteration type to graphically visualize the changes (Fig.5.8 to Fig. 5.10).

Quartz-Muscovite ± K feldspar ± garnet schist

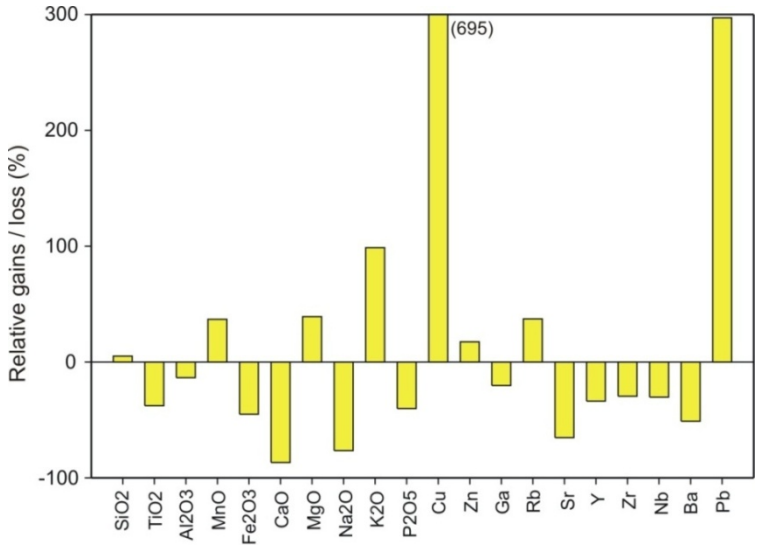

Fig.5.8 Relative percentage gains and losses for major and trace elements for quartz-muscovite-k feldspar schist (potassic altered rhyolite) with respect to least altered rhyolite precursor.

The quartz-muscovite-K feldspar schist show about 5% gain in SiO_2, 37% gain in MnO and 99 % gain in K_2O (Fig. 5.8). These rocks show very high losses of major oxides like CaO (-87%) and Na_2O (-76%) and high losses in TiO_2 (-38%), Al_2O_3 (-14%), Fe_2O_3 (-45%). Trace elements showing gains are copper (695%) zinc (+ 17%), rubidium (37%), lead (297%). Barium shows loss of about 51 %. There is also strong depletion in strontium (65 %).

Quartz-biotite-phlogopite ± garnet ± plagioclase ± staurolite ± gahnite schist

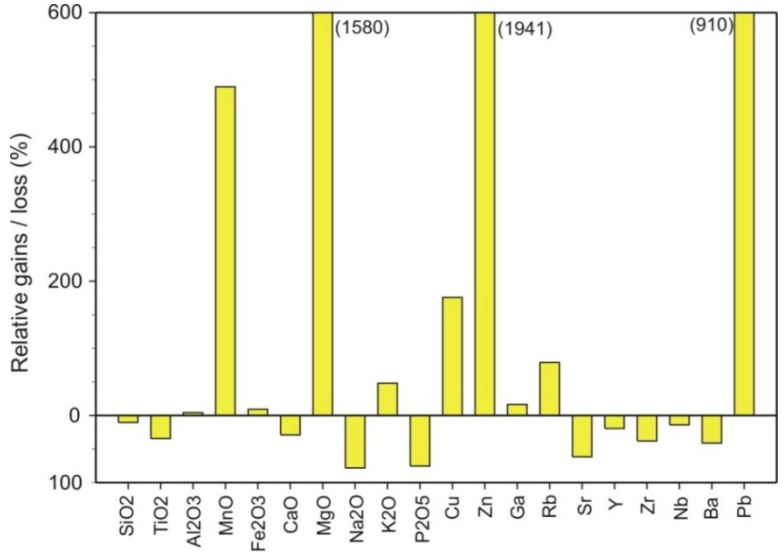

Fig.5.9 Relative percentage gains and losses for major and trace elements for quartz-biotite-phlogopite ± garnet bearing schist (magnesium altered rhyolite) with respect to the least altered rhyolite precursor.

The quartz-biotite-phlogopite-garnet schists show extreme gains in MgO (1580 %) and MnO (489 %) and also significant gains in K_2O (48%). The gains in MgO and K_2O are consistent with the mineralogy being dominated by phlogopite and spessartine garnet bearing rocks. Likewise, they show marked depletion in Na_2O (- 48 %) CaO (- 29%) and TiO_2 (-35%). Among trace elements, these rocks show high enrichment in Zn (1941 %) and Pb (+ 910%) and moderate gains in Rb (+ 79 %). Barium shows loss of about

41 %. The high zinc and lead contents are due to the fact that these rocks represent proximal alteration facies and frequently contain disseminated sulphides. Among trace elements losses are shown by strontium (62%), yttrium (20%) and zirconium (38%).

Tremolite – carbonate rocks

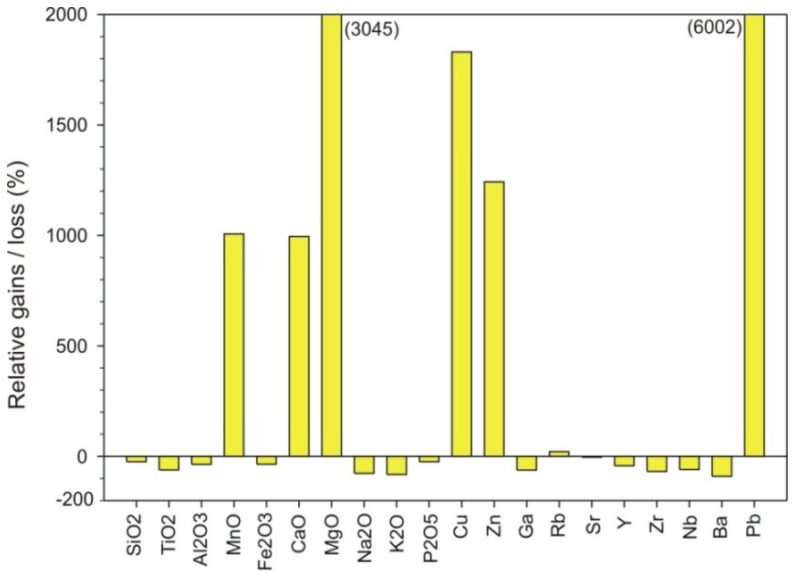

Fig 5.10 Relative percentage gains and losses for major and trace elements for tremolite carbonate rocks with resepect to the least altered rhyolite precursor.

Although the tremolite carbonate rocks are interpreted as metaexhalites which were formed by hydrothermal carbonate bearing precipitates on the sea floor, in this study, they have been compared with the precursor rhyolite, since it is believed that at least parts of these rocks could have also formed due to sub-surface replacement of rhyolite near to the site of venting. The rock shows extreme gains in MgO (+ 3045%), MnO (+1007%) and CaO (+995%) and high losses in Na_2O (-77%), K_2O (-82%) and TiO_2 (-61%). The base-metals

like zinc, copper and lead show very high values + 1243%, + 1831 % and + 6002 % respectively, which is consistent with the mineralized nature of this rock. Tantalum (Ta) also show high gains with + 452% increase over the unaltered rhyolite precursor (Fig. 5.10).

5.3.4 Alkali-Alumina Molar Ratios of rhyolites

Some recent studies on elemental mobility in altered rocks have shown that Alkali-alumina plots are an effective instrument for displaying chemical and mineralogical compositions of altered and unaltered rhyolites and rhyodacites (e.g. Davies and Whitehead, 2006). Molar ratio plots present alteration data in a readily interpretable manner. These plots can portray and interpret various aspects of hydrothermal alteration associated with VMS deposits (Davies and Whitehead, 2006). The process involves ratioing the mobile alkalies against an oxide such as Al_2O_3 which is considered to be essentially immobile (e.g. Jenner, 1996). Such diagrams are used in understanding the hydrothermal alteration in felsic volcanic rocks (e.g. Davies and Whitehead, 2006). Although such diagrams are primarily meant for rhyolites which have not undergone effects of metamorphism, in this study, we have tried to use these diagrams for the Bhuyari rhyolites which have undergone amphibolites facies metamorphism. The basic premise being that despite metamorphic overprints, changes in bulk chemistry attained during hydrothermal alteration will remain more or less unchanged.

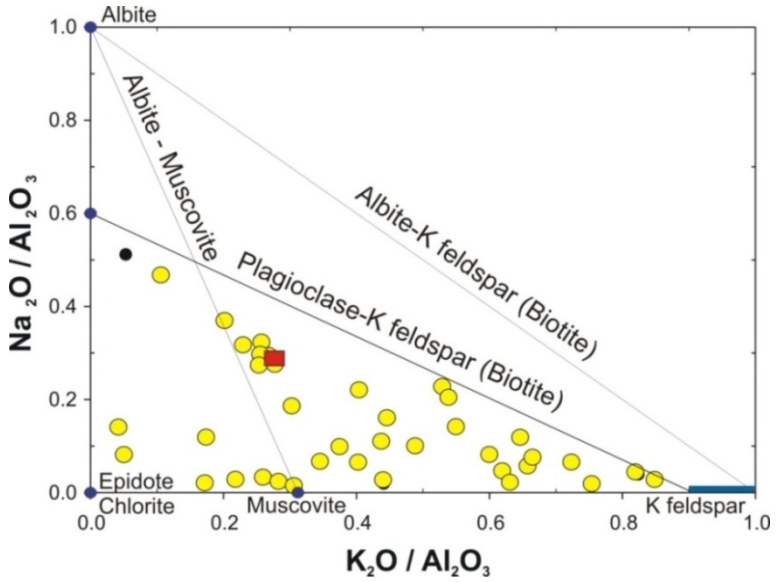

Fig. 5.11 Molar Ratio Plot for altered and least altered rhyolites showing Alkali-Alumina ratios for plagioclase, K-feldspar, Muscovite and alumina bearing ferromagnesian minerals (Davies and Whitehead, 2006). The square box represents the average composition of least altered rhyolite. Note that the samples plot predominantly along the plagioclase-K-feldspar and albite-muscovite join.

The major element data for all the altered and unaltered rhyolites were plotted in the diagrams. The average compositions of the least altered rhyolite plots below the plagioclase-K- feldspar (biotite) join in the diagram (Fig. 5.11). This is similar to unaltered Proterozoic and Paleozoic rhyolites which are enriched in K_2O and depleted in Na_2O. In contrast Archean rhyolites are enriched in Na_2O and plot above the Plag- K feldspar join (Davies and Whitehead, 2006). The results in the diagram (Fig. 5.11) clearly show that the rhyolites have undergone high degrees of alkali metasomatism during hydrothermal alteration. These signatures are preserved in spite of amphibolites-facies metamorphism. The spread of data along the plagioclase-K-feldspar join indicates destruction of plagioclase during alteration and subsequent formation of K-feldspar due to potassic alteration. This is consistent with the observed mineralogy of the alteration zones.

5.3.5 Discussion on gains and losses (mobility) of major and trace elements

Plotting of the major and trace element data in various alteration diagrams show that most show mobility with effects of alteration. It is known that most major elements except (Al_2O_3 and TiO_2), many trace elements, including base-metals and volatile metals and low field strength elements (LFSE) are considered mobile during intense hydrothermal alteration (Seiki and Date, 1980, Jenner, 1996 and Large et al, 2001b). In contrast, the high field strength elements (HFSE) and REE (except Eu) are considered immobile (e.g. MacLean, 1990; MacLean and Barrett, 1993; Barrett and MacLean, 1999) except in cases of very intense alteration (Campbell et al, 1984) or the presence of key complexing ions (e.g. Bau and Dulski, 1995).

In the alteration zones of Bhuyari Prospect, most major elements and some trace elements show wide variations due to the combined effects of hydrothermal alteration and metamorphism. When compared to least altered rhyolite, the quartz-muscovite-K feldspar schists show significant enrichment in K_2O and depletions in Na_2O. Similarly the biotite-phlogopite schists show extreme enrichments in MgO and depletion in Na_2O. Tremolite carbonate rocks show high CaO and MgO, they also have relatively high MnO contents. Most major and trace elements show variable mobility. Some trace elements like Nb, Zr and Y are relatively immobile although they too show some perturbations during intense alteration.

Na_2O depletion in footwall alteration zones is a defining feature of VMS deposits (e.g. Franklin et al, 1981, Large et al, 2001b, Barrett and MacLean, 1999). Strong losses in Na_2O and strontium are reported in footwall alteration zones in VMS deposits, for example in the Cambrian Boundary VMS deposit of Newfoundland (Piercey et al, 2013). Similarly, enrichments in K_2O-MgO-Fe_2O_3 and basemetal (Zn-Cu-Pb) are also documented in the Boundary VMS deposit.

5.3.6 Immobile elements during Hydrothermal Alteration

Due to low ionic potential, the low field strength elements (LFSE: Ba, Rb, Cs, Sr) are considered mobile, whereas the high field strength elements (HFSE: Nb, Th, Zr, Hf, Y, Al, Ti) have high ionic potentials and are considered immobile (see review by Jenner, 1996).

The chemical analyses of the least altered and altered rhyolites show wide variations in their major element contents due to the mobility of these elements during hydrothermal alteration. However, certain elements like Ti, Zr, Nb, Y remain relatively immobile during alteration, which is evident from a perusal of Fig.5.10.

Immobility is determined by plotting suspected immobile element pairs on x-y scatter plots. If elements are immobile they form a highly correlated linear trend, which ideally passes through the origin (MacLean and Barrett, 1993). The plots of Zr vs TiO_2 shows a linear pattern with most of the samples aligned along a straight line which passes through the origin, which also shows that their ratios are essentially unchanged during hydrothermal alteration (Fig. 5.12a).

In hydrothermally altered rocks, the immobile elements are preferred for use in discrimination diagrams over those which employ major elements. When the highly altered biotite-phlogopite-garnet bearing schist and muscovite-K feldspar bearing schists were plotted in the discrimination diagrams using immobile elements like Zr, Ti, Nb and Y (Winchester and Floyd, 1977), all the data plot in the rhyolite field showing a restricted range in their Zr/Ti and Nb/Y ratios, which proves that despite intense alteration certain trace elements are immobile and their ratios are preserved (Fig.5.12b). Significantly, this plot is consistent with the field and petrographic observations that phlogopite-bearing schists and muscovite-K feldspar schists represent highly altered rhyolite.

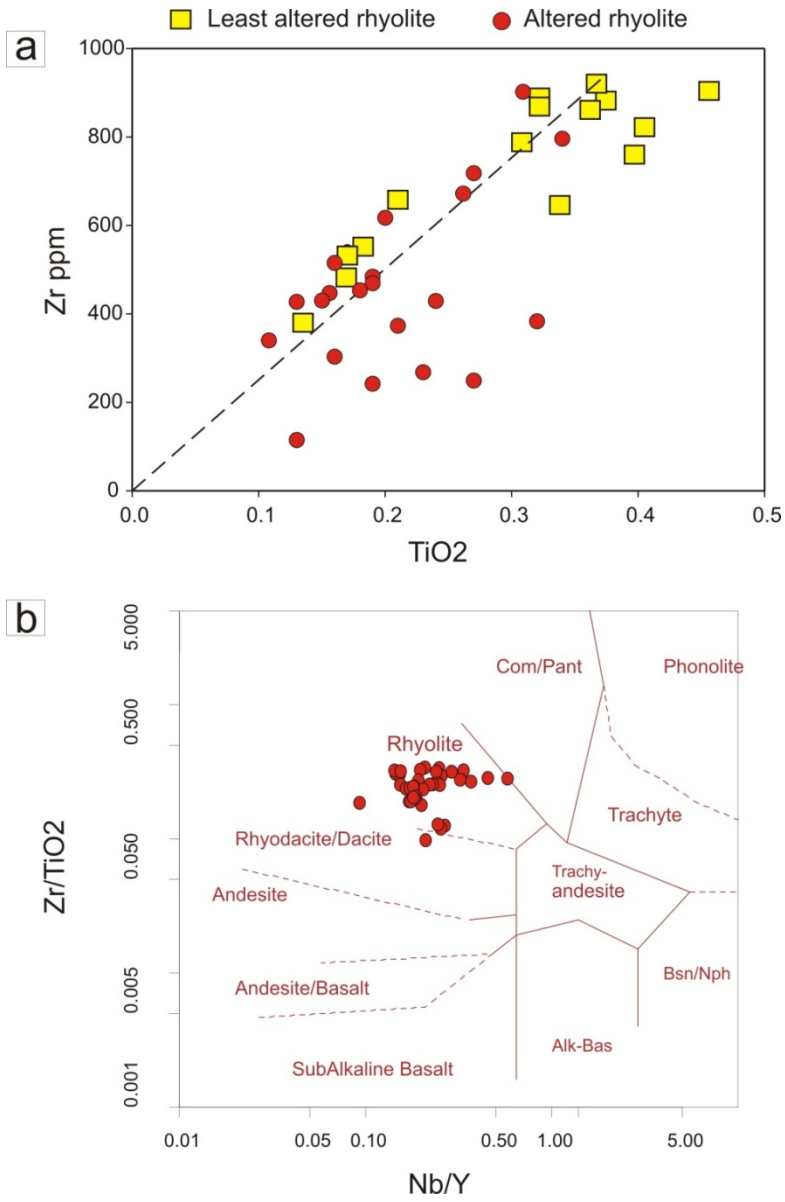

Fig. 5.12 Immobile elemet plots for altered and unaltered rhyolites. **a)** TiO_2 vs. Zr plot shows linear trends which are due to mass gains and losses of mobile elements (MacLean and Barret, 1993). TiO_2 and Zr show strong positive correlation (r = 0.76).

b) Discrimination diagram based on trace elements Zr/TiO_2 vs. Nb/Y (Winchester and Floyd, 1977) show that despite wide variations in major element compositions the unaltered and altered samples form a relatively tight cluster and plot well within the rhyolite field.

5.3.7 Rare Earth Elements of Alteration zones

The Rare Earth Elements (REE) concentrations in hydrothermal fluids are usually very low, but they tend to increase with decrease in PH (e.g. Piranjo, 1992). The behavior of REE in hydrothermal fluids are not well constrained. The transport of REE in hydrothermal fluids can take place in alkaline solutions as carbonate, sulphate or fluorine complexes.

Most studies related to mobility of REE in hydrothermal systems have come to the conclusion that REE generally remain inert during moderate to intensive hydrothermal alteration except in cases of advanced argillic alteration where REE form stable complexes during low PH and high F activity. However, many studies have shown that LREE (La to Sm and europium) show gains and losses in the alteration zones associated with modern and ancient VMS deposits (e.g Genna et al, 2014). Europium is known to be mobile during hydrothermal alteration (e.g. Campbell et al, 1984), where Eu depletion is greatest in the most intensely altered portions of the alteration zone and gradually decreases towards the periphery.

A total of 11 samples of altered and variably altered felsic volcanics were analysed for REE, including 3 samples from quartz-sericite-K-feldspar bearing rhyolite, 3 samples from highly altered biotite + plag +sulphide bearing rock and 4 samples from tremolite-carbonate rocks present as enclaves within the altered felsic volcanics. Detailed description of unaltered rhyolite REE patterns and characteristics are discussed in Chapter-4. The REE analyses of the altered rhyolites are given in Table 5.6.

In order to compare the REE of alteration zones, the data from altered rhyoites were plotted along with the REE data of unaltered rhyolite in chondrite normalized diagrams (Nakamura 1974) (Fig. 5.13). The REE patterns of unaltered rhyolite form a very coherent group showing a generally flat pattern with slight LREE enrichment. The REE in various altered rock types (altered rhyolites) are discussed here.

Table 5.6 REE analytical results for quartz-muscovite-K-feldspar ± garnet schist (Sl. Nos. 1-4), quartz-biotite-phlogopite ± garnet schists (5-7) and tremolite-carbonate rocks (8-11). Chondrite values are after Nakamura (1974).

Sl. Nos.	1	2	3	4	5	6	7	8	9	10	11
	PBS-2	PBR-9	PBR-24	PBR-32	PBS-20	PBS-31	PBS-48	PBC-4	PBC-7	PBC-15	PBC-16
La	69.2	82.9	39.9	7.4	124.4	75.2	94.3	5.8	3.11	0.04	0.93
Ce	140.8	133.4	127.6	17.3	185.7	156.0	194.4	19.8	9.40	0.78	4.61
Pr	16.4	18.5	5.4	1.9	27.6	17.7	22.3	1.5	0.51	0.01	0.43
Nd	72.2	78.7	23.1	8.2	111.2	73.2	93.4	6.3	1.58	0.04	2.05
Sm	17.3	19.8	6.1	2.6	22.3	15.3	21.2	8.0	1.40	0.05	3.13
Eu	2.8	3.7	1.1	0.6	2.5	1.4	2.3	0.1	0.05	0.00	0.02
Gd	17.4	18.4	6.1	2.6	18.2	12.1	20.9	2.6	0.45	0.02	0.68
Tb	3.4	3.7	1.2	0.7	2.9	1.9	4.0	0.6	0.07	0.00	0.12
Dy	25.3	21.0	6.2	4.2	17.9	10.2	32.4	7.9	0.58	0.01	1.01
Ho	3.0	4.0	1.0	0.9	1.8	0.9	4.6	359.2	20.20	0.60	32.20
Er	10.5	13.5	3.3	3.2	6.7	2.7	20.1	534.3	22.30	0.50	37.10
Tm	1.5	2.2	0.6	0.6	1.0	0.3	3.3	660.4	19.10	0.50	34.80
Yb	16.4	14.2	4.4	4.1	11.7	3.7	37.1	15.3	0.30	0.00	0.70
Lu	2.8	2.1	0.8	0.7	2.1	0.7	5.9	22.7	0.40	0.00	0.80
ΣREE	399.0	416.0	227.0	55.0	536.0	371.0	556.0	1644.0	79.00	3.00	119.00
La/Yb(N)	2.4	3.3	5.1	1.0	6.0	11.6	1.4	0.2	5.00	1.80	0.80
Eu/Eu*	0.5	0.6	0.6	0.7	0.4	0.3	0.3	0.1	0.14	0.08	0.03
(Gd/Lu)N	0.8	1.1	1.0	0.4	1.1	2.1	0.4	0.0	0.14	0.14	0.10
(La/Sm)N	2.1	2.2	3.4	1.5	2.9	2.5	2.3	0.4	1.15	0.46	0.15

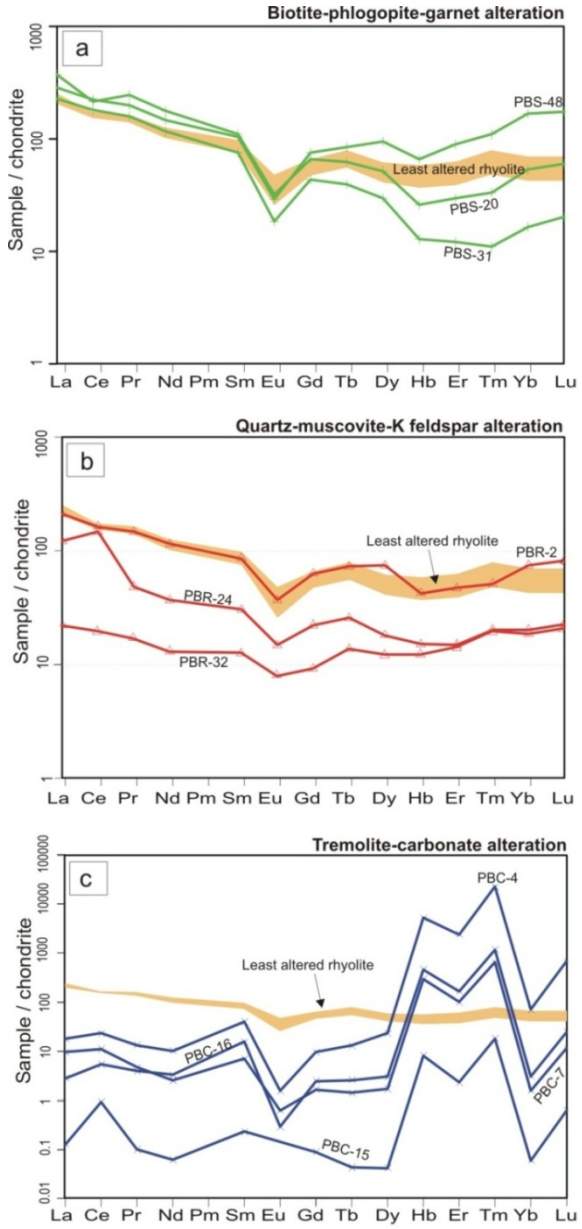

Fig.5.13 Chondrite normalized REE patterns (Nakamura 1974) of different groups of altered rhyolites, **a)** comparison of biotite-phlogopite-garnet bearing rocks with unaltered rhyolite show similar patterns (shaded profile is the composite pattern of 7 unaltered rhyolite) with pronounced vertical shifts in HREE, **b)** Muscovite-K-feldspar schists show similar pattern with unaltered rhyolite but showing depleted REE contents **c)** Tremolite-carbonate rock show markedly different REE profiles compared to least altered rhyolite.

REE in biotite-plagioclase-garnet rocks

The three phlogopite/biotite-garnet altered rocks PBS-20 (quartz-biotite-sericite-staurolite-garnet-gahnite rock), PBS-31 (quartz-biotite-plagioclase-gahnite rock) and PBS-48 (quartz-biotite-plagioclase-sphalerite rock) show very similar LREE contents and pattern; however the HREE show vertical shifts but still maintaining the pattern of the least altered rhyolite (Fig. 5.13a). All these rocks contain varying amounts of sulphides. Field and petrographic evidence indicates that all these rocks are rhyolites which have been intensely altered. From the Figure 5.13a, it is apparent that the LREE and mid REE patterns are almost similar to the precursor unaltered rhyolite, however there is some mobility in the HREE.

The total REE ranges from 371 to 556ppm (average 488ppm). The average total REE content (488ppm) is considerably higher than the average of least altered rhyolite (382ppm).

Sample PBS-31 show marked depletion /loss in HREE when compared to the precursor rhyolite. Sample PBS-20 also shows HREE depletion other than Yb and Lu which show no loss. The sample PBS-48 show enrichment in HREE compared to the precursor rhyolite. The intensely altered samples demonstrate HREE mobility and negligible or no LREE mobility. The overall patterns of the unaltered and intensly altered rhyolite are similar confirming the field and petrographic evidence that the biotite-garnet-plagioclase bearing schists represent intensely hydrothermally altered and metamorphosed massive rhyolites.

The LREE and MREE patterns are very similar to the unaltered rhyolite, whereas, there is slight perturbations in the HREE patterns (Fig. 5.13a). LREE is enriched in two samples compared to unaltered rhyolite,

whreas the HREE contents is diluted in two samples and enriched in one sample. The negative europium anomalies are also stronger in these rocks.

Enrichment in REE is documented in hydrothermally altered rocks relative to their protoliths in several studies. Proximal chloritic zones in VMS deposits at places have recorded gains in LREE and Eu for example in the Bracemac-McLeod deposit, Matagami, Canada (Genna et al, 2014).

REE in Quartz – Muscovite - K feldspar rocks

The three quartz-muscovite-K feldspar altered rhyolite contain total REE contents ranging from 55 to 416 ppm (average 274ppm), which is substantially lower than those of least altered rhyolite (avg. 352ppm) and the biotite (magnesium) altered rhyolite (avg. 488ppm). Their chondrite normalized patterns are similar, but two of the samples show dilutions in their total REE contents, which is possibly the result of silicification. The sample PBS-2 more or less retains the REE content of the least altered rhyolite, while the two other samples PBS-24 and PBS-32 show vertical shifts downwards while maintaining the pattern of the least altered rhyolite (Fig. 5.13b). All the three silicified samples show marked loss in REE which can be the result of dilution in total REE due to silicification, but their pattern is similar to the unaltered rhyolite as seen from the diagram.

Lower total REE contents are documented in highly altered host rocks and can be attributed to the presence of higher proportion of REE-free phases like quartz and sulphides together with the removal of REE by hydrothermal alteration (e.g. Cong Ling and Qiang Liu (2002). The rock type has similar REE patterns, with lower REE abundances and one sample shows a positive Ce anomaly. The lower LREE and europium in sericitic zones are attributed to destruction of volcanic glass and plagioclase (Genna et al, 2014).

REE in Tremolite-carbonate rocks

Four samples of tremolite-carbonate rocks occuring proximal to massive sulphides at Bhuyari show very different REE profiles when compared to least altered rhyolite (Fig. 5.13c). The total REE contents vary widely and ranges from 3 to 1644ppm. The lowest value of 3ppm is recorded for sample PBC-16. The highest value of 1644ppm is from sample PBC-4. The high total REE in this sample is similar to REE enrichment in some carbonatites. The high REE in sample PBC-4 is mainly due to higher HREE (Gd to Lu) contents, particularly holmium (359ppm), erbium (534ppm) and thulium (660ppm). The other two carbonate samples PBC-7 and PBC-16 also contain high HREE contents of 63 and 107ppm respectively. In comparison, the total HREE content of unaltered rhyolite is 23ppm.

It is observed that the REE pattern of the carbonate rocks markedly differ from the precursor rhyolite. However, the patterns of the four samples are remarkably similar despite the fact that total REE contents vary from 3ppm to 1644ppm (Fig. 5.13c). This clearly shows that these rocks were formed by a common set of processes and are different from the rhyolite. The chondrite normalized patterns are characterized by flat LREE and highly enriched and variable HREE. The four samples have identical REE signatures with extremely low LREE and mid REE and higher Ho, Er and Tm. The patterns also show negative Eu and Yb anomalies.

5.4 Summary and Interpretation of REE in Altered Rocks

Overall, the intensely altered rocks show depletion of REE contents with respect to unaltered rhyolites while broadly maintaining their similar chondrite-normalized patterns. The LREE in biotite-phlogopite schist show remarkably coherent behavior with LREE of unaltered rhyolite, however

HREE show perturbances. The muscovite-K feldspar altered rhyolite show high depletion in REE when compared to the phlogopite-rich rocks. The tremolite-carbonate rocks show vastly dissimilar REE pattern to unaltered rhyolite.

REE mobility during hydrothermal alteration has been investigated in several studies, for example in the VMS hosting rhyolite in the Abitibi province, the sericitised zones showed REE depletion up to 40% and chloritised zones showed only moderate losses up to 7 % when compared to unaltered rhyolites (Moulton et al, 2011). Generally, the REE was lost during alteration with major depletions associated with sericitization when compared to chloritization. The negative europium anomalies are prominent in the altered rhyolites. Chlorite altered zones in VMS bearing rhyolites showed upto 16% depletion of Europium (Moulton et al, 2011). A similar behavior of REE is documented in the intensely altered zones of massive sulphides of Paleoproterozoic Flin Flon- Snow Lake area, Manitoba, which show depleted REE profiles when compared to unaltered rocks, with greater europium anomalies (Campbell et al, 1984) with the greatest europium anomalies in the most altered rocks. These observations are supported by experimental studies that indicate REE mobility and Eu enrichment in hydrothermal fluids increases with decreasing pH and increasing temperatures (Haas et al., 1995).

These enrichment and depletions are not a primary geochemical signature of the rhyolite, rather, these variations reflect differences in the type and intensity of hydrothermal alteration and metamorphism. The present study has shown that the REE patterns of intensely altered rocks are similar to the unaltered protolith rhyolite. This result has important implication in the identification of similar highly altered lithologies in similar terrains.

5.5 Geochemical Proximity Indicators to Mineralized Zone

In this study, several major and trace elements display depletion or enrichment with increasing degree of alteration and proximity to ore. The increase in Alteration Index is accompanied by increase in Mg, K and Mn enrichment, whereas the concentration of Na_2O, CaO decrease with alteration intensity. These variations are also indicators to proximity of massive sulphides as seen from the alteration facies map and the sample locations (Fig.2.2b).

Characteristic and systematic enrichment and depletions of mobile elements are well documented in alteration zones of ore zones in VMS deposits worldwide. For example, a systematic increase in manganese content is noted in carbonates in the Roseberry VMS deposit in Tasmania, Australia (Large et al., 2001b). The Mn content of alteration carbonate increases towards ore both along strike and along strike. In Bhuyari, Sr is strongly depleted in highly altered Mg-altered and K-altered samples which are similar to the strongly altered footwall zones in Rosebery Zn-Pb-Cu VMS deposit in Australia (Large et al, 2001b).Some major and trace elements show consistent variations with intensity of alteration (AI).

Manganese enrichment

Manganese enrichment is observed in the quartz-biotite-phlogopite-±garnet± plagioclase ± gahnite ± staurolite schists (Mg-Fe alteration zone). The tremolite-carbonate rocks show more than 10 times the MnO contents present in unaltered rhyolite. The quartz-muscovite-K feldspar schists (potassic alteration zone) show around 40 % higher MnO values. Manganese enrichment in proximal alteration zones are characteristic of VMS deposits. For example, higher manganese content is recorded in the proximal carbonate alteration zones of the Rosebery VMS Zn-Pb-Cu ore lenses (Large et al., 2001b).

Sodium depletion.

Destruction of plagioclase during ore-related hydrothermal alteration has given rise to zones with very low sodium. The biotite-bearing zones contain low Na_2O contents (average: 0.75 wt. %). Sodium depletion is documented in the footwall alteration zones in most VMS deposits; for example, the footwall alteration zones of Rosebery Zn-Pb-Cu ore lenses contain less than 0.1 wt. % Na_2O, caused by destruction of albite and development of quartz, sericite and chlorite (Large et al, 2001b).

Magnesium and Potassium enrichment

At Bhuyari, Mg and K enrichment is a characteristic feature of the zoned footwall alteration. When compared to unaltered rhyolites the biotite-phlogopite schists show more than 8 times enrichments in MgO and the muscovite-K-feldspar rocks show >2 times increase in K_2O (Table 5.3). Elevated MgO and K_2O levels are a characteristic feature in VMS-related footwall alteration zones (Franklin et al., 1981). For example, in the case of Rosebery Zn-Pb-Cu deposit, the highest K_2O levels (>5 wt. %) is present in the stratabound footwall alteration zone below the ore lenses. At Bhuyari, samples with the highest enrichments in MgO and K_2O occur closest to the ore zones and such patterns can be used as a reliable proximity indicator to ore.

5.6 Discussion

Plotting of data in the Alteration Box Plot show that the chlorite ± sericite ± pyrite trend and sericite-chlorite ± pyrite alteration trends shown by the biotite-phlogopite schists are typical of chlorite-rich proximal footwall alteration systems in VMS deposits (Large et al, 2001a). This indicates that the many variants of the biotite-phlogopite rich rocks are metamorphosed chlorite-rich and chlorite-sericite altered proximal footwall alteration. This is

consistent with the field relations where these rocks form the core zones in the alteration system and also are associated with mineralization. The other important trend displayed by the altered rhyolites is the K-feldspar-sericite trend which is an uncommon alteration trend according to Large et al (2001a). Field relations show that this alteration broadly envelops the biotite-phlogopite alteration and also predates it, which suggest that it represents a phase of potassic alteration prior to more intense Mg-rich alteration. Other alteration diagrams show Na_2O depletion is a diagnostic feature of all altered rocks. Also, the geochemistry of the different alteration zone corroborates well with the observed mineralogy of these rocks when the data is plotted in the MgO-Al_2O_3-Alkali diagram, with Mg-enriched samples showing distinct trends towards the biotite and phlogopite nodes (Fig. 5.2b).

The phlogopite-chlorite-bearing rocks occurring as the core zone of alteration contains high MgO and low Na_2O and CaO, which is similar to high-Mg chloritic core zones of many zoned alteration systems in proximal VMS environments. This proximal alteration represents hydrothermal up-flow and discharge zones (e.g. feeder zones to the deposits) and form from high-temperature water rock interaction (e.g. Piercey, 2009).

Major elements show significant mobility in alteration zones. When compared to least altered rhyolite, K_2O, MgO and MnO show significant enrichments, whereas the Na_2O and CaO contents are depleted. Certain elements like TiO_2, Zr, Nb and Y show relative immobility when compared to other elements despite intense alteration and metamorphism. These immobile elements can be used for discrimination diagrams for understanding the protoliths of the highly altered rocks.

Detailed geochemical studies involving major, trace and REE of the alteration zones confirm that they represent intensely altered rhyolite. REE

signatures of highly altered rhyolites are similar to those of unaltered rhyolite which indicates that the biotite-phlogopite schists and muscovite-K feldspar schist have a rhyolitic protolith. REE contents and patterns of tremolite-carbonate rocks are different from unaltered rhyolite, suggesting a derivation from different source-perhaps as hydrothermal carbonate-bearing precipitates related to an exhalative vent on the seafloor.

These studies corroborate field-based and petrographic evidences for a rhyolitic protolith for the biotite-phlogopite-garnet-gahnite bearing schist and the muscovite-K-feldspar schists. The major and REE geochemistry of tremolite-carbonate rocks do not support a rhyolite protolith for these rocks. The vastly different REE signatures and low contents of trace elements like Zr, Nb and Y suggest that these may have alternate origins. The presence of relict banded nature, high proportion of spessartine garnets at places, close association with massive sulphides and lensoid nature suggest that these rocks could possibly represent meta-exhalites.

Geochemical proximity indicators have been identified for exploring these deposits. Constituents like MgO, MnO and K_2O show significant enrichment towards ore zones and proximal alteration zones. Na_2O show extreme depletion towards ore zones and proximal alteration zones.

5.7 Carbon and Oxygen Isotope studies of Carbonates

5.7.1 Introduction

The application of stable isotope ratios, to the characterization, interpretation and exploration of hydrothermal mineral deposits is one of the major recent advances in the field of economic geology (Misra, 2000). Applications of carbon isotopic composition of carbon-bearing minerals to the study of hydrothermal deposits are similar in principle to those for sulphur

(Ohmoto 1979). To facilitate inter laboratory comparisons, a set of international standards has been established for geologically important light stable isotopes: for carbon the accepted reference standard is PDB (Peedee Belemnite) and for oxygen it is SMOW (Standard Mean Oceanic Water) (e.g. Huston, 1999).

Carbon in VMS environments occurs broadly in two different modes: oxidized carbon in carbonate minerals and reduced carbon as graphite and organic matter. The quantity of carbon isotope data from both forms is very limited when compared to oxygen, sulphur and hydrogen data (Huston, 1999). As discussed previously, the carbonate-bearing rocks at Bhuyari are intimately associated with mineralization, the study of carbon and oxygen isotopes of the carbonates can provide constraints regarding the ore forming hydrothermal fluids involved in mineralization.

5.7.2 Carbonate Bearing Rocks around Bhuyari

Broadly, the carbonate occurrences around Bhuyari Prospect can be classified into two different types:

1) Type-1, as fine grained segregations in tremolite - carbonate rocks closely associated with sulphide mineralization and
2) Type-2, as egg-sized pockets within unaltered rhyolites distal from mineralized zone, approx. about 1km to the north of the sulphide-bearing zone (towards hanging wall side).

*The **Type-1 carbonate*** is the dominant form of carbonate present in the area and is closely associated with mineralized zone. They occur as three discrete outcrops on a small hillock south of Bhuyari village named CS hill-1 to 3 from south to north (Fig. 2.2b). During earlier exploration work by GSI,

the massive sulphide lens was intersected in the drill core close to the main tremolite-carbonate outcrop (Praveen et al, 2010). The carbonate minerals, which are identified as dolomite by EPMA studies, occur as fine-grained, sugary segregations within the tremolite-carbonate outcrops. In these outcrops, the mineral assemblages are dominated by tremolite with varying proportions of talc, carbonate, chlorite, actinolite, plagioclase, garnet etc. Carbonate occurs as segregations and patches in these rocks and is most often leached and weathered. Freshly broken surfaces show white, fine-grained, sugary carbonate which at places show the presence of fresh sulphides and brownish altered material which may be alteration products after some sulphides (See Chapter 2, Fig.2.9g).

Out of the 9 samples collected from near the mineralized area, 5 samples were collected from the southernmost tremolite-carbonate outcrop (CS Hill-1) and four samples from the outcrop just north of it (CS Hill-2) (Table 5.8). The northernmost outcrop (CS Hill-3) did not have any free carbonate and so samples were not collected. The location of the outcrops of tremolite-carbonate rocks from which the Type-1 carbonates are collected can be seen in the detailed geological map (Fig. 2.2b).

***Type-2 Carbonate*:** The type 2 carbonate occurs as discrete patches/ enclaves/ pods in grey, massive and least altered rhyolite around 1.5 km to the north of Bhuyari (Fig. 2.2a). Three samples were collected from this area. The location of isotiope samples (BYRC-1, BYRC-2 and BYRC-3) are shown in the map (Fig. 2.2a. Type-2 carbonate occurs as rounded enclaves within dark grey least altered rhyolite (Fig.2.9h) and are not associated with pervasive hydrothermal alteration. However, disseminated sulphides like pyrite are

present in this rock indicating that they have undergone minor degree of hydrothermal alteration. The carbonate is light yellow to dull white in color and form medium grained crystalline aggregates. The carbonate material was carefully removed from these locations and packed in polythene covers and sent for analysis. EPMA analyses of carbonate show that they are dolomite.

5.7.3 Methodology

Carbonate samples were analyzed in two batches. The first batch of 9 samples from the Type-1 carbonates were analysed at the Shizuoka University, Japan. The second batch of 3 sample comprising Type-2 carbonates was analyzed at NCGER, GSI, Bangalore.

At Shizuoka University, the instrument used is the Finnigan MAT 250 mass spectrometer. Carbon and oxygen isotopic composition of calcite were measured using the method described in Wada et al. (1982, 1984). Calcite from specific sampling points, such as grain core or grain boundary were sampled from a cut and polished slab using a cutter knife. The powder was collected in steel thimble and dropped into phosphoric acid at 60°C in an online reaction chamber, under vacuum conditions, which is connected to the inlet system of Finnigan MAT 250 mass spectrometer. Evolved gas was cryogenically purified to retain CO_2.

Samples analyzed at the NCGER lab, Bangalore, were analyzed by the SerCon Geo 20-20 Isotope Ratio Mass Spectrometer in continuous flow (CFIRMS) mode. The standard MAKMARB was analyzed to ensure accuracy and precision of the analysis. MAKMARB[1] gave $\delta^{13}C_{PDB}$ = +3.73 ± 0.16‰ and $\delta^{18}O_{PDB}$ = -10.85 ± 0.07‰.[1] Reported values for MAKMARB: $\delta^{13}C_{VPDB}$ =

+3.7 ± 0.1‰ and $\delta^{18}O_{VPDB}$ = -10.8 ± 0.2‰ . $\delta^{18}O_{SMOW}$ = 1.03086 $\delta^{18}O_{PDB}$ + 30.86 (Coplen, 1988)

5.7.4 Results

The $\delta^{13}C$ values for Bhuyari tremolite-carbonate rocks associated with sulphide mineralization, ranges from -3.12 to 1.24‰ and $\delta^{18}O$ values between 7.87 to 10.4‰. The results have been tabulated in Table 5.8 and summarized in Table 5.7.

The results are plotted in the $\delta^{13}C$ versus $\delta^{18}O$ plot. The $\delta^{13}C$ values show a fairly large spread between -3.12 to 1.24‰, whereas, the $\delta^{18}O$ values show a very restricted range between 7.8 to 10.4 ‰. The samples plot along a seawater-magmatic water mixing trend (Fig. 5.14).

There is no apparent difference between the $\delta^{13}C$ versus $\delta^{18}O$ values obtained for the carbonates from near mineralized zones and those distal from mineralized zone (Table. 5.7). The values for the carbonate patches/enclaves are lower and $\delta^{13}C$ ranges from -2.86 to -2.30 and $\delta^{18}O$ values between 7.80 to 8.04 ‰. These values are similar to those obtained for the carbonate rocks containing disseminated sulphides at Bhuyari Prospect (CS-II hill) and they also plot within the field of Thalanga hydrothermal carbonates (Herrmann and Hill, 2001). The values obtained for the large outcrop of tremolite carbonate rock (CS-1 hill) is higher and $\delta^{13}C$ ranges from 0.83 to 1.24 and $\delta^{18}O$ values between 9.88 to 10.4 ‰. This may be a function of lower temperature of hydrothermal fluids.

Table. 5.7 Table summarizing the details of the isotope analysis of the Type-1 and Type-2 carbonate samples.

Carbonate type	Sample No	Location	Sample description	delta 13 CPDB	delta 18 OSMOW
(Type-1) Spatially associated with mineralization	C-A1 to C-A5 (n=5)	CS Hill 1	Carb rocks without sulphides.	0.83 to 1.24	9.88 to 10.4
	C-B1 to C-B4 (n=4)	CS Hill 2	Carbonate rock with sulphides.	0.93 to -3.12	7.87 to 8.82
(Type-2) No spatial association with mineralization	BYRC-1 to BYRC-3 (n=3)	500-600m north of Bhuyari	Enclaves in unaltered rhyolite	-2.3 to -2.86	7.8 to 8.04

Out of the 9 carbonate samples collected from close to the mineralized zones, 5 samples (C-A1 to C-A5) collected from the tremolite carbonate rock adjacent to the massive sulphide zone form a very tight cluster and fall very close to the upper boundary of the hydrothermal carbonate field of Rosebery and Hercules VMS deposits of Australia (Khin Zaw and Large, 1990). The 4 samples (C-B1 to C-B4) collected from the second tremolite-carbonate hillock some distance away from the massive-sulphide zone show variation in $\delta^{13}C$ values from 0.93 to -3.12 and a more restricted $\delta\ ^{18}O$ values between 8.82 to 7.87. These values plot along with the Thalanga hydrothermal carbonates (Herrmann and Hill, 2001).

The $\delta^{13}C$ and $\delta\ ^{18}O$ values were plotted in the diagram of Hermmann and Hill (2001) for comparison with other similar carbonates from VMS deposits of Australia (Fig. 5.14). In these deposits, the origin of these carbonate rocks are inferred as of hydrothermal origin. The source of these carbonates may have inputs from seawater and magmatic fluids. The fields of

the Bhuyari carbonates are similar to the Thalanga VMS Zinc deposit in Australia.

Table: 5.8 Table showing the carbon and oxygen isotope data from tremolite carbonate rocks from Bhuyari prospect

Sl. No.	Sample No	Location	Description of sample and mode of occurrence	delta 13 CPDB*	delta 18 OSMOW
1	C-A1	CS hill-1	Mostly white coloured, fine-grd carbonate segregations occurring in outcrop of tremolite-talc rock	0.83 ± 0.06	10.26 ± 0.05
2	C-A2	CS-hill-1	Mostly fine-grained carbonate with minor tremolite in tremolite-talc rock	0.92 ± 0.01	10.08 ± 0.04
3	C-A3	CS-hill-1	Mostly white, fine-grd carbonate patches/segregations in tremolite-talc rock	1.24 ± 0.03	10.40 ± 0.06
4	C-A4	CS-hill-1	Mostly fine-grd carbonate	1.01 ± 0.01	10.02 ± 0.04
5	C-A5	CS-hill-1	Fine grained carbonate with minor tremolite	0.88 ± 0.02	9.88 ± 0.04
6	C-B1	CS-hill-2	Fine grained carbonate with specks of chocholate brown mineral in tremolite-talc-chlorite rock with disseminated sulphides	0.93 ± 0.03	8.21 ± 0.06
7	C-B2	CS-hill-2	Fine grained carbonate with tremolite and sulphide disseminations (galena)	-3.12±0.02	8.18 ± 0.03
8	C-B3	CS-hill-2	Fine grained carbonate with tremolite and sulphide disseminations (galena + sphalerite)	-1.38±0.02	8.82 ± 0.02
9	C-B4	CS-hill-2	Fine grained carbonate with large tremolite laths.	-3.05±0.03	7.87 ± 0.02
10	BYRC-1	Bhuyari North	Medium-grained crystalline carbonate as egg to tennis-ball sized rounded enclaves/pods within rhyolite	-2.30	7.80
11	BYRC-2	Bhuyari North	Medium-grained crystalline carbonate as egg to tennis-ball sized rounded enclaves/pods within rhyolite	-2.86	8.04
12	BYRC-3	Bhuyari North	Medium-grained crystalline carbonate as egg to tennis-ball sized rounded enclaves/pods within rhyolite	-2.74	7.84

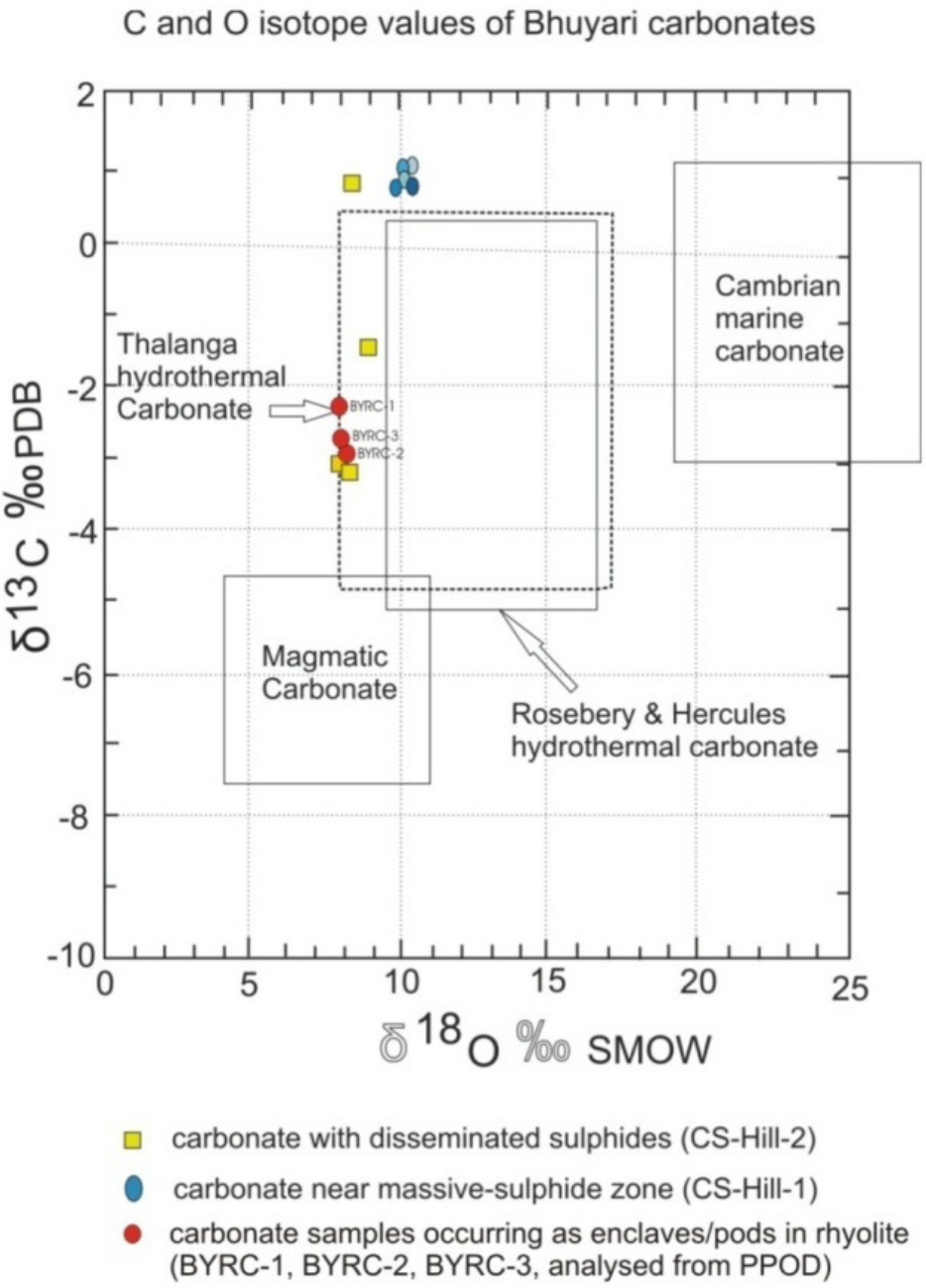

Fig.5.14 Stable carbon and oxygen isotope values from Bhuyari Prospect plotted in the $\delta^{13}C$ and $\delta\ ^{18}O$ diagram showing fields of Australian VMS-related carbonate rocks. Rosebery-Hercules field from Khin Zaw and Large (1990).Thalanga field from Hermmann and Hill (2001). Fields for magmatic and marine carbonates are from Ohmoto (1986) and Vezier and Hoefs (1976), respectively.

5.7.5 Discussion

In a detailed review of the carbon and oxygen isotope characteristics of Australian VMS deposits, Huston, 1999 showed that they are characterized by a restricted $\delta^{13}C$ range of between -5 and 0 per mil and have much wider range of $\delta^{18}O$ which exceeded 6 per mil in most deposits. The range of $\delta^{13}C$ observed is compatible with derivation from dissolved bicarbonate from seawater (Huston, 1999). The range of $\delta^{18}O$ values associated with VMS deposits is lower than typical values for marine carbonate (25-35‰). The VMS related carbonates have an observed $\delta^{18}O$ range of 7.5 to 20.0‰ which is interpreted to be the result of varying depositional temperatures. The range of $\delta^{18}O$ is suggestive of a fluid temperature in the range of 100 to 300°C (Huston, 1999). The lower and restricted values obtained for the Bhuyari carbonates (7.8 to 10.4 ‰) possibly reflect a lower range of temperature for hydrothermal fluids which deposited the carbonates.

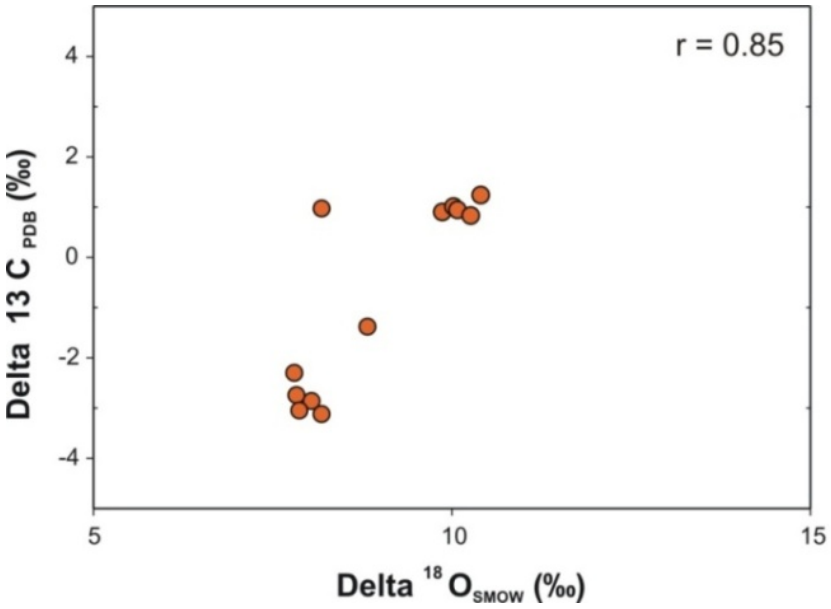

Fig.5.15 Scatter plot between showing strong positive correlation between $\delta^{13}C$ and $\delta^{18}O$ with a correlation coefficient of 0.85.

The $\delta^{13}C$ and $\delta\ ^{18}O$ values obtained for the Bhuyari carbonates show strong positive correlation (0.85) (Fig. 5.15). Positive correlations between $\delta^{13}C$ and $\delta\ ^{18}O$ as seen in this study are rare in carbonates related to VMS deposits as seen from the Australian examples. However, strong positive correlations between $\delta^{13}C$ and $\delta\ ^{18}O$ are seen in carbonates from some deposits like the South Herculus ($r = 0.91$) which have been interpreted to be the result of temperature variations (Khin Zhaw and Large, 1992).

These are comparable to the values obtained from similar tremolite-carbonate rocks from the Thalanga Volcanic-Hosted Massive Sulphide Deposit, from the Cambro-Ordovician Mount Windsor Sub-Province, Australia, which has $\delta^{13}C$ (2.5 to 0.5) and $\delta\ ^{18}O$ values (8 to 10.5). The isotopic ranges are also similar to hydrothermal carbonates associated with the Tasmanian VMS deposits of Hercules and Rosebery (Fig.5.14). There is no possibility of any sedimentary carbonate in Bhuyari since there is no record of marine carbonate within the bimodal volcanic sequence. Therefore, the $\delta^{13}C$ and $\delta\ ^{18}O$ signatures are indicative of a seawater-dominated hydrothermal system.

There are no major isotopic difference between the Type-1 carbonate occurring near mineralized zones and Type-2 carbonate located in unaltered rhyolites towards the hanging wall side. These two types of carbonates may have formed by the same low-temperature carbonate charged hydrothermal fluids. The presence of discrete patches of carbonate alteration in the rhyolite sequence further north towards the hanging wall side suggests that the carbonate-rich hydrothermal activity continued even after massive sulphide formation at Bhuyari.

Carbonates are associated with various mineral deposits and particularly with some Paleozoic VMS and epithermal deposits in Australia. Carbonates occur with ore zones in the Henty and Mount Julia gold deposits in

western Tasmania which is hosted by submarine volcaniclastic dacites. At Henty, carbonates occur as bedded carbonates and calcareous volcaniclastic rocks and are mainly found in the upper parts of the alteration zone. Based on stable isotopic data (carbon and oxygen) from the carbonates, it is interpreted that the carbonates formed by mixing of small amounts of magmatic CO_2 with seawater at and below the seawater interface (Callaghan, 2001). Many workers have proposed a exhalative origin for the carbonate at Henty (e.g. Halley and Roberts, 1997). The carbonate present in Rosebery and Hercules VMS deposits are interpreted to be associated with exhalative precipitates formed by hydrothermal systems (Large et al, 2001b). Exhalative carbonates are currently forming in the Ambitle Island in Papua New Guinea (e.g. Pichler and Dix, 1996).

The $\delta\ ^{18}O$ values have a relation with temperature of fluids. Higher temperature fluids near ore zones have lower $\delta\ ^{18}O$ when compared to those distal from ore. The carbonate near the ore zone at Rosebery VMS deposit in Australia has distinctly lower delta oxygen values ranging from 8.5 to 10 per mil when compared to other carbonates in the hanging wall and footwall of the deposit (10 to 14 per mil). This is very similar to the carbonates from Bhuyari which have low delta oxygen values ranging from 7.8 to 10.4 per mil.

In conclusion, it can be inferred that the $\delta^{13}C$ of carbonate from Bhuyari shows signatures of seawater derived hydrothermal fluid. The $\delta\ ^{18}O$ values are similar to most VMS deposits and their lower values possibly suggest lower temperature hydrothermal fluids. Carbonate was precipitated by low-temperature venting of hydrothermal fluids which may have been deposited after massive sulphide deposition. The carbonates may have altered the porous volcaniclatic rocks near the seafloor and some carbonate may have precipitated on the seafloor as exhalites which may have been a mixture of

carbonate and cherty exhalites. The laminated and bedded nature of the carbonate and differing REE signatures from rhyolite and also their low HFSE contents may indicate that at least part of these rocks were deposited as carbonate-rich exhalites on the seafloor near to the hydrothermal vent. The Type-1 carbonates associated with mineralization at Bhuyari formed from low temperature fluids near the hydrothermal vent possibly after deposition of massive sulphides. These low temperature carbonate-charged fluids permeated the fractured and permeable rhyolite below the hydrothermal vent and pervasively replaced the rhyolite below the seafloor. Part of the carbonate-charged hydrothermal fluids were exhaled from the hydrothermal vent and deposited on the seafloor along with other siliceous material to form carbonate-chert exhalites. The Type-2 carbonate occurring as pods within unaltered hanging- wall rhyolites north of Bhuyari may represent continuing hydrothermal activity.

******

Chapter 6

MINERAL CHEMISTRY

Contents

6.1 Introduction
6.2 Methodology
6.3 Results
6.4 Summary and Conclusions

6.1 Introduction

The study of mineral chemistry of individual minerals present in the different alteration zones is important to relate it with bulk chemistry of these rocks. Based on field, petrographic and geochemical studies, it is understood that the present metamorphic mineral assemblages in the alteration zones are ampibolite-facies equivalents of hydrothermal chlorite, sericite, K-feldspar and carbonate-bearing assemblages.

In metamorphosed VMS deposits, the mineralogy of metamorphic minerals found in the alteration zones provides vital clues for exploration of such deposits. These metamorphic minerals often contain anomalous contents of zinc, manganese, magnesium and barium giving rise to zincian staurolite, gahnite, spessartine garnet etc, which act as guides for the exploration of these deposits.

In the present work, detailed Electron Probe Micro Analyses (EPMA) studies have been carried out to cover most of the important minerals in the alteration zones at Bhuyari which has helped in detailed mineralogical characterization of the metamorphosed alteration zones. The variations in their mineralogy with respect to their alteration type and proximity to ore are documented and discussed. Mineral composition of the common minerals like

feldspar, biotite and garnet are studied and compared from the least altered as well as the highly altered rhyolites to understand variations in terms of their mineralogical composition and their position/location in the alteration system. These studies reveal that there are major variations in mineral compositions of several minerals depending on the type of alteration.

6.2 Methodology

Thin polished sections of rock samples were prepared at NCESS, Thiruvananthapuram. EPMA study of selected polished sections was carried out at EPMA Lab, NCEGR, GSI, Bangalore. The chemical composition of the major constituent minerals was determined using a CAMECA Sx100 electron microprobe. Operating conditions of the electron microprobe included an accelerating voltage of 15 kV and beam current of 12 nA for silicate and oxides. A beam current of 20 nA was used for sulphide analyses.

Additional EPMA data on selected co-existing mineral pairs and selected minerals used for geothermobarometry are dealt with separately in the chapter on metamorphism (Chapter 8).

6.3 Results

The detailed descriptions of the mineralogical compositions of the common minerals present in the different alteration zones as well as unaltered rhyolite are given below. The locations of sample numbers given in the tables are shown in the detailed map (Fig.2.2b).

Feldspars

Feldspars analyzed by EPMA from the altered and unaltered rhyolites are mainly microcline and plagioclase. The mineral chemistry of feldspars from different alteration zones are given in Tables 6.1, 6.2 & 6.3.

Microclines do not show much compositional variations like the plagioclases and are not present in the Mg-altered zones. Therefore, in this study, the plagioclase compositions have been investigated in detail as they are present in most alteration zones and also show compositional variations.

The plagioclase from the least altered rhyolite has a composition of oligoclase ($An_{16\ to}\ An_{26}$) (Fig. 6.1). Plagioclase is well developed in the altered rhyolites represented by biotite + plagioclase + garnet + gahnite bearing assemblages and their composition range from oligoclase to andesine (Table 6.2 and 6.3). Petrographic studies have shown that the plagioclases in the altered rhyolite are secondary and formed during metamorphism. Among the alteration assemblages, with the exception of tremolite-carbonate rocks, the anorthite content of metamorphic plagioclase varies from $An_{24\ to}\ An_{35.}$ Anorthite contents are lower in the phlogopite-plagioclase-gahnite assemblage (PBS-31) ($An_{23.7-24.4}$). The phlogopite-garnet assemblage without gahnite (PBS-26) has slightly higher $An_{29-32.6}$. The potassic altered rhyolite (PBS-1), with K-feldspar has higher anorthite contents (An_{34-35}). The tremolite carbonate rocks contain calcic plagioclases with $An_{77-88.}$ Although no clear and systematic variation could be discerned from the plagioclase compositions, it is observed that the lowest anorthite contents are present in the highly altered gahnite-plagioclase rocks and the highest anorthite contents are present in the tremolite carbonate rocks.

Plagioclase, although rare in metamorphosed alteration zones of massive sulphide deposits are known to be present in some VMS deposits. For example, porphyroblastic plagioclase with anorthite content-An_{10-22} is widespread in the metamorphosed alteration zones of the Proterozoic to early Paleozoic Bleikvassli Zn-Pb-(Cu) deposit, Norway (Cook, 1993). In Bleikvassli the plagioclase coexists with microcline in the K-feldspar bearing alteration zone (microcline gneiss).

Table-6.1 Representative mineral chemistry of feldspars from unaltered rhyolite

	1	2	3	4	5	6	7	8	9	10
	Oligoclase	**Oligoclase**	**Oligoclase**	**orthoclase**	**orthoclase**	**orthoclase**	**orthoclase**	**orthoclase**	**orthoclase**	**orthoclase**
Sample No.	**PBR-21/1**	**PBS-30/87**	**PBS-30/93**	**PBR-3/74**	**PBR-3/75**	**PBR-3/76**	**PBS-30/94**	**PBS-30/95**	**PBS-30/89**	**PBS-30/90**
SiO2	61.78	64.39	63.94	64.97	64.51	64.60	63.99	64.78	65.00	65.31
Al2O3	22.22	23.33	23.63	18.05	17.86	18.02	18.38	18.67	18.68	18.81
MnO	0.00	0.01	0.02	0.00	0.05	0.03	0.00	0.00	0.00	0.00
CaO	3.44	4.51	4.62	0.02	0.05	0.00	0.00	0.02	0.00	0.00
Na2O	9.41	7.07	7.86	0.75	0.72	0.94	0.50	0.66	0.65	0.77
K2O	0.10	0.22	0.18	15.65	15.64	15.30	15.80	15.79	15.95	15.00
Total	96.95	99.53	100.25	99.44	98.83	98.89	98.67	99.92	100.28	99.89
Cations on the basis of 8 oxygens:										
Si	2.81	2.83	2.45	2.63	3.01	3.01	2.99	2.99	2.99	3.00
Al	1.19	1.21	1.07	0.86	0.98	0.99	1.01	1.02	1.01	1.02
Ca	0.17	0.21	0.19	0.00	0.00	0.00	0.00	0.00	0.00	0.00
Na	0.83	0.60	0.58	0.06	0.07	0.08	0.05	0.06	0.06	0.07
K	0.01	0.01	0.01	0.81	0.93	0.91	0.94	0.93	0.94	0.88
Total	5.01	4.87	4.31	4.37	5.00	4.99	5.00	5.00	5.00	4.97
Mol.per cent end-members :										
Orthoclase	0.58	1.49	1.12	93.12	93.23	91.46	95.41	93.93	94.17	92.76
Albite	82.71	72.83	74.63	6.78	6.52	8.54	4.59	5.97	5.83	7.24
Anorthite	16.71	25.67	24.24	0.10	0.25	0.00	0.00	0.10	0.00	0.00
Total	100.00	100.00	100.00	100.00	100.00	100.00	100.00	100.00	100.00	100.00

Table-6.2 Representative Mineral chemistry of feldspars from altered rhyolite

	1	2	3	4	5	6	7	8	9	10
		andesine	andesine	andesine	andesine	andesine	andesine	andesine	andesine	orthoclase
Sample No.	**PBS-48/189**	**PBS-48/201**	**PBS-48/202**	**PBS-26/93**	**PBS-26/96**	**PBS-26/98**	**PBS-26/116**	**PBS-1/130**	**PBS-1/131**	**PBS-1/125**
								altered	altered	
SiO2	59.67	58.95	57.47	59.22	60.32	59.73	60.04	58.93	59.77	64.77
Al2O3	23.70	25.07	23.36	24.35	24.69	24.38	24.47	24.58	24.76	18.03
MnO	0.00	0.00	0.00	0.06	0.00	0.00	0.01	0.02	0.01	0.00
CaO	5.75	5.55	5.75	6.53	6.80	6.83	7.00	6.98	7.15	6.53
Na2O	7.68	6.42	7.68	7.57	7.73	7.88	7.48	7.18	7.22	0.79
K2O	0.12	0.14	0.12	0.05	0.03	0.04	0.03	0.17	0.13	15.50
Total	96.92	96.13	94.38	97.78	99.57	98.86	99.03	97.86	99.04	105.62
Cations on the basis of 8 oxygens:										
Si	2.73	2.70	2.37	2.69	2.69	2.69	2.69	2.68	2.35	2.89
Al	1.28	1.35	1.13	1.30	1.30	1.29	1.29	1.32	1.15	0.95
Ca	0.28	0.27	0.25	0.32	0.33	0.33	0.34	0.34	0.30	0.31
Na	0.68	0.57	0.61	0.67	0.67	0.69	0.65	0.63	0.55	0.07
K	0.01	0.01	0.01	0.00	0.00	0.00	0.00	0.01	0.01	0.88
Mol.per cent end-members :										
Orthoclase	0.72	0.96	0.72	0.29	0.17	0.23	0.17	1.00	0.76	69.87
Albite	70.22	67.02	70.22	67.52	67.17	67.46	65.80	64.40	64.14	5.41
Anorthite	29.05	32.02	29.05	32.19	32.65	32.31	34.03	34.60	35.10	24.72
	100.00	100.00	100.00	100.00	100.00	100.00	100.00	100.00	100.00	100.00

Table-6.3 Mineral chemistry of feldspars from altered rhyolite and tremolite-carbonate rocks

	11	12	13	14	15	16	17	18	19	20
							----------Tremolite-Carbonate Rocks----------			
	orthoclase	orthoclase	oligoclase	oligoclase	oligoclase	oligoclase	Bytownite	Bytownite	Bytownite	Bytownite
Sample No.	PBS-1/132	PBS-1/133	PBS-31/7	PBS-31/9	PBS-31/11	PBS-31/12	PBC-5/93	PBC-5/95	PBC-5/96	PBC-5/97
SiO2	63.80	64.05	62.74	62.90	62.10	63.34	45.33	50.22	48.67	46.06
Al2O3	17.86	18.06	23.06	23.25	23.17	24.28	34.41	33.19	33.86	33.88
MnO	0.00	0.00	0.00	0.06	0.04	0.03	0.07	0.01	0.02	0.01
CaO	0.00	0.00	4.98	4.89	5.02	4.62	17.27	16.11	16.61	17.59
Na2O	0.83	0.94	8.65	8.60	8.53	8.00	1.44	2.56	2.07	1.28
K2O	15.36	15.29	0.08	0.10	0.07	0.05	0.02	0.04	0.02	0.00
Total	97.85	98.34	99.51	99.80	98.93	100.32	98.53	102.14	101.25	98.82
Cations on the basis of 8 oxygens:										
Si	3.01	3.00	2.79	2.44	2.78	2.78	2.11	1.97	2.20	2.14
Al	0.99	1.00	1.21	1.06	1.22	1.25	1.89	1.53	1.80	1.86
Ca	0.00	0.00	0.24	0.20	0.24	0.22	0.86	0.68	0.80	0.88
Na	0.08	0.09	0.75	0.65	0.74	0.68	0.13	0.19	0.18	0.12
K	0.92	0.91	0.00	0.00	0.00	0.00	0.00	0.00	0.00	0.00
Mol.per cent end-members :										
Orthoclase	92.41	91.45	0.46	0.58	0.41	0.31	0.09	0.23	0.13	0.00
Albite	7.59	8.55	75.52	75.65	75.15	75.57	13.08	22.29	18.40	11.65
Anorthite	0.00	0.00	24.02	23.77	24.44	24.12	86.83	77.47	81.47	88.36
	100.00	100.00	100.00	100.00	100.00	100.00	100.00	100.00	100.00	100.00

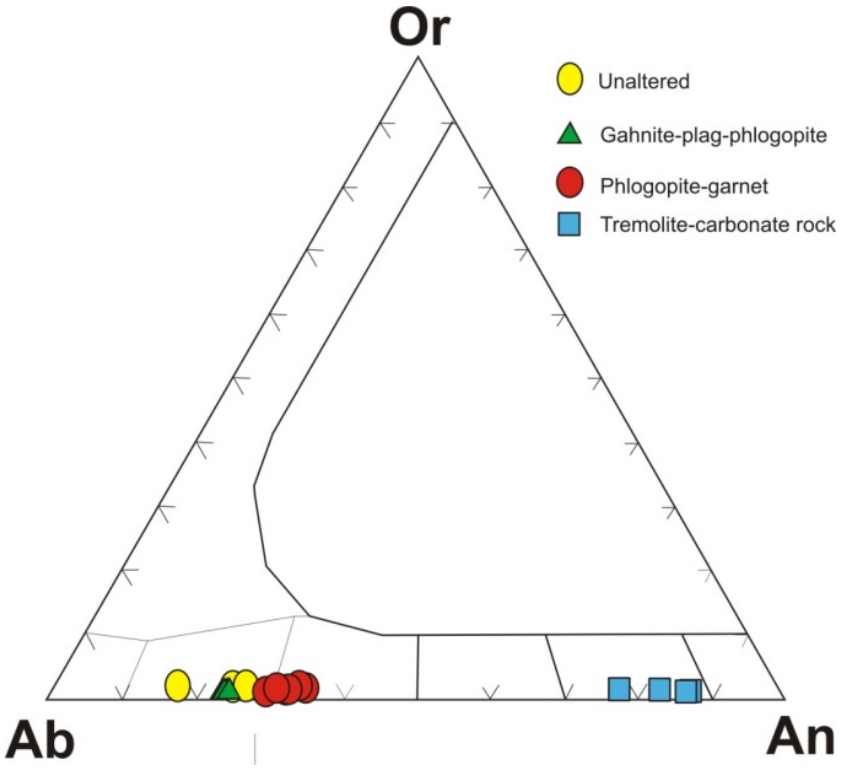

Fig. 6.1 Plagioclase compositions from various altered and unaltered rocks from Bhuyari (Feldspars of altered rocks are products of metamorphic recrystallization)

Biotite and Phlogopite

Biotite is the most widespread metamorphic mineral in the alteration zones of Bhuyari. A total of 34 biotite analyses are presented and studied from the unaltered as well as the representative alteration zones (Table 6.4, 6.5 and 6.6). The location of the sample numbers shown in the Tables 6.4, 6.5 and 6.6 are shown in the detailed map (Fig.2.2b). The biotite contents for 12 samples of least altered/ unaltered rhyolites are compared with those in the different alteration zones. Broadly, the results showed two distinct populations-biotites from least altered rhyolite show lower Mg number [Mg# = Mg/(Mg+Fe)] and the biotite from altered rhyolite shows higher Mg# and can be classified into

biotite and phlogopite respectively (Fig.6.2). When plotted in the biotite classification diagrams the unaltered biotite falls in the boundary between the siderophyllite-annite fields, whereas the altered biotite fall in the phlogopite field (Fig.6.2).

For the biotite from the unaltered rhyolites, the Mg number ranges from 0.24 to 0.28 as their MgO wt % ranges from 5 to 6 wt. %. Biotite is the major Ti-bearing mineral in the rhyolites. The unaltered/least altered biotite contain higher TiO_2 contents (1.9 to 2.9 wt.%) than the highly altered rhyolites (0.21 to 0.86 wt. %).

For biotite from altered rhyolites (biotite-phlogopite bearing schists) MgO ranges from 13.39 to 19.45 wt. % and the Mg # ranges from 0.64 to 0.8, which is considerably higher. An increase in Mg# is observed in the altered rhyolites towards the ore zone. The biotite-plagioclase-garnet assemblages distal to ore (sample-PBS-45) have lower Mg# (0.64 to 0.66) and the phlogopite-staurolite-garnet rocks proximal to massive sulphides (PBS-48) have highest Mg# (0.78 to 0.80). Those with Mg# more than 0.65 plot in the phlogopite field in the classification diagrams (Fig. 6.2). Increase in the X_{Mg} of biotite and chlorite has been documented in hydrothermally altered footwall rhyolites when compared to unaltered rhyolite at the Cambro-Ordovician Zn-Pb-Cu VMS deposit of Thalanga, Mount Windsor Sub Province, Northern Queensland, Australia (Paulick and Franz, 2001), and has been suggested as an indicator to identify fossil, metamorphosed, hydrothermal systems associated with massive sulphide deposits.

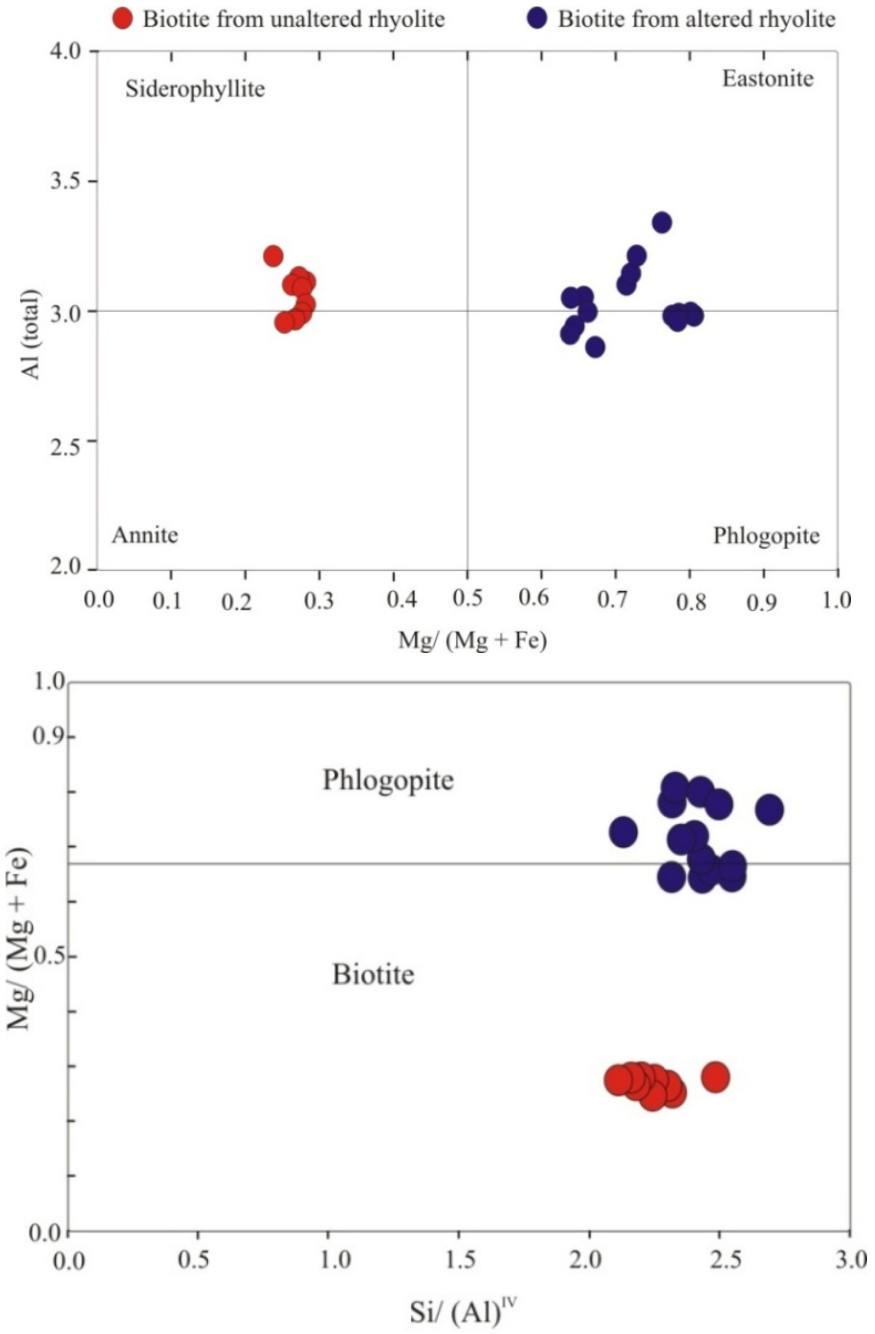

Fig.6.2 The compositions of biotite and phlogopite from unaltered rhyolite and altered rhyolite plotted in the biotite composition diagram show that the biotites in highly altered zones proximal to ore are more Mg-rich, while the biotite from unaltered rhyolite show lower Mg-contents.

Table-6.4 Mineral chemistry of biotite from least altered rhyolites from Bhuyari.

	1	2	3	4	5	6	7	8	9	10	11	12
Sample	**PBR-30/54**	**PBR-30/55**	**PBR-30/56**	**PBR-30/57**	**PBR-30/58**	**PBR-30/64**	**PBR-30/65**	**PBR-30/82**	**PBR-30/85**	**PBR-30/86**	**PBR-3/71**	**PBR-3/72**
SiO2	35.11	34.97	34.92	35.41	35.80	35.18	35.45	35.12	36.28	35.78	35.02	34.87
TiO2	2.77	2.99	2.19	2.31	1.89	2.83	2.81	2.59	2.35	2.48	2.30	2.10
Al2O3	16.09	16.75	16.31	16.35	17.62	16.47	16.32	16.82	16.86	16.81	15.71	15.71
FeO	26.16	25.99	27.01	27.63	27.45	26.65	26.21	26.41	27.05	26.88	26.64	26.29
MnO	0.62	0.63	0.74	0.68	0.64	0.64	0.55	0.74	0.69	0.70	0.79	0.78
MgO	5.57	5.21	5.94	6.05	4.82	5.64	5.74	5.74	5.99	5.80	5.05	5.21
CaO	0.01	0.02	0.00	0.03	0.55	0.02	0.01	0.03	0.05	0.02	0.00	0.00
Na2O	0.09	0.19	0.10	0.08	1.91	0.01	0.09	0.11	0.09	0.18	0.07	0.10
K2O	9.42	9.46	9.07	9.52	5.54	9.58	9.56	9.33	9.57	9.36	9.44	9.61
Total	95.84	96.21	96.28	98.06	96.22	97.02	96.74	96.89	98.93	98.01	95.02	94.66
Cations on the basis of 22 oxygens												
Si	5.52	5.48	5.49	5.48	5.53	5.48	5.52	5.47	5.53	5.51	5.59	5.59
Al iv	2.48	2.52	2.51	2.52	2.47	2.52	2.48	2.53	2.47	2.49	2.41	2.41
Al vi	0.51	0.57	0.51	0.46	0.74	0.51	0.52	0.55	0.55	0.56	0.55	0.55
Ti	0.33	0.35	0.26	0.27	0.22	0.33	0.33	0.30	0.27	0.29	0.28	0.25
Fe	3.44	3.41	3.55	3.58	3.55	3.47	3.41	3.44	3.45	3.46	3.56	3.52
Mn	0.08	0.08	0.10	0.09	0.08	0.08	0.07	0.10	0.09	0.09	0.11	0.11
Mg	1.31	1.22	1.39	1.40	1.11	1.31	1.33	1.33	1.36	1.33	1.20	1.24
Ca	0.00	0.00	0.00	0.00	0.09	0.00	0.00	0.01	0.01	0.00	0.00	0.00
Na	0.03	0.06	0.03	0.02	0.57	0.00	0.03	0.03	0.03	0.05	0.02	0.03
K	1.89	1.89	1.82	1.88	1.09	1.90	1.90	1.85	1.86	1.84	1.92	1.96
Fe/Fe+Mg	0.72	0.74	0.72	0.72	0.76	0.73	0.72	0.72	0.72	0.72	0.75	0.74
Mg/(Mg+Fe)	0.28	0.26	0.28	0.28	0.24	0.27	0.28	0.28	0.28	0.28	0.25	0.26

Table-6.5 Mineral chemistry of biotite/phlogopite from various altered rhyolites from Bhuyari

	13	14	15	16	17	18	19	20	21	22	23
Sample	**PBS-26/78**	**PBS-26/79**	**PBS-26/86**	**PBS-26/112**	**PBS-26/113**	**PBS-26/114**	**PBS-26/118**	**PBS-26/95**	**PBS-45/4**	**PBS-45/6**	**PBS-45/8**
oxides											
SiO2	38.91	36.88	38.31	38.53	36.92	37.76	38.99	38.38	36.71	37.50	37.88
TiO2	0.75	0.68	0.81	0.79	0.71	0.92	0.65	0.70	0.35	0.37	0.23
Al2O3	17.51	17.99	17.23	17.46	17.39	17.23	17.48	17.32	16.36	17.06	17.25
FeO	9.28	9.56	9.39	8.56	9.03	8.63	8.47	9.30	14.87	13.63	14.46
MnO	0.33	0.37	0.45	0.29	0.35	0.32	0.32	0.32	0.43	0.59	0.55
MgO	18.73	19.03	18.38	19.45	20.39	19.77	18.95	18.24	15.17	14.51	14.37
CaO	0.00	0.01	0.00	0.03	0.00	0.02	0.00	0.00	0.00	0.00	0.05
Na2O	0.29	0.24	0.24	0.24	0.19	0.21	0.26	0.20	0.19	0.20	0.21
K2O	9.35	8.02	9.11	9.03	8.07	8.60	9.12	9.47	8.95	9.23	9.27
Total	95.15	92.77	93.91	94.38	93.04	93.47	94.24	93.95	93.03	93.09	94.27
Cations on the basis of 22 oxygens											
Si	5.62	5.46	5.62	5.59	5.44	5.53	5.66	5.63	5.60	5.68	5.68
Al iv	2.38	2.54	2.38	2.41	2.56	2.47	2.34	2.37	2.40	2.32	2.32
Al vi	0.61	0.60	0.59	0.58	0.46	0.51	0.64	0.63	0.54	0.72	0.73
Ti	0.08	0.08	0.09	0.09	0.08	0.10	0.07	0.08	0.04	0.04	0.03
Fe	1.12	1.18	1.15	1.04	1.11	1.06	1.03	1.14	1.90	1.73	1.81
Mn	0.04	0.05	0.06	0.04	0.04	0.04	0.04	0.04	0.06	0.08	0.07
Mg	4.04	4.20	4.02	4.21	4.48	4.32	4.10	3.99	3.45	3.27	3.21
Ca	0.00	0.00	0.00	0.00	0.00	0.00	0.00	0.00	0.00	0.00	0.01
Na	0.08	0.07	0.07	0.07	0.05	0.06	0.07	0.06	0.06	0.06	0.06
K	1.72	1.51	1.70	1.67	1.52	1.61	1.69	1.77	1.74	1.78	1.77
Fe/Fe+Mg	0.22	0.22	0.22	0.20	0.20	0.20	0.20	0.22	0.35	0.35	0.36
Mg/ Mg + Fe	0.78	0.78	0.78	0.80	0.80	0.80	0.80	0.78	0.65	0.65	0.64

Table-6.6 Mineral chemistry of biotite/phlogopite from various altered rhyolites from Bhuyari

	24	25	26	27	28	29	30	31	32	33	34
Sample	**PBS-45/10**	**PBS-45/12**	**PBS-48/187**	**PBS-48/186**	**PBS-48/187**	**PBS-48/188**	**PBS-1/134**	**PBS-1/135**	**PBS-31/16**	**PBS-31/17**	**PBS-31/18**
SiO2	35.69	38.13	38.21	39.84	38.21	38.76	38.20	38.17	38.15	38.26	36.15
TiO2	0.34	0.24	0.47	0.36	0.47	0.43	1.68	1.94	0.75	0.86	0.68
Al2O3	16.45	16.89	16.87	19.34	16.87	17.08	16.40	16.26	18.01	17.93	18.10
FeO	14.67	13.37	8.73	8.25	8.73	8.85	13.47	12.87	10.87	11.39	11.16
MnO	0.58	0.36	0.72	0.59	0.72	0.68	0.96	0.84	0.43	0.39	0.47
MgO	14.67	14.73	17.30	14.80	17.30	17.83	13.39	14.86	15.71	16.03	16.79
CaO	0.04	-0.03	0.02	0.03	0.02	0.00	0.06	0.04	0.05	0.00	0.13
Na2O	0.18	0.17	0.20	0.20	0.20	0.20	0.15	0.11	0.18	0.23	0.20
K2O	8.48	9.52	9.76	9.51	9.76	9.63	9.63	9.71	9.51	9.51	8.24
Total	91.10	93.38	92.28	92.92	92.28	93.45	93.95	94.80	93.67	94.59	91.92
Cations on the basis of 22 oxygens											
Si	5.56	5.74	5.71	5.84	5.71	5.71	5.74	5.68	5.65	5.63	5.46
Al iv	2.44	2.26	2.29	2.16	2.29	2.29	2.26	2.32	2.35	2.37	2.54
Al vi	0.58	0.74	0.69	1.18	0.69	0.68	0.65	0.53	0.80	0.74	0.68
Ti	0.04	0.03	0.05	0.04	0.05	0.05	0.19	0.22	0.08	0.09	0.08
Fe	1.91	1.68	1.09	1.01	1.09	1.09	1.69	1.60	1.35	1.40	1.41
Mn	0.08	0.05	0.09	0.07	0.09	0.08	0.12	0.11	0.05	0.05	0.06
Mg	3.41	3.31	3.86	3.23	3.86	3.92	3.00	3.29	3.47	3.52	3.78
Ca	0.01	0.00	0.00	0.00	0.00	0.00	0.01	0.01	0.01	0.00	0.02
Na	0.05	0.05	0.06	0.06	0.06	0.06	0.04	0.03	0.05	0.06	0.06
K	1.68	1.83	1.86	1.78	1.86	1.81	1.85	1.84	1.80	1.78	1.59
Fe/Fe+Mg	0.36	0.34	0.22	0.24	0.22	0.22	0.36	0.33	0.28	0.28	0.27
Mg/ Mg + Fe	0.64	0.66	0.78	0.76	0.78	0.78	0.64	0.67	0.72	0.72	0.73

Garnet

Garnet is a common mineral in the metamorphosed alteration zones; they are widespread in the intensely altered zones and are also present occasionally as a minor constituent in the least altered/unaltered rhyolite. This provides an opportunity to study the variations of their chemical and mineralogical composition with respect to proximity to mineralized zones. Since all these garnets are metamorphic in origin, their composition reflects the bulk composition of the protolith. Garnet in the unaltered rhyolite are volumetrically minor (< 2%) and occur as discrete, <2mm, reddish garnets, while the highly altered biotite-phlogopite-gahnite bearing rocks and quartz-muscovite-K feldspar schists have higher garnet contents (up to 20 %) and their sizes range from < 1mm to 1cm. Garnets are generally rare in the tremolite-carbonate rocks. However, they are locally enriched in the banded/layered outcrop of tremolite-carbonate rocks.

Garnet analyses from unaltered and various types of altered rhyolites were compared to understand their compositional differences (Table 6.7, 6.8 and 6.9). The garnets are mostly almandine-spessartine solid solution, and have the following chemical composition (end member %): almandine (22.37 to 45.50 %), spessartine (32.72 to 57.85 %), pyrope (0.73 to 18.10 %), grossular (6.79 to 13.72 %). The Almandine (Alm), spessartine (Sps), Grossular (Gsr) and Pyrope (Prp) contents show wide variations in least altered and among the different types of metamorphosed alteration assemblages. In unaltered rhyolite, garnet compositions vary from $Alm_{43.6}$ to $Alm_{45.50,}$ $Sps_{32.5}$ to $Sps_{38.2}$, Gsr_{17} to $Gsr_{20.73}$ and $Prp_{0.7}$ o $Prp_{1.8}$. They form almandine-spessartine solid solutions and are basically almandine-rich.

In the various types of altered rhyolites, the garnet compositions vary from Alm_{11} to $Alm_{42.8}$, $Sps_{32.9}$ to $Sps_{57.8}$, $Gsr_{.8}$ to $Gsr_{33.8}$ and Prp_{6} to $Prp_{18.1}$. The garnets in the altered rhyolites are mostly spessartine-almandine solid solution

with enrichment in the spessartine component (33 to 56.5, avg. 45.19), which is significantly higher than those from unaltered garnets (avg. 34). The MnO contents (wt. %) are also significantly higher and ranges from 15.14 to 24.89. This shows that the predominant Mn-hosting mineral in the altered rocks are garnets. The almandine component ranges from 22.37 to 42.87, with an average of 33.40, which is lower than those from unaltered garnets (44.54).

Tremolite-carbonate rocks show MnO content of 21.91 wt. % and a high CaO content of 11.94 wt. %. The garnet has high spessartine component like the garnets from other proxminal alteration zones ($Sps_{47.3}$ to $Sps_{49.09}$), however they also possess high grossular component unlike the other garnets (Gsr.33.8 to $Gsr_{37.65}$) (Table 6.9). The high grossular content in a carbonate assemblage indicates that the protolith was Ca-rich and the participation of Ca(-Mn) minerals such as carbonate or epidote in the garnet-forming reaction (Paulick and Franz, 2001).

Garnets show zoning from core to rim, with higher spessartine and corresponding lower almandine contents towards the rim (Fig.6.3 & 6.4). Increasing spessartine contents from core towards the rims is indicative of decreasing temperatures during metamorphism (Tracey, 1982). Zoning in garnet with spessartine-rich rims are documented in garnets from altered and unaltered rhyolites, testifying for the uniform nature of metamorphic conditions. This may indicate retrogressive metamorphism towards the waning stages after peak metamorphism.

Spessartine-rich garnets as present in Bhuyari can form at much lower temperatures than required for their formation in metapelites where the garnet in isograd is at 500°C, because the temperature of garnet formation is considerably reduced in manganese and/or calcium-rich rocks (Spear, 1993).

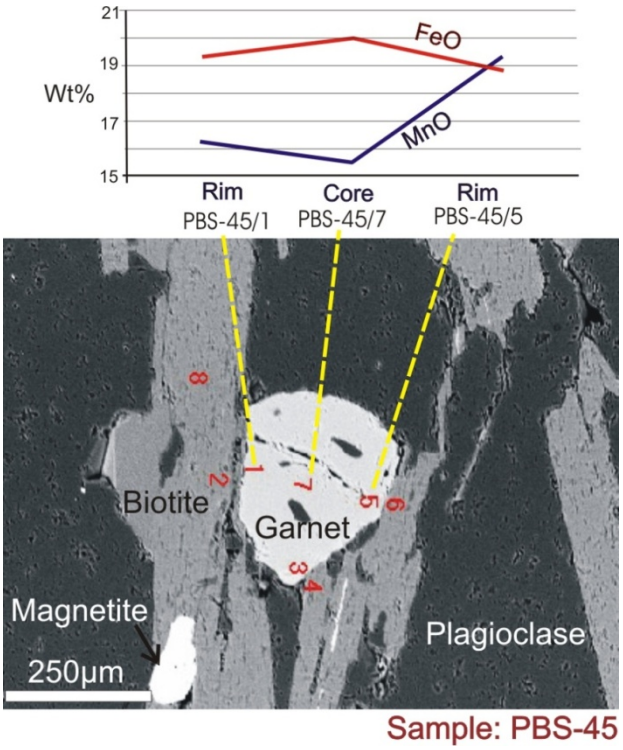

Fig.6.3 Back Scattered Electron (BSE) image of garnet-biotite-plagioclase assemblage showing analysed point locations. The garnet shows elevated MnO contents and corresponding lower FeO contents from the core to the rim indicating their zoned nature. *EPMA data of points shown in this figure are given in Table-6.9.*

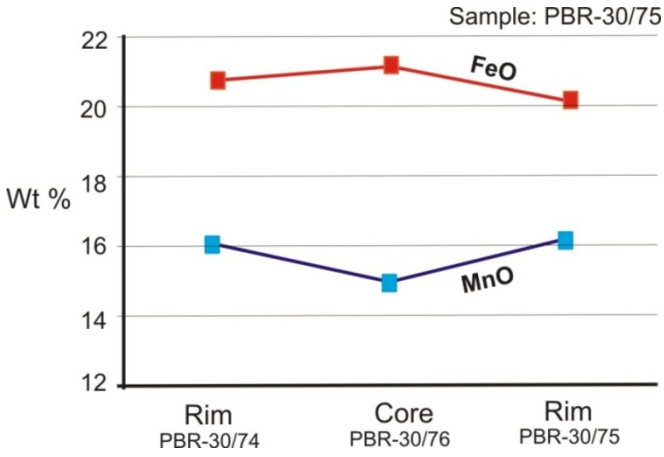

Fig. 6.4 Garnet from unaltered / least altered rhyolite showing zoned nature. Analyses are from sample No. PBR-30, *EPMA data for this figure are given in Table-6.7*

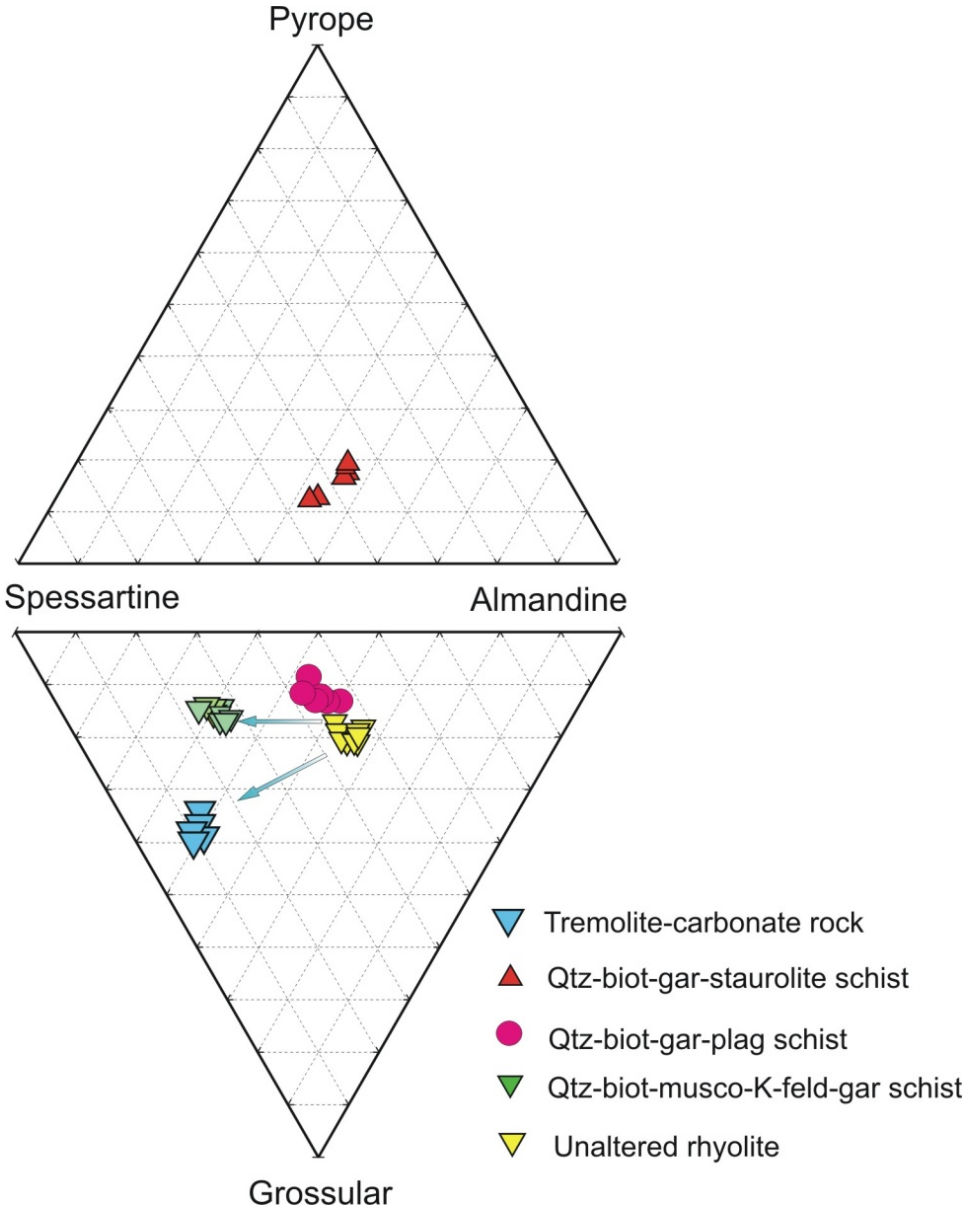

Fig. 6.5 The compositions of garnets from the Bhuyari area. Symbols are given for garnets from various alteration types. Garnets from altered rhyolite have spessartine-rich compositions when compared to those from unaltered rhyolite. Garnets from tremolite-garnet rocks show enrichment in grossular in addition to spessartine. Arrows show alteration vectors in terms of increase in spessartine content of garnet with alteration.

This study has documented that the alteration zones close to the mineralized zones are more spessartine-rich than those which occur in least altered rhyolites. Garnets from altered rhyolites hosting mineralization in the form of disseminated and vein sulphides (PBS-1 BR-4 and PBS-48, PBC-4 and PBC-5) have highest spessartine content (Sp_{54-58}), when compared to garnets from footwall alteration zones close to mineralization but lacking sulphides (PBS-26, Sp_{33-43}) and those from unaltered rhyolites (Sp_{32-38}). The increase in spessartine contents in different alteration types can be visualized in Fig 6.5. This shows that garnet compositions can be used as a reliable tool for identifying proximal ore-related hydrothermal systems in metamorphosed terrains.

Pyrope contents (mol. %) of the altered rhyolites (5-18) are much higher than those of unaltered rhyolites (0.7 to 1.7), however, there is no systematic relationship with proximity to mineralized zones. Almandine contents are lower for garnets from altered rhyolite (22-44) when compared to unaltered rhyolite (43-45). Grossular contents are also lower in altered rhyolites (7-15) when compared to garnets from unaltered rhyolite (17-21), except for those in carbonate-altered lithounits proximal to ore zones which has much higher grossular content (up to 37 mol %) (Table.6.9).

Overall, the most spessartine-rich garnet compositions are found in the alteration zones closest to the mineralized zones. Those from unaltered rhyolites further away from mineralization have lower spessartine and higher almandine contents. Grossular and pyrope contents of garnets also increase towards the mineralized zones.

Systematic enrichment of manganese in the garnets towards ore zones have been documented in several other metamorphosed massive sulphide deposits. In the Pegmont Pb-Zn deposit, garnets distal to ore zones are Fe-rich (and Mn-poor) and those proximal to the ore zones are (Mn-rich and Fe-poor). Similarly, Mn contents of garnet increase towards the ore zones in Broken Hill (South Africa) (eg. Spry et al, 2000).

Table 6.7 Representative mineral composition of garnets from unaltered rhyolite

	1	2	3	4	5	6	7	8	9	10	11
	PBR-3/70	**PBR-30/53**	**PBR-30/62**	**PBR-30/63**	**PBR-30/67**	**PBR-30/68**	**PBR-30/69**	**PBR-30/70A**	**PBR-30/74**	**PBR-30/75**	**PBR-30/76**
oxide									RIM-1	RIM-1	CORE-1
SiO2	36.86	37.1	36.96	37.52	36.82	37.21	37.11	36.21	37.42	37.39	37.40
TiO2	0.04	0.04	0.05	0.03	0.1	0.12	0.07	0	0.00	0.09	0.07
Al2O3	19.17	20.38	19.8	20.8	20.27	20.67	21.12	19.97	20.34	20.77	20.89
Fe2O3	0	1.43	1.92	0.45	1.26	1.06	1.4	1.08	2.94	1.15	2.00
FeO	19.49	19.5	18.95	19.31	19.05	19.3	19.36	18.33	18.04	19.12	19.30
MnO	15.32	14.96	15.57	15.9	15.1	14.72	15.11	16.71	16.03	16.19	14.95
MgO	0.18	0.43	0.36	0.33	0.45	0.46	0.44	0.28	0.36	0.33	0.45
CaO	6.84	7.01	6.93	6.94	7	7.47	7.02	5.89	7.67	6.78	7.45
total	97.9	100.85	100.54	101.27	100.06	101.02	101.63	98.47	102.80	101.81	102.51
Cations on the basis of 12 oxygens											
Si	3.06	2.99	2.99	3	2.99	2.98	2.96	2.99	2.96	2.98	2.96
Ti	0	0	0	0	0.01	0.01	0	0	0.00	0.01	0.00
Al	1.88	1.93	1.89	1.96	1.94	1.95	1.99	1.95	1.90	1.95	1.95
Fe3	0	0.09	0.12	0.03	0.08	0.06	0.08	0.07	0.18	0.07	0.12
Fe2	1.35	1.31	1.28	1.29	1.29	1.29	1.29	1.27	1.19	1.28	1.28
Mn	1.08	1.02	1.07	1.08	1.04	1	1.02	1.17	1.08	1.09	1.00
Mg	0.02	0.05	0.04	0.04	0.05	0.05	0.05	0.03	0.04	0.04	0.05
Ca	0.61	0.6	0.6	0.6	0.61	0.64	0.6	0.52	0.65	0.58	0.63
almandine	44.2	45.5	44.99	43.52	44.62	44.47	45.12	43.6	43.66	43.97	45.29
pyrope	0.73	1.68	1.4	1.3	1.77	1.8	1.72	1.13	1.35	1.28	1.72
grossular	19.85	19.66	19.31	19.63	19.82	21.01	19.68	17.05	20.73	18.96	20.49
spessartine	35.19	33.16	34.3	35.55	33.79	32.72	33.49	38.23	34.26	35.79	32.50

Table 6.8 Representative mineral composition of garnets from altered rhyolite

	12	13	14	15	16	17	18	19	20
Sample	**PBR-48/184**	**PBR-48/195**	**PBS-26/72**	**PBS-26/73**	**PBS-26/74**	**PBS-26/75**	**PBS-26/76**	**PBS-26/83**	**PBS-1/126**
SiO2	35.51	35.48	36.55	37.04	37.3	37.24	37.6	37.6	37.3
TiO2	0.03	0	0	0	0.03	0.06	0.05	0.05	0.04
Al2O3	20.25	20.21	20.97	20.77	20.69	20.74	20.74	21.11	20.33
Fe2O3	0.82	2.05	2.31	2.03	1.59	2.37	0.54	0.7	0.24
FeO	8.93	8.27	17.32	17.94	17.97	17.43	17.82	17.63	10.57
MnO	24.69	24.14	15.14	15.41	15	15.32	18.39	18.82	24.67
MgO	1.49	2.04	4.24	4.15	4.68	4.64	2.94	2.86	1.52
CaO	4.6	4.74	2.73	2.61	2.44	2.63	2.59	2.51	4.97
total	96.32	96.93	99.25	99.95	99.7	100.43	100.67	101.28	99.64
Cations on the basis of 12 oxygens									
Si	2.97	2.95	2.94	2.96	2.98	2.96	3	2.99	3.02
Ti	0	0	0	0	0	0	0	0	0
Al	2	1.98	1.99	1.96	1.95	1.94	1.95	1.98	1.94
Fe3	0.05	0.13	0.14	0.12	0.1	0.14	0.03	0.04	0.01
Fe2	0.63	0.57	1.16	1.2	1.2	1.16	1.19	1.17	0.72
Mn	1.75	1.7	1.03	1.04	1.01	1.03	1.24	1.27	1.69
Mg	0.19	0.25	0.51	0.49	0.56	0.55	0.35	0.34	0.18
Ca	0.41	0.42	0.24	0.22	0.21	0.22	0.22	0.21	0.43
almandine	22.37	22.84	42.35	42.87	42.12	41.87	40.25	40.01	24.06
pyrope	6.14	8.21	16.51	16.04	18.11	17.7	11.52	11.17	6.04
grossular	13.63	13.72	7.64	7.25	6.79	7.21	7.29	7.05	14.2
spessartine	57.85	55.23	33.5	33.84	32.98	33.21	40.94	41.77	55.71

Table 6.9 Representative mineral composition of garnets from altered rhyolite and tremolite-carbonate rocks

	21	22	23	24	25	26	27	28	29	30	31	32	33
Sample	**PBS-1/127**	**PBS-1/136**	**BR-4/6**	**BR-4/7**	**BR-4/8**	**PBS-45/1**	**PBS-45/5**	**PBS-45/7**	**PBC-5/92**	**PBC-4/95**	**PBC-4/96**	**PBC-4/97**	**PBC-4/98**
oxide						RIM	RIM	CORE					
SiO2	36.55	37.25	36.37	35.89	36.20	34.92	34.62	36.01	39.22	37.37	38.35	38.25	37.74
TiO2	0.05	0.05	0.06	0.09	0.05	0.02	0.05	0.02	0.10	0.03	0.17	0	0.05
Al2O3	20.06	20.42	20.82	20.70	20.99	21.24	20.00	20.80	21.36	21.49	21.03	21.49	21.36
Fe2O3	0.96	0.31	0.00	0.00	0.00	0.00	0.00	0.00	0.00	0	0	0	0
FeO	9.87	10.77	11.07	10.92	10.78	19.50	18.94	19.88	4.99	4.64	5.04	4.49	4.64
MnO	24.89	24.64	24.58	24.11	24.23	15.99	19.16	15.72	21.91	21.35	20.87	21.95	20.92
MgO	1.24	1.38	1.75	1.83	1.84	2.07	1.24	2.29	1.53	1.48	1.5	0.78	1.29
CaO	5.04	5.00	5.10	5.28	5.66	4.40	3.27	4.34	11.94	12.32	12.34	13.01	12.88
Total	98.66	99.82	99.75	98.82	99.75	98.14	97.28	99.06	101.05	98.68	99.3	13.01	12.88
cations on the basis of 12 oxygens													
Si	3.00	3.01	2.94	2.92	2.92	2.86	2.90	2.92	3.07	2.99	3.05	3.04	3.01
Ti	0.00	0.00	0.00	0.01	0.00	0.00	0.00	0.00	0.01	0	0.01	0	0
Al	1.94	1.95	1.98	1.99	1.99	2.05	1.97	1.99	1.97	2.02	1.97	2.01	2.01
Fe3	0.06	0.02	0.14	0.16	0.17	0.22	0.23	0.16	0.00	0	0	0	0
Fe2	0.68	0.73	0.61	0.58	0.56	1.11	1.09	1.19	0.33	0.31	0.34	0.3	0.31
Mn	1.73	1.69	1.68	1.66	1.65	1.11	1.36	1.08	1.45	1.45	1.41	1.44	1.41
Mg	0.15	0.17	0.21	0.22	0.22	0.25	0.15	0.28	0.18	0.18	0.18	0.09	0.15
almandine	24.07	24.61	24.27	24.07	23.51	43.31	42.33	43.75	11.04	10.38	11.29	10.14	10.40
pyrope	4.95	5.48	6.84	7.19	7.15	8.20	4.94	8.98	6.03	5.9	5.99	3.14	5.15
grossular	14.47	14.28	14.32	14.91	15.81	12.52	9.36	12.24	33.84	35.32	35.4	37.65	36.97
spessartine	56.50	55.63	54.57	53.83	53.52	35.97	43.37	35.04	49.09	48.39	47.33	49.07	47.48

Hornblende

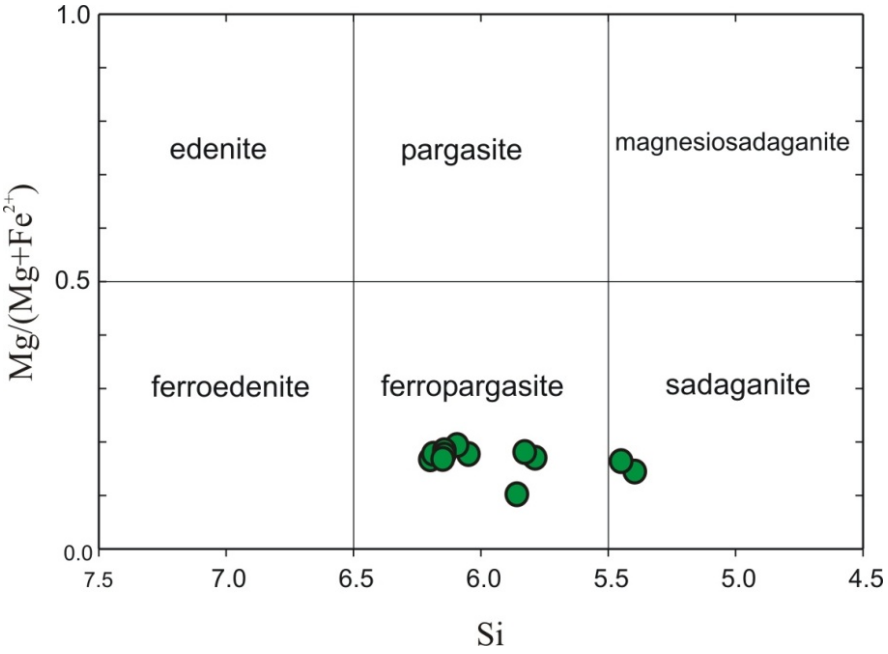

Fig.6.6 The compositions of amphibole plotted in the amphibole classification diagram after Leake et. al., 1997. The diagram parameters are $Ca_B > 1.5$ and $(Na + K)_A > 0.5$.

The hornblende data from the hornblende-bearing rhyolite (PBR-33) is provided in Table 6.10. The mineral composition is plotted in the hornblende classification diagram after Leake et. al.,1997 (Fig. 6.6). The hornblende composition from the least altered hornblende bearing rhyolites when plotted in the least altered rhyolites show that they are mostly iron-rich pargasite (ferropargasite) and sadaganite. This variety of hornblende which has higher Si and Fe contents and lower Mg contents, and more substitution of Al and Fe for silica. FeO (Total) ranges from 26.27 to 28.71wt. %. The MgO contents are low and range from 2.13 to 3.24 wt. %. CaO contents range from 9.71 to 10.97 Wt. %.

Table 6.10 Representative mineral compositions of hornblende from the hornblende- bearing rhyolite.

Sample No	1	2	3	4	5	6	7	8
PBR-33	PBR-33/27	PBR-33/28	PBR-33/29	PBR-33/31	PBR-33/33	PBR-33/34	PBR-33/35	PBR-33/36
SiO2	36.18	35.44	39.04	35.30	37.46	38.83	38.51	38.48
TiO2	0.81	0.75	0.79	0.76	0.88	0.70	0.70	0.67
Al2O3	13.48	20.01	12.37	21.89	16.25	12.47	12.29	13.89
Cr2O3	0.00	0.00	0.00	0.00	0.00	0.00	0.00	0.00
FeOT	28.71	26.95	28.53	26.27	28.13	28.69	28.31	27.76
MnO	1.15	1.08	1.21	1.11	1.15	1.16	1.10	1.10
MgO	2.76	2.46	2.86	2.13	2.77	3.24	3.02	2.98
CaO	10.70	10.10	10.97	9.71	10.25	10.95	10.54	10.69
Na2O	1.46	1.20	1.30	1.00	1.36	1.34	1.50	1.40
K2O	1.71	1.63	1.69	1.59	1.67	1.61	1.64	1.64
NiO	0.00	0.00	0.00	0.00	0.00	0.00	0.00	0.00
Total	96.96	99.62	98.76	99.76	99.92	98.99	97.61	98.61
Fe2O3	6.62	5.36	3.90	4.25	4.23	5.19	3.49	3.47
FeO	22.76	22.13	25.02	22.45	24.33	24.02	25.17	24.63
Total	97.62	100.16	99.15	100.19	100.34	99.51	97.96	98.96
Cations	23(O)	23(O)	23(O)	23(O)	23(O)	23(O)	23(O)	23(O)
Si	5.82	5.45	6.16	5.39	5.80	6.09	6.15	6.05
Ti	0.10	0.09	0.09	0.09	0.10	0.08	0.08	0.08
Al	2.56	3.63	2.30	3.94	2.97	2.31	2.31	2.57
Cr	0.00	0.00	0.00	0.00	0.00	0.00	0.00	0.00
Fe+3	0.80	0.62	0.46	0.49	0.49	0.61	0.42	0.41
Fe+2	3.06	2.85	3.30	2.87	3.15	3.15	3.36	3.24
Mn	0.16	0.14	0.16	0.14	0.15	0.15	0.15	0.15
Mg	0.66	0.56	0.67	0.49	0.64	0.76	0.72	0.70
Ca	1.84	1.66	1.85	1.59	1.70	1.84	1.80	1.80
Na	0.46	0.36	0.40	0.30	0.41	0.41	0.46	0.43
K	0.35	0.32	0.34	0.31	0.33	0.32	0.33	0.33
Total	15.81	15.68	15.74	15.61	15.74	15.73	15.80	15.76

Muscovite

The muscovite analyses are provided in Table 6.11a and Table 6.11b and the mineral chemistry data are plotted in the diagram of Guidotti and Sassi (1998) (Fig. 6.7). The analyses given in these tables are also used for geothermobarometric estimations in chapter-8 (section 8.3.3). Muscovite

compositions are compared between those from the mineralized zones and those from altered rocks close to mineralization but do not host mineralization. The samples BR-1 and PBS-1 are from the quartz-muscovite-K feldspar schist containing sulphide mineralization (pyrite, sphalerite, galena and chalcopyrite) as veins and disseminations and the samples PBS-26 and PBS-31 are from alteration zone occurring to the south of the mineralized zone. The MgO and FeO contents of muscovite within the mineralized zone ranges from 1.70 to 1.98 wt.% and 2.3 to 2.5 wt. % respectively. Whereas, the MgO and FeO contents of altered rocks lacking in sulphides ranges from 0.28 to 0.52 and 0.41 to 0.47 wt. % respectively. This shows that there is a marked increase in the phengite component of muscovite in the mineralised zones when compared to those outside mineralized zones.

Increase in phengitic composition of white micas has been documented with increasing proximity to proximal alteration zones in several VMS deposits, for example, spectral reflectance studies of hydrothermal alteration zones at the Hellyer Zn-Pb-Cu-Ag-Au VMS deposit in Australia, showed that phengitic white micas occupied the central regions of the footwall alteration pipe, whereas normal muscovite was present in the distal parts of the alteration zones (Yang et al, 2011). A similar pattern was recognized in the white micas in the hydrothermal alteration zones of VMS deposits in the Panorama district of Western Australia (Cudahy et al., 1999).

The composition of white mica is a function of physical and chemical conditions, mainly temperature, pressure and bulk chemical composition (e.g., Massonne and Schreyer, 1987; Velde, 1967). The Tschermak substitution, $Si^{iv}[Mg, Fe^{2+}]^{vi} = Al^{iv}Al^{vi}$, representing coupled octahedral and tetrahedral cation substitutions, is one of the most common causes for the compositional variation of white mica (Guidotti and Sassi, 1976, 1998) (Fig. 6.7). This substitution

results in white mica with compositions transitional from muscovite to celadonite, which is commonly termed phengite or phengitic white mica.

Although the muscovite in Bhuyari is a product of prograde metamorphism and do not represent the primary hydrothermal sericite or white mica, it can be assumed that the primary hydrothermal sericite/muscovite despite recrystallization and reconstitution via new growth during metamorphism has still retained its Mg-Fe compositional variations.

Table 6.11a EPMA analyses of muscovite from the altered rhyolites.

	1	2	3	4	5	6	7	8	9
Sample No.	**PBS-1/122**	**PBS-1/123**	**PBS-1/124**	**PBS-1/128**	**PBS-1/129**	**PBS-26/84**	**PBS-26/85**	**PBS-26/104**	**PBS-26/105**
SiO2	46.925	47.937	48.193	48.769	47.592	46.578	46.207	46.392	46.466
TiO2	1.153	1.16	1.409	1.388	1.343	0.217	0.06	0.309	0.319
Al2O3	29.695	30.665	30.629	30.369	30.192	35.107	35.081	34.608	36.361
FeO	2.535	2.653	2.485	2.521	2.536	0.587	0.67	0.493	0.405
MnO	0.078	0.037	0.107	0.179	0.053	0.039	0.06	0.023	0.025
MgO	1.878	1.976	1.91	1.872	1.763	0.769	0.808	0.743	0.282
CaO	0.022	0.011	0.023	0.014	0	0.008	0.017	0	0.008
Na2O	0.266	0.302	0.274	0.229	0.254	0.942	0.993	0.942	1.422
K2O	10.459	10.761	10.956	10.561	10.809	9.605	9.546	9.833	9.227
Total	93.011	95.502	95.986	95.902	94.542	93.852	93.442	93.343	94.515
Cations on the basis of 22 oxygens									
Si	6.45	6.42	6.43	6.49	6.44	6.24	6.22	6.26	6.17
Al iv	1.55	1.58	1.57	1.51	1.56	1.76	1.78	1.74	1.83
Al vi	3.26	3.27	3.24	3.25	3.26	3.78	3.79	3.76	3.86
Ti	0.12	0.12	0.14	0.14	0.14	0.02	0.01	0.03	0.03
Fe	0.29	0.30	0.28	0.28	0.29	0.07	0.08	0.06	0.04
Mn	0.01	0.00	0.01	0.02	0.01	0.00	0.01	0.00	0.00
Mg	0.38	0.39	0.38	0.37	0.36	0.15	0.16	0.15	0.06
Ca	0.00	0.00	0.00	0.00	0.00	0.00	0.00	0.00	0.00
Na	0.07	0.08	0.07	0.06	0.07	0.24	0.26	0.25	0.37
K	1.83	1.84	1.86	1.79	1.87	1.64	1.64	1.69	1.56
Al total	4.81	4.84	4.82	4.76	4.82	5.54	5.57	5.50	5.69
Fe/Fe+Mg	0.43	0.43	0.42	0.43	0.45	0.30	0.32	0.27	0.45
Mg/(Mg+Fe)	0.57	0.57	0.58	0.57	0.55	0.70	0.68	0.73	0.55

Table 6.11b EPMA analyses of muscovite from the altered rhyolites.

	10	11	12	13	14	15	16	17
	PBS-26/106	**PBS-26/107**	**PBS-26/8**	**BR-4/1**	**BR-4/2**	**BR-4/3**	**BR-4/4**	**BR-4/5**
SiO2	46.379	46.41	46.362	45.31	45.21	45.32	45.63	45.3
TiO2	0.339	0.407	0.384	1.47	1.41	1.6	1.35	1.42
Al2O3	35.732	35.012	33.142	30.84	31.34	30.96	31.39	29.4
FeO	0.458	0.466	1.182	2.46	2.37	2.33	2.66	2.13
MnO	0	0.044	0	0.04	0.06	0.04	0.1	0.1
MgO	0.352	0.516	1.122	1.79	1.7	1.68	1.93	2.08
CaO	0	0.041	0.034	0	0.02	0.03	0.02	0
Na2O	1.016	1.104	0.818	0.35	0.27	0.26	0.28	0.22
K2O	9.628	9.844	9.787	10.9	10.69	10.91	10.82	11.14
Total	93.904	93.844	92.831	93.16	93.07	93.13	94.18	91.79
Cations on the basis of 22 oxygens								
Si	6.20	6.23	6.31	6.25	6.23	6.25	6.23	6.35
Al iv	1.80	1.77	1.69	1.75	1.77	1.75	1.77	1.65
Al vi	3.84	3.77	3.63	3.27	3.32	3.28	3.28	3.20
Ti	0.03	0.04	0.04	0.15	0.15	0.17	0.14	0.15
Fe	0.05	0.05	0.13	0.28	0.27	0.27	0.30	0.25
Mn	0.00	0.01	0.00	0.00	0.01	0.00	0.01	0.01
Mg	0.07	0.10	0.23	0.37	0.35	0.35	0.39	0.43
Ca	0.00	0.01	0.00	0.00	0.00	0.00	0.00	0.00
Na	0.26	0.29	0.22	0.09	0.07	0.07	0.07	0.06
K	1.64	1.69	1.70	1.92	1.88	1.92	1.88	1.99
Al total	5.63	5.54	5.32	5.02	5.09	5.03	5.05	4.86
Fe/Fe+Mg	0.42	0.34	0.37	0.44	0.44	0.44	0.44	0.36
Mg/(Mg+Fe)	0.58	0.66	0.63	0.56	0.56	0.56	0.56	0.64

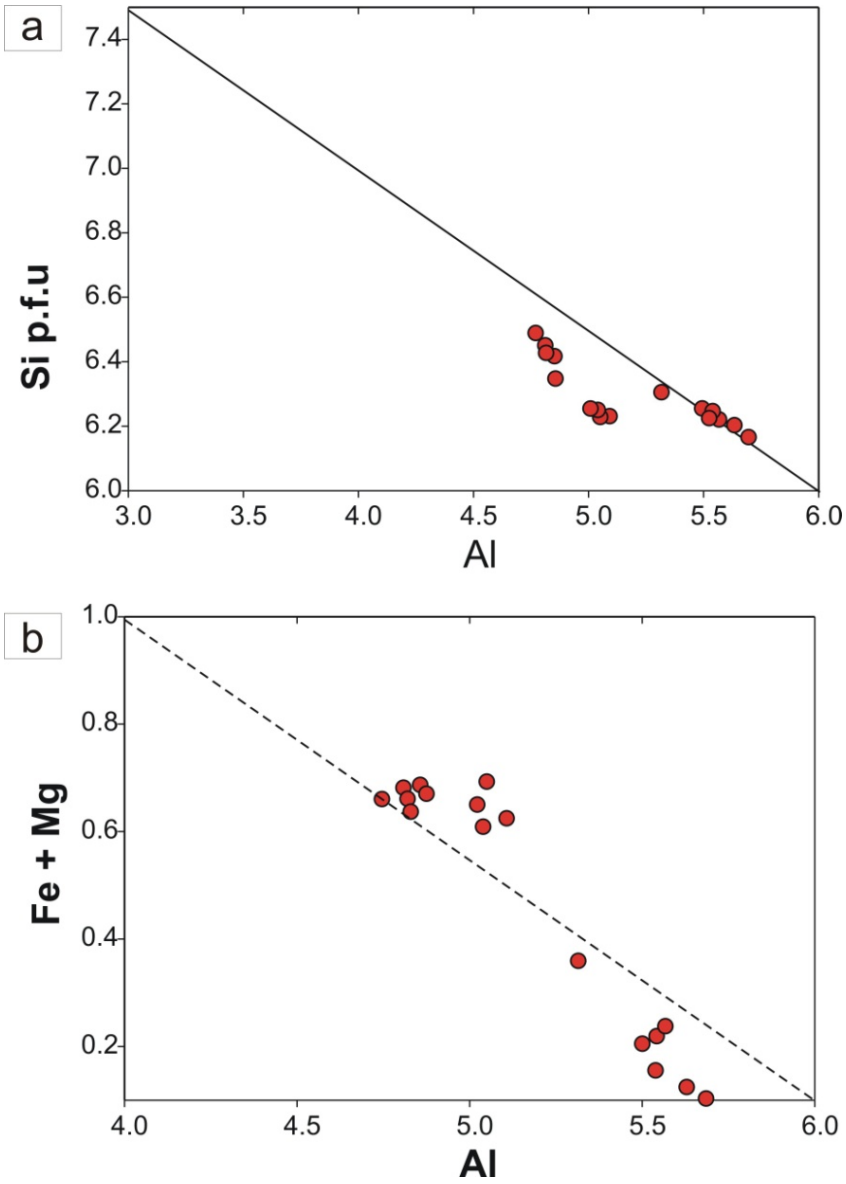

Fig. 6.7 Distribution of a) Si vs. Al and Fe+Mg vs. Al in muscovites from altered rocks from Bhuyari. The linear trends show that there is substiturion similar to the Tschermak substitution (Guidotti and Sassi, 1998). The muscovites are phengitic near the mineralized zones when compared to those distal from mineralized zones.

Gahnite (Zincian Spinel)

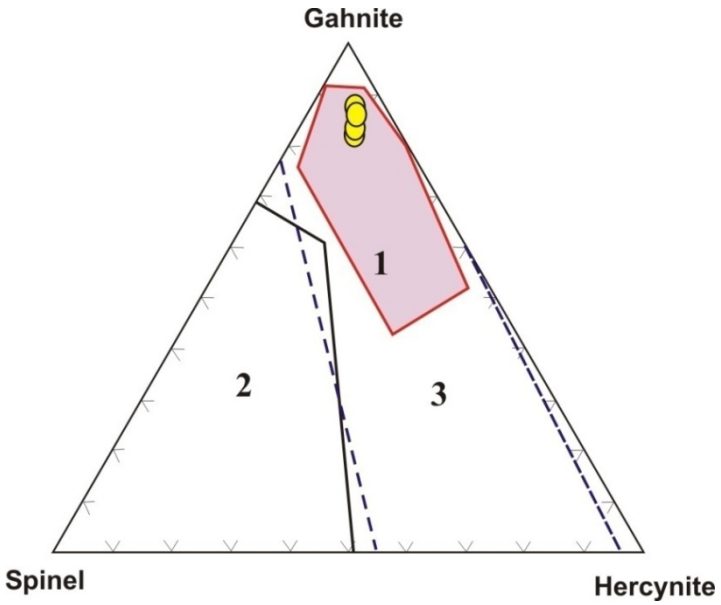

Fig. 6.8 Triangular plot showing the compositions of zincian spinels from the Bhuyari $ZnAl_2O_4$-$FeAl_2O_4$-$MgAl_2O_4$ contents. Compositional fields of spinels from metamorphosed massive sulfides in Fe-Al meta-sedimentary and meta-volcanic rocks **(1),** metamorphosed massive sulfide deposits and S-poor rocks in Mg-Ca-Al alteration zones **(2)** and unaltered and hydrothermally altered Fe-Al rich meta-sedimentary and meta-volcanic rocks **(3)** of worldwide localities are superimposed (after Heimann et al 2005).

A previous study in the area on gahnite suggested that they formed by desulphidation process in a prograde phase and also during a retrograde phase by breakdown of zinc-rich biotite. During this work, further petrographical and mineral chemistry was done to characterize the alteration zones in greater detail. Gahnite ($ZnAl_2O_4$) can form in a variety of ways- metamorphism of Zn-oxide phases, desulphidation of sphalerite, or breakdown of zinc-bearing silicates such as staurolite (Heimann et al, 2005 and references therein). In Bhuyari, the gahnite occurs in the quartz + phlogopite + plagioclase + gahnite + garnet assemblage towards the south of the massive sulphide zones. Detailed petrological description is given elsewhere (See Chapter-3, section 3.2.2.2).

Table 6.12 EPMA analyses of gahnite from the quartz-biotite/phlogopite-garnet-gahnite-chlorite assemblage.

	PBS-31/1	PBS-31/2	PBS-31/3	PBS-31/4
SiO2	0.02	0.56	0.13	0.08
TiO2	0.00	0.00	0.01	0.00
Al2O3	55.45	60.53	55.64	56.66
Cr2O3	0.00	0.01	0.00	0.04
Fe2O3	0.00	0	0	0
FeO	3.66	2.83	3.99	3.83
MnO	0.22	0.17	0.24	0.30
MgO	1.37	0.99	1.57	1.63
ZnO	37.21	37.77	36.82	35.93
on the basis of 4 oxygens				
Si	0.00	0.02	0.00	0.00
Al	1.99	2.02	1.98	2.00
Fe+3	0.00	0.00	0.00	0.00
Fe+2	0.09	0.07	0.10	0.10
Mn	0.01	0.00	0.01	0.01
Mg	0.06	0.04	0.07	0.07
Zn	0.83	0.79	0.82	0.79
Zn	0.83	0.79	0.82	0.79
Fe	0.09	0.07	0.10	0.10
Mg	0.06	0.04	0.07	0.07
	0.99	0.90	0.99181	0.96299
Gahnite	84.35	87.88	82.74	82.47
Hercinite	9.39	7.47	10.16	9.96
Spinel	6.26	4.66	7.10	7.56
	100.00	100.00	100.00	100.00

The gahnite compositions are tabulated in Table 6.2 and the end member compositions of gahnite, hercynite and spinel are calculated and plotted in the gahnite classification diagram of Heimannn et al (2005) (Fig. 6.8). Several grains of gahnite in this assemblage were analysed by EPMA. The analysed gahnites contains high mole % gahnite, (82.4 to 87.8) and low hercynite (7.5 - 10.2 mole %) and spinel (4.7 - 7.6 mole %). Gahnite with 55 - 90 mole % $ZnAl_2O_4$, 10 - 40 mole % $FeAl_2O_4$ and 5 - 20 mole % $MgAl_2O_4$ are considered to be the best guides to ore (Spry and Scott, 1986a).

Gahnite is proposed as an indicator mineral for metamorphosed VMS deposits in view of its close association with mineralized zones (e.g.Spry et al. 2000; Heimann et al, 2005). The additional data confirms the earlier studies and all gahnite composition are similar to those present in metamorphosed massive sulphides (Fig. 6.8).

Zincian Staurolite

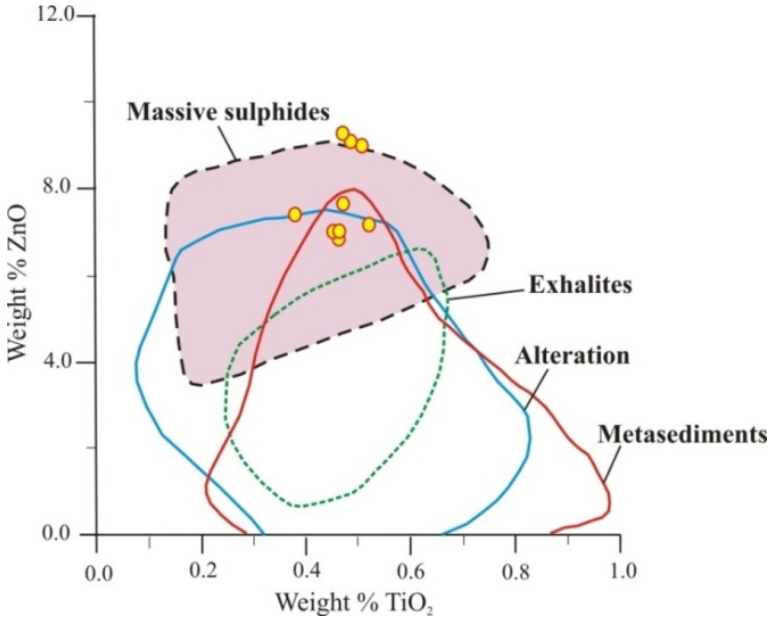

Fig. 6.9 TiO_2 - ZnO plot for staurolites from different geological settings (metamorphosed massive sulphide deposits, metaexhalative gahnite-quartz rocks, pegmatites, aluminous metasediments and marbles) from Spry et al (2000).

Staurolite occurs in the magnesium-rich alteration zone proximal to massive sulphides at Bhuyari. These staurolites contain very high zinc contents with ZnO contents reaching 9 wt. %. The staurolite analyses are provided in the Table 6.13. Spry and Scott (1986b) suggested that the Fe/Zn ratio of staurolite can serve as a vector to ore.

In massive sulphides, metaexhalites and related alteration zones, staurolite typically contain between 5 and 9 wt. % ZnO, generally in the presence of quartz. In quartz bearing rocks in contact with sphalerite and or/gahnite, the elevated Zn stabilizes staurolite and prevents is breadown during metamorphism. Although zincian staurolite can form in multiple ways, the most common mode of formation associated with massive sulphides is similar to gahniute, zincian staurolite forms by desulphidation of sphalerite.

Staurolite in massive sulfide deposits generally contains 4–9 wt% ZnO whereas they contain 0-7 wt% ZnO in the alteration zones (Spry et al 2000). Spry and Scott (1986b) have shown that staurolite formed by desulfidation of sulfides in the Appalachians and Scandinavian Caledonides contain higher ZnO (7–9wt%) than those did not form by desulfidation mechanism (6wt% ZnO) as in Broken Hill, Australia, Gamsberg, South Africa and Geco, Ontario.

The staurolite bearing rock at Bhuyari is a hard, light coloured, quartz - rich rock with profuse development of staurolite (light yellow colour) occurring as patches in a quartz-rich groundmass. In hand specimen the rock appears mainly to be composed of quartz + staurolite. Staurolite appears to make up up to 40% of the rock. Zaleski et al (1991) showed that in quartz-bearing rocks in contact with sphalerite and/or gahnite, the elevated Zn stabilizes staurolite and prevents its breakdown during metamorphism.

Staurolite porphyroblasts at Bhuyari attain up to a few cm in size and are typically euhedral. Textural evidence gives indication of formation of staurolite in a prograde environment and is formed during the late stages or post deformation. The randomly oriented staurolite crystals with numerous quartz, biotite, garnet and muscovite inclusions support a late origin. Textural evidence for desulphidation reactions involving sphalerite is present in the form of sphalerite inclusions within zincian staurolite (Fig.6.10a). At places staurolite also gives evidence for formation by breakdown of biotite (Fig. 6.10b). Staurolite is the only silicate mineral that can accommodate significant Zn, and acts as a collector mineral during prograde metamorphism (Stoddard 1979).

The staurolites have extremely high zinc contents (6.84 to 9.24 wt.% ZnO) which are perhaps the highest ever reported from massive sulphides. Iron (FeO) contents range from 4.8 to 6.35, magnesium contents range from 1.61 to 1.93 with X_{Mg} (Mg/(Mg+Fe^{2+}) ranging from 0.34 to 0.37. The mineral chemistry data is plotted in the diagram of Spry et al (2000), and the zincian staurolites of Bhuyari fall well within the field of staurolites associated with massive sulphides (Fig. 6.9).

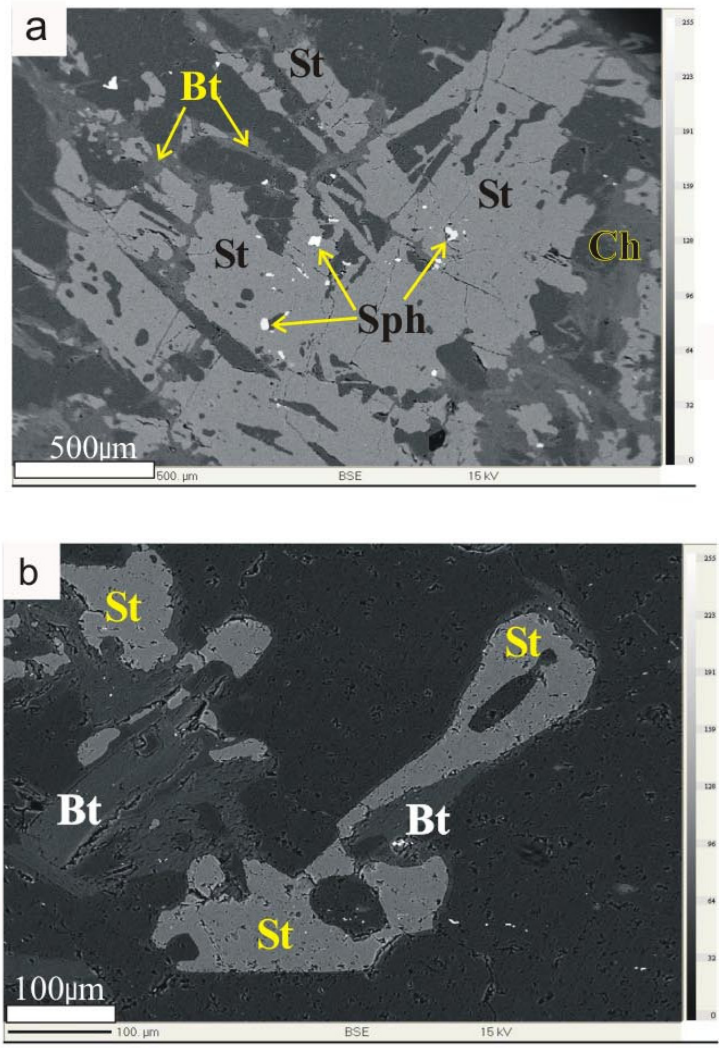

Fig. 6.10 a) BSE image showing staurolite porphyroblasts (St) with inclusions of sphalerite (Sph) giving evidence for development of zincian staurolite from desulphidation reaction involving sphalerite. **b)** Staurolite forming pseudomorphs after biotite, giving evidence for zincian staurolite formation from zinc-rich biotite.

Table 6.13 EPMA analyses of staurolite from the biotite-staurolite-garnet schists from Bhuyari.

	1	2	3	4	5	6	7	8	9
Sample No.	**PBS-26/5**	**PBS-26/6**	**PBS-26/7**	**PBS-26/12**	**PBS-26/13**	**PBS-26/14**	**PBS-26/15**	**PBS-26/16**	**PBS-26/17**
SiO2	27.51	27.24	27.81	28.02	26.96	26.90	28.03	27.54	27.29
TiO2	0.51	0.48	0.47	0.38	0.52	0.46	0.47	0.45	0.47
Al2O3	53.30	53.60	53.50	54.21	52.75	52.53	53.18	53.11	52.97
Cr2O3	0.00	0.02	0.01	0.00	0.00	0.07	0.01	0.00	0.00
Fe2O3	0.00	0.00	0.00	0.00	0.00	0.00	0.00	0.00	0.00
FeO	5.05	5.14	4.83	5.93	5.83	5.81	6.15	6.24	6.35
MnO	0.96	0.90	0.79	1.27	1.22	1.29	1.26	1.28	1.25
MgO	1.61	1.71	1.43	1.73	1.76	1.84	1.93	1.86	1.84
ZnO	8.96	9.04	9.24	7.38	7.14	6.84	7.61	6.98	6.95
CaO	0.00	0.00	0.02	0.00	0.00	0.03	0.00	0.03	0.02
Na2O	0.25	0.17	0.20	0.20	0.15	0.14	0.15	0.16	0.16
Number of metal atoms on 48 oxygen basis									
Si	8.04	7.95	8.10	8.07	7.99	8.00	8.12	8.06	8.02
Ti	0.11	0.11	0.10	0.08	0.12	0.10	0.10	0.10	0.10
Al	18.35	18.44	18.36	18.40	18.43	18.42	18.16	18.31	18.35
Cr	0.00	0.00	0.00	0.00	0.00	0.02	0.00	0.00	0.00
Fe+3	0.00	0.00	0.00	0.00	0.00	0.00	0.00	0.00	0.00
Fe+2	1.23	1.26	1.18	1.43	1.45	1.45	1.49	1.53	1.56
Mn	0.24	0.22	0.20	0.31	0.31	0.33	0.31	0.32	0.31
Mg	0.70	0.75	0.62	0.74	0.78	0.82	0.84	0.81	0.81
Zn	1.93	1.95	1.99	1.57	1.56	1.50	1.63	1.51	1.51
Ca	0.00	0.00	0.01	0.00	0.00	0.01	0.00	0.01	0.00
Na	0.14	0.10	0.11	0.11	0.09	0.08	0.09	0.09	0.09
Mg/(Mg+Fe2+)	0.363	0.373	0.346	0.343	0.350	0.361	0.359	0.347	0.341

Tremolite

Tremolite analyses are provided in Table No.6.14, and plotted in the amphibole classification diagram of Leake et al (1997). Most of the data plot within the field for tremolite with one data falling in the actinolite field (Fig. 6.11). The tremolite-carbonate rock type represents amphibolite facies metamorphism of magnesium and calcium rich protolith most likely consisting of Mg-chlorite and dolomite. The tremolite-carbonate rocks contain a varied mineralogy with varying proportions of chlorite (penninite), tremolite, dolomite, bytownite, zoisite, spessartine-grossular. Tremolite microanalyses show relatively uniform compositions close to the magnesian end member with Mg numbers (100*Mg/[Mg + Fe]) of more than 90.

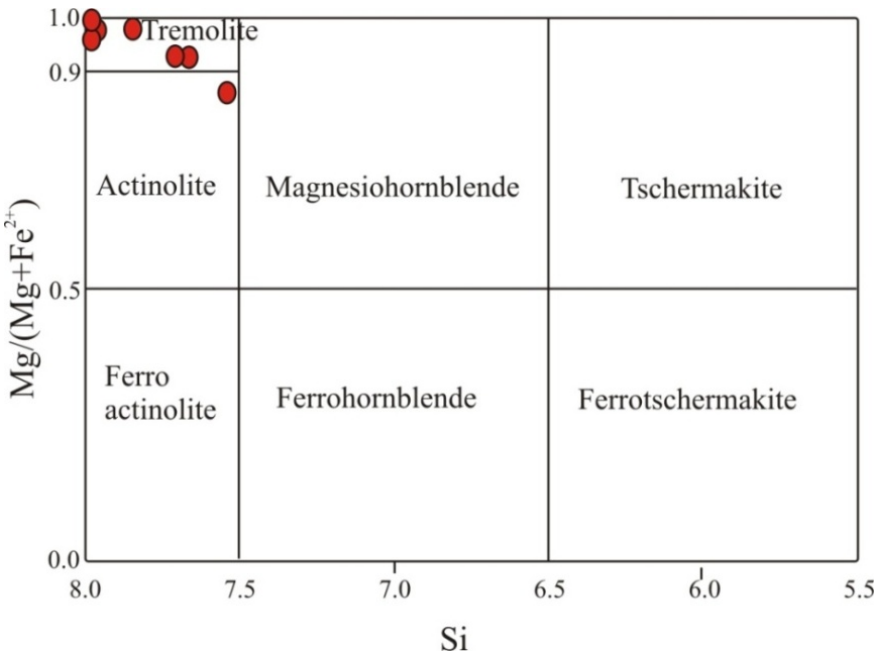

Fig.6.11 Amphiboles from the tremolite-carbonate rocks plot predominantly in the tremolite and some in the actinolite field in a plot of Si versus Mg/(Mg+fe) (after Leake et al, 1997). Values of X_{Mg} [$(Mg/(Mg+Fe^{2+})$] range from 0.91 to 0.99

Table 6.14 EPMA analysis of amphiboles from tremolite-carbonate rocks

	PBC-5/98	PBC-5/99	PBC-8/49	PBC-8/35	PBC-5/94	PBC-8/36	PBC-8/37
SiO2	56.144	55.765	55.024	54.896	52.522	54.661	54.567
TiO2	0.08	0.07	0.02	0.03	0.04	0.02	0.02
Al2O3	3.02	3.40	0.46	0.28	4.81	0.71	0.83
FeOT	3.59	3.60	0.67	0.44	6.26	0.50	1.09
MnO	1.25	1.34	0.47	0.51	1.67	0.48	0.46
MgO	21.09	20.71	25.16	22.77	18.99	21.78	20.77
CaO	13.21	13.12	9.92	11.44	10.98	11.79	11.30
Na2O	0.33	0.46	0.19	0.15	0.31	0.11	0.20
K2O	0.27	0.23	0.09	0.05	0.20	0.05	0.03
Total	98.95	98.69	92.03	90.56	95.77	90.11	89.26
Cations :	23(O)	23(O)	23(O)	23(O)	23(O)	23(O)	23(O)
Si	7.69	7.67	7.88	8.02	7.51	8.00	8.00
Ti	0.01	0.01	0.00	0.00	0.00	0.00	0.00
Al	0.49	0.55	0.08	0.05	0.81	0.12	0.14
Fe+3	0.00	0.00	0.08	0.00	0.04	0.00	0.00
Fe+2	0.41	0.41	0.00	0.05	0.70	0.06	0.14
Mn	0.14	0.16	0.06	0.06	0.20	0.06	0.06
Mg	4.31	4.24	5.37	4.96	4.05	4.77	4.59
Ca	1.94	1.93	1.52	1.79	1.68	1.85	1.79
Na	0.09	0.12	0.05	0.04	0.08	0.03	0.06
K	0.05	0.04	0.02	0.01	0.04	0.01	0.01
Total	15.12	15.13	15.07	14.98	15.12	14.93	14.87
$Mg/(Mg+Fe^{2+})$	0.913	0.911	0.999	0.989	0.852	0.987	0.971

Table 6.16 Representative mineral chemistry of chlorite from various altered rocks of Bhuyari. Serial numbers from 1 to 9 (tremolite-carbonate rocks), 10-12 (quartz-staurolite-garnet-biotite-chlorite schist) and 13-14 (quartz-phlogopite-garnet schist)

Sr. No.	1	2	3	4	5	7	8	9	10	11	12	13	14
Sample. No.	PBC-8/31	PBC-8/32	PBC-8/33	PBC-8/50	PBC-8/27	PBC-8-25	PBC-7-18	PBC-8-19	PBS-26/87	PBS-26/89	PBS-26/97	PBS-48/190	PBS-48/191
SiO2	33.19	32.51	32.62	32.57	32.78	32.87	33.29	33.93	27.85	27.30	27.33	27.06	28.48
TiO2	0.04	0.01	0.00	0.00	0.00	0.00	0.02	0.03	0.21	0.17	0.04	0.09	0.04
Al2O3	13.90	13.86	13.85	13.39	13.52	13.98	14.54	14.23	22.16	21.74	23.07	19.84	20.19
FeO	0.98	1.09	1.03	1.00	1.16	1.10	0.98	0.84	12.19	12.84	10.93	12.94	13.34
MnO	0.03	0.15	0.13	0.16	0.12	0.09	0.08	0.10	0.45	0.48	0.64	1.16	1.26
MgO	34.14	34.14	33.39	33.57	34.14	34.63	34.71	34.58	22.79	23.13	25.15	23.90	23.85
CaO	0.05	0.02	0.01	0.20	0.03	0.09	0.01	0.08	0.04	0.05	0.01	0.01	0.03
Na2O	0.04	0.00	0.01	0.06	0.05	0.10	0.02	0.09	0.05	0.05	0.02	0.03	0.06
K2O	0.01	0.03	0.02	0.05	0.01	0.02	0.01	0.04	1.12	1.31	0.03	0.02	0.01
Formula on the basis of 28 oxygen atoms													
Si	6.49	6.26	6.49	6.36	6.46	6.41	6.42	6.37	5.52	5.80	5.36	5.87	5.65
Al iv	1.51	1.74	1.51	1.64	1.54	1.59	1.58	1.63	2.48	2.20	2.64	2.13	2.35
Sum	8.00	8.00	8.00	8.00	8.00	8.00			8.00	8.00	8.00	8.00	8.00
Al vi	1.70	1.89	1.74	1.83	1.61	1.63	1.73	1.91	2.72	1.88	2.69	1.73	2.38
Ti	0.01	0.00	0.00	0.00	0.00	0.00	0	0	0.03	0.03	0.01	0.01	0.01
Fe3+	0.11	0.08	0.12	0.09	0.08	0.01	0.08	0.13	0.03	0.00	0.03	0.00	0.06
Fe2+	0.05	0.10	0.05	0.07	0.11	0.17	0.06	0.01	1.99	2.52	1.77	2.51	2.15
Mn	0.01	0.02	0.02	0.03	0.02	0.01	0.01	0.02	0.08	0.09	0.11	0.21	0.21
Mg	9.95	9.79	9.89	9.78	10.02	10.07	9.97	9.67	6.73	7.33	7.35	7.73	7.05
Ca	0.01	0.00	0.00	0.04	0.01	0.02	0	0.02	0.01	0.01	0.00	0.00	0.01
Na	0.03	0.00	0.01	0.05	0.04	0.08	0.01	0.06	0.04	0.04	0.02	0.03	0.04
K	0.00	0.01	0.01	0.02	0.00	0.01	0	0.02	0.57	0.71	0.01	0.01	0.01
Mg/(Mg + Fe)	0.99	0.99	0.99	0.99	0.99	0.98	0.99	0.99	0.77	0.74	0.81	0.76	0.77

Chlorite

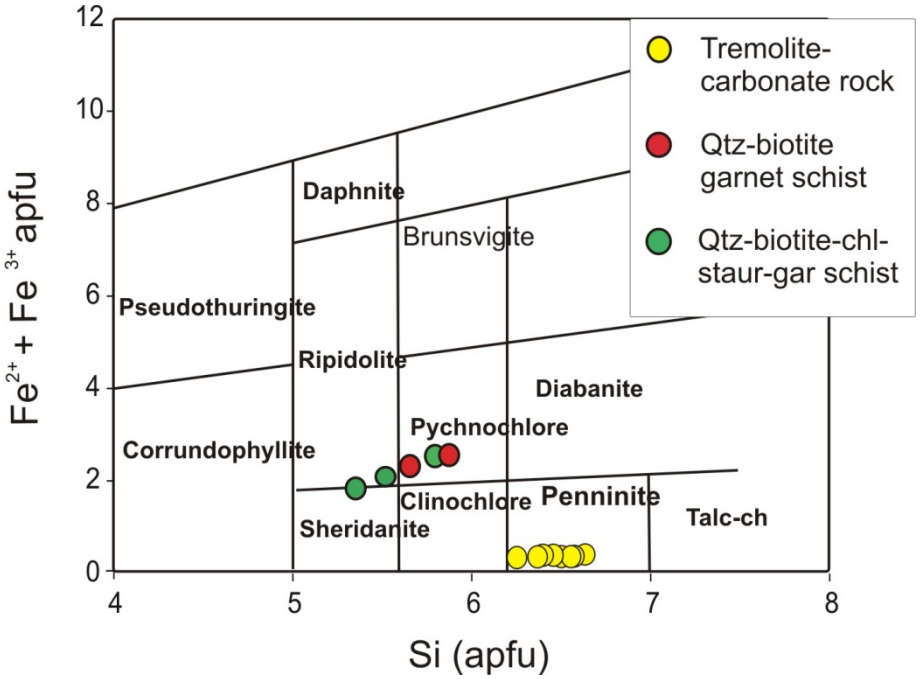

Fig. 6.12 Chlorite compositions from different alteration assemblages, tremolite-carbonate rocks, quartz-phlogopite-garnet schist and quartz-staurolite-biotite-garnet-chlorite schist. Chlorite classification diagram after Hey (1954).

Chlorite is ubiquitous in the magnesium enriched alteration zones at Bhuyari. A total of 14 chlorite analyses from different assemblages are given in Table 6.16 and are plotted in the chlorite classification diagram. The Si apfu versus Fe (total) plot shows that the chlorites show a range of compositions falling in sheridanite, pychnochlore and penninite fields. These chlorites are generally Mg-rich. Chlorites from the biotite-phlogopite schists plot in the pychnochlore and ripidolite fields. Chlorites from the tremolite-carbonate rocks fall in the peninite field (Fig. 6.12). The chlorites from quartz-phlogopite-garnet schist and from the quartz-staurolite-garnet-biotie schist are retrograde products after phlogopite, staurolite, biotite and garnet.

The chlorite present in the tremolite-carbonate rocks is penninite, which is a Mg-rich chlorite. Textural evidence shows that the peninite occurs as flaky, euhedral grains formed in a prograde event which is replaced by secondary iron-rich chlorite during retrogression.

The chlorites in the Mg-rich alteration zone have Mg# values ranging from 7.4 to 7.6, whereas the peninite from tremolite-carbonates which are adjacent to the massive sulphides contain very high Mg# values above 9. The chlorite in the phlogopite-garnet schist which is part of the magnesium-rich alteration zone is pychnochlore. The chlorite in the staurolite-garnet-biotite rock is sheridanite and pychnochlore. There is a systematic increase in Mg/ Mg+Fe contents of chlorites from alteration zone distal from the massive sulphide to those proximal to the massive sulphides. The chlorites in the biotite-garnet-plagioclase rock which forms the main Mg-altered footwall alteration assemblage has Mg/ (Mg+Fe) ranging from 0.76 to 0.77, for the staurolite-biotite-garnet rock near adjacent to the tremolite-carbonate rocks the Mg/(Mg + Fe) is 0.74 to 0.81 and for the tremolite-carbonate rock which is closest to the massive sulphide zone it is 0.98 to 0.99 (Table. 6.16).

(Paulick et al, 2001) documented an increase in Mg numbers of chlorite with increasing stratigraphic level and proximity to the mineralized zones at Thalanga VMS deposit in Australia. A similar pattern has been documented for a number of other VMS deposits, including Seneca, Corbet, and South Bay and Hellyer, however a trend of iron-enrichment in proximal chlorite is also documented in several VMS deposits such as Heath Steele, Home and Herculus (references in Paulick et al, 2001).

Dolomite

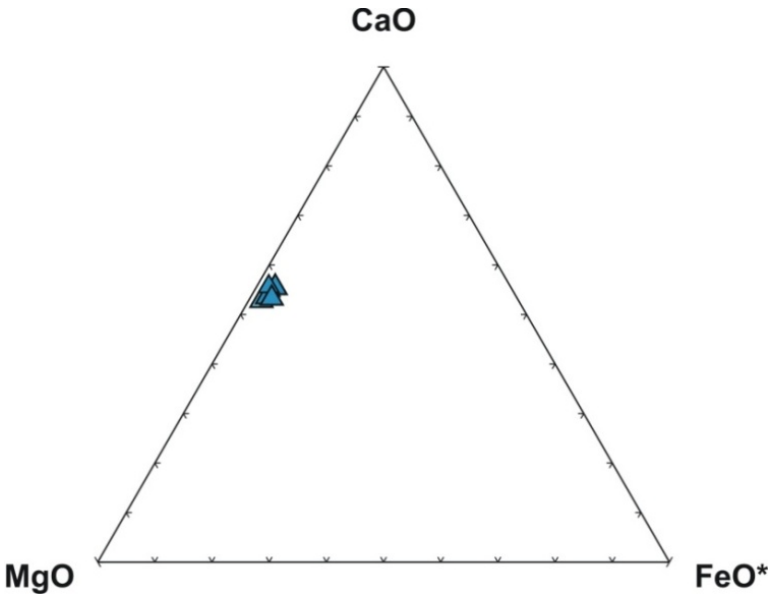

Fig.6.13 Carbonate composition plotted in the CaO-MgO-FeO* (FeO*= FeO + MnO) diagram (wt%) of carbonates

The carbonate occurring in the tremolite-carbonate rocks are dolomitic in composition. The analytical data of dolomite is given in Table 6.15. The data is plotted in the classification diagram for carbonate (Fig. 6.13). In the CaO-MgO-FeO* plot the dolomite samples plot in a tight cluster (Fig. 6.13).

Dolomite is restricted to the tremolite-carbonate outcrops and is not present in any other alteration zones. The main carbonate mineral in the tremolite-carbonate rocks is dolomite. Dolomite occurs as granular aggregates. They occur as groundmass for the tremolite porphyroblasts. At places however, they form monomineralic crystalline aggregates. EPMA analyses (6 numbers) of dolomite are given in Table 6.18. The dolomite has higher MnO contents ranging from 0.59 to 1 wt %. They contain around 0.02 to 0.03 Mn cation per formula unit. Similar manganese content is present in the hydrothermal dolomite associated with the Thalanga Zn-Cu-Pb VMS deposit

(Herrmann and Hill, 2001). The manganese enrichment in the carbonate is expected in proximal hydrothermal fluids related to ore bodies. Manganese enrichment is widely studied in various metaexhalites and coticulres (Spry et al, 2000).

Table 6.17. Representative mineral chemistry of carbonates from tremolite-carbonate rocks.

	1	2	3	4	5	6
	PBC-8/26.	**PBC-8/46**	**PBC-8/47**	**PBC-8/51**	**PBC-8/52**	**PBC-8/53**
SiO2	0.06	0.02	0.13	0.02	0.111	0.123
TiO2	0.00	0.00	0.06	0	0.008	0
Al2O3	0.02	0.00	0.18	0.49	0.243	0.245
Cr2O3	0.00	0.02	0.00	0	0.02	0
Fe2O3	0.00	0.00	0.00	0	0	0
FeO	0.41	0.38	0.33	0.399	0.314	0.414
MnO	0.92	1.04	0.59	0.868	0.763	0.84
MgO	20.81	19.85	18.54	20.586	18.913	19.154
CaO	27.50	25.65	21.91	26.143	24.588	24.203
on the basis of 6 O						
Si	0.00	0.001	0.000	0.000	0.004	0.004
Ti	0.00	0.000	0.000	0.000	0.000	0.000
Al	0.00	0.000	0.000	0.000	0.010	0.010
Cr	0.00	0.001	0.000	0.000	0.001	0.000
Fe+3	0.00	0.000	0.000	0.000	0.000	0.000
Fe+2	0.01	0.011	0.011	0.011	0.009	0.012
Mn	0.03	0.030	0.030	0.030	0.023	0.025
Mg	1.00	1.013	1.013	1.013	1.004	1.015
Ca	0.95	0.941	0.941	0.941	0.938	0.922
Total	2.00	1.996	1.995	1.995	1.990	1.989
C	2.000	2.004	2.005	2.005	2.010	2.011

6.4 Summary and Conclusions

The EPMA analyses of metamorphic minerals from the alteration zones and from the least altered rhyolites show marked differences in compositions. Systematic compositional variations have also been observed in certain minerals based on their proximity from mineralized zones. The important results of this study are as follows-

Biotite shows increase in X_{Mg} contents towards the mineralized zones. The biotite from least altered rhyolite can be classified as normal biotite (Mg number: 0.24 to 0.28) whereas, those form the alteration zones close to ore zones are phlogopite (Mg number: 0.64 to 0.8).

Muscovite show higher MgO and FeO contents within the mineralized zones (1.7 to 2 and 2.3 to 2.5wt.%) when compared to those from proximal alteration zones (0.3 to 0.5 and 0.41 to 0.47 wt.%).

Plagioclase do not show systematic compositional variations from altered and unaltered rhyolites. However, anorthite contents are significantly higher in altered rhyolites (24-35) when compared to least altered rhyolite (17-26). The highest anorthite contents are present in the tremolite-carbonate rocks (77-88).

Garnet show systematic increase in spessartine contents (32.5 to 38.2 mol. %) from least altered rhyolite to those from proximal alteration zones and mineralized zones (36 to 57.8 mol. %).

Zincian staurolite Presence of zincian stauroltie with extremely high ZnO contents upto (9 wt. %) in staurolite are similar to those developed in metamorphosed massive sulphide deposits (Spry et al, 2000).

Gahnite: The gahnites from Bhuyari has very high gahnite component (gahnite mol. % 82.47 to 87.88) and falls well within the field of gahnites from metamorphosed massive sulphides (after Heimann et al, 2005).

Indicator Minerals (and mineral chemistry) for Mineral Exploration

Since most of the metamorphic minerals in the alteration zones are refractory during sedimentation, they have the potential for occurring in heavy mineral separates in sediments and therefore are valuable exploration aids for locating ore bodies in VMS districts (e.g. Averill, 2001). It is well known that mineral chemistry of some minerals in the metamorphic alteration zones such as Fe/Zn ratios of staurolite can serve as vectors to ore (Spry and Scott, 1986b). The composition of gahnite has been shown to be an effective exploration guide to metamorphosed massive sulphide deposits (Spry and Scott, 1986a; Heimann et al, 2005).

In Betul belt, the presence of refractory and resistant minerals like gahnite, staurolite and garnet are present in the stream sediments which occur downstream of these deposits. These minerals can also be sometimes found in areas covered by soil and regolith. Earlier studies in other parts of Betul Belt have indicated that gahnite and zincian staurolite can be used as indicator minerals in mineral exploration (Ghosh and Praveen, 2008).

Gahnite in Bhuyari is present only in close proximity to mineralized zones, and therefore the very presence of gahnite in stream sediment or soil or regolith can indicate the presence of sphalerite-bearing mineralized zones in the up-stream areas or within soil cover and is therefore a very good indicator for mineralization in Betul Belt. However, the other metamorphic minerals like staurolite and garnet are present both in proximal alteration zones as well as from moderate to weakly altered zones. The zinc content of staurolite (up to

9 wt. %) occurring adjacent to the mineralized zone at Bhuyari is the highest reported for Betul Belt. Such high Zn-staurolites can be used as reliable proximity indicators to ore and can be differentiated from low-Zn staurolites occurring in less altered rocks.

In this study, it is proposed that in addition to gahnite and zincian staurolite, garnet can also be used as a indicator mineral when found in stream sediment, soil, regolith or even in alteration zones. Garnet is widespread in weakly altered, moderately altered and intensely altered rocks and is also easy to find in the stream sediments. In Bhuyari, the highest spessartine content (57.8 mol. %) is found in the quartz-phlogopite-garnet rocks which contain disseminated and vein mineralization and is also adjacent to massive sulphide zones, and the lowest spessartine content (32 mol. %) is found in the least altered rhyolite. Therefore, it is proposed that the spessartine content of garnet can be used as a criterion to determine the proximity to ore zones.

In addition to these refractory and resistant minerals, certain minerals like biotite and muscovite can also be potentially used as indicator minerals. In areas of sparse outcrops, rapid assessment for mineralization potential can be carried out by EPMA studies to determine the phlogopite content of biotite and phengite component of muscovite to understand the proximity of these outcrops to hidden mineralized zones if any. In this study it is found that high Mg-biotite (phlogopite) and Mg-Fe muscovite (phengite) are associated with the intensely altered rhyolite within and/or proximal to mineralized zones.

******

Chapter 7

SULPHIDE MINERALIZATION

Contents

7.1. Introduction
7.2 Objectives of this Study
7.3 Methodology
7.4. Surface Indications and Nature of Sulphide Mineralization
7.5 Sulphide Texture and Mineralogy
7.6 Mineral Chemistry of Sulphides
7.7 Discussion

7.1 Introduction

Volcanic-associated massive sulphide deposits (VMS) are predominantly stratiform accumulations of sulphide minerals that precipitate from the hydrothermal fluids at or below the sea floor. The deposits are characterized by a zone of massive ore containing more than 50% sulphides by volume and underlain by a stringer zone containing less than 25% sulphides by volume (Franklin et al, 1981). The massive ore zone is typically lensoid in cross-section invariably has a sharp contact with the hanging wall and diffuse and gradational contacts with the footwall rocks. The schematic diagram of a typical undeformed VMS deposit as described by Franklin et al (1981) is show in Fig. 7.1. The ore zone is essentially composed of discontinuously banded and brecciated ore of Fe-sulphides (pyrite + pyrrhotite) - chalcopyrite-sphalerite ± galena. The ore also contain a wide variety of accessory and silicate minerals including magnetite, bornite, native silver, native gold, electrum, Ag-sulphides and Ag-bearing sulphosalts. These deposits commonly contain Fe-rich siliceous (and sometimes manganiferous) sediments, thought to represent chemical precipitation on the sea-floor (exhalites) during the

waning stages of hydrothermal activity. Gahnite is an accessory mineral in virtually all deposits metamorphosed to amphibolite facies (e.g. Misra 2000 and references therein).

VMS deposits have been broadly categorized as Cu-Zn group and Zn-Pb-Cu group. Iron sulphides like pyrite and pyrrhotite are the most abundant ore minerals in the typical massive ores of Cu-Zn deposits. Upward and lateral zonation of Cu (chalcopyrite) to Zn (sphalerite) and Pb (galena) is a common feature. The massive sulphide ores in Kuroko-type deposits (Kuroko or black ore) is characterized by the absence of pyrrhotite. The Kuroko deposits are also characterized by an abundance of galena especially at the stratigraphically upper parts of the massive ore. Bornite and tetrahedrite-tennantite also form other important constituents of the black ores. These minerals are rare in the Cu-Zn group of VMS deposits. The Kuroko ores are also characterized by the presence of barite and bedded anhydrite-gypsum-pyrite ore (Sekkoko), which are absent in the Cu-Zn group (Franklin et al, 1981, Franklin 1993).

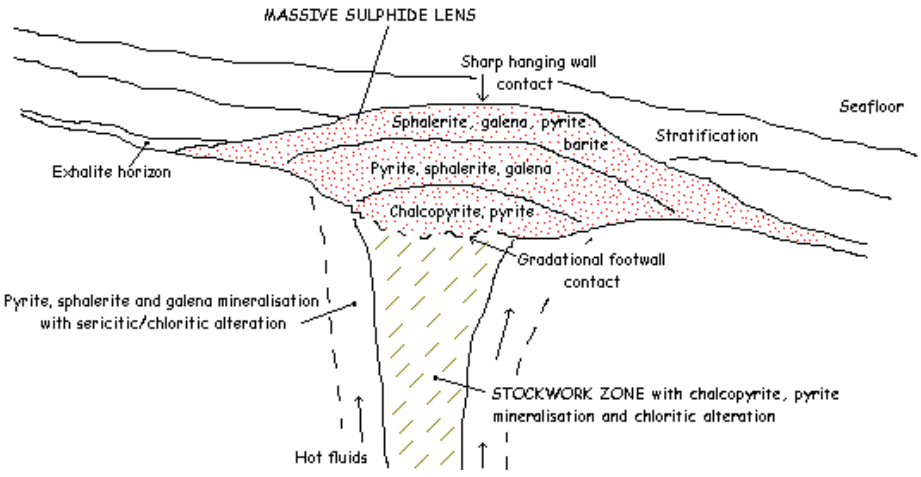

Fig.7.1 Schematic diagram showing the typical volcanogenic massive sulphide deposit (after Franklin et al, 1981). The diagram shows a discordant feeder zone with inner chloritic alteration along with disseminated and stockwork sulphides which is followed upwards by stratiform massive sulphides.

The stringer zone underlies the massive ore zone and is omnipresent in most VMS deposits (Fig. 7.1). Where present, it occurs as a conical to cylindrical shaped mappable body comprising of anastomosing veinlets, veins and irregular replacement bodies of sulphide and quartz. The sulphides are dominated by chalcopyrite and pyrite. The metals contained in VMS deposits are thought to have been derived through the leaching of large volumes of underlying rock by modified seawater hydrothermal fluids (Ohomoto 1986), or they were derived more directly from magmatic hydrothermal fluids (Yang and Scott, 1996), based on studies of melt inclusions, suggest that magmatic contributions to the hydrothermal fluid were responsible for ore formation at some recent sea-floor and ancient VMS deposits (Misra, 2000).

Most Proterozoic and Archean VMS occur in highly deformed terrains and therefore such primary sulphide morphology is rarely preserved. In such deformed examples, the massive sulphide zones and its discordant stringer zone are generally brought in parallelism with the regional foliation. Relationship between alteration zones and the associated sulphides are also obscured in such cases, and requires careful field mapping accompanied by petrological and geochemical studies to decipher it.

In Betul Belt, several small (<3 mt) base-metal deposits and prospects hosted by the felsic volcanic rocks have been explored by the Geological Survey of India. These deposits are inferred to have formed by submarine volcanic-exhalative processes (Raut and Mahakud, 2004, Praveen et al, 2005; Golani et al, 2006; Praveen et al, 2007). The sulphide mineralization in Betul Belt can broadly be classified as Zn-Pb-Cu and Zn-Cu type. Mineralization is zinc-rich and dominantly contains sphalerite, pyrite, galena, chalcopyrite and pyrrhotite. High contents of silver and cadmium are also associated with these ores (Mahakud et al, 2001). Incidence of gold (up to 1.4 ppm) has been

reported from felsic tuff associated with the deposits (Mahakud, 1993) and high barium contents up to (0.33%) have been reported from the sulphide-rich ores (Ramachandra and Pal, 1992). The ore bodies are generally transposed parallel to the regional foliation and consist of massive, semi-massive and disseminated sulphides which are enclosed by intensely altered felsic volcanic rocks (Praveen et al, 2007).

In Bhuyari, exploration by GSI has shown that the massive sulphide mineralization (> 50 volume % sulphides) occurs as a small tabular body with an inferred strike length of approximately 100m and width ranging from <1m to a few meters (Praveen et al, 2010). The massive sulphide body is dominated by sphalerite and pyrite with subordinate galena and chalcopyrite. This massive sulphide body is enclosed by semi-massive (< 50 vol. % sulphides), disseminated and vein mineralization which extends for more than 200m along strike. This type of mineralization is enclosed by the highly altered biotite-phlogopite-bearing schists and quartz-muscovite-K feldspar schists occuring parallel to the massive sulphide body and to the south of it. The sulphides contain zinc is the predominant metal with subordinate Pb and Cu. Silver (Ag) and cadmium (Cd) are the other associated metals. Major gangue minerals comprise of quartz, chlorite, biotite, muscovite, plagioclase, garnet and gahnite.

7.2 Objectives of this Study

The objectives of the study are to study and characterize the sulphide textures and mineralogy so that it can be integrated with other field-based and geochemical studies to understand the VMS mineral system in the area.

7.3 Methodology

Thin polished sections of sulphide-bearing samples from Bhuyari were prepared at NCESS, Thiruvananthapuram. The ore microscopic studies were

carried out in petrological Lab, GSI, Bangalore. EPMA studies of ore minerals were carried out at GSI Labs, in Bangalore and Faridabad. Based on EPMA studies, representative mineral compositions of various sulphide phases like sphalerite, pyrite, galena, chalcopyrite and pyrite were analyzed and studied.

7.4 Surface Indications and Nature of Sulphide Mineralization

The rocks exposed around Bhuyari, particularly the tremolite-carbonate rocks that forms small hillocks south of Bhuyari and the altered rhyolite exposed in the river valley show ample evidence for sulphide mineralization in the form of various secondary minerals like malachite (copper carbonate), azurite (copper carbonate) and smithsonite (zinc carbonate) which occur as coatings and encrustations.

Malachite is widespread in the altered rhyolites and tremolite-carbonate rocks in the area. It forms greenish encrustations and veins parallel to the mineralized zones in the altered massive (quartz-porphyritic) rhyolite in the Kanhan valley and its vicinity (Fig.7.2a). Malachite also occurs as greenish and greenish-blue patches in the tremolite-carbonate rocks (Fig. 7.2.c). At places, azurite (blue encrustations) is present associated with malachite in the tremolite-carbonate veins in the area. Whitish powdery coatings and encrustations of snithsonite (zinc carbonate) is found profusely in the biotite-altered schsits in the Kanhan river valley (Fig.7.2b). Material excavated from a dug well south of Bhuyari shows fresh sulphides in the form of galena, pyrite, sphalerite and minor chalcopyrite. These sulphides are coarse grained, recrystallised and aligned parallel to the foliation (Fig.7.2d).

At places freshly broken outcrops show the presence of disseminated and vein mineralization consists mainly of sphalerite with subordinate pyrite, galena, chalcopyrite and pyrrhotite (Fig. 7.3a and 7.3b). Disseminated pyrite

occurs as a halo in the altered rocks surrounding the mineralized zone. Based on the presence of disseminated, vein and stringer mineralization in the altered rhyolites south of the massive sulphide zone, the altered rhyolites occurring to the south of the massive sulphides are inferred to represent the stratigraphic footwall of the mineralized zone. This observation is supported by the presence of unaltered rhyolites and lack of mineralization in the hanging-wall side towards north of the massive sulphide zone (Fig. 2.2b).

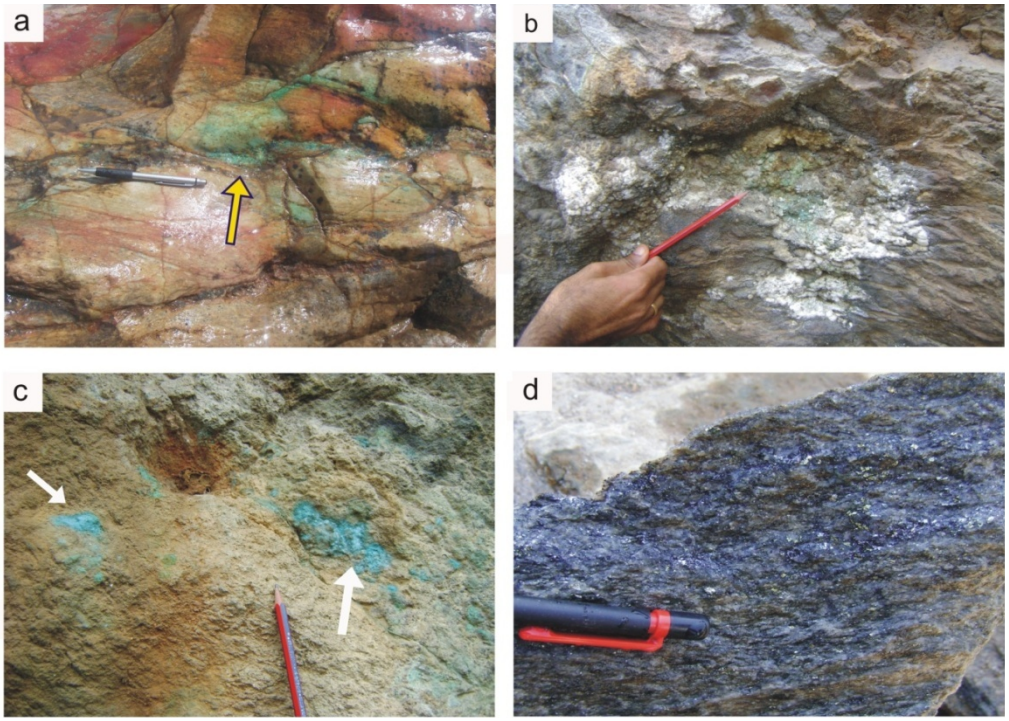

Fig.7.2 Photographs showing surface indications for mineralization. a) Malachite staining on red silicified rhyolite b) white encrustations of smithsonite (zinc carbonate) on biotite-phlogopite schist in the Kanhar River bed south of Bhuyari. (c) Malachite patches (arrows) on tremolite-carbonate rocks south of Bhuyari d) mineralized quartz-muscovite-biotite-K-feldspar schist with sphalerite, galena and pyrite along foliation sample from a well near sample PBS-2.

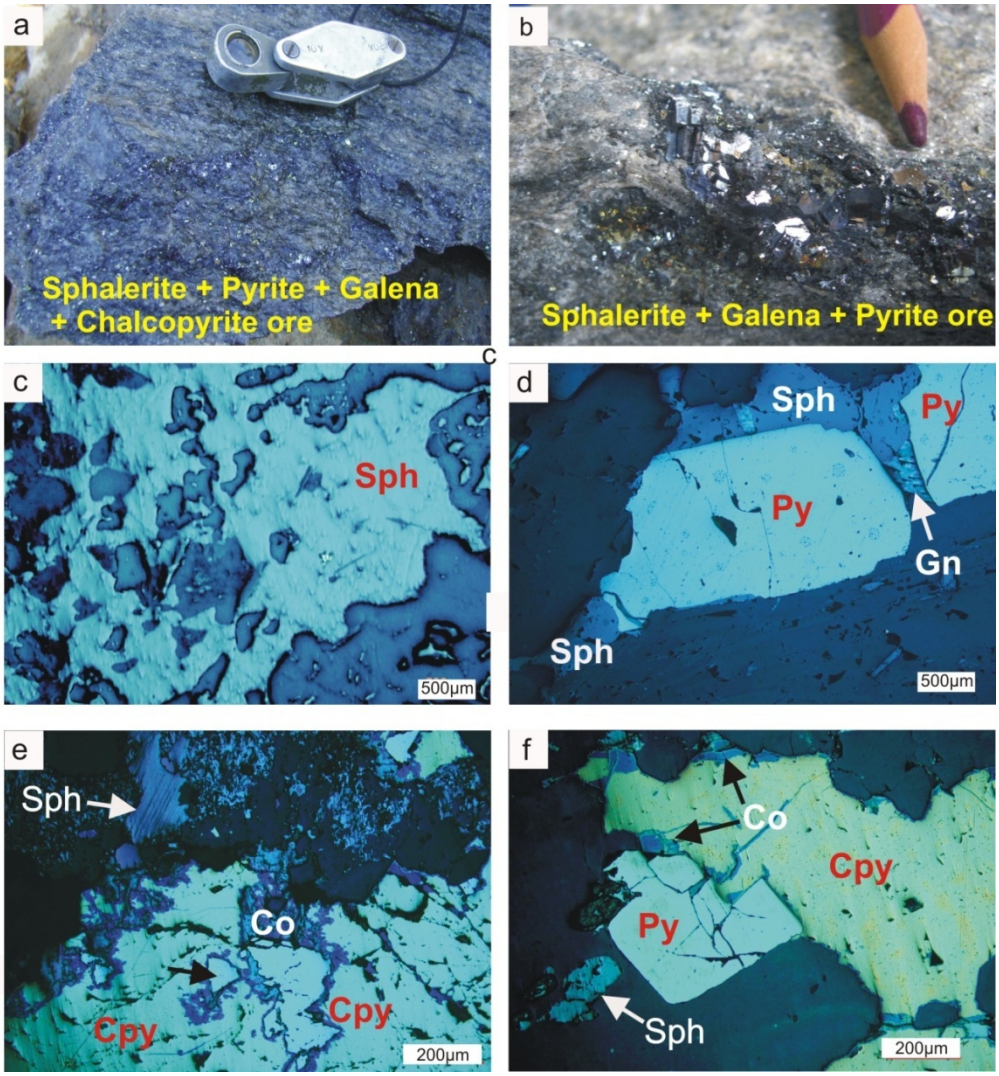

Fig: 7.3 Photographs of mineralized outcrops (a) semi-massive sphalerite ore occurring as bands along foliation plane of highly altered (b) disseminated recrystallised sphalerite-galena-pyrite ore (c) massive sphalerite ore with interstitial silicates (gangue), (d) stringer veins with cubic recrystallized pyrite (Py) and sphalerite (Sph), (e) chalcopyrite (Cpy)-rich zones overprinting sphalerite (Sph), chalcopyrite show alteration to bluish covelite (Co), (f) chalcopyrite (Cy) and euhedral pyrite (Py) show straight grain margins, sphalerite (Sph) also seen.

7.5 Sulphide Texture and Mineralogy

In semi-massive portions, sulphides occupy intergranular spaces of the host rock minerals and are of replacement type (Fig.7.3c). Relict host rock patches are commonly present within the massive and semi-massive sulphides (Fig.7.3c). Mostly such primary textures are obscured and effects of deformation and metamorphism has resulted in the sulphides occurring as recrystallized veins and stringers parallel to the foliation planes in the rock (Fig. 7.3d).

Sulphide zones show effects of metamorphic recrystallization and are medium to coarse grained. Sphalerite, galena and pyrite are typically recrystallized into 1-3mm grains in which pyrite are euhedral (Fig.7.3b). Sphalerite also occurs as massive and remobilized aggregates with interstitial silicates (Fig. 7.3c). Galena forms recrystallized aggregates along with sphalerite and pyrite (Fig. 7.3b). Chalcopyrite is associated with pyrite and occur as remobilized veins and bands adjacent to the massive sulphide zone towards south. Chalcopyrite is generally associated with pyrite and is at places altered to bluish covelite (Fig. 7.3e & f).

Although, the primary textures have been modified by recrystalization and grain-size coarsening, the textural evidences indicate that chalcopyrite-pyrite assemblage overprints the earlier sphalerite-galena-pyrite assemblage (Fig.7.3e & f). This may suggests a sulphide evolution from initial low temperature (sphalerite-pyrite) to higher temperature chalcopyrite-rich assemblage. Textures also indicate that chalcopyrite and euhedral pyrite formed last in paragenesis (Fig. 7.3e & f) when compared to an earlier sphalerite-pyrite episode.

7.6 Mineral Chemistry of Sulphides

Electron Probe Micro Analyses (EPMA) of sulphide minerals were carried out at EPMA Lab, GSI, Faridabad. The analyzed sulphides contain low proportion of trace elements like cobalt, nickel, arsenic and silver (Tables 7.1 to 7.3). The sphalerite analyses show a clear variation in mineral chemistry in terms of proximity to the central alteration zone and massive sulphides. The Fe content of sphalerite close to the massive sulphide zone show high and ranges from 7.7 to 9.2 wt. % (Sample BR-4 and 5) (Table 7.1), whereas, the Fe content of sphalerite distal to the massive sulphide zone (sample: BYR-6) ranges from 4.5 wt. % to 5.4 wt. % (Table.7.3). The sphalerite with higher Fe content could represent primary sphalerite whereas; the sphalerite distal to the proximal alteration zone could represent remobilized and recrystallised sphalerite, which could have lost some of its Fe content. This is supported by the almost monomineralic sphalerite-rich zones when in the distal areas, whereas, in the proximal zones, the sphalerite coexists with galena, chalcopyrite, pyrite.

At places sphalerite contain up to 0.5 wt. % copper which may be due to minute inclusions of chalcopyrite in sphalerite which is supported by ore petrographic studies. Pyrite contain Fe contents ranging from 46.16 to 47.66 wt. %. Chalcopyrite contains Fe content ranging from 29.42 to 30.16 wt. %. (Table. 7.2). Galena contain Pb contents ranging from 83.4 to 87.61 wt.%. The Pb content of galena also shows variation from close to massive sulphide zone and distal to massive sulphide zone. Pb contents of galena close to massive sulphides range from 85.7 to 87.6 wt.% and Pb content of galena distal to massive sulphide show Pb contents ranging from 83.4 to 85 wt. %.

Table-7.1 Mineral chemistry by EPMA of galena and sphalerite from ore proximal to massive sulphide zone

	1	2	3	4	5	6	7	8	9	10	11
	galena	galena	galena	galena	galena	sph	sph	sph	covelite	covelite	covelite
	BYR-4/11	BYR-4/20	BYR-4/22	BYR-5/1	BYR-5/2	BYR-4/17	BYR-4/36	BYR-4/39	BYR-4/3.	BYR-4/4	BYR-4/9
S	13.84	13.6	13.74	13.48	13.27	33.24	33.31	33.19	32.46	32.33	32.89
Fe	0.06	0	0	0	0	9.03	9.23	8.09	1.36	1.96	2.16
Co	0	0	0	0	0	0.01	0.02	0	0	0.02	0
Ni	0	0	0	0	0	0	0	0	0.01	0	0
Cu	0	0.05	0	0	0	0.07	0	0.48	64.09	63.7	63.71
As	0	0	0	0	0	0	0	0.05	0.03	0.08	0
Ag	0	0.05	0	0	0	0	0.05	0	0.02	0.19	0.18
Pb	87.61	86.17	86.88	85.68	86.34	0	0	0	0.05	0.12	0
Zn	0	0	0	0	0	56.83	56.93	58.05	0.07	0.26	0
Total	101.5	99.94	100.62	99.34	99.64	99.32	99.6	100.12	98.26	98.65	99

Table-7.2 Mineral chemistry by EPMA of pyrite and chalcopyrite from ore proximal to massive sulphide zone

	12	13	14	15	16	17	18	19	20	21
	pyrite	pyrite	pyrite	pyrite	pyrite	cpy	cpy	cpy	cpy	cpy
Sample	BYR-4/2	BYR-4/12	BYR-4/16	BYR-4/19	BYR-5/7	BYR-4/6	BYR-4/15	BYR-4/18	BYR-4/24	BYR-4/34
S	52.46	53.01	53.21	53.79	53.11	34.39	34.89	35.32	34.47	34.28
Fe	46.18	46.17	46.39	46.16	47.58	29.79	29.89	30.16	29.63	29.98
Co	0.05	0.03	0.05	0.07	0.08	0.02	0	0	0	0
Ni	0	0	0	0	0	0	0	0	0	0.03
Cu	0.03	0	0	0.09	0	33.84	33.29	32.86	33.84	34.25
As	0	0.26	0.05	0.1	0.07	0.03	0.08	0.01	0	0.07
Ag	0.04	0	0.02	0.03	0	0.03	0	0.04	0	0
Pb	0	0	0	0	0	0	0	0	0	0
Zn	0.01	0	0.02	0	0	0	0.02	0.17	0	0
Total	98.95	99.5	99.76	100.24	100.88	98.11	98.18	98.67	97.98	98.6

Table-7.3 Mineral chemistry by EPMA of sphalerite from ore distal to massive sulphide zone

	22	23	24	25	26	27	28	29	30	31
Sulphide	**Sph**	**Sph**	**sph**	**sph**	**sph**	**sph**	**galena**	**galena**	**galena**	**galena**
Sample	**BYR-6/8**	**BYR-6/10**	**BYR-6/12**	**BYR-6/16**	**BYR-6/18**	**BYR-6/20**	**BYR-6/14**	**BYR-6/15**	**BYR-6/19**	**BYR-6/21**
S	32.04	32.47	32.95	33.41	33.34	33.01	12.82	13.03	13.68	12.7
Fe	4.51	5.29	5.33	5.23	5.31	5.41	0	0	0.07	0
Co	0	0	0	0	0	0	0	0	0	0
Ni	0	0	0	0	0	0	0.01	0	0	0
Cu	0.38	0.01	0	0	0	0	0	0	0	0
As	0	0	0.02	0.03	0.03	0	0	0	0	0
Ag	0	0.08	0.06	0	0.04	0.01	0	0	0	0
Pb	0	0	0	0	0	0	83.44	85.06	84.97	83.65
Zn	60.67	60.71	61.19	61.14	60.95	60.7	0.03	0.37	2.51	0.56
Total	98.06	98.68	99.61	99.81	99.74	99.2	96.36	98.49	101.23	97.14

7.7 Discussion

Surface indications of mineralization in the form of malachite, azurite and cerussite encrustations present on the outcrops of highly altered rhyolites indicate that the mineralized system is exposed on the present level of erosion. Exploration by GSI shows that the ore zones occur as multiple bands which are parallel to the E-W regional foliation with shallow to moderate dips (20-30°) towards south (Fig.7.4). The original morphology of the ore bodies and alteration zones is not preserved due to deformation effects. Mineralization enclosed within the highly altered rhyolite indicates that the sulphides are syngenetic to rhyolite emplacement and hydrothermal alteration and therefore are similar to other VMS deposits worldwide. The massive sulphide lens occurs near the top of the alteration zone which suggests that this was the top of the hydrothermal system where the massive sulphides were vented out on the seafloor. Close association of tremolite-carbonate rocks which have field as well as geochemical signatures of metaexhalites are consistent with this interpretation. Most part of the disseminated and semimassive sulphide ores could have possibly formed by replacement processes close to the seafloor or just below the seafloor (sub-seafloor). The disseminated and vein pyrite-chalcopyrite bearing zones adjacent to the massive sulphides may represent stringer zones characteristic of VMS deposits.

Remobilization has not caused large scale transport of the sulphides, which is evident from their close spatial association with their alteration zones. Alteration systems in VMS deposits are a syngenetic feature, and any large scale mobilization of sulphides will result in separation of the sulphides from their enclosing/associated alteration zones. The recrystallization effects are related to the main deformational event, which is the N-S compression and resultant E-W foliation in the rocks. The sulphides have undergone coarsening of grain sizes as part of metamorphic recrystallization.

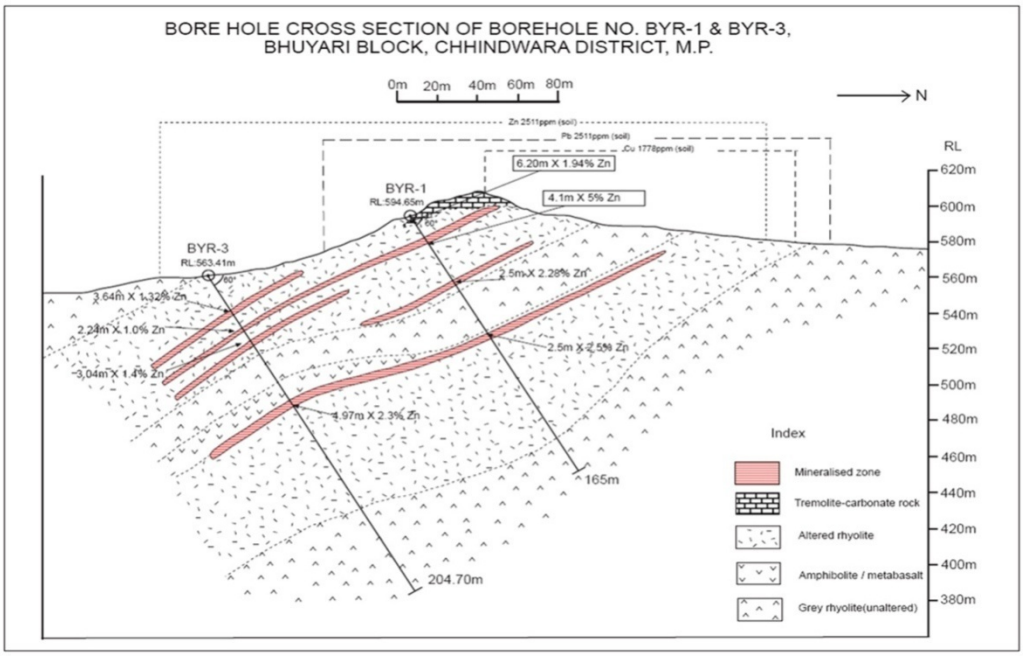

Fig.7.4. Geological cross section along N-S of the central part of the mineralized zone at Bhuyari based on GSI boreholes (Praveen et al, 2010).

Sulphide paragenesis suggests that the initial low-temperature sphalerite-pyrite mineralization was followed by higher temperature chalcopyrite-pyrite mineralization as indicated by ore textures. Sulphide mineralogy is similar to the well-known Kuroko VMS Zn-Pb-Cu deposits of Japan, with pyrite, sphalerite, chalcopyrite and galena as the major minerals. The lack of pyrrhotite in the ore zones are also similar to the Kuroko ores, however, the Bhuyari ores lack barite and anhydrite which are common in the Kuroko ores.Proterozoic VMS deposits commonly occur as clusters of several deposits extending over vast volcanic provinces. The numerous base-metal prospects associated with the felsic volcanics of Betul Belt including Bhuyari are examples of such clustering of VMS-type deposits. This suggests that there is a potential for the discovery of additional VMS deposits in the felsic volcanic sequence of Betul Belt.

******

Chapter 8

METAMORPHISM AND GEOTHERMOBAROMETRY

Contents

8.1 Introduction
8.2 Metamorphic Mineral Assemblages
8.3 Use of Petrogenetic Grid for estimating Pressure-Temperature
8.4 Geothermobarometry
8.5 Conclusion

8.1 Introduction

Metamorphosed terrains which have undergone amphibolite to granulite facies metamorphism provide challenges for the recognition of the pre-metamorphic ore-related hydrothermal alteration zones which are crucial for the exploration of VMS deposits. However, at the Bhuyari VMS Prospect metamorphosed to amphibolite facies, careful alteration facies mapping using metamorphic mineral assemblages has helped in delineating mineralogically and chemically distinct alteration zones associated with zinc-rich mineralization. The results show that major element chemistry of these alteration zones closely reflects their protolith composition.

Bonnet and Corriveau (2007), in their review of VMS alteration in metamorphosed felsic rocks have shown that alteration mapping based on visual estimates of rock types, mineral modal abundance, and mineral assemblages are effective in qualitatively measuring the variations in major elements associated with the premetamorphic hydrothermal alteration and in establishing the chemical zonation with a reasonable degree of confidence.

Such zonation reflects major element mobility during fluid-rock reaction in the upflow zone (e.g. Al, Fe, Mg, Ca, Na, and K) and represents geochemical indicators of the type and intensity of alteration (Barrett and MacLean, 1994a; Large et al., 2001b). These tools are also applicable to metamorphosed, weakly to intensely altered rocks whose precursor is known (e.g. Hallberg, 2001). Medium to high grade metamorphism converts the hydrothermal mineral assemblages into various characteristic mineral assemblages that form by reactions involving primary hydrothermal chlorite, sericite, smectite and carbonate in various proportions in different zones. Rock composition and physical conditions, such as pressure and temperature (e.g. Rosenberg et al., 2000) constrain mineral assemblages, mineral composition, and modal mineral abundance of metamorphic rocks, including those forming metamorphosed hydrothermal alteration zones and those affected by synmetamorphic sulphidation and oxidation processes.

As pressure and temperature change, mineral phases react with each other to form new mineral assemblages. The changes in mineralogy during metamorphism obey the phase rule; hence the pressure-temperature stability field of different metamorphic assemblages can be predicted, and experimentally reproduced and calibrated for the most common rock compositions and then graphically represented using petrogenetic grids and phase diagrams (AFM, A'CF, A'KF, etc) (e.g. Spear, 1993 and Bonnet and Corriveau, 2007). The plotting of the composition of altered rocks and unaltered precursors in phase diagrams allows their respective stable mineral assemblages and modal mineral abundance to be determined. Alteration vectors may be represented graphically using chemical diagrams or on AFM,

A'CF, or A'KF phase diagrams, as discussed above, in order to visualize the whole-rock composition and the mineralogical assemblages of the altered rocks and their precursors (Bonnet and Corriveau, 2007). This allows (1) the chemical changes associated with the hydrothermal alteration to be determined by comparing the metamorphic characteristics of the altered rocks and their precursors, and by extrapolation, their compositions; (2) the establishment of the link between the metamorphic assemblages observed and the primary hydrothermal mineralogical assemblages; and (3) the development of metallogenic models (Roberts et al., 2005). The field models can then be refined with lithogeochemical studies (Large et al., 2001c).

The metamorphosed alteration assemblages containing garnet, muscovite, biotite, staurolite at Bhuyari show some similarities with typical metapelites, which can lead to their wrong identification as metasedimentary rocks. This could actually be due to - as is true in the case of most of the hydrothermally altered rocks - considerable addition and depletion of mobile elements like Mg, Fe, Ca, Na and K.

Major element data of the altered as well as least altered rhyolites were plotted in the different diagrams like AKFm, A'KF and MgO-SiO_2-CaO diagram to study and visualize the connection between the alteration assemblages and bulk chemical composition. The connection between the different metamorphic mineral assemblages at Bhuyari and typical semi-pelites consisting of quartz + biotite+ plagioclase (+ staurolite, cordierite, aluminosilicate, garnet) is easily demonstrated with an AKFm plot (Fig.8.1). The altered protolith with variable contents of K_2O, MgO and FeO will move in different directions during prograde metamorphism. The AKFm plot is

particularly useful in representing Mg-rich chloritic alteration and K-Al rich sericitic alteration. These trends are visible in the AKFm plot where most samples plot in between the biotite and muscovite fields with trends towards the K apex (Fig. 8.1). The biotite in these assemblages is highly Mg-rich (phlogopitic) and could have formed by metamorphism of hydrothermal Mg-rich chlorite. Similarly the trends towards the muscovite node reflect primary sericite alteration.

The A'KF diagram is useful in accounting for all Mg-Fe minerals, K-bearing minerals and aluminum bearing minerals which make up most of the minerals present in the magnesium-rich and potassic alteration zones (Fig. 8.2). Aluminum is assumed to go into feldspar and mica along with the alkali metals. This diagram is particularly useful to represent sericitic alteration (K-Al) localized close to the apex K (Bonnet and Corriveau, 2007). The altered rhyolites when plotted in the A'KF diagram show that the majority of samples plot close to the biotite and phengite which clearly reflects the assemblages in the Bhuyari alteration zones which are dominated by phyllosicates like biotite-phlogopite and muscovite-phengite. The remaining samples plot close to staurolite and K-feldspar fields which again reflect the presence of these minerals in the alteration zones. The lack of aluminosilicates in the assemblage is reflected in the empty space near the andalusite – kyanite - sillimanite fields. A trend towards K-feldspar is very evident in the samples from the muscovite-K feldspar altered zone which shows that this assemblage was derived from rhyolites affected by intense sericite alteration (Fig.8.2).

The tremolite-carbonate rocks of Bhuyari were plotted in the MgO-SiO_2-CaO diagram which is the standard diagram for carbonate rocks

(Fig.8.3). The plots fall near the dolomite and tremolite areas. This is consistent with the mineralogy of the tremolite carbonate rocks, which are predominantly composed of tremolite and carbonate with minor proportions of other minerals like talc, chlorite, garnet, plagioclase, zoisite, actinolite, serpentine etc. Tremolite-carbonate-chlorite bearing assemblages associated with ore zones at Thalanga VMS deposit, Australa, are inferred to represent metamorphosed dolomite + chlorite (or Mg-smectite) assemblages which formed by hydrothermal alteration and addition of carbonate to permeable rhyolite volcaniclastics in the upper few meters of the seafloor substrate (Herrmann and Hill, 2001). This supports the view that the carbonate-bearing rocks were originally deposited on or close to the paleo seafloor by hydrothermal venting and were syngenetic with massive sulphide deposition. The close spatial association with massive sulphide zones and carbonate rocks at Bhuyari is consistent with this hypothesis.

Overall, the metamorphic mineral assemblage in the various alteration zones broadly reflects the bulk composition as seen from the plots. The alteration trends are also clearly evident with the predominant trends towards biotite and muscovite end members, which is consistent with the phyllosilicate dominant alteration at Bhuyari. Minor trends towards staurolite and garnet are also discernible, which correspond to argillic alteration. The AKFm and A'KF plots clearly show that the various assemblages at Bhuyari comprising garnet, staurolite, gahnite, biotite and muscovite were derived from metamorphism of chloritic and sericite-altered rhyolitic protolith, which is evident from the trends radiating from the least altered rhyolite field towards sericite and chlorite nodes (Figs.8.1 & 8.2). These plots also show that the metamorphic

mineral assemblages do not represent metapelites and that their precursors are clearly derived from rhyolitic protoliths.

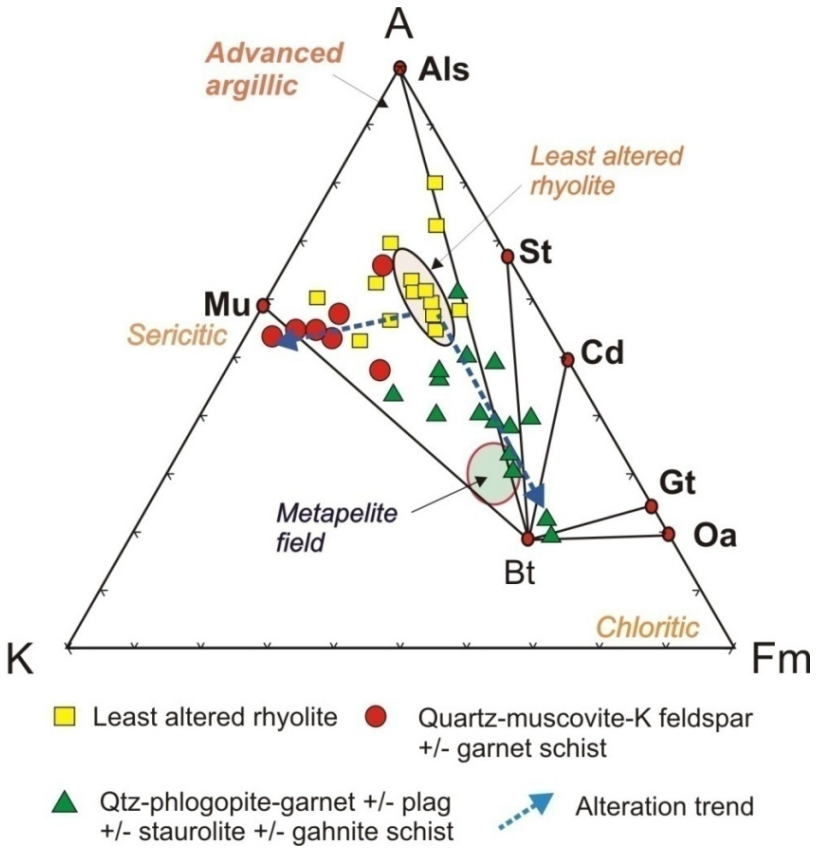

Fig 8.1 AKFm diagram after Arnold and Sandiford (1990) showing the distribution of bulk rock compositions of least altered and altered rock types. The least altered rhyolites (LA) plot in a tight cluster shown by shaded ellipse. The field for ideal bulk composition of pelitic and semipelitic rocks is also shown for comparison (Arnold and Sandiford, 1990). Apices are **A**: $A1_20_3$, **K**: K_20, **Fm**: FeO+MgO, projected from albite, quartz and vapour (in excess). Note that there are distinct trends towards muscovite, biotite and staurolite apices. The inferred nature of premetamorphic hydrothermal alteration is given in italics (advanced argillic, sericitic, chloritic). The alteration vectors (dotted arrows) show trends towards sericitic and chloritic alteration.

Abbreviations: Als-aluminosilicate, St-staurolite, Cd-cordierite, Gt-garnet, Oa-orthoamphibole, Bt-biotite, Mu-muscovite.

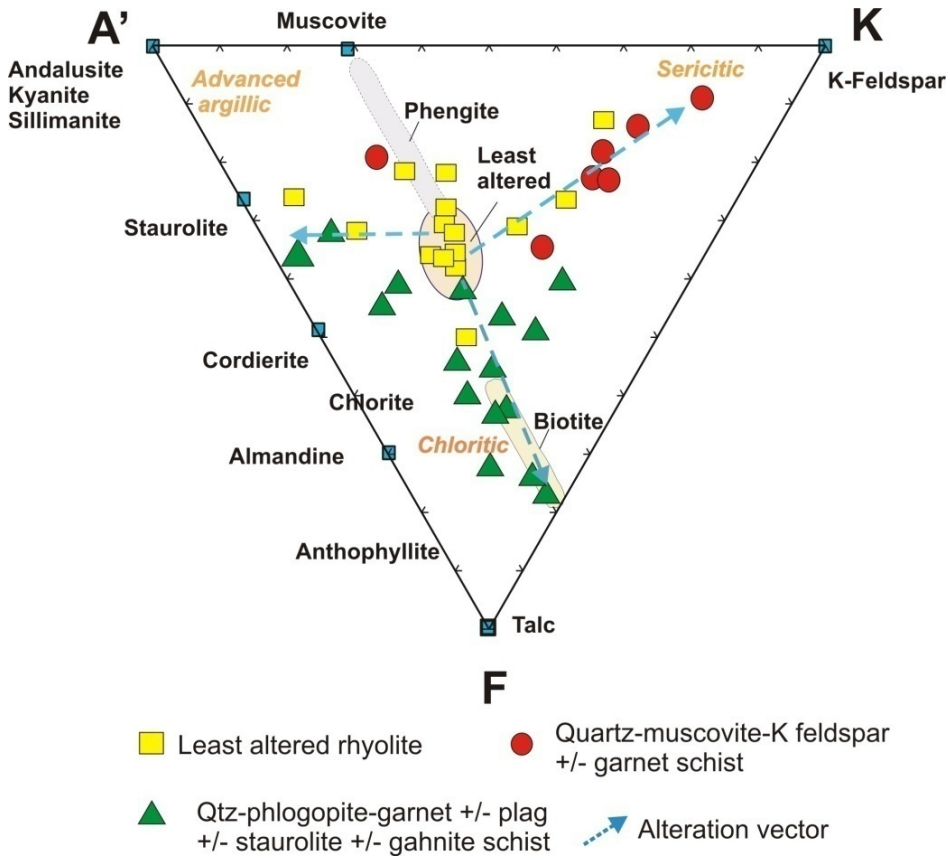

Fig. 8.2 Ternary diagram showing alteration vectors and their control on modal composition and mineral paragenesis of metamorphosed hydrothermal alteration zones (modified from Bonnet and Corriveau, 2007) A'KF diagram. A' = (Al_2O_3 + Fe_2O_3) - (K_2O + CaO + Na_2O), K = K_2O and F = (FeO + MgO). Green boxes indicate ideal end member locations in the diagram. Fields for phengite (Fe-Mg bearing muscovite) and biotite are also shown. The unaltered rhyolites plot in a tight cluster. The fields for nature of premetamorphic hydrothermal alteration are from (Bonnet and Corriveau, 2007) and are shown in italics (advanced argillic, sericitic, chloritic). Alteration vectors (dotted lines) originate from the unaltered rhyolites and show distinct trends towards the biotite and sericite-K-feldspar end member compositions. A trend towards staurolite is also apparent.

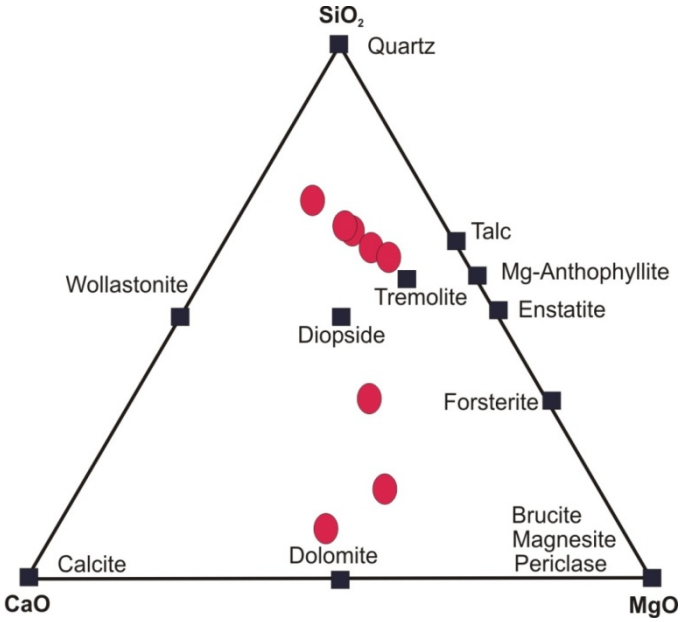

Fig 8.3 Molar proportions of tremolite-carbonate rocks plotted in the MgO-SiO_2-CaO diagram. The plot closely reflects the tremolite-dolomite dominated mineralogy of the carbonate rocks of Bhuyari

8.2 Metamorphic Mineral Assemblages

Aluminosilicate is absent from the mineral assemblage at Bhuyari. However, fibrolite clots (sillimanite) is present in some metamorphosed alteration zones in the central part of Betul Belt, for example at Muariya and Dehelwara prospects which are about 40km to the east of Bhuyari. This indicates that the eastern part of Betul Belt around Bhuyari experienced intermediate P-T conditions. The absence of the index mineral kyanite in the assemblages supports the assumption that the pressures did not cross 8 kb during peak metamorphism. It is therefore reasonable to assume that the rocks at Bhuyari underwent amphibolite facies metamorphism.

Mineral assemblages in the altered felsic volcanics have similar metamorphic minerals as metapelites due to extensive metasomatism and

resultant bulk composition prior to metamorphism. The mineral assemblages containing garnet, biotite, staurolite, plagioclase and K-feldspar provide clear evidence for amphibolite facies metamorphism. The presence of tremolite in the carbonate altered rocks also supports this view. The mafic volcanics at Bhuyari have typical amphibolite facies mineral assemblage of plagioclase + hornblende + quartz. This is a diagnostic assemblage developed in mafic volcanic rocks in amphibolite facies (e.g. Bucher and Frey, 2013).

The tremolite-carbonate rocks provide evidence for amphibolite facies metamorphism with the assemblage containing tremolite + dolomite + talc + chlorite + grossular + anorthite + zoisite. These rocks are also enriched in sulphides like galena, sphalerite and chalcopyrite. Tremolite occurs as coarse porphyroblasts (up to several centimeters) sometimes forming monomineralic aggregates. The absence of wollastonite and diopside in this rock can be taken as evidence that these rocks never surpassed the amphibolite facies metamorphism. The present assemblage of tremolite-bearing rocks possibly represents peak metamorphic assemblage.

Presence of garnet, staurolite and biotite in the magnesium rich alteration zone and tremolite, zoisite, grossular and anorthite in the meta-carbonate rocks offer good scope for constraining the P-T conditions during metamorphism. Garnets are ubiquitous in most altered mineral assemblages at Bhuyari. The garnets are spessartine-rich in the magnesium- rich alteration zones as well as locally grossular rich in the tremolite-carbonate rocks. In metapelites, garnets generally form at 500° C at the garnet-in isograd. However, temperatures of garnet formation are significantly reduced in manganese-rich and calcium-rich rocks (Spear, 1993). The tremolite carbonate rock also locally contains grossular-rich garnets.

The textural relationships in the garnet-staurolite rocks give evidence for late formation of staurolite after garnet and biotite. The staurolite forming reaction following Spear (1993) is as follows.

Garnet + Chlorite + Muscovite = Staurolite + Quartz + H_2O.

At Bhuyari, the staurolite porphyroblasts replace and form pseudomorphs after biotite. Large porphyroblasts of staurolite contain inclusions of garnet. Staurolite is a common mineral constituent in metapelitic rocks of medium grade amphibolite facies domains, with an upper stability limit generally defined by the reaction:

Staurolite + Muscovite + Quartz = Biotite + Al_2SiO_5 + H_2O (± garnet, Zn-rich spinel)

According to the experiments of Richardson (1968), the first appearance of staurolite with quartz alone occurs at 540°C at 3 kbar in pure H_2O and staurolite with biotite, almandine, muscovite, and quartz should first appear at a T of the order of 20°–30°C higher, reduced slightly by impurities in the fluid and Mn in garnet (Holdaway et al., 1997).

According to (Holdaway et al., 1997) garnet-biotite calibration, the first appearance of the assemblage staurolite-biotite-almandine is at 574ºC. According to the garnet-biotite calibration of Powell and Holland (1990), the first appearance of staurolite-biotite-almandine is at some temperature below the average staurolite zone T of 574°C. This is also consistent with the estimate of Guidotti (1974). Richardson (1968), Dutrow and Holdaway (1989), and Holdaway et al., (1995) all indicate that at 3 kbar, staurolite and quartz break down at a temperature of 625°C.

At Bhuyari, the peak metamorphic conditions were attained with the development of staurolite + garnet + biotite bearing assemblages in the

magnesium rich alteration zones and with phengite-microcline-plagioclase-garnet in the potassium-rich alteration zones and with development of tremolite-dolomite-plagioclase in the carbonate alteration zones. The complete absence of diopside and sillimanite in the carbonate and aluminous alteration zones suggest that temperatures were limited to sub 600° C, which is suggestive of intermediate pressure and temperature metamorphism. Textural evidence shows that the assemblages were formed in a single prolonged metamorphic event. Final retrogressive metamorphism evidenced in the form of second generation gahnite and chlorite forming events could be linked to intrusion of granites towards the north.

8.3 Use of Petrogenetic Grid for Estimating Pressure-Temperature

When the metamorphic mineral paragenesis and reactions are well preserved in the field, the P-T conditions of metamorphism can be reasonably well constrained by the relevant petrogenetic grid. For the mineral assemblages in Bhuyari, the KFMASH grid is suitable since most of the mineral assemblage excluding that of the tremolite-carbonate rocks can be accounted for. The Bhuyari mineral assemblage gives an indication for amphiboite facies metamorphism. The thermobarometry of rocks in the amphibolite facies indicates that they form in the approximate T range of 500-700°C and at pressures ranging from 3 to 12 kbar (e.g. Essene, 1989). Pressures in the amphibolite facies may be estimated by a comparison of prograde index minerals of metapelites relative to key invariant points on a petrogenetic grid, which may be mappable as bathograds (Carmichael, 1978).

The presence of prograde staurolite in the rocks is a key indicator to the staurolite zone of metamorphism, which is reasonably well-constrained. Droop

(1985) indicates, on the basis of a number of thermometers and barometers, that the garnet + chlorite + muscovite staurolite + biotite isograd occurs at about 7 kb and 580'C. The slightly lower pressure estimates obtained by GPMB (4 to 5.1 kb) and by GMPQ (4.6 to 5.7 kb) may be an artifact of retrogression effects.

Based on the KFMASH petrogenetic grid (Fig. 8.4) and the mineral assemblage staurolite + biotite + gahnite likely attained peak temperature in the range of 600 to 620° and pressures ranging from 6 to 7 kb. This compares favourably with the temperatures obtained from GM thermometer and GPMQ barometer, except for the slightly higher pressure estimates in the KFMASH grid which are in the range of 6-7 kb.

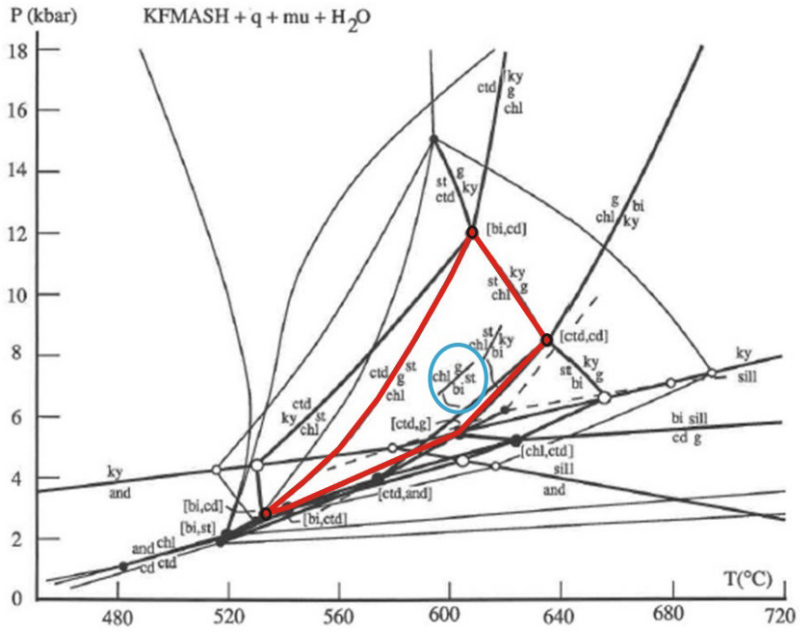

Fig.8.4 Pressure-Temperature projection in KFMASH after Powell and Holland (1990) showing the stability field of biotite + garnet + staurolite assemblage (shown in red lines). The mineral assemblage comprising biotite + staurolite + garnet is highlighted (blue circle) which corresponds to a pressure of 6-7 kb and temperatures of 590-610°C.

The KFMASH petrogenetic grid by Holland and Powell (1990) takes into account the reactions involving staurolite, garnet, biotite, chlorite, aluminosilicate and excess phases –muscovite, quartz and H_2O and is ideal for the assemblage at Bhuyari. The stability field for the biotite + garnet + staurolite field is shown within the red lines. Based on the KFMASH grid, the stability field for biotite + staurolite + garnet field corresponds to a pressure of 6-8 k bars and a temperature of 590 to 610°C (Fig.8.4).

8.4 Geothermobarometry

The metamorphic mineral assemblages in the alteration zones of the Bhuyari Zn-Pb (Cu) deposit closely resemble those developed in metamorphosed pelitic rocks. Therefore, the geothermobarobeters applicable for metapelites can be used for the alteration zone assemblages at Bhuyari. Other studies have also shown that routine normal geothermobarometric calculations and calibration methods such as those used in metapelitic assemblages can be applied to rocks which have been intensely altered by hydrothermal activity prior to regional metamorphism, provided appropriate caution is taken (eg. Cook, 1993).

For this study, Electron Microprobe Analyses (EPMA) of the various metamorphic minerals occurring in equilibrium was determined to estimate pressure-temperature conditions. To determine the peak conditions of regional metamorphism the following methods were attempted

1. Garnet-biotite thermometry
2. Ti in biotite thermometry
3. Phengite barometry
4. Garnet-Plagioclase-muscovite-biotite- barometry
5. Garnet-Muscovite thermometry and
6. Garnet-Muscovite-Plagioclase-Quartz barometry

These methods give a fair approximation of the PT conditions during metamorphism and are used in conjunction with standard PT grids for metapelites. The metamorphosed alteration zones contain various mineral assemblages that are amenable for pressure-temperature determinations.

8.4.1 Garnet Biotite Thermometry

The garnet-biotite Fe-Mg exchange geothermometer is the most widely used thermometer for estimating temperature of equilibration of medium-grade pelitic metamorphic rocks. This geothermometer was first proposed by Ferry and Spear (1978) based upon the exchange of Fe^{2+} and Mg between garnet and coexisting biotite. The important experimental work of Ferry and Spear (1978) and Perchuk and Lavrent'eva (1983) form the basis for this widely used geothermometer. This was subsequently improved upon by various workers (e.g., Ganguly and Saxena, 1984; Bhattacharya et al., 1992; Kleemann and Reinhardt, 1994). The mineral assemblages in the metamorphosed alteration zones in Bhuyari are ideal for employing the garnet-biotite thermometer in view of the widespread presence of coexisting prograde garnet and biotite. However, the relatively Mn-rich compositions of the garnet render most of the calibrations which rely on Mg-Fe exchange reactions to give inaccurate results. Similarly, the effect of high Mg-content of the biotite in some of the samples is also uncertain. These may be the reason for relatively wide range of temperatures achieved for garnet-biotite pairs (Table 8.3).

At Bhuyari, textural evidence indicates that the biotite-garnet is a peak equilibrium assemblage in the rocks (Fig. 8.5). Coexisting biotite and garnet show straight mutual grain contacts indicative of formation in a prograde event (Figs. 8.5a, b &c). Staurolite occurring as incipient grains within biotite gives

evidence for formation by breakdown of biotite (Figs. 8.5c & d). These porphyroblasts are also variably affected by a retrogressive event which is manifested in the form of chloritisation of biotite (Fig. 8.5d) and at places by sericitisation of staurolite. This retrogressive event could have affected the Mg-Fe systematics of the peak metamorphic conditions. This is also reflected in the variable Mg/Fe ratios of the analysed garnets from various alteration types. Therefore, as far as possible, care was taken to use the garnet analyses which contained the highest Mg/Fe ratios (representing peak-T) as suggested by Holdaway et al (1997).

EPMA data of 13 garnet-biotite pairs from different alteration assemblages were used for obtaining the peak metamorphic temperatures attained during metamorphism (Table 8.1 and 8.2). In most of these rocks the mineral assemblage consists of quartz, feldspar, biotite, garnet, staurolite and muscovite with variable amount of accessory sulphides. Core and rim areas were analyzed from the coexisting biotite and garnet (Fig. 8.5a &b). The results are summarized in Table-8.3. The obtained results show a temperature range from a low of 268°C to a high of 775°C. The lower temperatures possibly are a result of the unusually Mn-rich garnets present in the assemblage at Bhuyari, which may cause the shifts towards lower temperature where most calibrations are prepared for ideal almandine garnet and biotie Fe-Mg exchange parameters. However, the obtained values provide us with a reference point that the temperatures are probably on the lower side than that is expected. Also, it shows that these garnet-biotite thermometers do not yield precise results if they contain high content of manganese in the garnet structure.

P-T values obtained for PBS-45,(garnet + biotite + plagioclase assemblage) are more consistent with the mineral paragenesis at Bhuyari. It gives a T range between 376 to 638°C at a assumed minimum pressure of 4kb (Table 8.3).

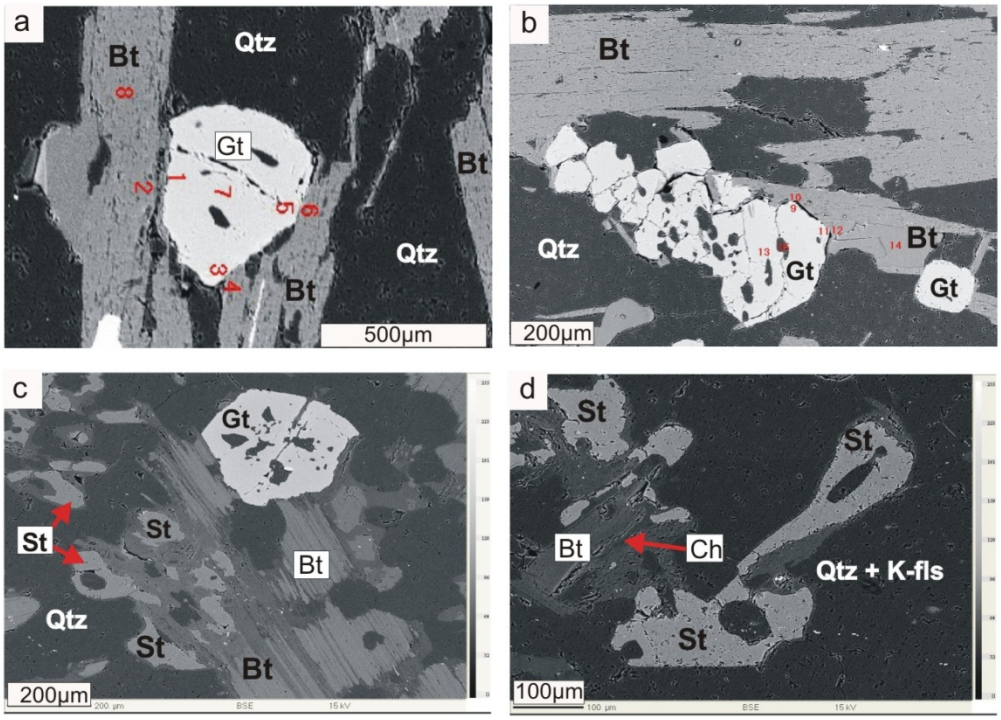

Fig 8.5 Texture of garnet + staurolite + biotite + muscovite + chlorite rock as seen in Back scattered Electron (BSE) images a) Coexisting biotite and garnet forming an equilibrium assemblage, the analysis points on garnet and biotite by EPMA are shown. b) Garnet porphyroblasts with quartz and biotite (Bt) inclusions, c) Staurolite showing incipient growth replacing biotite. d) Garnet + staurolite appear to an equilibrium assemblage; c) staurolite replaces and form pseudomorphs after biotite in a quartz + K-feldspar rich groundmass, chloritisation of biotite is seen.

Table-No. 8.1 Table showing EPMA data of 12 garnet analyses from garnet + biotite bearing assemblages used for P-T studies.

	1	2	3	4	5	6	7	8	9	10	11	12
	rim 1	rim 2	core 1	rim 4	rim 5	core 5	rim 1	rim	rim	rim-1	rim-4	rim
Analysis	PBS-45/1	PBS-45/3	PBS-45/7	PBS-45/9	PBS-45/11	PBS-45/13	PBR-3/70	PBS-26/81	PBS-26/76	PBR-30/53	PBR-30/63	PBR-3/69
SiO2	34.92	36.45	36.01	35.38	37.04	36.68	36.86	37.15	37.40	37.10	37.52	37.17
TiO2	0.02	0.04	0.02	0.05	0.00	0.00	0.04	0.00	0.00	0.04	0.03	0.15
Al2O3	21.24	21.14	20.80	20.55	20.99	21.08	19.17	20.68	20.74	20.38	20.80	19.35
Cr2O3	0.00	0.00	0.03	0	0.00	0.00	0.00	0.00	0.00	0.00	0.00	0.00
Fe2O3	0.00	0.00	0.00	0.00	0.00	0.00	0.00	0.00	0.00	1.43	0.45	0.00
FeO	19.50	18.64	19.88	19.35	18.97	19.82	19.49	18.41	18.31	19.50	19.31	19.05
MnO	15.99	17.32	15.72	18.39	18.39	15.64	15.32	17.73	18.39	14.96	15.90	11.99
MgO	2.07	1.52	2.29	1.32	1.55	2.04	0.18	3.26	2.94	0.43	0.33	0.32
CaO	4.40	3.80	4.34	3.09	3.93	4.39	6.84	2.46	2.59	7.01	6.94	9.91
Total	98.14	98.91	99.09	98.12	100.87	99.65		99.69	100.37	100.85	101.27	97.95
Cations on the basis of 12 oxygens												
Si	2.86	2.98	2.92	2.93	2.97	2.96	3.06	2.99	3.00	2.99	3.00	3.06
Ti	0.00	0.00	0.00	0.00	0.00	0.00	0.00	0.00	0.00	0.00	0.00	0.01
Al	2.05	2.03	1.99	2.00	1.98	2.01	1.88	1.96	1.96	1.93	1.96	1.88
Cr	0.00	0.00	0.00	0.00	0.00	0.00	0.00	0.00	0.00	0.00	0.00	0.00
Fe3	0.22	0.01	0.16	0.13	0.07	0.07	0.00	0.06	0.05	0.09	0.03	0.00
Fe2	1.11	1.26	1.19	1.21	1.20	1.27	1.35	1.18	1.17	1.31	1.29	1.31
Mn	1.11	1.20	1.08	1.29	1.25	1.07	1.08	1.21	1.25	1.02	1.08	0.84
Mg	0.25	0.18	0.28	0.16	0.19	0.25	0.02	0.39	0.35	0.05	0.04	0.04
Ca	0.39	0.33	0.38	0.27	0.34	0.38	0.61	0.21	0.22	0.60	0.60	0.87
Almandine	43.31	42.60	43.75	43.69	41.79	44.12	44.20	40.62	40.25	45.50	43.52	42.84
Pyrope	8.20	6.19	8.98	5.31	6.09	8.10	0.71	12.82	11.51	1.68	1.30	1.28
Grossular	12.52	11.13	12.24	8.94	11.09	12.52	19.89	6.96	7.31	19.66	19.63	28.55
Spessartine	35.97	40.09	35.04	42.06	41.03	35.26	35.20	39.60	40.93	33.16	35.55	27.33

Table-No.8.2 Table showing EPMA data of 12 biotite analyses from garnet + biotite bearing assemblages used for P-T studies

	PB545/2	PB545/4	PB545/8	PB545/10	PB545/12	PB545/14	PBR-3/71	PBS-26/82	PBR-26/76	PBR-30/54	PBR-30/64	PBR-3/72
	rim 1	rim 2	core 1	rim 4	rim 5	core 5	rim 1	rim	rim	Bt-core-1	Bt-rim-4	Biotite rim
SiO2	35.65	36.71	37.88	35.09	38.13	36.36	35.022	34.29	34.21	35.112	35.179	34.87
TiO2	0.21	0.35	0.23	0.34	0.24	0.35	2.295	0.61	0.51	2.77	2.83	2.10
Al2O3	16.15	16.36	17.25	16.45	16.89	16.30	15.711	18.76	19.28	16.09	16.47	15.71
FeO	14.27	14.87	14.46	14.67	13.37	14.13	26.64	19.90	10.71	26.16	26.65	26.29
MnO	0.48	0.43	0.55	0.58	0.36	0.41	0.79	0.58	0.68	0.62	0.64	0.78
MgO	14.57	15.17	14.37	14.67	14.73	15.03	5.049	19.90	20.59	5.57	5.64	5.21
CaO	0.01	0.02	0.03	0.55	0.02	0.01	0	0.01	0.02	0.01	0.02	0.00
Na2O	0.09	0.19	0.08	1.91	0.01	0.09	0.066	0.14	0.17	0.09	0.12	0.10
K2O	9.42	9.46	9.52	5.54	9.58	9.56	9.444	6.42	5.55	9.42	9.58	9.61
Total	90.85	93.56	94.37	89.80	93.33	92.24	95.02	100.62	91.72	95.84	97.11	94.66
Si	5.58	5.59	5.67	5.49	5.74	5.60	5.59	4.91	5.11	5.53	5.48	5.59
Al iv	2.42	2.41	2.33	2.51	2.26	2.40	2.41	3.09	2.89	2.47	2.52	2.41
Al vi	0.57	0.52	0.72	0.53	0.73	0.55	0.55	0.07	0.51	0.52	0.51	0.55
Ti	0.02	0.04	0.03	0.04	0.03	0.04	0.28	0.07	0.06	0.33	0.33	0.25
Fe	1.87	1.89	1.81	1.92	1.68	1.82	3.56	2.38	1.34	3.45	3.47	3.52
Mn	0.06	0.06	0.07	0.08	0.05	0.05	0.11	0.07	0.09	0.08	0.08	0.11
Mg	3.40	3.44	3.21	3.42	3.30	3.45	1.20	4.25	4.59	1.31	1.31	1.24
Ca	0.00	0.00	0.00	0.09	0.00	0.00	0.00	0.00	0.00	0.00	0.00	0.00
Na	0.03	0.06	0.02	0.58	0.00	0.03	0.02	0.04	0.05	0.03	0.03	0.03
K	1.88	1.84	1.82	1.11	1.84	1.88	1.92	1.17	1.06	1.89	1.90	1.96
Mg/(Mg+Fe)	0.65	0.65	0.64	0.64	0.66	0.65	0.25	0.64	0.77	0.28	0.27	0.26
Fe/(Fe+Mg)	0.35	0.35	0.36	0.35	0.33	0.34	0.73	0.36	0.22	0.71	0.71	0.72

Table 8.3. Table showing the P-T estimates based on garnet-biotite EPMA results as per calibrations of by various workers.

	Reference Pressure		(Temperatures in Degree Centigrade)					
Sample	Min pr	kbar	Bhattacharya et al (1992)	Dasgupta et al (1991)	Ferry and Spear (1978)	Perchuk and Larrenteva (1983)	Thompson (1976)	Holdaway and Lee (1977)
PBS-45/2	4	7	496	638	481	528	525	511
PBS-45/4	4	7	413	516	375	459	434	431
PBS-45/14	4	7	460	566	422	490	476	468
PBS-45/8	4	7	506	626	494	536	536	521
PBS-45/10	4	7	400	504	368	454	428	425
PBS-45/12	4	7	414	503	376	459	435	431
PBS-26/1	4	7	557	775	584	588	609	584
PBS-26/77	4	7	441	550	388	467	446	441
PBS-3/69	4	7	382	456	395	472	452	446
PBR-3/70	4	7	268	312	279	388	347	351
PBR-30/53	4	7	378	344	412	484	467	460
PBS-30/63	4	7	348	318	380	462	438	434
PBS-30/81	4	7	306	361	323	421	388	388

8.4.2 Ti in Biotite Thermometer

The concentration of Ti in biotite has long been considered to be a function primarily of changing temperature conditions in metamorphic rocks and has been suggested as a potential geothermometer (Dymek,1983; Patiño Douce,1993). The Ti-saturation surface generated for biotites from peraluminous metapelites at low-to-medium pressures contains useful information with petrologic and crystallographic implications. A reformulation of the surface PT expression results in an empirical Ti-in-biotite geothermometer for biotites in peraluminous metamorphic rocks. The geothermometer is valid over a range of 480 to 800 °C and has an estimated precision of ±24 °C (Henry et al., 2005). Further, the systematics of Ti in biotite provides a means to assess the approach to chemical equilibrium of biotite in metamorphic rocks. In magnesian biotite, Ti primarily substitutes via a Ti-tschermaks substitution controlled by octahedral-tetrahedral layer misfit (Henry et al., 2005).

The metamorphic mineral assemblage at Bhuyari is broadly similar to metapelite mineralogy. However, the Ti in biotite thermometer is suitable for the metamorphic mineral assemblage in Bhuyari since it satisfies most of the criteria as laid down by Henry et al (2005), i.e.

1. presence of ilmentite and rutile in the assemblage,
2. presence of quartz in the rock,
3. biotite X_{Mg} should be between 0.275 to 1.0 and Ti should be between 0.04 and 0.6 apfu.

The mineral assemblage in Bhuyari does not qualify in the strictest sense to Henry et al (2005) due to the absence of graphite and aluminosilicate in the rocks. Graphite is not reported or observed from any of the rocks near

Bhuyari prospect; however, the rocks at Bhuyari contain garnet, staurolite and gahnite as aluminium-bearing minerals. The sample PBR-30 which has been selected for the thermometry at places contain accessory metamorphic almandine-spessartine garnet in an assemblage containing quartz, plagioclase, biotite, muscovite and accessory and ilmentite/rutile. Moreover, the biotite in this sample meets the specifications and range of Ti from 0.22 to 0.352 and X_{Mg} ranging from 0.263 to 0.283. A total of 10 biotite analyses were used for Ti in biotite thermometry (Table 8.5). The temperature calculated as per Ti content and X_{Mg} in biotite range from a low value of 571°C to a high value of 652°C calculated for a constant pressure assumed at 6.5 kb (Table 8.4)

The Ti-in-biotite (TIB) geothermometer of Henry et al (2005) is based on the Ti-saturation surface of near-isobaric natural biotite data for peraluminous metapelites equilibrated at 4-6 kbar. This surface is evaluated in terms of temperature (T) vs. X_{Mg} vs. Ti, and is solved specifically for T. Temperatures can be determined either by plotting biotite Ti and Mg/(Mg+Fe) values on the simple binary diagram (Fig. 8.6) or by calculating T from the expression:

$$T = ([\ln(Ti) - a - c(X_{Mg})^3]/b)^{0.333}$$

Where T is temperature in degrees C, Ti is the apfu normalized to 22 oxygens, X_{Mg} is Mg/(Mg+Fe), and the a, b and c parameters are given below.

Coefficient	Value
a	-2.3594
b	4.6482e-9
c	-1.7283

This expression is valid in the range X_{Mg} = 0.275 -1.0, Ti = 0.04 - 0.6 apfu and T = 480-800°C.

When the Ti (apfu) values of biotite from a garnet-biotite bearing assemblage were plotted in the diagram of Henry et al (2005) it showed a range of temperatures from 571 to 661°C with an average temperature of 629°C based on the isotherms (Fig. 8.6 & Table. 8.4). The EPMA data of the biotites used in the plot are given in (Table 8.5).These results are fairly consistent with the observed equilibrium mineral assemblages in the area.

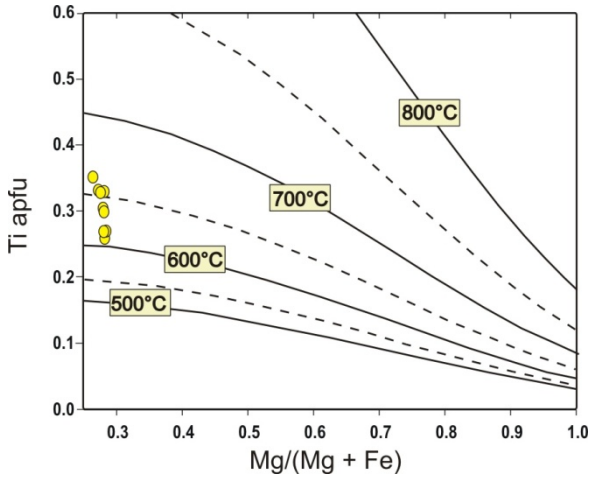

Fig.8.6 The Ti apfu versus Mg/(Mg + Fe) plot for the biotite sample PBR-30, showing the temperature isotherms of Henry et al (2005)

Table 8.4 Parameters used to determine the temperature using the Ti-in biotite thermometer as per Henry et al (2005).

Sample No.	a	b	c	Ti	X(Mg)	T°(C)
PBR-30/54	-2.359	0.000	-1.728	0.328	0.275	650.598
PBR-30/55	-2.359	0.000	-1.728	0.352	0.263	661.836
PBR-30/56	-2.359	0.000	-1.728	0.259	0.282	608.424
PBR-30/57	-2.359	0.000	-1.728	0.269	0.281	615.503
PBR-30/58	-2.359	0.000	-1.728	0.220	0.238	571.415
PBR-30/64	-2.359	0.000	-1.728	0.332	0.274	652.497
PBR-30/65	-2.359	0.000	-1.728	0.329	0.281	651.714
PBR-30/82	-2.359	0.000	-1.728	0.303	0.279	637.375
PBR-30/85	-2.359	0.000	-1.728	0.269	0.283	615.986
PBR-30/86	-2.359	0.000	-1.728	0.287	0.283	627.893
a, b and c are surface fit coefficients						

Table 8.5 EPMA analyses of biotite from biotite-garnet bearing sample (PBR-30) used for estimating thermometry based on the Ti in biotite

	1	2	3	4	5	6	7	8	9	10
	PBR-30/54	PBR-30/55	PBR-30/56	PBR-30/57	PBR-30/58	PBR-30/64	PBR-30/65	PBR-30/82	PBR-30/85	PBR-30/86
SiO2	35.11	34.97	34.92	35.41	35.8	35.18	35.45	35.12	36.28	35.78
TiO2	2.77	2.99	2.19	2.31	1.89	2.83	2.81	2.59	2.35	2.48
Al2O3	16.09	16.75	16.31	16.35	17.62	16.47	16.32	16.82	16.86	16.81
FeO	26.16	25.99	27.01	27.63	27.45	26.65	26.21	26.41	27.05	26.88
MnO	0.62	0.63	0.74	0.68	0.64	0.64	0.55	0.74	0.69	0.7
MgO	5.57	5.21	5.94	6.05	4.82	5.64	5.74	5.74	5.99	5.8
CaO	0.01	0.02	0	0.03	0.55	0.02	0.01	0.03	0.05	0.02
Na2O	0.09	0.19	0.1	0.08	1.91	0.01	0.09	0.11	0.09	0.18
K2O	9.42	9.46	9.07	9.52	5.54	9.58	9.56	9.33	9.57	9.36
ZnO	0.22	0.15	0	0.13	0.12	0.08	0.13	0.15	0.17	0.03
Si	5.52	5.48	5.49	5.48	5.53	5.48	5.52	5.47	5.53	5.51
Al iv	2.48	2.52	2.51	2.52	2.47	2.52	2.48	2.53	2.47	2.49
Al vi	0.51	0.57	0.51	0.46	0.74	0.51	0.52	0.55	0.55	0.56
Ti	0.328	0.352	0.259	0.269	0.220	0.332	0.329	0.303	0.269	0.287
Cr	0.00	0.00	0.00	0.00	0.00	0.00	0.00	0.00	0.00	0.00
Fe	3.44	3.41	3.55	3.58	3.55	3.47	3.41	3.44	3.45	3.46
Mn	0.08	0.08	0.10	0.09	0.08	0.08	0.07	0.10	0.09	0.09
Mg	1.31	1.22	1.39	1.40	1.11	1.31	1.33	1.33	1.36	1.33
Zn	0.03	0.02	0.00	0.01	0.01	0.01	0.01	0.02	0.02	0.00
Ca	0.00	0.00	0.00	0.00	0.09	0.00	0.00	0.01	0.01	0.00
Na	0.03	0.06	0.03	0.02	0.57	0.00	0.03	0.03	0.03	0.05
K	1.89	1.89	1.82	1.88	1.09	1.90	1.90	1.85	1.86	1.84
Fe/Fe+Mg	0.72	0.74	0.72	0.72	0.76	0.73	0.72	0.72	0.72	0.72
Mg/(Mg+Fe)	0.275	0.263	0.282	0.281	0.238	0.274	0.281	0.279	0.283	0.283

8.4.3 Phengite geochemistry and barometry

Muscovite/sericite occur in most rock types in Bhuyari, including least altered rhyolite and in the various other alteration types. Muscovite is especially an important constituent of the quartz-biotite-muscovite-K-feldspar

± garnet schist and also in the quartz-biotite-plagioclase-muscovite schist which occur towards the footwall of the ore zones. These alteration types occur in close proximity to the mineralized zones at Bhuyari.

The mineral assemblage with phengite, K-feldspar, biotite, garnet, staurolite and quartz is ideal for correct and optimal results for the determination of pressure by phengite barometry. The stability field of the critical assemblage phengite-K-feldspar-phlogopite- quartz ranges, in the presence of excess H_2O, from at least 350° C to about 700° C but has an upper pressure limit in the range 16-22 kbar, when K-feldspar and phlogopite react to form phengite and a K, Mg-rich siliceous fluid (Massone and Schreyer, 1987).

Detailed petrographic study of the mineral assemblages is necessary prerequisite to thermobarometric applications. Mineral textures should be evaluated in order to distinguish retrograde assemblages with preserved equilibrium assemblages (Essene (1989). In the quartz-K-feldspar-biotite-muscovite-garnet schist, muscovite occur as < 0.5mm flakes and define the foliation along with biotite in a ground mass dominated by quartz and K-feldspar and minor sulphides (Fig.3.2b). In this assemblage, muscovite texturally appears fresh and unaltered. Muscovite/phengite occurs as colourless flakes and along with brown biotite and garnet in the garnet-mica bearing rocks (Fig.8.5c). In the potassic altered rocks, muscovite is an important constituent which occur with secondary K-feldspar porphyroblasts (Fig.8.5 d).

For interpretation of barometry, it is important that the muscovite is prograde rather than a retrograde product. Texturally, the prograde muscovite can be identified based on their larger flakes when compared to the retrograde fine-grained muscovite which can be called sericite. The prograde muscovite coexists with phlogopite-garnet and plagioclase and form a higher proportion

in the rock, whereas the retrograde sericite occur as alteration products of garnet, staurolite and muscovite. The muscovite and biotite defines the penetrative foliation present in the rocks of the Bhuyari area, which is part of the ENE-WSW trending regional foliation in the eastern part of Betul Belt.

Textural evidence indicates that most metamorphic mineral assemblages at Bhuyari formed syn and / or post peak metamorphism. The presence of muscovite flakes along with biotite aligned along the foliation shows that the muscovite is pre- or syn-deformational and has participated in the deformation process (Fig.3.2). Retrograde muscovite/sericite in contrast is generally unoriented and occurs as irregular disseminations, frequently forming pseudomorphs after staurolite or garnet. At places, the staurolite crystals have been entirely replaced by sericite with only the relict outlines of staurolite preserved (Fig.3.5f).

Muscovite is generally consumed in prograde enviroinments with the development of staurolite and garnet. However, at many places, muscovite is documented to be preserved and continue in the garnet and staurolite bearing high grade assemblages as in the metamorphosed alteration zones of Cu-Zn-Au massive sulphide deposits of Snow Lake, Manitoba in the Paleoproterozoic Trans Hudson Orogen (Menard and Gordon, 1997). In their study (Menard and Gorton, 1997) observed that although most chlorite was consumed during garnet formation in prograde metamorphism, muscovite continued to be preserved even in higher grade assemblages containing staurolite + garnet + biotite + plagioclase and kyanite + biotite + chlorite. The preservation of prograde muscovite with phengitic composition at Bhuyari, inferred by textural and mineralogical studies provides us the opportunity to apply the phengite barometry application to understand the pressure conditions achieved during peak regional metamorphism in the area.

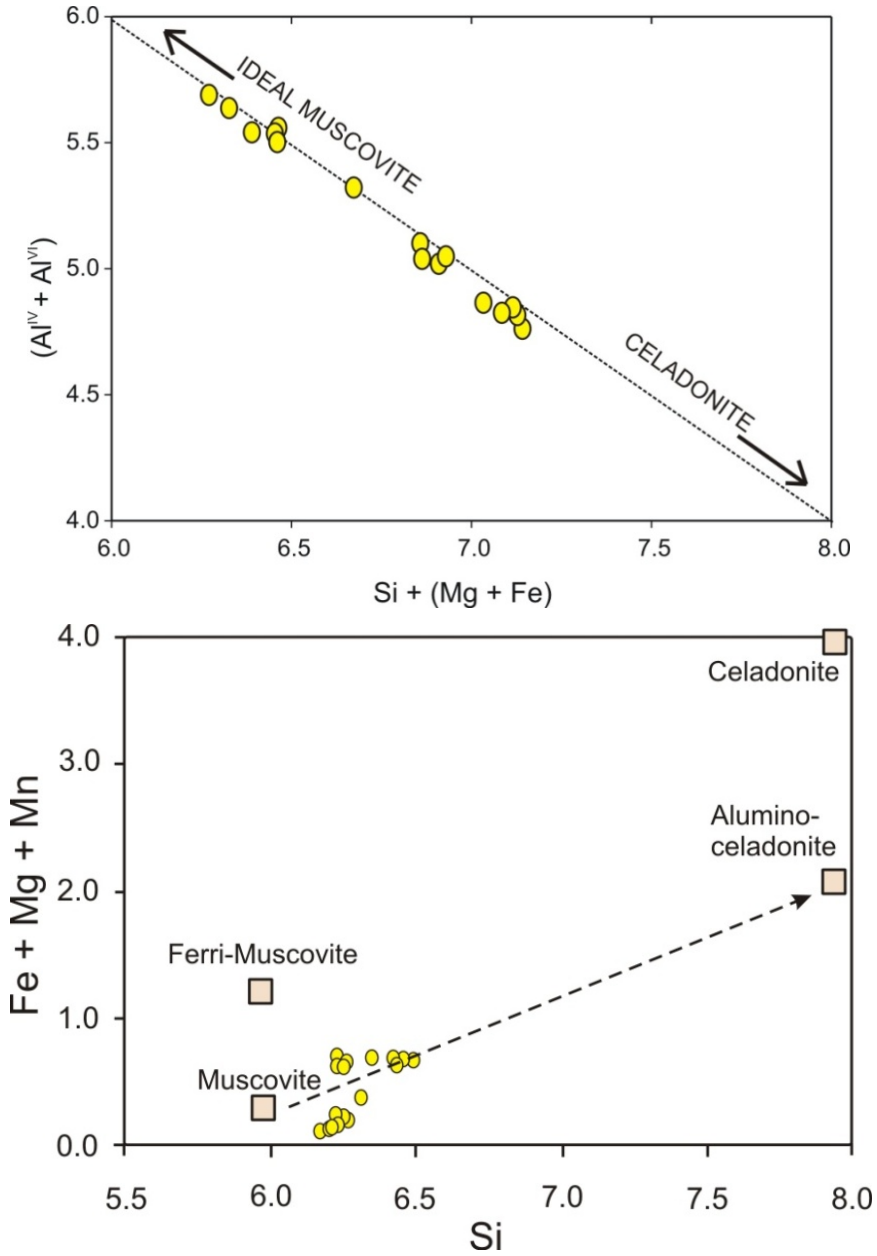

Fig 8.7 a) Si + (Mg +Fe) vs. Al^{VI} +Al^{IV} plot for the muscovites from altered rocks from Bhuyari show clear evidence for tschermakitic or phengitic substitution. b) Si vs Σ (Fe_T + Mg + Mn) for white-micas. The ideal compositions of muscovite, ferrimuscovite, celadonite and aluminoceladonite taken from Guidotti and Sassi (1998).

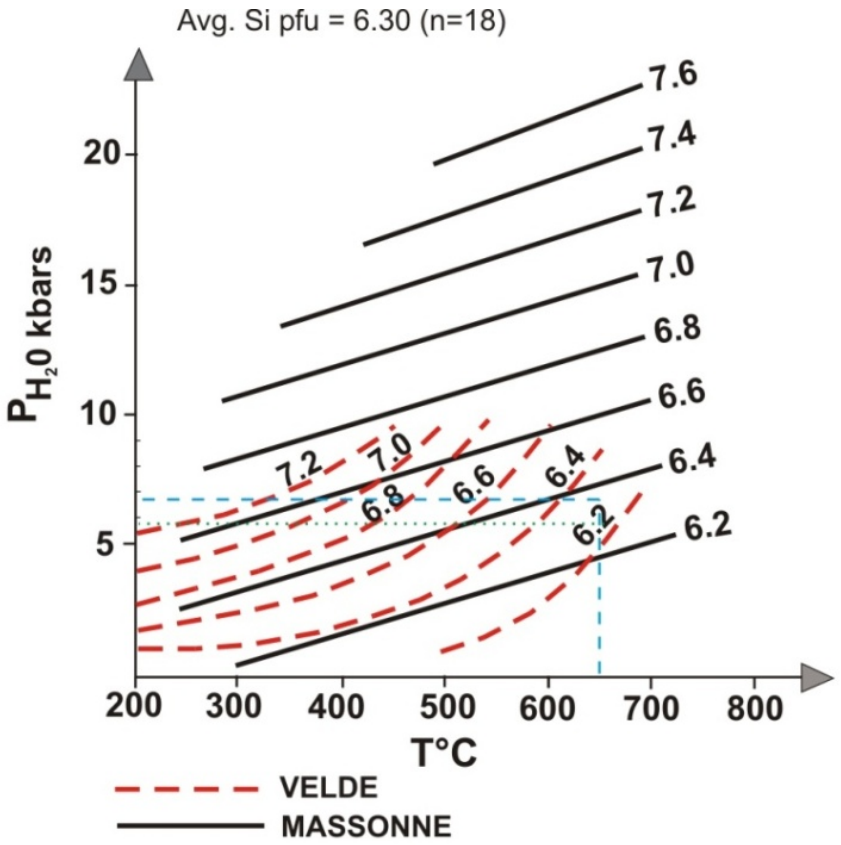

Fig.8.8 Average Si apfu of phengite from Bhuyari plotted in the Si-isopleths of phengite in the assemblage phengite + biotite + K-feldspar + quartz + H_2O according to Velde (1967) and Massonne (1981)

The muscovite in Bhuyari is phengitic and contains a consistently high Si content in the range of 6.17 to 6.49 (calculated per 22 oxygen atoms) with an average Si content of 6.30 apfu (mineral chemistry analyses are given in Chapter-6:Tables 6.11a & 6.11b). Phengite (Ernst, 1963) refers to Fe- and Mg-rich white micas (Velde, 1965) that obey the substitution Al^{IV} +Al^{VI}= (Mg, Fe^{+2})^{VI} + Si, but Guidotti and Sassi (1976) suggest that the term "celadonitic muscovite" be used instead of phengite.

There is a strong, almost linear increase of the Si content per formula unit (p.f.u.) of phengite, ideally $KAl_{2-x}Mg_x[Al_{1-x}Si_{3+x}O_{10}]$ $(OH)_2$ with pressure, as well as a moderate decrease of Si (or x) with temperature. The most siliceous phengite with Si near 3.8 p.f.u. becomes stable near 20 kbar depending on temperature (Massone and Schreyer, 1987).

The stability field of the critical assemblage phengite- K-feldspar-phlogopite- quartz ranges, in the presence of excess H_2O, from at least 350° C to about 700° C but has an upper pressure limit in the range 16-22 kbar (Massone and Schreyer, 1987).

The observed (Mg + Fe) rich muscovite/sericite compositions from Bhuyari are most likely related to their protolith composition, which were affected by Mg- metasomatism. However, the certain studies indicate that the metamorphic muscovites can have their Mg-Fe contents reset during metamorphism and may also be the product of regional metamorphism. For example, experimental data from Velde (1965) indicate that the increase in the phengitic and 'celadonitic' components of white-mica is mainly controlled by pressure conditions, and not by bulk composition. This increase results from the substitution between silica and aluminium according to a tschermakitic or phengitic substitution (i).

Muscovite, represented by the formula $K_2Al_4(Al_2Si_6O_{20})$ $(OH)4$, is known to deviate markedly from the ideal composition by substitution (Guidotti and Sassi, 1998) of:

(i) $(Mg, Fe^{2+})^{VI+}Si^{IV} \leftrightarrow Al^{VI} + Al^{IV}$ (tschermakitic or phengitic substitution)

(ii) Fe^{3+} Al^{VI} (ferrimuscovite substitution)

(iii) Na + K (paragonitic substitution)

(iv) (Na, K) + Si ↔ Ca+ Al (margaritic substitution)

Two balanced reactions have been proposed for the phengite formation (Essene, 1989):

(a) Phengite = K-feldspar + Chlorite + Quartz + Water

(b) Phengite = K-feldspar + Phlogopite + Quartz + Water.

The most important control for the application of the barometer proposed is the presence of the buffering phase K-feldspar under equilibrium conditions (Essene, 1989). In the absence of K-feldspar the phengite barometry provides only a minimum estimate of pressure. Petrographic studies of muscovite-bearing rocks at Bhuyari shows that the muscovite/phengite is commonly associated with K-feldspar and is a preserved equilibrium assemblage formed during amphibolite facies metamorphism of potassic alteration zones. The muscovite/phengite flakes texturally appear fresh and unaltered by retrogression, and are in equilibrium with quartz, potash feldspar, biotite and pyrite. Therefore, this assemblage is considered suitable for applying phengite barometry. Phengite is partly able to withstand the effects of later retrogression effects and therefore is able to provide useful information regarding pressure (Evans and Patrick, 1989).

The average Si content of phengite (6.30) was plotted in the diagram using Si-isopleth diagrams of Velde (1965) and Massone (1981) for an assumed peak temperatures of 650°C (Fig. 8.8). This shows that the estimated pressure is 5.8 kb according to the calibration of Massone (1981) and 6.8 k bars according to Velde (1965).

8.4.4 Garnet-Plagioclase-Muscovite-Biotite Barometry

The metamorphic mineral assemblages at Bhuyari do not contain aluminosilicate. Therefore, geobarometers using aluminosilicates such as the

garnet-aluminosilicate-plagioclase- quartz (GASP) barometer cannot be applied. The biotite-garnet-muscovite-plagioclase barometer of Holland and Powell (1998) was tried to assess the PT conditions. For this purpose, the garnet-staurolite-biotite-plagioclase assemblage and the biotite-muscovite-plagioclase-garnet schist were used and were represented by sample PBS-26 and PBS-1 respectively (Table 8.7).

A total of five sets of analyses contained the data from closely associated biotite-garnet-muscovite-plagioclase were used for this purpose (Table 8.6). These five (BGMP) analyses includes 3 groups of analyses from the staurolite + garnet + biotite +muscovite + plagioclase + K-feldspar assemblage (sample PBS-26), and two sets from the quartz + muscovite + biotite + garnet + plagioclase assemblage (sample PBS-1).

The six group of analyses were plotted in the program based on calibrations of Holland and Powell (1998), which gave a range of pressures from a low of 3.49 to a high of 5.14 kb and a temperature range of 456 to 529°C.

8.4.5 Garnet-Muscovite-Plagioclase-Quartz Geobarometer

The garnet-muscovite (GM) thermometer and the garnet-muscovite-plagioclase-quartz (GMPQ) barometer can be used in assemblages that lack aluminosilicate or biotite (Wu and Zhao, 2006). The GM geothermometer and the GMPQ geobarometer have been simultaneously calibrated under conditions of temperature conditions in the range of 450–760°C and for pressure conditions in the range of 0.8–11.1 kbar by Wu and Zhao (2006). Since muscovite is ubiquitous in greenschist-to amphibolite facies metapelites, the GM geothermometer and GMPQ geobarometer are very important in

determining the metamorphic P–T conditions of metapelitic rocks Wu and Zhao (2006). The Fe and Mg exchange between coexisting garnet and muscovite is the basis of the GM thermometer.

The PT conditions of Bhuyari were estimated using the spread sheet calculator provided by Wu and Zhao (2006) along with their online paper. According to Wu and Zhao (2006) application of the GM thermometer and the GMPQ barometer to metapelitic rocks with muscovite of Mg >0.13 or Fe <0.04 atoms on the basis of 11 oxygens is not recommended. This criterion is met only by the sample PBS-26, which is the staurolite-biotite-garnet-muscovite bearing rock. Three selected sets from the data used previously for GPMB barometry were used for this purpose (Table 8.7). Using this spread sheet the garnet-muscovite thermometer gave a temperature range from 624-637°C and the the garnet-muscovite-plagioclase-quartz (GMPQ) geobarometer results range from 4.6 kb to 5.7 kb.

Table.8.6 P-T estimate based on Biotite-Garnet-Muscovite-Plagioclase based on EPMA analyses of coexisting phases.

	Sample		Si	Ti	Al	Fe	Mn	Mg	Ca	Na	K	Pressure	Temperature
	PBS-1/135	Biotite	5.68	0.22	2.85	1.6	0.12	3.29	0.01	0.03	1.84		
1	PBS-1/137	Garnet	2.97	0	1.98	0.66	1.62	0.18	0.51	0	0	3.99 kbars	495°C
	PBS-1/129	Muscovite	6.44	0.14	4.82	0.29	0.01	0.36	0	0.07	1.87		
	PBS-1/131	Plagioclase	2.35	0	1.15	0	0	0	0.3	0.55	0.01		
	PBS-1/134	Biotite	5.74	0.19	2.91	1.69	0.12	3	0.011	0.04	1.85		
2	PBS-1/136	Garnet	3.01	0	1.95	0.73	1.69	0.17	0.43	0	0	3.35 kbars	481°C
	PBS-1/128	Muscovite	6.49	0.14	4.76	0.28	0.02	0.37	0	0.06	1.79		
	PBS-1/130	Plagioclase	2.68	0	1.32	0	0	0	0.34	0.63	0.01		
	PBS-26/78	Biotite	5.62	0.08	2.98	1.12	0.04	4.04	0	0.08	1.72		
3	PBS-26/81	Garnet	2.99	0	1.96	1.18	1.21	0.39	0.21	0	0	3.49 kbars	456°C
	PBS-26/84	Muscovite	6.24	0.02	5.54	0.07	0	0.15	0	0.24	1.64		
	PBS-26/93	Plagioclase	2.69	0.00	1.30	0.01	0.00	0.00	0.32	0.67	0.00		
	PBS-26/95	Biotite	5.63	0.08	3.00	1.14	0.04	3.99	0	0.06	1.77		
	PBS-26/75	Garnet	2.96	0	1.94	1.16	1.03	0.55	0.22	0	0	5.14 kbars	529°C
4	PBS-26/105	Muscovite	6.17	0.03	5.69	0.04	0	0.06	0	0.37	1.56		
	PBS-26/98	Plagioclase	2.69	0.00	1.29	0.00	0.00	0.00	0.33	0.69	0.00		
5	PBS-26/112	Biotite	5.59	0.09	2.99	1.04	0.04	4.21	0	0.07	1.67		
	PBS-26/74	Garnet	2.98	0	1.95	1.20	1.01	0.56	0.21	0	0	4.23 kbars	502°C
	PBS-26/107	Muscovite	6.23	0.04	5.54	0.05	0.01	0.10	0.01	0.29	1.69		
	PBS-26/116	Plagioclase	2.69	0.00	1.29	0.00	0.00	0.00	0.34	0.65	0.00		

Table 8.7 Three groups of muscovite-plagioclase-garnet analyses from sample PBS-26 for determining temperature based on GM geothermometer and GMPQ geobarometer based on calibrations by Wu and Zhao (2006)

Sample No.	SiO2 Wt.%	TiO2 Wt.%	Al2O3 Wt.%	FeO Wt.%	MnO Wt.%	MgO Wt.%	CaO Wt.%	Na2O Wt.%	K2O Wt.%	Computed temperature	Computed pressure
PBS-26/84											
Muscovite	46.58	0.22	35.11	0.59	0.04	0.77	0.01	0.94	9.61		
Plagioclase	59.22	0.00	24.35	0.21	0.06	0.00	6.53	7.57	0.05	624°C	4.57 k bars
Garnet	37.15	0.00	20.68	18.41	17.73	3.26	2.46	0.00	0.00		
PBS-26/95											
Muscovite	46.47	0.32	36.36	0.41	0.03	0.28	0.01	1.42	9.23		
Plagioclase	59.73	0.01	24.38	0.13	0.00	0.00	6.83	7.88	0.04	630°C	5.70 kbars
Garnet	37.24	0.06	20.74	19.56	15.32	4.64	2.63	0.00	0.00		
PBS-26/107											
Muscovite	46.41	0.41	35.01	0.47	0.04	0.52	0.04	1.10	9.84		
Plagioclase	60.04	0.03	24.47	0.04	0.01	0.00	7.00	7.48	0.03	637°C	5.00 kbars
Garnet	37.30	0.03	20.69	17.97	15.00	4.68	2.44	0.00	0.00		

8.5 Conclusion

The study of the relationship between metamorphic mineral assemblages and geochemistry of alteration zones indicate that the biotite-phlogopite-bearing rocks represent metamorphosed chlorite-rich protoliths and the muscovite - K- feldspar-rich rocks represent metamorphosed sericite - K-feldspar-rich protoliths. The tremolite-carbonate rocks are inferred to represent metamorphosed equivalents of dolomite-chlorite bearing protoliths. This study also shows that these rocks do not have a pelitic origin and they actually represent hydrothermally altered and metamorphosed felsic volcanic rock.

Based on a combination of mineral assemblages, plotting in PT grid and geothermobarometric estimates the assemblages at Bhuyari reflect peak temperatures in the range of 580 to 650°C and pressures of 5.8 to 7 kb. The observed pressures range corresponds to roughly 20 to 25 km crustal depth. Such a depth range is explained as a result of crustal thickening during the Betul Orogeny.

******

Chapter 9

SUMMARY AND CONCLUSIONS

The Betul Belt in central India is a unique lithotectonic segment of the Indian Precambrian Shield, in the sense that it preserves a record of Proterozoic submarine feslic volcanism and associated base-metal mineralization. The felsic volcanic rocks of Betul Belt hosts several small base-metal deposits which have been described as belonging to Volcanogenic Massive Sulphide Deposits (VMS) in recent years.

However, these deposits have not been characterized in detail and several aspects including the volcanic facies, alteration zones, geochemistry, petrogenesis and tectonic setting are least understood. This work aims at addressing these issues by a combination of detailed field mapping of volcanic and alteration facies, geochemistry and mineral chemistry of unaltered rhyolites and altered rhyolites, carbon and oxygen isotope studies and characterization of sulphide mineralization by ore petrography and mineral chemistry. Geothermobarometric studies were also carried out to constrain metamorphic conditions.

Detailed field mapping shows that the unaltered rhyolite preserve primary volcanic features like porphyritic texture and flow banding. These unaltered rhyolites grade into altered rhyolites towards the mineralized zones. Volcanic facies newly identified in this study, viz., peperite and associated deep-water sediments establishes contemporaneous volcanism and sedimentation in deep water conditions. Such moderate to deep-water conditions are considered to be favourable for massive sulphide formation. The tectonic setting that favours such deep-water conditions, ambient

submarine bimodal volcanism and clastic sedimentation is a continental back arc rift. Alteration facies mapping around Bhuyari prospect shows three distinct metamorphosed alteration zones containing a high-Mg core represented by biotite-phlogopite-garnet bearing schists which are enveloped by potassic-rich envelop characterized by muscovite-K feldspar bearing schists. Tremolite-carbonate rocks occur as pockets in three discrete outcrops close to the massive sulphide lenses.

Petrographic studies indicate that different metamorphic mineral assemblages in altered rhyolite correspond to variations in bulk chemistry of pre-metamorphic hydrothermal alteration zones. The inner core zone of the alteration system contains assemblages containing biotite-phlogopite, garnet, staurolite, gahnite and plagioclase. The outer zone of the alteration system contains K-feldspar, muscovite and garnet. Most minerals show evidence for formation in a single prograde metamorphic event. Petrography of tremolite-carbonate rocks shows wide variation in mineralogy with several assemblages including variable tremolite, dolomite, talc, chlorite, garnet, zoisite and sphene.

Texture of metamorphosed alteration zones shows that most minerals represent the late stage of deformation. This is evidenced by the relatively random orientation of the garnet, staurolite, gahnite and plagioclase porphyroblasts. Earlier episode of mineral formation is evidenced by the foliated nature of phlogopite, muscovite and biotite, which indicates that these minerals were crystallized during the peak deformation event.

Major, trace and REE analyses of the unaltered rhyolites from Bhuyari and surrounding areas were carried out to constrain their geochemical features. The rhyolites contain high silica contents (SiO_2 - 72 to 80%) suggestive of

high-silica rhyolites. The rhyolites are all aluminous (metaluminous to peraluminous) and most samples have A/CNK (molar Al_2O_3/Na2O + K_2O + CaO ratio) close to unity. The rhyolites contain high HFSE and REE contents, the Zr (380 to 912ppm) and Y (89-163ppm) and Nb (21-39ppm) contents are particularly high. The Zr and Nb contents are comparable to rhyolites from several well known VMS areas like those from the Proterozoic Bathurst camp in Canada. The total REE contents of the rhyolites are also high and reaches about 100 times chondritic values. The high concentration of HFSE and REE is a characteristic geochemical feature and recognized in VMS terrains from Archean to recent. The high SiO_2, HFSE and REE broadly fit the definition of high-silica rhyolite (Barrie et al, 1993). The zircon saturation temperatures calculated for the rhyolite are in the range of 872 to 991°C and are indicative of high temperature evolution of the rhyolites of the area.

Rhyolite classification plots based on VMS prospectivity show that they belong to FIIIb type which is considered highly prospective for VMS deposits (Lesher et al, 1986; Hart et al, 2004). Trace element characteristics show that the rhyolites have within-plate, A-type affinities and more specifically belong to the A-2 type, which are the crustally-derived anorogenic sub-type. Geochemical study corroborates field and petrographic evidence for a rhyolitic protolith for the biotite-phlogopite-garnet bearing and muscovite – K-feldspar bearing schists. These rocks were likely the result of syngenetic hydrothermal chlorite-sericite and sericite- K-feldspar alteration of rhyolites. Tremolite-carbonate rocks do not point to a rhyolitic protolith based on major, trace and REE geochemistry.

Geochemistry of alteration zones have shown that the phlogopite-chlorite-bearing rocks occurring as the core zone of alteration contains high MgO and low Na_2O and CaO. This is similar to high-Mg chloritic core zones

of many zoned alteration systems in proximal VMS environments. Proximal alteration represents hydrothermal up-flow and discharge zones (e.g. feeder zones to the deposits) and form high-temperature water-rock interaction. These zones represent high-temperature alteration zones. The muscovite - K-feldspar rocks are metamorphic equivalents of sericite – K-feldspar rocks. They possibly represent low-temperature, acidic alteration. Carbonate-rich zones may represent partly metaexhalites and partly altered rhyolites.

Carbon and Oxygen isotopes of carbonate samples were analyzed to understand the nature and origin of hydrothermal fluid that deposited the carbonate. The $\delta^{13}C$ of carbonate shows signatures of seawater-derived hydrothermal fluid. The $\delta\ ^{18}O$ values are similar to most VMS deposits and their lower values possibly suggest lower temperature hydrothermal fluids. Carbonate was precipitated by low-temperature venting of hydrothermal fluids which may have been deposited after massive sulphide deposition. The carbonates may have altered the porous volcaniclatic rocks near the seafloor and some carbonate may have precipitated on the seafloor as exhalites as a mixture of carbonate and cherty exhalites. The laminated and bedded nature of the carbonate and differing REE signatures compared to rhyolite and also their low HFSE contents indicate that at least part of these rocks were deposited as carbonate-rich exhalites on the seafloor near to the hydrothermal vent.

Detailed mineral chemistry of unaltered and altered rhyolite shows that there exist variations in composition of the minerals with respect to distance from the centre of the alteration system. Biotite shows increase in X_{Mg} content towards the mineralized zones. The biotite from least altered rhyolite have Mg numbers ranging from 0.24 to 0.28, whereas, those form the alteration zones close to ore zones have Mg numbers ranging from 0.64 to 0.80 and are phlogopitic. Garnet shows an increase in spessartine contents from least

altered rhyolite ($Sps_{32.5}$ to $Sps_{38.2}$), to those from proximal alteration zones and mineralized zones ($Sps_{32.9}$ to $Sps_{57.8}$). Plagioclases do not show systematic compositional variations from altered and unaltered rhyolites. However, anorthite contents are significantly higher in altered rhyolites (An_{24-35}) when compared to least altered rhyolite (An_{17-26}). Muscovite shows higher MgO contents at or near the mineralized zones (1.7 to 2 wt.%) when compared to those from proximal alteration zones (0.3 to 0.5 wt.%). The phengite component of muscovite is highest within the mineralized zone (Si + Fe +Mg = 6.9 to 7.1) when compared to those in the alteration zones (Si + Fe + Mg = 6.3 to 6.4). Presence of zincian stauroltie and gahnite with extremely high ZnO contents (up to 9 wt. % in staurolite and up to 40 wt. % in gahnite) are similar to those developed in metamorphosed massive sulphide deposits. Gahnite, zincian staurolite, spessartine garnet and high Mg-biotite and Mg-muscovite (phengite) are associated with the intensely altered rhyolite at or proximal to mineralized zone and therefore can be used as indicator minerals in identifying similar fossil hydrothermal systems associated with metamorphosed VMS deposits in felsic volcanic terrains.

The mineralised zones are present close to or near the top of the alteration zones. The close spatial association of massive sulphide zones with the tremolite-carbonate rocks indicates that the massive sulphides were deposited by hydrothermal fluids on the seafloor. Sulphide mineralogy consists of sphalerite, galena, pyrite and chalcopyrite. They show recrystallization and remobilization effects. Ore petrography and EPMA-based studies on sulphide texture and mineralogy show several characteristic features typical of VMS deposits. Sulphide paragenesis indicates that initial low temperature sphalerite and pyrite mineralization was followed by higher temperature chalcopyrite-pyrite mineralization as indicated by ore textures.

Mineral chemistry of sulphides show that the Fe content of sphalerite increases near the massive sulphide zone when compared to distal parts. Similarly the Pb-content of galena increases with proximity to massive sulphide zones.

Mineral assemblages in the metamorphosed alteration zones give indications for amphibolites facies metamorphism. The relationship between mineral assemblages and geochemistry of alteration zones indicate that the Mg-rich biotite-phlogopite schists were formed by metamorphism of chlorite-rich protoliths and the muscovite - K- feldspar-rich rocks were formed by metamorphism of sericite - K-feldspar-rich protoliths. The tremolite-carbonate rocks are inferred to represent metamorphosed equivalents of dolomite-chlorite bearing protoliths. These rock types do not appear to have a sedimentary origin. The alteration system at Bhuyari therefore, represents a metamorphosed zoned alteration system with an Mg-rich core and a K-rich outer zone which is similar to those associated with some metamorphosed VMS deposits worldwide.

The peak metamorphic conditions were attained with the development of staurolite + garnet + biotite bearing assemblages in the magnesium rich alteration zones and with phengite-microcline-plagioclase-garnet assemblage in the K-rich alteration zone and with development of tremolite-dolomite-plagioclase in the carbonate alteration zones. The mafic volcanics at Bhuyari also have typical amphibolite facies mineral assemblage of plagioclase + hornblende + quartz.

Textural evidence shows that the assemblages were formed in a single prolonged metamorphic event. Final retrogressive metamorphism evidenced in the form of second generation gahnite and chlorite. The presence of prograde staurolite in the rocks constrain the conditions of metamorphism since the

garnet + chlorite + muscovite staurolite + biotite isograd occurs at PT of about 7 kb and 580°C. Based on the KFMASH petrogenetic grid and the mineral assemblage staurolite + biotite + garnet the likely peak temperature and pressure attained was in the range of 590 to 610°C and 6 to 7 kb.

Geothermobarometry results obtained using EPMA data of coexisting minerals areconsistent with mineral assemblages. The PT values obtained for garnet-biotite thermometry range between 376 to 638°C at an assumed minimum pressure of 4kb. The temperature calculated as per Ti-content and X_{Mg} in biotite range from 571 to 652°C calculated for a constant pressure assumed at 6.5 kb. Based on Si content of phengite, the pressure obtained for peak metamorphism at 650°C is in the range of 5.8 to 6.8 kb. Based on the biotite-garnet-muscovite-plagioclase barometer of Holland and Powell (1995) the range of PT obtained is 3.49 to 5.14 kb and 480 to 529°C. The garnet-muscovite thermometer gave a temperature range of 624-637°C and the garnet-muscovite-plagioclase-quartz geobarometer gave a pressure of 4.6 to 5 kb. The estimated pressure of 5.8 to 7 kb roughly corresponds to 20 to 25 km crustal depth. Such a depth range is explained as a result of crustal thickening during the Betul Orogeny.

The geochemical features of unaltered rhyolite supported by primary volcanic textures identified as part of this study are consistent with their emplacement in a continental back-arc basin which may have developed in a zone of convergence between the Bundelkhand Craton in the north and the Bastar Craton in the south during the early Proterozoic, and possibly followed the sequence of events as given below:

1. Initial back-arc rifting resulted in basaltic-magma upwelling and pooling in the sub-crustal levels, prompting partial melting of the crust and generation of felsic melts.
2. Continued rifting with greater mantle inputs generated high-temperature rhyolites with elevated HSFE and REE contents. These rhyolites formed submarine dome and lava complexes in relatively deep-water conditions. Associated peperite indicates contemporaneous ambient deep-water sedimentation. The sub-crustal/shallow crustal magma reservoir supplied heat to form long-lived hydrothermal convection system which leached metals from the volcanic pile and gave rise to massive sulphide deposits on the seafloor.
3. Further widening of the rift and associated mantle upwelling resulted in voluminous mafic volcanism represented by massive and pillowed metabasalts present to the north of Bhuyari.
4. Culmination of the volcanic cycle is followed by deposition of clastic sedimentary rocks evidenced by presence of shales and phyllites to the north of the bimodal volcanics in the central part of Betul Belt.
5. Closure of the rift-basin by N-S directed compression resulted in EW trending regional foliation and amphibolite facies metamorphism which produced various metamorphic mineral assemblages in the alteration zones.

The integrated geochemical, mineralogical, isotope and geothermobarometric studies on the base-metal deposit of Bhuyari in the eastern Betul Belt shows that it represents a typical VMS deposit which has been later deformed and metamorphosed to amphibolites facies during or closely following the Betul Orogeny. The deposit formed during voluminous

submarine volcanism in moderate to deep-water conditions. Hydrothermal fluids mainly comprised sea-water with possible minor magmatic component. Sulphides were deposited on the sea-floor and near the sea-floor. Hydrothermal alteration consisted of a Mg-K-Fe core and a K-Fe outer envelope. Mg-carbonate alteration formed by low-temperature hydrothermal fluids close to the sea-floor. Amphibolite facies metamorphism converted the alteration zone into metamorphic mineral assemblages with porphyroblasts of garnet, Zn-staurolite, Zn-spinel (gahnite), plagioclase, biotite-phlogopite, tremolite etc based on their position in the alteration zones. Certain index minerals and elemental enrichments in minerals from rocks close to or within the mineralized zones were identified. The minerals like Mn-garnet, Zn-spinel and Zn-staurolite are resistant during erosion and their presence in stream sediments and regolith can be used as guides for locating such deposits.

******

REFERENCES

Acharya, S.K. and Roy, A (2000) Tectonothermal history of the Central Indian Tectonic Zone and reactivation of major faults/shear zones. Jour. Geol.Soc.India. v. 55, pp.239-256.

Alam, M., Naushad, M., Wanjari, N and Ahmad, T (2009) Geochemical characterizations of mafic magmatic rocks of the Central Indian Shield: Implication for Precambrian crustal evolution. In: (Eds.) Talat Ahmad, Francis Hirsch, and Punya Charusiri, Journal of the Virtual Explorer, vol. 32, paper 8, doi:10.3809/jvirtex.2009.00246.

Allen, R.L., Lundstrom, I., Ripa, M., Simeonov, A and Christofferson, H (1996) Facies analysis of a 19 Ga continental margin, back arc felsic caldera province with diverse Zn-Pb-Ag (Cu-Au) sulphide and Fe oxide deposits, Bergslagen region, Sweden. Econ. Geol., v. 91, pp. 979-1008.

Allen, R.L., Weihed, P. and Svenson, S.A. (1997) Setting of an Zn-Cu-Au-Ag massive sulphide deposits in the evolution and facies architecture of a 1.9 Ga massive volcanic arc, Skellefte dist., Sweden. Econ. Geol., v.91, pp.1022-1053.

Allen, R.L., Weihed, P., Blundell, D., Crawford, T., Davidson, G., Galley, A., Gibson, H., Hannington, M., Herzig, P., Large, R., Lentz, D., Maslennikov, V., McCutcheon, S., Peter, J and Tornos, F (2002) Global comparisons of volcanic-hosted massive sulphide districts, in Blundel, D., Neubauer, F., and von Quadt, A., eds., The timing and location of major ore deposits in an evolving orogen, The Geological Society. London, p.13-37.

Appel, P.W.U (1979) Stratabound copper sulphides in a banded iron-formation and in basaltic tuffs in the early Precambrian Isua supracrustal belt, West Greenland: Econ. Geol. v.74, p. 45-52.

Arnold, J and Sandiford, M (1990) Petrogenesis of cordierite-orthoamphibole assemblages in the Springton region, south Australia, Contributions to Mineralogy and Petrology, v. 106, pp. 100-109.

Averill, S.A (2001) The application of heavy indicator mineralogy in mineral exploration with emphasis in base metal indicators in glaciated metamorphic and plutonic terrains, in McClenaghan, M.B., Bobrowsky, P.T., Hall, G.E.M., and Cook, S.J., eds., Drift exploration in glaciated terrain: Geological Society of London Special Publication 185, p.69-81.

Baker, P. E (1968) Comparative volcanology and petrology of the Atlantic island-arcs: Bulletin of Volcanology, v. 32, pp. 189–206.

Balaram, V., Ramesh, S.L and Anjaiah, K.V (1996) New trace and REE data in the thirteen GSF reference samples by ICP-MS. Geostandards Newsletter, v.20, pp.71-78.

Barrett, T.J and MacLean, W.H (1991) Chemical, mass, and oxygen isotope changes during extreme hydrothermal alteration of an Archean rhyolite, Noranda, Quebec: Econ.Geol., v.86, pp.406-414.

Barrett, T.J., Cattalani, S and MacLean, W.H (1993) Volcanic lithogeochemistry and alteration at the Delbridge massive sulphide deposit, Noranda, Quebec: Journal of Geochemical Exploration, v.48, pp.135-173.

Barrett, T.J., and MacLean, W.H. (1994a) Chemostratigraphy and hydrothermal alteration in exploration for VMS deposits in greenstone and younger volcanic rocks: Geological Association of Canada Short Course Notes, v. 11, pp. 433–467.

Barrett, T.J and MacLean, W.H (1994b) Mass changes in hydrothermal alteration zones associated with VMS deposits of the Noranda area: Exploration and Mining Geology, v. 3, pp. 31–160.

Barrett, T.J and MacLean, W.H (1999) Volcanic sequences, lithogeochemistry, and hydrothermal alteration in some bimodal volcanic-associated massive sulphide systems. In: Barrie CT, Hannington MD (eds.) Volcanic-associated massive sulphide deposits: processes and examples in modern and ancient settings. Reviews in economic geology, v.8, pp.101-131.

Barrett, T.J and MacLean, W.H and Tennant, S.C (2001) Volcanic sequence and alteration at the Parys Mountain Volcanic-Hosted Massive Sulphide Deposit, Wales, United Kingdom: Applications of Immobile element Lithogeochemistry. Econ. Geol. v.96, pp. 1279-1305.

Barrett, T.J and MacLean, W.H and Areback, H (2005) The Palaeoproterozoic Kristineberg VMS deposit, Skellefte district, northern Sweden. Part II: chemostratigraphy and alteration. Minerallium Deposita. v.40, pp.368-395.

Barrett, T.J., Dawson, G.L., and MacLean, W (2008) Volcanic stratigraphy, alteration, and sea-floor setting of the Paleozoic Feitais massive sulfide deposit, Aljustrel, Portugal: Econ. Geol. v. 103, pp. 215–239.

Barrie, C.T., Ludden, J.n and Green, A.H (1993) Geochemistry of volcanic rocks associated with Cu-Zn and Ni-Cu deposits in the Abitibi Sub-province. Econ.Geol., v.88, pp.1341-1358.

Barrie, C.T (1995) Zircon thermometry of high-temperature rhyolites near volcanic-associated massive sulfide deposits, Abitibi subprovince, Canada. Geology v. 23, pp.169-172.

Barrie, C.T., Cathles, L.M., Erendi, A., Schwaiger, M and Murray, C (1999) Heat and fluid flow in volcanic-associated massive sulphide-forming hydrothermal systems, in Barrie, C.T and Hannington, M.D., eds. Volcanic Associated Massive Sulphide Deposits: Processes and Examplesin Modern and Ancient Enviroinments, Reviews in Economic Geology 8, Society of Economic Geologists, pp. 201-219.

Bau, M and Dulski, P (1995) Comparative study of yttrium and rare-earth element behaviours in fluorine- rich hydrothermal fluids: Contributions to Mineralogy and Petrology, v. 119, pp. 213-223.

Bea, F (1996) Residence of REE, Y,Th and U in granites and crustal protoliths; implications for chemistry of crustal melts. J. Petrol, v.37, pp.521-552.

Bhattacharya, A., Mohanty, L., Maji, A., Sen, S.R and Raith, M (1992) Non-ideal mixing in the phlogopite-annite boundary: Constraints from experimental data on Mg-Fe partitioning and a reformulation of the biotite-garnet thermometer. Contributions to Mineralogy and Petrology, v. 111, pp. 87-93.

Bonnet, A.L and Corriveau, L (2007) Alteration vectors to metamorphosed hydrothermal systems in gneissic terranes, in Goodfellow, W.D., ed, Mineral Deposits of Canada: A synthesis of major deposit-types,

District Metallogeny, the evolution of geological provinces, and exploration methods: Geological association of Canada, Mineral deposits division, Special publication, No. 5, pp. 1035-1049.

Brooks, E.R (1995) Paleozoic fluidization, folding and peperite formation, northern Sierra Nevada, California. Canadian Journal of Earth Sciences, v. 32, pp.314-324.

Bryan, S.E., Holcombe, R.J. & Fielding, C.R (2001) Yarrol terrane of the northern New England Fold Belt: forearc or backarc? Australian Journal of Earth Sciences v.48, pp.293–316.

Bucher, K and Frey, M (2013) Petrogenesis of metamorphic rocks. Springer.

Busby-Spera, C.J and White, J.D.L (1987) Variation in peperite textures associated with differing host-sediment properties. Bulletin of Volcanology, v. 49, pp. 765-775.

Callaghan (2001) Geology and host rock alteration of the Henty and mount Julia gold deposits, western Tasmania. Econ. Geol. v. 96, pp. 1073-1088.

Campbell, I.H., Coad, P., Franklin, J.M., Gorton, M.P and Thurston, P.C (1982) Rare earth elements in volcanic rocks associated with Cu-Zn massive sulphidemineralsiation: A preliminary report: Canadian Journal of Earth sciences, v.19, pp. 619-623.

Campbell, I.H., Lesher, C.M., Coad, P., Franklin, J.M., Gorton, M.P., and Thurston, P.C (1984) Rare-earth element mobility in alteration pipes below massive Cu-Zn-sulfide deposits; Chemical Geology, v. 45, pp. 181-202.

Campbell, K.A., Nesbitt, E.A. & Bourgeois, J (2006) Signatures of storms, oceanic floods and forearc tectonism in marine shelf strata of the Quinault Formation (Pliocene), Washington, USA. Sedimentology. v. 53,pp. 945–969.

Carmichael, D. M (1978) Metamorphic bathozones and bathograds: a measure of the depth of postmetamorphic Postmetamorphic uplift and erosion on the regional scale. American Journal of Science, v.278,pp.769-97.

Cas, R.A.R and Wright, J.V (1987) Volcanic successions- modern and ancient. A geological approach to processes, products and successions: London, Allen and Unwin, 529p.

Chakraborty, K and Roy, A (2012) Mesoproterozoic differential metasomatism in subcontinental lithospheric mantle of Central Indian Tectonic Zone: Evidence from major and trace element geochemistry of Padhar Mafic Ultramafic Complex. Geol. Soc. India, v. 80, pp. 628-640.

Chaturvedi, R.K (2001) A review of the geology, tectonic features and tectono-lithostratigraphy of Betul Belt. Geol.Surv.India- Special Publication Series, v.64, pp. 299-315.

Christiansen, E.H (2005) Contrasting processes in silicic magma chambers: evidence from very large volume ignimbrites. Geological Magazine, v.142, pp. 669-681.

Christiansen, E.N and McCurry (2008) Contrasting origin of Cenozoic silicic volcanic rocks from the western Cordillera of the United States. Bulletin of Volcanology, v.70,pp. 251-267.

Clemens, J.D., Holloway, J.R and White, A.J.R (1986) Origin of A-type granite, experimental constraints. American Mineralogist.v.19, pp.111-131.

Cong Ling and Qiang Liu (2002) Behavior of the REEs and other trace elements during fluid-rock interaction related to ore-forming processes of the Yinshan transitional deposit in China. Geochemical Journal, v. 36, pp. 443 to 463.

Cook, N.J (1993) Conditions of metamorphism estimated from alteration lithologies and ore at the Bleikvassli Zn-Pb-(Cu) deposit, Nordland, Norway. Norsk Geologisk Tidsskrift, 73: 226-233.

Coplen, T. B. (1988) Normalization of oxygen and hydrogen isotope data. Chem. Geol. (Isotope Geoscience Section) 72, 293–297.

Corfu, F., Hanchar, J.M., Hoskin, P.W.O., Kinny, P (2003) Atlas of zircon textures: Reviews in Mineralogy and Geochemistry, v. 53, pp. 469-500.

Crawford, A.R (1978) Narmada-Son lineament of India, traces into Madagascar. Journal of Geological Soceity of India, v. 19, pp.144-153.

Cudahy, T.J., Okada, K., Ueda, K., Brauhart, C., Morant, P., Huston, D., Cocks, T., Cocks, P.,Wilson, J., Ong, C., Mason, P., Huntington, J.F (1999) Mapping the Panorama VMS style alteration and host rock mineralogy, Pilbara Block, using airborne hyperspectral VNIR-SWIR data. CSIRO Exploration and Mining Report 661F. 86pp.

Dasgupta, S., Sengupta, P., Guha, D., and Fukuoka, M (1991) A refined garnet-biotite Fe-Mg exchange geothermometer and its application in amphibolites and granulites. Contributions to Mineralogy and Petrology. v. 109. Pp. 130-137.

Davies, J.F and Whitehead R.E (2006) Alkali-alumina and MgO-alumina molar ratios of altered and unaltered rhyolites. Exploration and Mining geology, v. 15, Nos. 1-2, pp 75-88.

Deb, M (2000) VMS deposits: Geological characteristics, genetic models, and a review of their metallogenesis in the Aravalli range. In: Deb,M.(ed.) Crustal Evolution and Metallogeny in the Northwestern Indian Shield. Narosa, New Delhi, pp.328-363.

Deb, M., Thorpe, R.J., Krstic, D., Davis, D. and Corfu, F. (2001) Zircon U-Pb and galena Pb isotope evidence for an approximate 1.0 ga terrane along the western margin of the Aravalli-Delhi orogenic belt, northwestern india. Precambrian Research, v. 108, pp. 195-213.

Dora, M.L and Praveen, M.N (2007) Prospecting for basemetal mineralization in Bhuyari Block, Chhindwara district, M.P, E-I stage. GSI report for the Field Season 2003-04.

Droop, G.T.R (1985) Alpine metamorphism in the south-east Tauern window, Austria, P-T variations in space and time. Journal of Metamorphic Geology, v. 3, pp. 371-402.

Dusel-Bacon., Wooden, J.L and Hopkins, M.J (2004) U-Pb zircon and geochemical evidence for bimodal mid-Paleozoic magmatism and syngenetic base-metal mineralisation in the Yukon-Tanana terrane, Alaska: Geological society of America Bulletin, v. 116, pp. 989-1015.

Dutrow, B.L., and Holdaway, M.J. (1989) Experimental determination of the upper thermal stability of Fe staurolite + Quartz at medium pressures. Journal of Petrology, v. 30, pp. 229-248.

Dymek, R.F (1983) Titanium, aluminum and interlayer cation substitutions inbiotite from high-grade gneisses, West Green land. American Mineralogist, v.68, pp.880.899.

Eby, G.N (1990) The A-type granitoids: A review of their occurrence and chemical characteristics and speculations on their petrogenesis. Lithos, v.26, pp.115-134.

Eby, G.N (1992) Chemical Subdivision of the A-Type granitoids: Petrogenetic and Tectonic implications. Geology, v. 20, pp.641-694.

Ernst, W. G (1963) Petrogenesis of glaucophane schists. Journ. Petrol. v.4,p p.1-30.

Essene, E.J (1989) The current status of thermobarometry in metamorphic rocks. In: Daly, J., Cliff, R., Yardley, B. (Eds.), Evolution ofMetamorphic Belts. Geological Society Special Publication, v.43, pp. 1–44.

Evans, B.W and Patrick, E.B (1987) Phengite-3T in high-pressure metamorphosed granitic orthogneiss, Seward Peninsula, Alaska. Canadian Mineralogist, vol. 25, pp. 141-158.

Ferry, J.M. and Spear, F.S (1978) Experimental calibration of the partitioning of Fe and Mg between biotite and garnet. Contributions to Mineralogy and Petrology, 66, 113–117.

Fisher. R.V (1961) Proposed classification of volcaniclastic sediments and rocks. Geological Society of America Bulletin, v.72. pp.1409-1414.

Franklin, J.M., Lyden, J.W. and Sangster, D.F (1981) Volcanic associated massive sulphide deposits. Econ. Geol., 75th Anniversary Volume, pp. 485-627.

Franklin, J.M (1993) Volcanic-associated massive sulphide deposits, *in* Kirkham, R.V., Sinclair, W.D., Thorpe, R.I., and Duke, J.M., eds., Mineral deposit modeling: Geological Association of Canada Special Paper, v. 40, pp. 315–334.

Franklin, J.M (1995) Volcanic-associated massive sulphide base metals: Geological Survey of Canada, Geology of Canada, no.8.pp. 158-183.

Franklin, J.M, H.L. Gibson, I.R. Jonasson, and A.G. Galley (2005) Volcanogenic Massive Sulphide Deposits: in Hedenquist, J.W., Thompson, J.F.H., Goldfarb, R.J., and Richards, J.P., eds., Economic Geology, 100th Anniversary Volume, The Economic Geology Publishing Company, pp.523-560.

Frost, B.R., Barnes, C.G., Collins, W.J., R.J., Ellis, D.J., Frost, C.R (2001) A geochemical classification for granitic rocks. Jour. Petrol. V.42, pp.2033-2048.

Gaboury, D and Pearson, V (2008) Rhyolite geochemical signatures and association with volcanogenic massive sulphide deposits: Examples from the Abitibi belt, Canada v.103, pp.1531-1562.

Galley, A, Hannington M, Taylor B, Paradis, S (2000) Exploration criteria developed from the results of VMS Camiro Project 94E07, In: Gemmell J, Pongratz J (eds) Volcanic enviroinments and massive sulphides. Centre for Ore deposit and Exploration Studies (CODES), Hobart, Tasmania, Australia, pp 53-55.

Ganguly, J. and Saxena, S.K. (1984) Mixing properties of aluminosilicate garnets: Constraints from natural and experimental data, and applications to geothermobarometry. American Mineralogist, 69, 88–97.

Genna, D., Gaboury, D and Roy, G (2014) Evolution of a volcanogenic hydrothermal system recorded by the behavior of LREE and Eu: Case study of the Key Tuffite at Bracemac-McLeod deposits, Matagami, Canada. Ore Geology Reviews, v. 63. Pp.160-177.

Ghosh, B and Praveen, M.N (2007) Garnet-Gahnite-Staurolite relations and occurrence of Ecandrewsite from the Koparpani base metal prospect, Betul Belt, central India, Neues, Jahr.fur.Min. Abhand. v.184, pp. 105-116.

Ghosh, B., Praveen, M. N and Shrivastava, H. S (2006) Gahnite chemistry from metamorphosed Zn-Pb-Cu sulphide occurrences of Betul Belt, Central India. Geol. Soc. Ind., v.67, pp.17-20.

Ghosh, B and Praveen, M.N (2008) Indicator minerals as guides to base metal sulphide mineralisation in Betul Belt, central India. J. Earth Syst. Sci. **117**, No. 4, August 2008, pp. 1–16

Glazner, A.F., Coleman, D.S and Bartley, J.M (2008) The tenuous connection between high-silica rhyolites and granodiorite plutons. Geology, v.36, pp.1047-1050.

Golani, P.R, Bandyopadhyay and Anupendu Gupta (2001) Gavilgarh-Tan Shear: A prominent ductile shear zone in Central India with multiple reactivation history.Geol.Surv.Ind. Spl.Pub.No.64.pp.265-272.

Golani, P.R and Dora, M.L (2003) Final report on the specialized thematic mapping in Gavilgarh-Tan shear zone area in Kanhan and Pench river valley sectors of Chhindwara district, Madhya Pradesh, Geol. Surv. India, (unpublished progress report).

Golani, P.R., Dora, M.L and Bandopadhyay, B.K (2006) Base metal mineralization associated with hydrothermal alteration in felsic volcanic rocks in Proterozoic Betul Belt at Bhuyari, Chhindwara District, Madhya Pradesh. Geol. Soc. India,v.68, pp.797-808.

Gill, J. B (1981) Orogenic andesites and plate tectonics: New York, Springer-Verlag, 390 p.

Green, T.H and Pearson, N.J (1987) An Experimental study of Nb and Ta partitioning between Ti-rich minerals and silicate liquids at high pressure and Temperature, Geochim.Cosmochim.Acta, v.51, pp.55-62.

Guidotti, C.V (1974) Transition from the staurolite to sillimanite zone, Rangely Quadrangle, Maine. Geological Society of America Bulletin, v.85,pp.475- 490.

Guidotti, C.V., and Sassi, F.P (1976) Muscovite as a petrogenetic indicator mineral in pelitic schists: Neues Jahrbuch fur Mineralogie Abhandlungen, v.127, pp. 97-142.

Guidotti, C, V and Sassi, F (1998) Petrogenetic significance of Na–K white micamineralogy: recent advances for metamorphic rocks. European Journal of Mineralogy, v.10, pp.815–854.

Haas, J.R., Shock, E.L., and Sassani, D.C (1995) Rare earth elements in hydrothermal systems: estimates of standard partial molal thermodynamic properties of aqueous complexes of the rare earth elements at high pressures and temperatures; Geochimica et Cosmochimica Acta, v. 59, p. 4329-4350.

Halley, S.W. and Roberts, R.H (1997) A shallow water, gold rich VMS deposit in Western Tasmania, Economic Geology, v.92, pp.438-447.

Hart, T.R., Gibson, H.L and Lesher, C.M (2004) Trace element geochemistry and petrogenesis of felsic volcanic rocks associated with volcanogenic massive Cu-Zn-Pb sulphide deposits. Econ.Geol, V.99, pp.1003-1013.

Hannington, M.D., K.H., Poulsen, J.F.H., Thompson, and R.H. Sillitoe (1999). Volcanogenic gold in the massive sulphide environment. Reviews in Econ.Geol.,v.8, pp.325-356.

Hallberg, A (2001) Rock classification, magmatic affinity, and hydrothermalalteration at Boliden, Skellefte district, Sweden - a desk-top approach to whole rock geochemistry, *in* Weihed P., ed., Economic Geology Research: Sveriges Geologiska Undersökning, v. 833, pp. 93-131.

Hashiguchi, H, Yamada R and Inoue T (1983) Practical applications of low Na_2O anomalies in footwall acid lava for delimiting promising areas around the Kosaka and Fukazawa Kuroko deposits, Akita Prefecture, Japan. In: Ohmoto H, Skinner BJ (eds) The Kuroko and related volcanogenic massive sulphide deposits. Econ.Geol.Monograph 5. pp 387-394.

Heimann, A., Spry, P.G and Teale, G.S (2005) Zincian spinel associated with metamorphosed Proterozoic base-metal sulphide occurrences, Colorado: A re-evaluation of gahnite composition as guide in exploration; Can. Min., v. 43, pp. 601-622.

Hekinian, R., Fevrier, M., Bischoff, J.L., Picot, P., and Shanks, W.C (1980) Sulfide deposits from the East Pacific Rise near 21o N: Science, v. 207, no. 4438, pp. 1433–1444.

Henry, D. J., Guidotti, C. V. and Thomson, J. A. (2005) The Ti-saturation surface for low-to-medium pressure metapelitic biotite: Implications for Geothermometry and Ti-substitution Mechanisms. American Mineralogist, volume 90, pages 316-328.

Herrmann, W and Hill, A.P (2001) The Origin of Chlorite-Tremolite-Carbonate rocks associated with the Thalanga Volcanic-Hosted Massive Sulphide Depost, North Queensland, Australia, Econ. Geol. V.96.,pp. 1149-1173

Hey, M.H (1954) A new review of the chromites, Mineral. Mag. V. 30, pp.277-292.

Hildreth, W (1979) The Bishop Tuff; Evidence for the origin of compositional zonation in silicic magma chambers, in Chapin, C.E. and Elston, W.E., eds., Ash-flow tuffs: Geological Society of America Special Paper, v.180, pp. 43–75.

Hildreth, W (1981) Gradients in silicic magma chambers: implications for lithospheric magmatism. Jour. Geophysical Research. v. 86, pp.10153–10192.

Hodges D.J and Manojlovic P.M (1983) Application of lithogeochemistry to exploration for deep VMS deposits in high grade metamorphic rocks, Snow Lake, Manitoba. Journal of Geochemical Exploration 48: 201-224.

Holdaway, M.J., Mukhopadhyay, B., Dutrow, B.L. (1995) Thermodynamic properties of stoichiometric staurolite. Am. Mineral., v.80, pp.520-533.

Holdaway, M.J., Mukhopadhyay, B, Dyar, M.D, Guidotti, C.V and Dutrow, B.L (1997) Garnet-biotite geothermometry revised: New Margules parameters and a natural specimen data set from Maine. American Mineralogist, v. 82, pp.582–595.

Holland, T.J.B and Powell, R (1990) An enlarged and updated internally consistent thermodynamic dataset with uncertainties and correlations:

The system K_2O-Na_2O-CaO-MgO-MnO-FeO-Fe_2O_3-Al_2O_3-TiO_2-SiO_2-C-H_2-O_2. Journal of Metamorphic Geology, v.8,pp. 89-124.

Holland, T.J.B and Powell, R (1998) An internally consistent thermodynamic data set for phases of petrological interest: Journal of metamorphic geology, v.16, pp.309-343.

Huston, D.L (1999) Stable isotopes and the genesis of volcanic-hosted massive sulphide deposits: a review, in volcanic-associated massive sulphide deposits: processes and examples in modern and ancient settings, Reviews in Economic Geology, vol. 8, pp. 157-179.

Hutchinson, R.W (1973) Volcanogenic sulphide deposits and their metallogenic significance. Econ. Geol., v.68, pp.1223-1246.

Hutchinson, R.W (1980) Massive base-metal sulphides as guides to tectonic evolution. Geol. Assoc. Canada Spec. Paper 20, pp.659-684.

Irvine, T.N and Baragar, W.R.A (1971) A guide to the chemical classification of the common rocks: Canadian Journal of Earth Sciences, v.8,pp.523-548.

Jain, S.C., Yedekkar, D.B., Nair,K.K.K (1991) Central Indian Shear Zone: a major Precambrian crustal boundary.Journ. Geol. Soc. India. v.37, pp.521-548.

Jenner, G.A (1996) Trace element geochemistry of igneous rocks: Geochemical nomenclature and analytical geochemistry. In: Wyman, D.A. (ed) Trace element geochemistry of volcanic rocks: Applications for massive sulphide exploration, Geological Association of Canada, Short Course Notes 12, pp.51–77.

Klau, W and Large, D.E (1980) Submarine exhalative Cu-Pb-Zn deposits, a discussion on their classification and metallogenesis. Geol.Jahrb., D 40, pp.13-58.

Keranen, K and Klemperer, S.L (2008) Discontinuous and diachronous evolution of the main Ethiopian rift: Implications for development of continental rifts. Earth and Planetary Science Letters.v.265,pp.96-111.

Khin Zhaw, and Large, R.R (1990) δ^{18} O and δ^{13} C isotopic variation of hydrothermal carbonates from the Rosebery, Hercules and South Hercules deposits, western Tasmania: Interplay of Cambrian vs Devonian systems [abs]: Geological Society of Australia, International Conference on Geochronology, Cosmochronology and Isotope Geology, 7th, Canberra, Australia, September 24-29, 1990, Abstracts, no.27.

Kleemann, U. and Reinhardt, J. (1994) Garnet-biotite thermometry revisited: The effect of Alvi and Ti in biotite. European Journal of Mineralogy, 6, 925–941.

King, P.L., Chappell, B.W., Allen, C.M and White, A.J.R (2001) Arc A-type granites the high-temperature felsic granites?Evidences from fractionated granites of the Wangrah suite.Australian Journal of Earth Sciences, v.38, pp.501-514.

Large, R.R (1977) Chemical Evolution and zonation of massive sulphide deposits in volcanic terrains. Econ. Geol., v.72, pp.549-572.

Large, R.R (1992) Australian volcanic-hosted massive sulfide deposits: features, styles, and genetic models. Econ.Geol., v.87, pp.471-510.

Large, R.R., Allen, Gemmell, G.B., Paulick, H., and Huston, D.L (2001a) The Alteration Box Plot: A simple approach to understanding the relationships alteration lithology and lithogeochemistry associated with VMS deposits: Economic Geology, v. 96, pp. 957-971.

Large, R.R., Allen, R.L., Blake, M.D and Herrmann.W (2001b) Hydrothermal Alteration and Volatile element halos for the Rosebery K Lens Volcanic-hosted massive sulphide deposit, Western Tasmania, Economic Geology, v.96, pp.1055-1072.

Large, R.R., McPhie, J., Bruce, G.J., Herrmann, W and Davidson, G.J (2001c) The Spectrum of Ore Deposit Types, Volcanic Environments, Alteration Halos, and Related Exploration Vectors in Submarine Volcanic Successions: Some Examples from Australia. Econ.Geol., v.96, pp.913-938.

Le Bas, M. J., Le Maitre, R.W., Streckeisen, A and Zanettin, B (1986) A chemical classification of volcanic rocks based on the total alkali-silica diagram. Journal of Petrology,v.27, pp.745-750.

Leake, B.E., Wooley, A.R., Arps, C.E.S., Birch, W.D., Gilbert, M.C., Grice, J.D., Hawthorne, F.C., Kato, A., Kisch, H., Krivovichev, V.G., Linthout, K., Laird, J., Mandarino, J.A., Maresch, W.V., Nickel, E.H., Rock, N.M.S., Schumacher, W.V., Smith, D.C., Stephenson, N.C.N., Ungaretti, L., Whittaker, E.J.W. and Youzhi, G. (1997) Nomenclature of amphiboles: Report of the Subcommittee on Amphiboles of the International Mineralogical Association, Commission on New Minerals and Mineral Names. American Mineralogist, 82, 1019-1037.

Lentz, D.R (1996) Trace element systematic of felsic volcanic rocks associated with massive-sulphide deposits in the Bathurst Mining Camp: petrogenetic, tectonic and chemostratigraphic implications for VMS exploration; in Wyman, D.A., ed., Trace Element Geochemistry of Volcanic Rocks: applications for Massive Sulphide exploration; Geological Association of Canada, Short Course Notes, v.12. pp. 359-402.

Lentz, D.R (1998) Petrogenetic evolution of felsic volcanic sequences associated with Phanerozoic volcanic-hosted massive sulphide systems: the role of extensional geodynamics: Ore Geology Reviews, v.12. pp. 289-327.

Lentz, D.R (1999) Petrology, geochemistry, and oxygen isotope interpretation of felsic volcanic and related rocks hosting the Brunswick 6 and 12 massive sulphide deposits (Brunswick Belt), Bathurst mining camp, New Brunswick, Canada, Econ.Geol. v.94, pp.57-86.

Lesher, C.M., Goodwin, A.M., Campbell, I.H and Gorton, M.P (1986) Trace element geochemistry of ore associated and barren, felsic metavolcnic rocks in the Superior Province Canada: Canadian Journal of Earth Sciences, v.23, pp.222-237.

Long, D.G.F (2004) The tectonostatigraphic evolution of the Huronian basement and the subsequent basin fill: geological constraints on impact models of the Sudbury event. Precambrian Research, v.129, pp. 203–223.

Lydon, J.W (1984) Some observations on the mineralogical and chemical zonation patterns of volcanogenic sulphide deposits of Cyprus: Geological Survey of Canada Paper 84-1A, p.611-616.

Mandal, B., Sen, M.K and Rao, V.V (2013) New seismic images of the Central Indian Suture Zone and their tectonic implications. Tectonics, v. 32, pp. 908–921.

MacLean, W.H (1990) Mass change calculations in altered rock series: Mineralium Deposita, v. 25, pp. 44-49.

MacLean, W.H and Barrett, T.J (1993) Lithogeochemical techniques using immobile elements: Journal of Geochemical exploration, v. 48, pp. 109-133.

MacDonald, R.W.J., Barrett, T.J and Sherlock, R.L (1996) Geology and Lithogeochemistry at the Hidden Creek Massive Sulphide deposit, Anyonx, west-Central British Columbia: Exploration and Mining Geology, v.5. pp.369-398.

Mahakud, S.P (1993) Final report on the detailed exploration for polymetallic mineralization in Bhanwara-Tekra block, Kherli Bazar-Bargaon area, Multai tehsil, Betul, M P, Geol. Surv. Ind., unpublished progress report.

Mahakud, S.P., Raut, P.K and Mishra, V.P (2000) Geological set-up of Kherli Bazar polymetallic deposit, Betul district, Madhya Pradesh. In: Tectonomagmatism, Geochemistry and metamorphism of Precambrian Terrains, (eds. K C Gyani and P Kataria). Proceedings of the National Seminar, Udaipur University, pp. 395-406.

Mahakud, S.P., Raut, P.K., Hansda, C., Ramteke, P.F., Chakraborty, C., Praveen, M.N and Sisodiya, D.S (2001) Sulphide mineralisation in the central part of Betul Belt around Ghisi-Muariya-Koparpani area, Betul district, Madhya Pradesh. Geol. Surv. India,Spl. Pub., v.64, pp.377-385.

McBirney A.R (1963) Factors governing the nature of submarine volcanism: Bull. Volcanol.v.26. pp. 455-469.

Majumdar, R., Van Loon, A.J., and Arima, M (2006) Soft-sediment deformation structures in the Earth's oldest seismites. Sedimentary Geology, v. 186, pp.19-26.

Massone, H.J. (1981) Phengite: Eine experimentelle Untersuchung ihres Druck-Temperatur-Verhaltens im System K,O-MgO-AlrO3-SiOr-H,O. Unpublished Ph.D. thesis, University of Bochum, Bochum, Germany (not seen, extracted from Contributions to Mineralogy and Petrology, v. 96, pp.519-522)

Massone, H.J and Schreyer, R (1987) Phengite geobarometry based on the limiting assemblage with K-feldspar, phlogopite and quartz. Contributions to Mineralogy and Petrology, v. 96, pp. 212-214.

McPhie, J., Doyle, M., and Allen, R (1993) Volcanic Textures: A Guide to the interpretation of Textures in Volcanic Rocks; Codes Key Center, Tasmania, 198p.

Morris, G.A., Larson, P.B and Hooper, P.R (2000) "Subduction style" magmatism in a non-subduction setting; the Colville Igneous Complex, NE Washington state, USA, J. Petrol. v.41. pp. 43-67.

Moulton, B.J.A., Fowler, A.D., Ayer, J.A., Berger, B.R and Langevin, P.M (2011) Archean sub-aqueous high silica rhyolite coulees: Examples from the Kidd-Munro Assemblage in the Abitibi Subprovince. Precambrian Resaearch, v. 189, pp. 389-403.

Menard, T and Gordon,T.M (1997) Metamorphic P-T paths from the eastern Flin Flon belt and Kisseynew domain, Snow Lake, Manitoba. The Canadian Mineralogist, v. 35, pp. 1095- 1115.

Mishra, M.K., Devi., S.J., Kaulina,T., Das, K.C., Kumar, S and Ahmad, T (2011) Petrogenesis and tectonic setting of the Proterozoic mafic magnmatic rocks of the Central Indian Tectonic Zone, Betul area, Geochemical constraints, In R.K. Srivastava (Ed) Dyke swarms: Key for geodynamic interpretation, Springer Verlag (2011) pp. 189-202.

Misra, K.C (2000) Understanding mineral deposits, Kluwer Academic Publishers. 845p.

Nakamura, N (1974) Determination of REE, Ba, Fe, Mg, Na and K in carbonaceous and ordinary chondrites: Geochim. Cosmochim.Acta. v. 38, pp. 757-775.

Ohmoto, H and Rye, R.O (1979) Isotopes of Sulphur and Carbon, in Barnes, H.L. Ed., Geochemistry of Hydrothermal ore deposits, John Wiley and Sons, pp. 509-567.

Ohmoto, H and Skinner, B. J (1983) The Kuroko and related volcanogenic massive sulfide deposits: Econ. Geol. Mon. 5, 604 p.

Ohmoto, H (1986), Stable isotope geochemistry of ore deposits: Reviews in Mineralogy, v.16, pp.491-560.

Ohmoto, H (1996) Formation of volcanogenic massive sulfide deposits: The Kuroko perspective: Ore Geology Reviews, v.10, pp. 135-177.

Pankhurst, R.J., Leat, P.T., Sruoga, P., Rapela, C.W., M'Arquez, M., Storey, B.C and Riley, T.R (1998) The Chon-Aike silicic igneous province of Patagonia and related rocks in West Antartica: A silicic LIP, J. Volcan. Geotherm. Res. v.81, pp.113-136.

Patiño-Douce, A.E (1993) Titanium substitution in biotite: an empirical model with applications to thermometry, O2 and H2O barometries, and consequences form biotite stability. Chemical Geology, v.108, pp.133.162.

Patiño-Douce, A.E (1997) Generation of metaaluminous A-type granite by low-pressure melting of calc-alkaline granitoids, Geol. 25 (8) pp.743-746.

Paulick, H., Herrmann, W., Gemmell, J.B (2001) Alteration of felsic volcanics hosting the Thalanga massive sulfide deposit (Northern Queensland, Australia) and geochemical proximity indicators to ore: Economic Geology, v.96, pp.1175-1200

Paulick, H and Franz, G (2001) Greenschist facies regional and contact metamorphism of the Thalanga Volcanic-Hosted Massive Sulphide Deposit (northern Queensland, Australia) Mineralium Deposita, v. 36, pp. 786-793.

Perchuk, L.L and Lavrent'eva, I.V (1983) Experimental investigation of exchange equillibria in the system cordierite-garnet-biotite. In: Saxena, S.K. (ed) Kinetics and equilibrium in mineral reactions, Advances in physical geochemistry, v. 3, pp.199-239. Springer-Verlag, New York.

Pearce, J. A., Harris, N. B. W., and Tindle, A. J (1984) Trace element discrimination diagrams for the tectonic interpretation of granitic rocks. J. Petrol., v.25, pp.956-83.

Piercey, S.J., Paradis, S., Murphy, D.C and Mortensen, J.K (2001) Geochemistry and paleotectonic setting of felsic volcanic rocks in the Finyalson lake volcanic-hosted massive sulphide (VHMS) district, Yukon, Canada. Econ. Geol. v. 96, pp.1877-1905.

Pearce, S.J., Peter, J.M., Mortensen, J.K., Paradis, S., Murphy, D.C and Tucker, T.L (2008) Petrology and U-Pb Geochronology of Footwall Porphyritic Rhyolites from the Wolverine Volcanogenic Massive Sulphide Deposit, Yukon, Canada: Implications for the Genesis of Massive Sulphide Deposits in Continental Margin Enviroinments, Eco.Geol. v.103, pp.5-33.

Piercey, S.J (2009) Lithogeochemistry of volcanic rocks associated with volcanogenic massive sulphide deposits and application to exploration, in submarine volcanism and mineralization: Modern through ancient, (eds) B.Cousens and S.J.Piercey; Geological Association of Canada, short courses 29-30, May 2008, Quebec City, Canada, pp. 15-40.

Piercey, S.J., Squires, G.C and Brace, T.D (2013) Lithostratigraphic, Hydrothermal, and Tectonic Setting of the Boundary volcanogenic massive sulphide deposit, Newfoundland Appalachians, Canada: Formation by subsea floor replacement in a rifted Cambrian arc.

Pichler, T and G. R. Dix (1996) Hydrothermal venting within a coral reef ecosystem, Ambitle Island, Papua New Guinea. Geology, v.20, pp.435–438.

Piranjo, F (1992) Hydrothermal Mineral Deposits. Principles and Fundamental Concepts for the Exploration Geologist. pp.709, Springer-Verlag.

Powell, R and Holland, T (1990) Calculated mineral equilibria in the pelite system, KFMASH ($K2O$-FeO-MgO-Al_2O_3-SiO_2-H_2O) American Mineralogist, Volume 75, pages 367-380.

Praveen, M.N., Ghosh, B., Shrivastava, H.S., Kumaran, G.S., Roy, S and Sisodiya, D.S (2005) Metamorphic mineral assemblages associated with sulphidemineralisation in Betul Belt: A possible hydrothermal

origin. In: Sinha, A. and Singh, S.K. (eds), Proceeding volume of 1st Indian Mineral Congress "Showcasing the Indian Mineral Industry in the 21st Century", ISM, Dhanbad, India. Allied Publishers, New Delhi, pp.193-218.

Praveen, M.N., Ghosh, B., Shrivastava, H.S., Dora, M.L and Gaikwad, L.D (2007) Sulphide mineralisation in Betul Belt: Classification and general characteristics. Geol. Soc. Ind. v. 69: pp. 85-91.

Praveen, M.N and Ghosh, B (2007) Multiple origin of gahnite associated with hydrothermal alteration from Bhuyari basemetal prospect of Proterozoic Betul Belt. Geol. Soc. India, v.69,pp.233-241.

Praveen, M.N and Ghosh, B (2009) Submarine volcanic facies and its implication as possible tracker of sulphide mineralization-a study from Jilharidev area, Betul Belt, central India, Current Science, v.97.No.5,pp.670-679

Praveen.M.N., Dora., M.L, Srivastav, H.S and Mishra, M.N (2010) Report on the exploration for base metal mineralization in Bhuyari Block, Chhindwara District, M.P. Unpublished prog. rep. GSI.

Radhakrishna, B.P (1989) Suspect tectono-stratigraphic terrane elements in the Indian sub-continent. Journal Geological Society India. v.34,pp.1-24.

Ramchandra, H.M. and Pal, R.N (1992) Progress Report on the study of geochemistry and Cu-Pb-Zn mineralisation in Kherli Bazar area, Betul, M.P. (unpublished), Geol. Surv. Ind.

Raut, P.K and Mahakud, S.P (2004) Geology, geochemistry and tectonic setting of volcanosedimentary sequence of Betul Belt, Madhya Pradesh and genesis of zinc and copper sulphide mineralisation, Geol.Surv.India, Spl.Pub., v.72, pp.133-146.

Richardson, S.W (1968) Staurolite stability in a part of the system Fe-Al- Si-O-H. Journal of Petrology, v.9, pp.467–488.

Robert F., Poulsen K.H., Cassidy K.F., and Hodgson C.J (2005) Gold Metallogeny of the Superior and Yilgarn Cratons, in Economic Geology 100th Anniversary Volume, 1001-1034.

Rona, P.A (1986) Black smokers, massive sulphides and vent biota at the Mid Atlantic Ridge. Nature, v.321,pp 33-37.

Roy, A., Ramachandra, H.M., Bandopadhyay, B.K (2000) Supracrustal belts and their significance in the crustal evolution of Central India.Geol.Surv. India. Spl. Pub., v.55, pp.361-380.

Roy, A and Prasad, M.H (2001) Precambrian of central India: a possible tectonic model. Geol. Surv. India. Spl. Pub., v.64, pp.177-197.

Roy, A and Prasad, M.H (2003) Tectonothermal events in Central Indian Tectonic Zone (CITZ) and its implications in Rhodinian crustal assembly.Journal of Asian Earth Sciences,v.22, pp.115-129.

Roy, A., Chore, S.A., Viswakarma, L.L and Chakraborty, K (2004) Geology and petrochemistry of Padhar mafic-ultramafic complex from Betul Belt: A study on arc type magmatism in Central Indian Tectonic Zone. Geol. Surv. India. Spec. Publ.,v.84, pp. 297-318.

Rosenberg, J.L., Spry, P.G., Jacobson, C.E., and Vokes, F.M (2000) The effects of sulfidation and oxidation during metamorphism on the compositionally varied rocks adjacent to the Bleikvassli Zn-Pb-(Cu) deposit, Nordland, Norway: Mineralium Deposita, v. 35, pp. 714-726.

Ruks, T.W., Piercey, S.J., Ryan, J.J, Villeneuve, M.E and Creaser, R.A (2006) Mid to late Proterozoic K-feldspar Augen granitoids of the Yukon-

Tanana Terrane, Yukon, Canada: Implications for crustal growth and tectonic evolution of the northern cordillera; Geological Society of America Bulletin, v. 118.,pp.1212-1231.

Ryerson, F.J and Watson, E.B (1987) Rutile saturation in magmas: Implications for Ti-Nb-Ta depletion in island arc basalts, Earth Planet. Sci. Lett.,v.86, pp.225-239.

Sangster, D.F (1972) Precambrian volcanogenic massive sulphide deposits in Canada: A review: Geological Survey of Canada Paper 72-22, 44 p.

Sangster, D.F., and Brook, W.A (1977) Primitive lead in an Australian Zn-Pb-Ba deposit: Nature, v. 270, pp. 423.

Sangster, D.F. and Scott, S.D (1976) Precambrian strata-bound massive Cu-Zn-Pb sulphide ore of North America. In Handbook of strata-bound and stratiform ore deposits, K.H. Wolf (ed.), v.6, pp.129-222. Amsterdam: Elsevier.

Shand (1943) Eruptive Rocks, John Wiley and Sons.

Shanks III and Pat, W.C (2012) Historical evolution of descriptive and genetic knowledge and concepts in volcanogenic massive sulfide occurrence model: U.S. Geological Survey Scientific Investigations Report 2010–5070 –C, chap. 3, 6 p.

Shikazono, N., Hoshino, M., Utada, M., Nakata, M., Ueda, A (1998) Hydrothermal carbonates in altered wall rocks at the Uwamuki Kuroko deposits, Japan: Mineralium Deposita, v.33, pp.346-358.

Shrivastava, S.K and Chellani, S.K (1996) Special thematic mapping of Archean-Proterozoic rocks of Bordehi and Kherli areas, Betul District, Madhya Pradesh, Rec. Geol. Surv. India, v. 129 (6), pp. 91-95.

Shrivastava, H.S, Ramteke, P, F, Praveen, M.N, Chakraborty, U (2007) Detailed exploration for basemetal mineralisation in Muariya Block, Chhindwara district, M.P, unpublished progress report, GSI.

Sillitoe, R.H (1982) Extensional habitats of rhyolite-hosted massive sulfide deposits. Geology, v.10, pp.403–407.

Spiess, F.N., MacDonald, K.C., Atwater, T., Ballard, R., Carranza, A., Cordoba, D., Cox, e., Diaz Garcia, V.M., Francheteau, J., Guerrero, J., Hawkins, J., Haymon, R., Hessler, R., Juteau, J., Kastner, M., Larson, R., Luyendyk, B., Macdougall, J.D., Miller, S., Normark, W., Orcutt, J., and Rangin, E (1980). East Pacific Rise: Hot springs and geophysical experiments. Science, v.207, pp.1421-33.

Schmincke, H.U (1967) Fused tuff and peperites in south-central Washinton, Geol.Soc. Amer. Bull. v.78, pp. 319-330.

Seiki, Y and Date, J (1980) Computer application to the alteration data of the footwall dacite lava at the Ezuri Kuroko deposits, Akito Prefecture, Mining Geology, v. 30, pp. 241-250.

Skjerlie, K.P and Johnston, A.D (1992) Vapour-absent melting at 10 Kbar of a biotite and amphibole-bearing tonalite gneiss: implications for the generation of A-type granites. Geology, v. 20, pp.263-266.

Slack, J.F., Grenne, T and Bekker A (2009) Seafloor-hydrothermal Si-Fe-Mn exhalites in the Pecos greenstone belt, New Mexico and the redox state of ca. 1720 Ma deep seawater. Geosphere, v. 5, pp. 302-314.

Slaughter, J., Kerrich, O.M and Wall, V.J (1975) Experimental and Thermodynamic study of equillibria in the system CaO-MgO-SiO_2-H_2O-CO_2. American Journal of Science, v. 275, pp. 143-162.

Solomon, M. (1976) "Volcanic" Massive sulphide deposits and their host rocks-a review and an exploration, In: Wolf, K.A. (eds), Handbook of strata-bound and stratiform ore posits. 11, Regional studies and specific deposits: Amsterdam, Elsevier, pp.21-50.

Spear, F.S (1993) Metamorphic phase equilibria and pressure-temperature-time paths. Mineral. Soc Am Monogra. pp. 1-788.

Spry, P.G and Scott, S.D (1986a) The stability of zincian spinels in sulphide systems and their potential as exploration guides for metamorphosed massive sulphide deposits: Economic Geology, v.81,pp. 1146-1163.

Spry, P.G and Scott, S.D (1986b) Zincian spinel and staurolite as guides to ore in the Appalachians and Scandinavian Caledonides: Canadian Mineralogist, v. 24, pp.147–163.

Spry, P.G., Peter, J.M and Slack, J. F (2000) Meta-exhalites as exploration guides to ore; Review Econ. Geol. V.11,pp.163–201.

Stanton, R.L (1986) Stratiform ores and geological processes, Trans. Inst. Min. Metall. 95(B), pp.167– 178.

Sreejith, C and Ravindra Kumar, G.R (2013) Petrogenesis of high-K metagranites in the Kerala Khondalite Belt, southern India: a possible magmatic-arc link between India, Sri Lanka, and Madagascar, Journal of Geodynamics, v. 63, pp.69-82.

Stein, J.H., Hannah, J.L., Zimmerman, A., Markey, R.J., Sarkar, S.C., Pal, A.B (2004) A 2.5 Ga porphyry Cu-Mo-Au deposit at Malanjkhand, Central India: Implications for late Archean continental assembly. Precambrian Research, v. 34, pp. 89-226.

Sun, S.S and McDonough, W.F (1989) Chemical and isotopic systematic of ocean floor basalts; implication for mantle composition and processes, In:

Magmatism in the ocean basins. Saunders, A.D. and Norry, M.J. (Editors), Geological Soceity of London, London.v.42, pp.313-345.

Taylor, S.R and McLennan, S.M (1985) The continental crust: Its composition and evolution. Blackwell Scientific Publications, Oxford, 312p.

Thompson, A. B (1976) Mineral reactions in pelitic rocks II' Calculation of some P-T-X (Fe-Mg) phase relations. American Journal of Science, 276,425454

Thurston, P.C (1981) Economic evaluation of Archean felsic volcanic rocks using REE geochemistry: Geological Soceity of Australia, special edition, v.7, pp.439-450.

Thurston, P.C and Fryer, B.J (1983) The geochemistry of repetitive cyclical volcanism from basalt through rhyolite in the Uchi-Confederation greenstone belt, Canada: Contributions to Mineralogy and Petrology, v.83, pp. 204-226.

Van Loon, A.J (2009) Soft sediment deformation structures in siliciclastic sediments: an overview. Geologos, v. 15 (1), pp.3-55.

Velde, B (1965) Phengite micas: Synthesis, stability and natural occurrence: American Journal of Science, v. 263, p. 886-913.

Velde, B (1967) Si^{4+} Content of natural phengites. Contributions to Mineralogy and Petrology, v. 14, pp. 250-258.

Vezier, J and Hoefs, J (1976) The nature of O18/O16 and C13/C12 secular trends in sedimentary carbonate rocks: Geochimica et Cosmochimica Acta, v.40,pp.1387-1395.

Wada H., Fujii, N and Niitsuma N (1984) Analytical method of stable isotope for ultra-small amounts of carbon dioxide with MAT-250 mass spectrometer. Geoscience Reports of Shizuoka University, 10, 103–112.

Wada H., Niitsuma N and Saito T (1982), Carbon and oxygen isotopic measurement of ultra-small samples. Geoscience Reports of Shizuoka University, v. 7, pp.35–50.

Wall V.J and England R.N (1979) Zn-Fe spinel-silicate-sulfide reactions as sensors of metamorphic intensive variables and processes. Geological Society of America Abstracts with Programs, 11, 354.

Watson, E.B and Harrisson, T.M (1983) Zircon saturation revisited: temperature and composition effects in a variety of crustal magma types. Earth Planet Sci. Lett., v.64, pp.295-304.

Whalen, J. B., Currie, K. L and Chappell, B. W (1987) A-type granites: geochemical characteristics, discrimination and petrogenesis. Contrib. Mineral. Petrol.v.95, pp.407–419.

Whalen, J.B., Stuik, L.C and Hurley, M.G (1998) Bedrock geology of the Endako map area, Central British Columbia; in Current Research, 1998-A; Geological Survey of Canada, pp.113-123.

Watson, E.B (1996) Dissolution, growth and survival of zircons during crustal fusion: kinetic principles, geological models and implications for isotopic inheritance. Trans R SocEdinb Earth Sci, v.87, pp. 43-56.

Wilson, M (1989) Igneous petrogenesis: A global tectonic approach: London, Unwin Hyman, 466p.

White, J.D.L., McPhie, J and Skilling, I.P (2000) Peperite: a useful genetic term. Bulletin of Volcanology, v. 62, pp 65-66.

Winchester, J.A and Floyd, P.A (1977), Geochemical discrimination of different magma series and their differentiation products using immobile elements,Chemical Geology, v.20, pp.325-343.

Wu Chung-Ming and Zhao Guochun (2006) Recalibration of the Garnet–Muscovite (GM) geothermometer and the Garnet–Muscovite–Plagioclase–Quartz (GMPQ) geobarometer for metapelitic assemblages. Journal of petrology, v. 47, No. 12, pp. 2357-2368.

Yang, K., and Scott, S.D (1996) Possible contribution of a metal-rich magmatic fluid to a sea-floor hydrothermal system. Nature, v. 383, pp.420–423.

Yang. K., Huntington, J.F., Gemmell, J.B and Scott, K.M (2011) Variations in composition and abundance of white mica in the hydrothermal alteration system at Hellyer, Tasmania, as revealed by infrared reflectance spectroscopy. Journal of Geochemical Exploration, v.108, pp. 143–156.

Yedekar, D.B., Jain,S.C., Nair, K.K.K and Dutta, K.K (1990) The central Indian collision suture. Precambrian of central India, GSI.Sp. Publ., v.28, pp.1-37.

Zaleski, E., Froese, E and Gordon, T.M (1991) Metamorphic petrology of Fe-Zn-Mg-Al alteration of the Linda volcanogenic massive sulphide deposit, Snow Lake, Manitoba, Can.Min. v. 29, pp. 995-1017.

******

APPENDIX

Copy of research paper (Praveen and Ghosh, 2009) describing the volcanic facies in the area.

Submarine volcanic facies and its implication as possible tracker of sulphide mineralization – a study from Jilharidev area, Betul belt, central India

M. N. Praveen[1] and Biswajit Ghosh[2,*]

[1]Geological Survey of India, Southern Region, Kerala Unit, Thiruvananthapuram 695 014, India
[2]Department of Geology, University of Calcutta, 35 Ballygunge Circular Road, Kolkata 700 019, India

Felsic volcaniclastic rock forms part of host rock sequences in many of the base metal prospects in the Betul belt. However, the volcanic facies, fragmentation processes and depositional environments in mineralized areas are poorly understood because of the effects of synvolcanic hydrothermal alteration and subsequent regional metamorphism. A section in the Kanhan river valley, which exposes volcanics with relatively well preserved primary textures was mapped in detail to understand the disposition of the felsic volcanics namely rhyolite and to identify the various volcanic facies present within them (viz. massive, flow-banded, autobreccia and hyaloclastite). Four different facies types were distinguished based on phenocryst type, size and abundance. Presence of hyaloclastite autoclastic rocks and pillow lava and absence of pyroclastic deposits suggest a deep, submarine, passive, effusive-type volcanic setting. Autobreccia and hyaloclastite in the felsic volcanic sequence of the present study area lying within Betul Belt has similarities with well-known volcanic-hosted massive sulphide (VHMS) bearing areas in other parts of the world. Proper identification of the volcanic facies within highly altered host rocks near the deposits can help in building up facies models that would establish the genetic relationship between sulphide mineralization and the host-rock facies which in turn will have important implications for base metal exploration in the area.

Keywords: Autobreccia, base metal exploration, Betul belt, hyaloclastite, massive rhyolite, submarine volcanic facies.

THE felsic volcanic rocks belonging to the bimodal volcanic sequence of the Mesoproterozoic Betul belt contain a number of small base metal occurrences. It is being recognized that mineralization is of volcanic-hosted massive sulphide (VHMS) type and based on metal ratios, they range in spectrum from Zn–Cu to Zn–Pb–Cu type[1]. Felsic volcaniclastics occur along with the massive rhyolites and form part of the host rock successions for sulphide mineralization[1–3]. However, the fragmentation processes and depositional environments of these volcaniclastics are poorly understood. Recognition of primary volcanic facies near the prospects is difficult because of the effects of synvolcanic mineralizing hydrothermal alteration and subsequent regional metamorphism.

It is well known that volcanic setting and facies have significant influences on the style of mineralization, alteration patterns and metal content of VHMS deposits[4,6]. This study is an attempt at distinguishing the different phases of rhyolites and their associated facies based on primary volcanic textures that can be readily identified in the field. Their possible mode of origin is also discussed. For this purpose, a section in the Kanhan river valley near Jilharidev temple, 5 km north of Bhuyari Zn–Pb–Cu prospect was selected as the study area and mapped in detail to delineate the different rhyolite flows. Since primary volcanic textures are well preserved in the area, individual volcanic facies could be distinguished and studied in detail. This study indicates that fragmented felsic rocks present in the area are formed by autoclastic processes like flow-fragmentation (autobrecciation) and quench fragmentation and may have formed in a deep-water environment.

Regional geology

The study area is in Betul belt, an approximately 135 × 15 km, east–west trending, Mesoproterozoic inlier surrounded by sedimentary rocks of the Gondwana Supergroup towards the north and west and the Deccan basalts in the south and east. The Sausar belt is exposed to the southeast of Betul belt (Figure 1). The Betul belt which constitutes the central part of the E–W to ENE–WSW Central Indian Tectonic Zone (CITZ)[7] contains three distinct suites of rocks, viz. supracrustal rocks, ultramafic-mafic suite, and syn- to post-kinematic granite suite. The belt is traversed by a number of ENE–WSW ductile shear zones with sub-vertical to steep northerly dips and show

*For correspondence. (e-mail: bghosh_geol@hotmail.com)

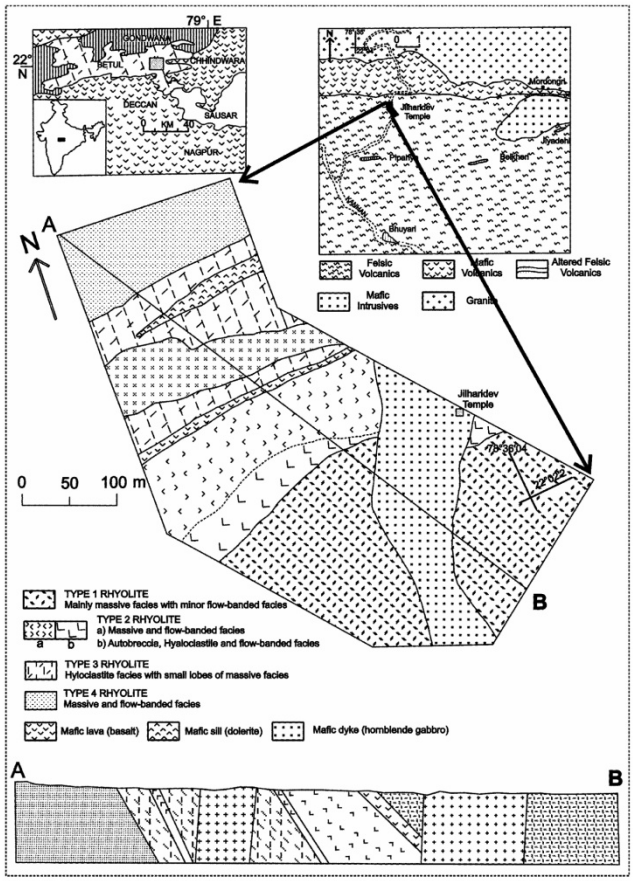

Figure 1. Detailed geological map of (mapping carried out on 1 : 1000 scale) Kanhan river section showing the different rhyolite flows. Inset map towards top left shows location map showing the Betul belt inlier (after Golani and Dora[37]), black box shows area of regional map shown towards top right. Inset map towards top right shows simplified regional map around Jilharidev area, black rectangle in Kanhan river near Jilharidev temple shows area covered by detailed map. Geological section drawn at the bottom of the figure is along the line A–B of the geological map.

low to medium grade metamorphism[7]. The tectonic setting may be nearer to the arc environment[7].

The central and eastern part of the Betul belt contains the bimodal volcanic sequence belonging to the Bargaon Group[8]. Available whole rock geochemical data indicate the dominantly bimodal nature of the volcanics and their tholeiitic affinity[1,3]. This part of the Betul belt contains several small base metal prospects namely those located at Banskhapa–Pipariya, Bhanwra–Tekra, Bargaon–Tarora, Ghisi, Muariya, Koparpani, Dehalwara and Bhuyari[1–3,9]. Zn–Pb–Cu and Zn–Cu ore bodies are associated with metamorphosed hydrothermal alteration zones which contain various assemblages of metamorphic minerals which include chlorite, biotite, garnet, staurolite, sillimanite, gahnite, anthophyllite, actinolite and tremolite[10]. Ghosh and Praveen[11] proposed that most of these minerals formed in a single metamorphic regime of continually decreasing growth kinetics generally linked to progressive cooling. Mahakud *et al.*[2] reported that the rocks were metamorphosed to staurolite–almandine subfacies of

Figure 2. Field photographs of ***a***, pillow lava; ***b***, mafic autobreccia with clasts showing crude lineation (arrows); ***c***, Apophyses of porphyritic granite in mafic volcanics showing chilled margins; ***d***, massive facies of type-1 rhyolite showing large, abundant quartz (dark grains) and feldspar (white) phenocrysts; ***e***, photomicrograph of type-1 rhyolite showing quartz phenocryst in a fine grained quartz-rich groundmass; ***f***, field photographs of flow-banded facies of type-1 rhyolite with contorted flow banding.

almandine–amphibolite facies, and subsequently subjected to retrograde metamorphism.

The eastern part of the bimodal volcanic region is dominated by felsic volcanics (Figure 1). Felsic volcanics are composed of massive rhyolite, flow-banded rhyolite, felsic volcaniclastics and thin horizons of felsic chert. Felsic volcanics are intensely altered near mineralized areas like Bhuyari. A sequence of mafic volcanics (basalt) occurring to the north of the felsic volcanics is composed dominantly of pillow lavas (Figure 2 *a*). Massive and volcaniclastic facies are also present. The mafic volcaniclastics are composed of angular raft like clasts which display a crude lineation and many clasts are flattened and stretched (Figure 2 *b*), indicating that these are products of autobrecciation. The mafic volcanics are intruded by younger porphyritic granites (Figure 2 *c*). These granites form the northern contact of the Betul belt in this area with the Gondwana Supergroup. The granites show minimum deformation and are related to the younger Navegaon granite as described by Mahakud *et al.*[12]. A regional ENE–WSW to EW trending schistosity with moderate southerly dips is developed in the rocks. The general E–W trend of the volcanics is deduced from the contact between the felsic and mafic volcanics, which is also sub-parallel to the regional schistosity.

The Bhuyari base metal prospect towards the south of the study area has many features similar to typical VHMS deposits and contains disseminated, vein and minor massive Zn–Pb–Cu sulphides[9,13]. The prospect area is dominated by massive, quartz-porphyritic rhyolite which is intensely altered close to the ore bodies. Chemical analyses of felsic volcanic rocks at Bhuyari prospect show that they are rhyolitic in composition[9]. Primary textures like relict flow banding are only occasionally preserved in the rhyolites. Ore bodies are hosted by hydrothermally altered and metamorphosed massive rhyolite which has given rise to

various assemblages of metamorphic minerals like quartz–muscovite schist, quartz–biotite–muscovite–garnet ± plagioclase ± staurolite ± gahnite schist and tremolite–carbonate rock. The tremolite–carbonate rocks are very localized in nature and based on their close spatial association with massive sulphide mineralization and preservation of relict soft-sediment, deformation structures are interpreted as meta-exhalites related to a mineralizing hydrothermal vent[13]. Metamorphosed hydrothermally altered felsic volcanics occur as lensoid bodies conformable to the volcanic sequence near Pipariya, Belkheri and Jiyadehi villages (Figure 1). At these places, the altered rocks consist of quartz–sericite ± garnet schist, quartz–chlorite–garnet schist and quartz–biotite–chlorite ± garnet schist and their alteration pattern is similar to those in other prospects of Betul belt. Outcrops of altered rocks at Belkheri contain specks of sphalerite, galena and chalcopyrite along with disseminated pyrite and pyrrhotite. Bed rock values of altered rock from Pipariya and Belkheri show anomalous values for zinc and lead. Such garnet bearing quartzo-feldspathic schist rocks showing bed rock base metal anomalies have been observed to occur between Kohat and Lawagoghri, a few kilometres to the south of Bhuyari[9] and it was proposed that these rocks may represent an exhalative component of the felsic volcanics.

Brief overview on submarine felsic volcanics

Submarine silicic lavas can be divided into three main types: lava domes, laterally extensive lava flows and largely intrusive high-level domes (cryptodomes) that intrude the sediment pile and barely breach the sediment surface[14]. De Rosen-Spence *et al.*[15] found that the rhyolitic to dacitic Archean flows of the Rouyn-Noranda area vary from above-vent domes to more extensive tabular masses, however they commonly formed stacked sequences of lavas with their boundaries being marked by variations in the abundance and size of quartz and plagioclase phenocrysts. For rocks related to intrusions and lavas, individual facies correspond to various different textural components of the body, based on which Allen[14] identified massive coherent lava, flow banded coherent lava, autobreccia and hyaloclastite as the main original facies within the silicic volcanic units hosting volcanic associated mineralization at Benambra, southeastern Australia. Submarine volcaniclastics could form by autobrecciation (flow-fragmentation), quench fragmentation, pyroclastic fragmentation and resedimentation[5]. Submarine lavas consist of at least 30% by volume of autoclastic rocks (hyaloclastite and autobreccia). Autobreccias result from the fracturing of solidifying magma under the influence of shear stresses induced by the flow of nearby magma. They can form in intrusive magma masses but are more common in the margins of lava flows and may also occur within lavas[16,17]. Autobreccias are usually coarse aggregates with minimal finely granulated debris and they may form substantial proportions of lavas[16]. Autobreccias have been identified in all submarine lava types from basaltic[18] to rhyolitic[15].

Hyaloclastites are products of quench fragmentation, which may occur when hot magma and cold water come in contact, producing thermal stresses which lead to cooling contraction granulation[17,19,20]. Rittman[21] originally applied the term 'hyaloclastite' to the broken, spalled glassy shells of basaltic pillows but its definition has evolved to include all quench-fragmented aggregates, irrespective of composition[5]. Hyaloclastite may form when subaerial lavas flow into water[22,23], when lavas are erupted subaqueously[24], or when magma intrudes water-saturated sediments[25]. Hyaloclastite can consist of large glassy blocks through to finely granulated sand and silt-size glassy fragments. Fragments generally have curviplanar surfaces and may be equant and blocky or blade-like and splintery in shape[5].

Volcanic facies of the Jilharidev area

Primary volcanic features and textural characteristics of the rhyolites in the eastern part of Betul belt are best exposed in the N–S trending Kanhan river section occurring to the north of the Bhuyari base metal prospect (Figure 1). The present study is restricted to the identification of rhyolite types and facies in a single section in the Kanhan river across the strike of the volcanics, lateral tracing of the rhyolite type and facies was not attempted due to thick forest cover and scanty outcrops.

Depending on the nature and size of the phenocrysts and their relative proportions, four different types of rhyolites (Types 1–4) and based on structures and textures present in them, four different facies (massive coherent lava, flow banded lava, autobreccia and hyaloclastite) were recognized. Besides rhyolites, the mapped area also contains (1) 10–20 m wide conformable metabasic sill; (2) 10 m wide mafic extrusive (basalt) with ill-preserved pillows and (3) few 50–100 m wide mafic intrusive rocks represented by dolerite and hornblende gabbro. Structurally, most rocks in the area are massive in nature and display minimum deformation. Only a crude foliation could be identified at places with strike parallel to the E–W trend of the volcanics and moderate dips to the south. Although no pronounced hydrothermal alteration is present in the rocks, the rhyolites at many places show extensive development of 1–3 cm long hornblende along with discrete crystals of magnetite and rare garnets; such hornblende-bearing rhyolites are common in Betul belt[3,9] and may represent low intensity hydrothermal alteration. Pyrites is ubiquitious in the rhyolites of the area and occur as disseminations and rarely as 1 cm clots, the presence of pyrite also indicates hydrothermal activity. The weathering of pyrite gives the rhyolites a deep red surface

Table 1. Different types of volcanic facies of the Jilharidev area

Type	Mode of occurrence	Phenocryst	Groundmass	Dominant structural/textural pattern	Comments
Type-1	Massive coherent facies, locally flow banded	Quartz and feldspar-phyric (together 20%), equal proportion of quartz and plagioclase phenocrysts evenly distributed, quartz phenocrysts are generally <3 mm and feldspar phenocrysts are <5 mm in size. The quartz phenocrysts are rounded to euhedral in shape and show varying degrees of resorbtion of grain margins whereas feldspars are generally euhedral plagioclase laths	Finer grained mosaic of mainly quartz, minor feldspar and sericite	Flow banding, porphyritic	Features in this rhyolite (viz. the large and abundant phenocrysts, mostly massive nature and absence of hyaloclastite) are similar in character to sub-volcanic rhyolite domes and sills. which are common in rhyolite lava complexes[5,26]
Type-2	Massive (60%) autoclastics (30%) flow banded (10%)	Aphyric to sparsely feldspar-phyric	Fine grained feldspar and quartz	Brecciated/fragmented (flow fragmentation), microbreccia (quench fragmentation), flow banding, porphyritic, Nodular devitrification texture (1–3 cm diameter)	Autobreccia with hyaloclastite matrix indicates that auto-brecciation and quench fragmentation occurred simultaneously. These features together with presence of widespread planar flow banding in this rhyolite gives evidence for extrusion of lava on to the sea floor
Type-3	Hyaloclastite (80%) with small lobes of massive facies	Dominantly feldspar-phyric (15–20%) with (~3%) quartz	Fine grained feldspar and quartz	Microbreccia, porphyritic, ill-developed flow banding	Appears to have been em-placed as an extrusive flow, which has had extensive interaction with seawater
Type-4	Mainly massive with intermittent thin flow banding	Aphyric to sparsely feldspar-phyric	Cryptocrystalline quartzo-feldspathic material	Planar flow banding, porphyritic, nodular devitrification texture (<1 cm diameter)	Presence of planar flow banding and extensive nodular devitrification textures indicate that this rhyolite was originally glass-rich extrusive lava

colour. Characteristics of different types of volcanic facies are given in Table 1.

Type-1 rhyolite

Type-1 rhyolites occur mainly as massive coherent facies and are only locally flow banded. Type-1 rhyolites are strongly quartz and feldspar-phyric, with about 20% quartz + feldspar phenocrysts and quartz phenocrysts are generally less than 3 mm and feldspar phenocrysts are less than 5 mm in size. This rhyolite has an equal proportion of both quartz and plagioclase phenocrysts evenly distributed in a quartzo-feldspathic groundmass (Figure 2 *d*). The quartz phenocrysts are rounded to euhedral in shape and show varying degrees of resorbtion of grain margins (Figure 2 *e*), whereas feldspars are generally euhedral plagioclase laths. The groundmass consists of a finer grained mosaic of mainly quartz and minor feldspar and sericite. Flow banding is present as mm to cm thick alternating layers of light siliceous and dark phyllosilicate rich layers. Evidence for viscous flow is provided by contorted flow banding (Figure 2 *f*). Disseminated pyrite is commonly present in the rock and at places the pyrite forms centimetre sized aggregates. At places 1–3 cm long hornblende along with discrete grains of magnetite and rare garnets are present (Figure 3 *a*).

Many of the features in this rhyolite (viz. the large and abundant phenocrysts, mostly massive nature and absence of hyaloclastite) are similar in character to sub-volcanic rhyolite dome and sills. Such domes and sills are common in rhyolite lava complexes[5,26].

Type-2 rhyolite

Type-2 rhyolite is sparsely feldspar-phyric with up to 5% (<1 mm) feldspar phenocrysts and quartz phenocryst are

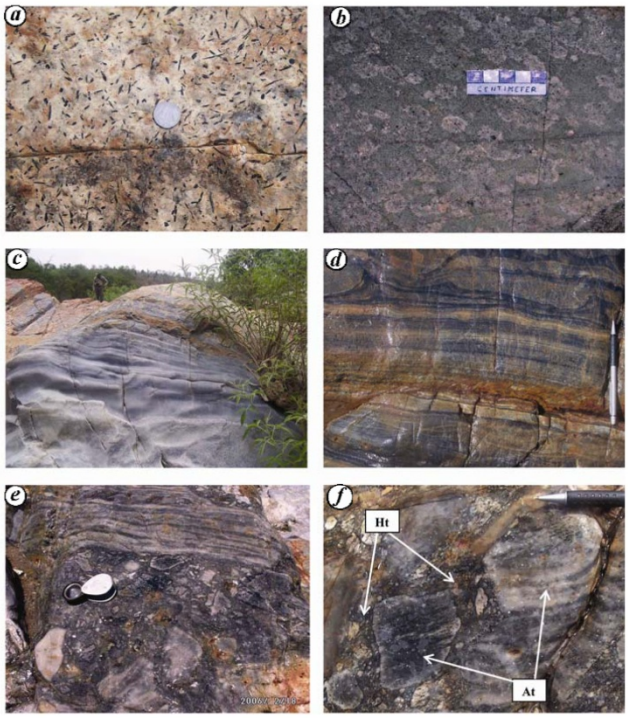

Figure 3. Field photographs: ***a***, Randomly oriented hornblende grains in type-1 rhyolite; ***b***, White, rounded and coalesced devitrification structures in type 2 rhyolite; ***c***, Flow banded facies of type-2 rhyolite showing flow-banding parallel to strike; ***d***, Flow banded facies of type-2 rhyolite showing flame-like extensions (near top of photograph); ***e***, Flow banded facies adjacent to autobreccia facies in type-2 rhyolite, note bigger clasts towards bottom of photograph show flow banding; ***f***, Large, adjacent autobreccia clasts (At) showing continuation of flow-band between them and hyaloclastite microbreccia (Ht) occurring in the matrix.

absent. Volumetrically this rhyolite contains approximately 60% massive facies, 30% autoclastics (autobreccia and hyaloclastites) and about 10% flow-banded facies. The massive facies is aphyric to sparsely feldsparphyric rhyolite and quartz phenocrysts are absent or rare. At places the massive facies rock show 1–3 cm, rounded, white coloured quartzo-feldspathic aggregates. They form discrete and interconnected masses with bulbous, cauliflower-like margins (Figure 3 *b*). These textures are similar to nodular devitrification textures as described by Allen[14], where they are similar to other devitrification structures like large spherulites and lithophysae. When devitrification spreads radially outwards from a smaller number of nuclei or spreads further out from flow bands, more irregular, nodular to cauliflower shaped devitrification was formed; they commonly exhibit sharp, finely bulbous margins, which are devitrification fronts. They can form interconnected structures. Growth of such textures requires a coherent glassy host and they are therefore to be expected only in lavas, shallow intrusions, or strongly welded glassy pyroclastic rocks[14].

Type-2 rhyolite displays spectacular development of flow-banded facies, which occur in a number of parallel zones ranging from few centimetres to several metres wide within the massive and autoclastic facies, the layering in the flow bands is mostly planar with strike generally parallel to those of the volcanic sequence (Figure 3 *c*). Flow banding is considered to be a record of the movement of the lava mass[27]. Flow bands consist of alternating mm to cm thin light and dark coloured layers.

The pale siliceous layers are considered to represent devitrified glass and the dark phyllosilicate layers are nondevitrified altered glass and such layering is formed when devitrification commences from numerous nuclei along a primary flow foliation and progresses a short distance from the flow fabric as relatively planar devitrification fronts[14]. At places wispy, flame-like textures are found extending from the flow bands (Figure 3 *d*); these may have developed due to compaction and shearing of flow-bands in a semi-molten state.

A 10–40 m wide horizon of *in situ* and clast rotated autoclastic rocks which consist of both autobreccia and hyaloclastite occur intercalated with flow banded facies within the type-2 rhyolite near the contact with the type-1 massive rhyolite (Figure 1). Although autobreccia and hyaloclastite occur together in this rhyolite, they have formed by different processes and can be differentiated based on certain textural features.

Autobreccia consists of large, blocky to medium sized clasts, which routinely preserve flow-banding and commonly occur adjacent to flow-banded rhyolite (Figure 3 *e*), indicating that they formed by breaking up of flow-banded rhyolite. Autobreccias can be distinguished from hyaloclastite by the flow-banded character of the clasts and by the paucity of granule sized clasts[14,16]. Locally, *in situ* autobreccia is preserved in which flow-bands continue into adjacent clasts (Figure 3 *f*), *in situ* breccias occur as pockets within more widespread disorganized aggregates. Unequivocal evidence for brecciation to have occurred during flow of the lava is provided by lineated flow-banded clasts which preserve a flow fabric (Figure 4 *a*), these clasts are tightly packed, flattened and stretched to elongate shapes giving evidence for plastic moulding or accommodation of shapes, such features are formed when the breaking magma is plastic[5].

Hyaloclastite can be distinguished from autobreccia by their lack of flow banding and plastic deformation textures. Hyaloclastite can also be differentiated because they can also occur as small granule sized clasts and frequently they occur as fine-grained microbreccia between the intergranular spaces of larger flow-banded clasts of autobreccia (Figure 3 *f*). De Rosen-Spence *et al.*[15] suggested that autobrecciation and quench fragmentation can occur simultaneously, where initial autobrecciation, particularly of viscous magma which breaks by brittle fracture, would give water access to the interior of the flow, so triggering quench fragmentation. Kokelaar[20] also suggested that hyaloclastite may result from the dynamic stressing of chilled lava surfaces as lava continues to flow.

At places, the autoclastic facies is mainly composed of hyaloclastite, these consist of clasts which show a size range from sand sized microbreccia to block sized clasts, and more commonly contain pebble sized clasts. They form closely spaced, polygonal fragments with curviplanar and serrated margins that are common (Figure 4 *b*). Certain groups of clasts display jigsaw-fit textures (Figure 4 *c*), these occur as isolated in a more disorganized hyaloclastite matrix. Occurrence of such jigsaw-fit textures between groups of clasts is considered a diagnostic feature of *in situ* hyaloclastite[28]. Also, these breccias do not show flow-banding and are not intimately associated with flow bands or show flow fabric, these evidences indicate that parts of the autoclastics in flow-2 rhyolite have formed exclusively by quench-fragmentation.

Minimum deformation in the rocks together with the unequivocal evidences as given above for the presence of autobreccia and hyaloclastite clearly indicates that fragmentation was caused by primary autoclastic processes. Autobreccia with hyaloclastite matrix in type-2 rhyolite indicates that autobrecciation and quench fragmentation occurred simultaneously. These features together with the presence of widespread planar flow-banding in this rhyolite give evidence for extrusion of lava on to the sea floor. A thin 10 m wide outcrop of pillowed metabasalt separates type-2 rhyolite from type-3 rhyolite, pillows are not well-developed and outcrops of this metabasalt are scanty. The rock is fine grained and composed of chloritized amphibole and plagioclase.

Type-3 rhyolite

This rhyolite mainly consists of hyaloclastite facies which encloses small lobes of massive facies. Volumetrically, it contains almost 80% of hyaloclastite. Massive coherent rhyolite is represented by a moderately to strongly porphyritic rhyolite characterized by 15–20%, less than 2 mm phenocrysts of plagioclase feldspar (Figure 4 *d*). Quartz phenocrysts are up to 3% and not readily apparent to the naked eye, however small (<1 mm) rounded phenocrysts can be seen with a hand lens. Massive coherent lava exists as small lobes within more extensive hyaloclastite of the same rhyolite. Flow banding, although present, is not well developed. Hyaloclastite consists of mm to cm sized angular fragments that show polygonal to splintery shapes with curviplanar margins (Figure 4 *e*). Clasts are monomictic and preserve the same phenocryst size and abundance of the massive coherent facies. Rarely, do they contain coarse block sized clasts. Absence of flow banded clasts and the predominance of small clasts ranging from sand sized to less than 2 cm distinguish this breccia as hyaloclastites.

Type-3 rhyolite appears to have been emplaced as an extrusive flow, which has had extensive interaction with seawater. It is distinguished from type-2 rhyolite on the basis of its moderately to strongly porphyritic nature, absence of autobreccia and by the predominance of hyaloclastite microbreccia. A 20 m wide concordant amphibolite (meta-dolerite) sill is present within this rhyolite. The rock is medium grained and composed mainly of green coloured amphibole, chlorite and plagioclase.

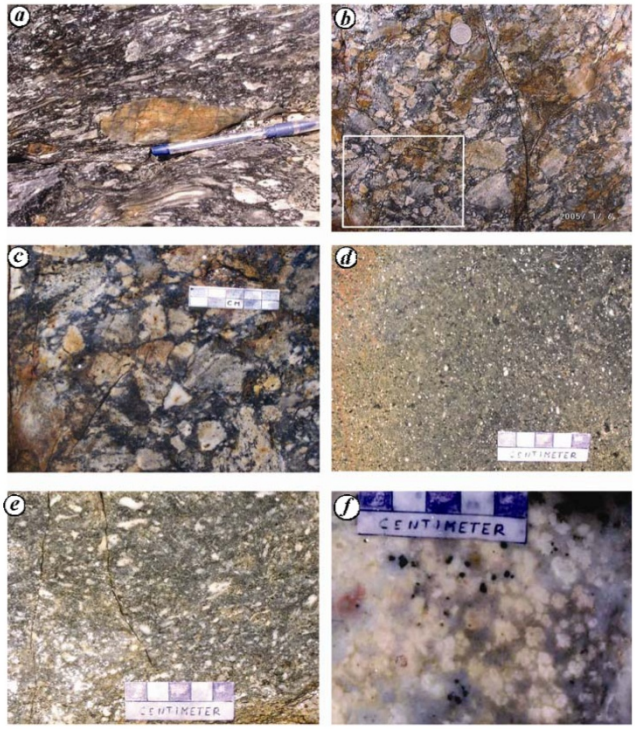

Figure 4. Field photographs: ***a***, Autobreccia facies of type-2 rhyolite with plastically stretched flow-banded clasts; ***b***, Hyaloclastite facies of type-2 rhyolite showing closely packed, large as well as fine grained angular clasts with curviplanar margins; ***c***, Magnified photograph of the area in the square shown in Figure 4 *b* showing a group of clasts with jigsaw-fit textures (centre of photograph); ***d***, Massive facies of type-3 rhyolite with abundant feldspar phenocrysts; ***e***, Hyaloclastite facies of type-3 rhyolite with finely granulated clasts; ***f***, Nodular devitrification texture in type-4 massive rhyolite with white, cauliflower-like aggregates.

Type-4 rhyolite

Type-4 rhyolite is an aphyric to sparsely feldspar-phyric rhyolite with up to 3%, less than 1 mm feldspar phenocrysts. This rhyolite has a smooth surface appearance on account of the lack of phenocrysts and clasts. Most of the rhyolite is composed of massive coherent facies with intermittent thin zones of flow-banded facies. Massive coherent lava consists of extremely fine grained cryptocrystalline quartzo-feldspathic material and ranges from being aphyric to sparsely feldspar porphyritic with up to 3% less than 1 mm euhedral feldspar phenocrysts. Nodular devitrification textures are common in this rhyolite, they are similar but smaller in size to those in type-2 rhyolite, generally less than 1 cm in diameter and has a distinct cauliflower-like shape, they occur as discrete and coalesced aggregates (Figure 4 *f*). Flow banding is extremely planar and thinly layered with layering parallel to the E–W strike of the volcanics with vertical dips. Flow-banding is not associated with autobreccia. This rhyolite could at places be confused for thinly laminated chert, because of the straight, apparently sedimentary laminations and fine grain size of the rock. However, presence of feldspar phenocrysts and nodular devitrifying textures provide unequivocal evidence for a volcanic parentage. Presence of planar flow banding and extensive nodular devitrification textures indicate that this rhyolite was originally glass-rich extrusive lava.

Discussion

In the study area in Kanhan river section near Jilharidev, four different types of rhyolite emplacement can be distinguished mainly based on their phenocryst-mineralogy, phenocryst size and abundance. This indicates that multiple phases of extrusive and some related intrusive phases were associated with this lava complex. These might be similar to the submarine dome and lava complex as described by Cas[5] which are nonexplosive silicic volcanic centres dominated by coherent lavas, cross cutting dykes and feeders, hyaloclastites and autobreccia. Also, the presence of multiple types of rhyolite and associated facies in the study area indicate that they comprise a proximal (volcanic centre or vent area) to medial facies association. De Rosen-Spence *et al.*[15] have identified systematic proximal to distal variations in Archean lavas, where the proximal facies consists mainly of massive lavas and medial facies consists of lava lobes in hyaloclastite breccia. Proximal facies association as described by Allen *et al.*[26] consists of multiple generations of lavas and *in situ* hyaloclastite breccia.

At Jilharidev area, the common association of hyaloclastite in the felsic volcanic succession together with the presence of pillow basalt lavas indicates that the volcanics were extruded in a submarine setting. Volcanic facies association of lavas and autoclastic rocks at Jilharidev area indicate passive submarine volcanism rather than explosive pyroclastic eruption. The facies association within the felsic volcanics comprising massive, flow-banded and autoclastic (autobreccia and hyaloclastite) facies are considered to be products of effusive rhyolitic eruptions that are formed at submarine volcanic centres[6,29] and represent ambient submarine volcanism[5].

Explosive eruptions are generated by volatiles of varying origins. The most common volatiles are exsolved magmatic volatiles, such as water and carbon dioxide (magmatic explosions[30]) or superheated external water in contact with the magma (phreatic explosions) or a combination of magmatic volatiles and superheated external water which are known as phreato-magmatic explosions[20,31,32]. In case of submarine lava-forming eruptions, the non-explosive nature of the eruption could be due to the ambient hydrostatic pressure of the seawater column being high enough to suppress the explosive expansion of magmatic volatiles and the explosive expansion of superheated seawater in contact with the erupting magma[5]. McBirney[33] estimated that practical maximum water depths for explosive eruption of acid magmas with known volatile contents are probably in the range of 500–1000 m.

Explosive silicic eruptions are characterized by vesicular, pumiceous clasts, whereas dense non-vesicular clasts are related to lava flows[29]. No evidence of pyroclastic deposits is found in the study area. Since all other primary volcanic textures are relatively well preserved, any original vesicular clasts could have been easily recognized. However, in the present case, the clasts in the volcaniclastics are dense and completely lacking in vesicles or amygdules. The non-vesicular nature of the rhyolites at Jilharidev together with the conspicuous absence of pumiceous clasts suggest that rhyolite extrusions were not associated with pyroclastic eruptions. It would be therefore reasonable to infer that they were emplaced at sufficient water depths so that vesiculation of volatiles could not take place due to high hydrostatic pressures. Additional evidence for deep water setting for the emplacement of these volcanics is the presence of massive sulphide at the nearby Bhuyari prospect. On the basis of studies in several VHMS deposits, it is generally agreed upon that a water depth of more than 500 m is required for the formation of massive sulphides[5]. Massive sulphide occurrences within the felsic volcanics in many other places of Betul belt may indicate prevalence of a regional deep marine setting for the emplacement of the volcanics.

It is interesting to note that the presence of autobreccia and hyaloclastite in the felsic volcanic sequence of Betul belt has similarities with the well-known VHMS bearing areas in other parts of the world. Autobreccia and hyaloclastite form host-rock successions for the Kuroko massive sulphide deposits, Japan[34], the Silurian Currawong and Wilga depoits, Australia[14,35], Que River and Hellyer deposits in Tasmania[22] and the Archean Golden Groove VHMS succession in Western Australia[36]. It is probable that the autobreccia and hyaloclastite (similar to that recorded in the presently studied Jilharidev area) may be found at many base metal prospects of the Betul belt. Proper identification of the volcanic facies within highly altered host rocks near the deposits can help in building up facies models that would establish the genetic relationship between sulphide mineralization and the host–rock facies and in turn, this will have important implications for base metal exploration in the area.

1. Praveen, M. N., Ghosh, B., Shrivastava, Dora, M. L. and Gaikwad, L. D., Sulphide mineralisation in Betul belt: classification and general characteristics. *Geol. Soc. India*, 2007, **69**, 85–91.
2. Mahakud, S. P., Raut, P. K., Hansda, C., Ramteke, P. F., Chakraborty, U., Praveen, M. N. and Sisodiya, D. S., Sulphide mineralisation in the central part of Betul belt around Ghisi–Muariya–Koparpani area, Betul district, Madhya Pradesh. *Geol. Surv. India Spl. Pub.*, 2001, **64**, 377–385.
3. Raut, P. K. and Mahakud, S. P., Geology, geochemistry and tectonic setting of volcanosedimentary sequence of Betul belt, Madhya Pradesh and genesis of zinc and copper sulphide mineralisation. *Geol. Surv. India*, *Spl. Pub.*, 2004, **72**, 133–146.
4. Morton, R. L. and Franklin, J. M., Two-fold classification of Archean volcanic-associated massive sulphide deposits. *Econ. Geol.*, 1987, **82**, 1057–1063.
5. Cas, R. A. F., Submarine volcanism: eruption styles, products, and relevance to understanding the host–rock successions to volcanic-hosted massive sulphide deposits. *Econ. Geol.*, 1992, **87**, 511–541.
6. Large, R. R., McPhie, J., Bruce, G. J., Herrmann, W. and Davidson, G. J., The spectrum of ore deposit types, volcanic environments, alteration halos, and related exploration vectors in submarine vol-

canic successions: some examples from Australia. *Econ. Geol.*, 2001, **96**, 913–938.
7. Roy, A. and Prasad, M. H.., Precambrian of central India: a possible tectonic model. *Geol. Surv. India Spl. Pub.*, 2001, **64**, 177–197.
8. Shrivastava, S. K. and Chellani, S. K., Geology of Amla-Kherli Bazar area, district Betul, Madhya Pradesh. *Rec. Geol. Surv. India*, 1994, **128**, 91–95.
9. Golani, P. R., Dora, M. L. and Bandopadhyay, B. K., Base metal mineralization associated with hydrothermal alteration in felsic volcanic rocks in Proterozoic Betul belt at Bhuyari, Chhindwara District, Madhya Pradesh. *Geol. Soc. India*, 2006, **68**, 797–808.
10. Praveen, M. N. *et al.*, Metamorphic mineral assemblages associated with sulphide mineralisation in Betul belt: a possible hydrothermal origin. In Proceeding volume of 1st Indian Mineral Congress Showcasing the Indian Mineral Industry in the 21st Century (eds Sinha, A. and Singh, S. K.), ISM, Dhanbad, India, Allied Publishers, New Delhi, 2005, pp. 193–218.
11. Ghosh, B. and Praveen, M. N., Garnet–gahnite–staurolite relations and occurrence of ecandrewsite from the Koparpani base metal sulphide prospect, Betul belt, Central India. *N. Jb. Miner. Abh.*, 2007, **184**, 105–116.
12. Mahakud, S. P., Raut, P. K. and Mishra, V. P., Geological set-up of Kherli Bazar polymetallic deposit Betul district, Madhya Pradesh, Proceedings of the National Seminar on Tectonomagmatism, Geochemistry and Metamorphism of Precambrian Terrains (eds Gyani, K. C. and Kataria, P.), University Department of Geology, Udaipur, 2000, p. 438.
13. Praveen, M. N. and Ghosh, B., Multiple origin of gahnite associated with hydrothermal alteration from Bhuyari basemetal prospect of proterozoic Betul belt. *Geol. Soc. India*, 2007, **69**, 233–241.
14. Allen, R. L., False pyroclastic textures in altered silicic lavas, with implications for volcanic-associated mineralisation. *Econ. Geol.*, 1988, **83**, 1424–1446.
15. De Rosen-Spence, A. F., Provost, G., Dimroth, E., Gochnaver, K. and Owen, V., Archean subaqueous felsic flows, Noranda, Quebec, Canada, and their Quaternary equivalents. *Precambrian Res.*, 1980, **12**, 43–77.
16. MacDonald, G. A., *Volcanoes*, Englewood Cliffs, New Jersey, Prentice-Hall, 1972, p. 510.
17. Cas, R. A. F. and Wright, J. V., *Volcanic Successions – Modern and Ancient. A Geological Approach to Processes, Products and Successions*, Allen and Unwin, London, 1987, p. 529.
18. Ballard, R. D., Holcomb, R. D. and van Alden, T. H., The Galapagos rift at 86°W: sheet flows, collapse pits and lava lakes of the rift valley. *J. Geophys. Res.*, 1979, **84**, 5407–5422.
19. Fisher, R. V. and Schmincke, H. U., *Pyroclastic Rocks*, Springer-Verlag, 1984, p. 472.
20. Kokelaar, B. P., Magma–water interactions in subaqueous and emergent basaltic volcanism. *Bull. Volcanol.*, 1986, **48**, 275–289.
21. Rittman, A., *Volcanoes and their Activity*, John Wiley, New York, 1962, p. 305.
22. Waters, A. C., Determining direction of flow in basalts. *Am. J. Sci.*, 1960, **258**, 350–366.
23. Jones, J. G. and Nelson, P. H. H., The flow of basalt lava from air to water – its structural expression and stratigraphic significance. *Geol. Mag.*, 1970, **107**, 13–19.
24. Carlisle, D., Pillow breccias and their aquagene tuffs, Quadra Island, British Columbia. *J. Geol.*, 1963, **71**, 48–71.
25. Kokelaar, B. P., Fluidization of wet sediments during the emplacement and cooling of various igneous bodies. *J. Geol. Soc. London*, 1982, **139**, 21–33.
26. Allen, R. L., Weihead, P. and Svenson, S. A., Setting of an Zn–Cu–Au–Ag massive sulphide deposits in the evolution and facies architecture of a 1.9 Ga massive volcanic arc, Skellefte dist., Sweden. *Econ. Geol.*, 1997, **91**, 1022–1053.
27. McPhie, J., Doyle, M. and Allen, R., *Volcanic Textures: A Guide to the Interpretation of Textures in Volcanic Rocks*, Codes Key Center, Tasmania, 1993, p. 198.
28. Yamagishi, H., Studies on the Neogene subaqueous lavas and hyaloclastites in southwest Hokkaido. *Rep. Geol. Surv. Hokkaido*, 1987, **59**, 55–117.
29. McPhie, J. and Allen, R., Facies architecture of mineralized submarine volcanic sequences: Cambrian Mount Read volcanics, Western Tasmania. *Econ. Geol.*, 1992, **87**, 587–596.
30. Sparks, R. S. J., The dynamics of bubble formation and growth in magmas: a review and analysis. *J. Volcanol. Geotherm. Res.*, 1978, **3**, 1–37.
31. Sheridan, M. F. and Wohletz, K. H., Hydrovolcanic explosions: the systematics of water-pyroclast equilibration. *Science*, 1981, **212**, 1387–1389.
32. Sheridan, M. F. and Wohletz, K. H., Hydrovolcanism: basic considerations. In Explosive Volcanism (eds Sheridan, M. F. and Barberi, F.). *J. Volcanol. Geotherm. Res.*, 1983, **17**, 1–29.
33. McBirney, A. R., Factors governing the nature of submarine volcanism. *Bull. Volcanol.*, 1963, **26**, 455–469.
34. Cas, R. A. F., Allen, R. L., Yamagishi, H., Ishikawa, Y. and Ohguchi, T., Eruptive style, products and setting of kuroko volcanics, Miocene Green Tuff Belt, Japan. *Geol. Soc. Austr. Abstr.*, 1990, **25**, 34.
35. Allen, R. L., Reconstruction of the tectonic, volcanic, and sedimentary setting of strongly deformed Cu–Zn massive sulphide deposits at Benambra, Victoria. *Econ. Geol.*, 1992, **87**, 825–854.
36. Clifford, B. A., Volcanic-sedimentary facies associations hosting the volcanogenic massive sulphide mineralisation at Golden Groove, Western Australia. In Pacific Rim Congress Gold Coast, Queensland, 26–29 August 1987, Proc. Parkville Australia, Australasian Inst. Mining Metallurgy, 1987, pp. 871–875.
37. Golani, P. R. and Dora, L. M., Final report on the specialized thematic mapping in Gavilgarh – Tan shear zone area in Kanhan and Pench river valley sectors of Chhindwara district, Madhya Pradesh. *Geol. Surv. India*, 2003 (unpublished progress report).

ACKNOWLEDGEMENTS. We thank Mr H. S. Shrivastava, GSI, Bhopal for stimulating discussion; Mr M. L. Dora, GSI, Nagpur for support, and Mr A. Majumdar, GSI, Jabalpur for technical assistance.

Received 28 February 2008; revised accepted 24 July 2009

******